TRIM25 ACTIVATION AND MODULATION OF ANTI-VIRAL IMMUNITY

Jacint Sanchez

Immokalee, Florida

B.S., University of South Florida

A Dissertation presented to the Graduate Faculty

of the University of Virginia in Candidacy

for the Degree of Doctor of Philosophy

Interdisciplinary Program in Biophysics

University of Virginia

December 2017

ABSTRACT

TRIM25 is a member of the tripartite motif family of E3 ligases. This family of proteins regulate many cellular processes, including development, cell growth, differentiation, cancer, and innate immune response. TRIM25 is best characterized as an important factor for anti-viral innate immunity, but also functions in diverse RNA-dependent pathways. Previous TRIM25 studies have identified cellular substrates and touched on its E3 ligase activity, but provided little insight into the requirements for TRIM25 catalytic activation. By elucidating the mechanisms involved in TRIM25 anti-viral activation, we can provide a fundamental understanding of TRIM25-mediated processes. This work employs structural, biophysical, and biochemical techniques complemented with cell biology to analyze TRIM25's tertiary and quaternary structures, as well as essential factors for TRIM25 mediated anti-viral activity.

The cellular PRRs RIG-I and ZAP independently modulate an effective anti-viral innate immune response through induction of IFN signaling and translational inhibition of viral proteins, respectively. The E3 ligase TRIM25 enhances both RIG-I and ZAP anti-viral activities through polyubiquitination. In order for ubiquitin synthesis to occur, TRIM25 must be catalytically activated by substrate-induced higher-order oligomerization.

The TRIM25 coiled-coil domain is the initial site of oligomerization. Structural studies reveal that the coiled-coil subunits are antiparallel in orientation and composed of heptad-hendecad-heptad repeats of hydrophobic residues. This pattern is maintained within other TRIMs as well. Many RING E3 ligases

require dimerization for catalytic activity. However, the central antiparallel coiled-coil dictates that the catalytic RING domains remain sequestered at opposite ends of the dimer.

Further structural and biochemical studies revealed that the RING domain is a second site for TRIM25 oligomerization. Purified RING protein is monomeric in solution, as demonstrated with analytical ultracentrifugation. A structure of the RING domain in complex with a ubiquitin-conjugated E2 protein demonstrated that the interaction requires RING dimerization. Mutations designed to disrupt RING dimerization reduced TRIM25 E3 ligase activity and anti-viral activity *in vitro*. Furthermore, purified full-length TRIM25 forms a tetrameric species in solution and the introduction of either L69A or V72A result in only dimeric TRIM25.

Full-length TRIM25 co-purifies with nucleic acids. Biochemical studies revealed that RNA enhances TRIM25 E3 ligase activity. A mutational analysis identified a cooperative nucleic acid-binding mechanism within TRIM25. Lys and Arg residues within the coiled-coil, Linker 2 region, and SPRY domain coordinate nucleic acid binding as well as grant binding specificity to RNA over DNA. Moreover, a reduction in RNA binding affinity correlated with a reduction of TRIM25-mediated anti-viral activity.

Overall, this thesis provides a biochemical and structural basis for understanding the mechanisms of TRIM25 catalytic activation, and how this modulates an RNA-dependent cellular anti-viral response.

To my parents,

Gregorio and Maria Sanchez

ACKNOWLEDGEMENTS

I am grateful to my thesis advisor, Owen Pornillos, for his encouragement and guidance throughout this research. As a rotation student in Owen's lab, and a new student to the field of crystallography, I crystallized my first protein immediately. In my naivety I asked Owen, "Is crystallography supposed to be difficult?" In the years to follow, I have repeatedly learned that yes, yes it is difficult. Discussions with Owen and Barbie Ganser-Pornillos have greatly shaped my development as well as influenced my future directions as a scientist. I thank Yueping Wan and Marcin Roganowicz for the production and expression of many TRIM25 constructs. I thank members of my committee Daniel Engel, Robert Nakamoto, and Jochen Zimmer for useful comments and advice; members of the Michaela Gack Lab, our collaborators who performed the virus assays; and people in the Biophysics department for various help and reagents. I thank the past and current members of the Pornillos Lab for scientific and non-scientific discussions, FPLC time, birthday parties, and a terrific environment for doing science; Katarzyna Okręglicka and Michael Chi, for structural and biochemical studies on the coiled-coil and RING domains, respectively; Katarzyna Skorupka for countless things; Jordan Welker, Yueping Wan, and Marcin Roganowicz for the production and expression of many TRIM25 constructs; Jonathan Wager for many things crystallography-related; Kaneil Zadrozny for an endless effervescent attitude. Daria Dawidziak and Iga Kucharska for always lending a helpful hand; and Jacek Plewka for competitive racquetball. I thank all the friends and acquaintances I met in Charlottesville

making the past few years very memorable; Adam Greene, Cait Hamele, and Maddie Hamele-Greene for being awesome roommates. Finally, I thank my family for their love and support; my parents for their inspirational hard-working attitude; Guadalupe Sanchez and Joseph Billadello for their support of my intellectual pursuits; my grandparents for being my biggest fans; and my better half Katarzyna Zawada, for everything, past, present, future.

Table of Contents

CHAPTER 1

INTRODUCTION TO VIRUSES AND INNATE IMMUNITY

The Global Health Burden of Viruses

Viruses are the most numerous and genetically diverse organisms on the planet. They are environmentally ubiquitous and capable of infecting organisms from all three domains of life. Through various processes, viruses have greatly impacted the evolution of cellular life (Koonin, Senkevich, and Dolja 2006; Forterre and Prangishvili 2009; Feschotte and Gilbert 2012). Of importance, viruses have caused some of the most dramatic and deadly disease pandemics in human history. In the past century, outbreaks of Influenza, Smallpox, HIV (human immunodeficiency virus), Ebola, Zika, SARS (severe acute respiratory syndrome), MERS (Middle East respiratory syndrome) have underscored the importance of understanding the host cellular mechanisms involved in developing an antiviral immune response. Effective vaccination and quarantine strategies have resulted in the eradication of the smallpox virus and the near-eradication of the poliovirus. However, there remain many viruses within the human population that require massive eradication efforts. Viruses are under constant evolutionary pressure to alter their genetic make-up, which challenges the development of effective vaccines. Additionally, it is not easy to predict where and when most infectious agents will re-emerge.

The infectious properties of viruses enable them to spread horizontally between hosts across many species. Arthropods, other mammals, and humans themselves serve as main reservoir species for many human viruses. Mass migrations, trade and travel have all greatly contributed to spreading infectious diseases worldwide. Mass migrations, often the result of natural disasters and

war, can create an environment of poor hygiene and malnutrition, which hasten the spread of infectious diseases. Economic trade led to the development of large cities where viral diseases such as measles, rubella, and smallpox may have gained a foothold after the human population reached a density high enough to support endemic infections.

The 1918 H1N1 influenza virus pandemic left a notable scar on human health. This pandemic virus infected over 500 million people worldwide and resulted in the deaths of 50 to 100 million people (Taubenberger and Morens 2006). Influenza, like many other viruses, disproportionately affects juveniles, the elderly, and the immunocompromised. The world health organization estimates there are 3-5 million cases of severe illness, and up to 500,000 deaths worldwide every year attributed to influenza ("WHO | Influenza (Seasonal)" 2017). The impact of this pandemic was not limited to the initial outbreak. All influenza A pandemics since that time, except those from avian viruses such as H5N1 and H7N7, have been decedents of the 1918 virus. The H2N2 and H3N2 viruses, which caused pandemics in 1957 and 1968 respectively, are composed of key genes from the 1918 virus (Kilbourne 2006; Taubenberger and Morens 2006; Taubenberger et al. 2017).

Acquired Immune Deficiency Syndrome (AIDS) was first recognized as a new disease in 1981 (Centers for Disease Control (CDC) 1981; Greene 2007). A retrovirus, termed the human immunodeficiency virus type 1 (HIV-1), was subsequently identified as the causative agent of one of the most devastating emerging diseases in recent history (Barré-Sinoussi et al. 1983; Gallo et al. 1984;

Popovic et al. 1984). Since its identification, the pandemic form of HIV-1 has infected at least 60 million people and caused more than 25 million deaths. The annual number of new HIV infections in the United States has been reduced by more than two-thirds since the height of the epidemic in the 1980s due to public health education and advances in anti-retroviral therapies (CDC 2017). In 2016, there were an estimated 1.8 million new cases of HIV in, and 37 million people living with HIV worldwide (Center for Disease Control and Prevention 2017).

From March 2014 through March 2016, West Africa experienced the largest outbreak of Ebola virus in history since its discovery in 1976 (Breman et al. 2016). On August 8th, 2014 the World Health Organization (WHO) declared the epidemic to be a "public health emergency of international concern" ("WHO | Statement on the 1st Meeting of the IHR Emergency Committee on the 2014 Ebola Outbreak in West Africa" 2014). The degree of morbidity and mortality, its zoonotic origins and its possible spread to other countries and continents alarmed the world to the presence of this outbreak. The total number of suspected human cases of Ebola infection reached nearly 30,000, approximately half of those cases were laboratory-confirmed, and a death count of over 11,000 ("2014-2016 Ebola Outbreak in West Africa | Ebola Hemorrhagic Fever | CDC" 2017).

Virus life cycle

In order to develop strategies for antiviral therapy we first need to understand the life cycle of the virus as well as the accompanying host cell

response against an invading virus. These studies may provide strategic insight into drug development directed at enhancing the host immune response at critical junctures of viral infection.

All viruses share a canonical replication cycle involving six steps: attachment, entry, uncoating, replication, assembly, and egress. **Attachment**. Viruses attach to specific receptor site(s) on host cell outer membrane through viral attachment proteins in the capsid or embedded within the viral envelope. The specificity of this interaction determines the cell type(s) that can be infected by a particular virus. **Entry**. Viruses enter the cell when the viral envelope fuses directly with the cell membrane, or the host membrane engulfs the virus. **Uncoating**. Once inside the cell, the viral capsid is disassembled, and the viral nucleic acid is released. **Replication**. The replication mechanism depends on the viral genome. A virus may carry its own polymerases, or usurp the host polymerase machinery, to replicate the virus genome. **Assembly**. The viral mRNA directs the host cell to synthesize viral proteins and to assemble new virions. **Egress**. The last stage of viral replication is the release of new virions produced in the host. Newly formed viruses are then able to infect adjacent cells or a new host organism to repeat the replication cycle.

Innate Immunity: Pathogen-Associated Molecular Patterns and Pattern Recognition Receptors

The process of infection exposes several viral components to host defense mechanisms. The immune system constitutes the first line of defense during infection and has evolved under selective pressure imposed by infectious microorganisms. As a result, host multicellular organisms have developed

various defense mechanisms that have the capacity to be triggered by infection and to protect the host organism by eliminating the invading pathogen and neutralizing their virulence factors. These phylogenetically ancient defense mechanisms, collectively known as the innate immune system, use germline-encoded receptors for the recognition of microbial pathogens.

Immune recognition is a unique biological process in that the immune system continually selects against targets that it has evolved to recognize. While most other host molecular recognition processes involve products of the same genome, immune recognition is mediated between products encoded on different genomes. This directs the evolution of innate immunity towards the recognition of conserved molecular constituents of the pathogen (Medzhitov and Janeway 1997).

During infection, pathogens present to the host cell evolutionarily conserved microbial structures termed pathogen-associated molecular patterns (PAMPS) (**Fig. 1**). PAMPs are highly conserved molecules within a class of pathogens that have essential functions in microbial fitness or survival and are distinguishable from the host "self" (Janeway 2013; Nürnberger and Brunner 2002). For example, teichoic acids and LPS are common components of gram-positive and gram-negative bacteria, respectively (Gourbeyre et al. 2015; Jeong and Lee 2011; Iwasaki and Medzhitov 2010; Finlay and McFadden 2006; Aderem and Ulevitch 2000; "LPS/TLR4 Signal Transduction Pathway" 2008); and double-stranded RNA is a structural signature of several groups of RNA viruses (F. Jiang et al. 2011; Gerlier and Lyles 2011; Ferrao and Wu 2012; Berke, Li, and

Fig. 1. Viral infection exposes viral PAMPs to cellular PRRs.

PRR recognition of viral PAMPs activate an anti-viral innate immune response. Cellular factors like NF-KB and type-I interferons initiate a broad cellular defense to restrict the virus life cycle.

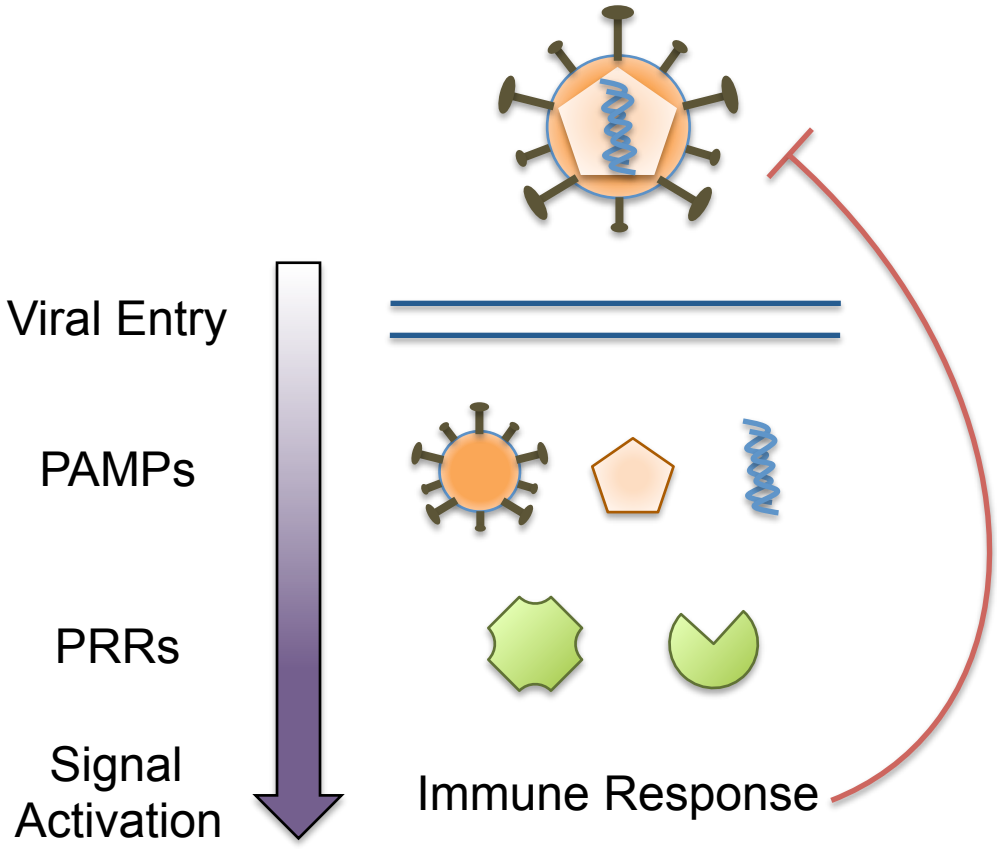
Viral Entry
PAMPs
PRRs
Signal Activation
Immune Response

Modis 2013; Mogensen 2009). Pathogens of varied biochemical compositions and life cycles, including viruses, bacteria, protozoa, and fungi are recognized through surprisingly similar overlapping mechanisms by host pattern recognition receptors (PRRs) (Akira, Uematsu, and Takeuchi 2006), demonstrating the breadth and plasticity of the innate immune response.

Innate immune detection of PAMPs is mediated by a structurally diverse set of PRRs. Functionally, PRRs are divided into two types: membrane-bound receptors localized at cellular or endosomal membranes, and cytosolic receptors that circulate throughout the cytoplasm. The family of toll-like receptors (TLRs) are membrane-bound receptors that aid in recognition of pathogens during a membrane-associated lifecycle step. Membrane-bound receptors provide a substantial innate immune response but are not capable of fully sampling intracellular cytosolic pathogens and their derivatives. Cytoplasmic PRRs like retinoic acid-inducible gene I (RIG-I)-like receptors (RLRs) and nucleotide-binding oligomerization domain (NOD)-like receptors (NLRs) fill in that defensive gap. An extensive property of the innate immune system is that no single class of pathogen is sensed by only one type of PRR. Rather, during infection, a number of PRRs are engaged by a given pathogen via various PAMPs, securing a rapid and potent inflammatory response.

Upon PAMP recognition, PRRs communicate the presence of abnormal host factors as a consequence of cellular stress, inflammation, or infection (Akira, Uematsu, and Takeuchi 2006; “LPS/TLR4 Signal Transduction Pathway” 2008; Mogensen 2009; Iwasaki and Medzhitov 2010; Jeong and Lee 2011; Berke, Li,

and Modis 2013; Gerlier and Lyles 2011; Killip, Fodor, and Randall 2015). RIG-I, TLR3, TLR7, TLR8, and TLR9 are all examples of PRRs with a similar substrate of non-self RNA (Akira, Uematsu, and Takeuchi 2006; Mogensen 2009; F. Jiang et al. 2011; Berke, Li, and Modis 2013) (**Fig. 2**). RNA recognition by these PRRs leads to the activation of the transcription factors interferon regulatory factor-3 (IRF-3) and nuclear factor κB (NF-κB). Activated IRF3 and NF-κB accumulate in the host cell nucleus and bind to target promoters to induce the expression of type-I interferons (IFNs) (Rawlings, Rosler, and Harrison 2017; Schneider, Chevillotte, and Rice 2014).

Interferon and Interferon Stimulated Genes

The type-I IFN system provides a robust antiviral state, effective against all types of viruses. Knockout mice that are defective in IFN signaling have high mortality rates in response to various viral infections (Ryman et al. 2000; van den Broek et al. 1995; Hwang et al. 1995; Grieder and Vogel 2017; Bray 2001; Bouloy et al. 2001). Similarly, humans with genetic defects in interferon signaling have a higher incidence of death due to viral disease (Dupuis et al. 2003).

Virus infection induces the production of intracellular IFN that can then be secreted into the extracellular space. These extracellular cytokines circulate in the body and trigger susceptible cells to express potent antiviral mechanisms, thus limiting viral spread. Upon IFN binding to cell surface receptors, a signal is transmitted through the membrane and into the cell, lead to dramatic changes in cellular properties.

Fig. 2. Intracellular sensing of viral RNA by the innate immune system.

Upon cell entry, the invading RNA virus releases its genome into the host cytoplasm. Distinct pattern recognition receptors are able to recognize various 5' RNA cap structures gained by the viral RNA. In the absence of a cap structure, the 5'-triphosphate of RNA is sensed by RIG-I. RIG-I nucleates filament formation of mitochondria antiviral-signaling protein (MAVS), resulting in the production of type I IFNs and the production of pro-inflammatory cytokines. ZAP recognizes CpG dinucleotides in RNA. ZAP coordination with RNA-induced silencing complex (RISC) results in the translational inhibition of viral RNAs. The fidelity in which ZAP recognizes self vs. non-self RNA is currently unknown. The 2', 5'-oligoadenylate synthetase (OAS)/RNase L system induces degradation of viral and cellular RNAs. Autocrine and paracrine IFN binds to cell surface type I IFN receptor (IFNR) and initiates the JAK-STAT signaling cascade. Among hundreds of proteins encoded by IFN-stimulated genes (ISGs), antiviral proteins like RIG-I, ZAP and TRIM25 provide an enhancement in cellular defense. Viral RNA, exonucleases, and ISGs are recruited to antiviral stress granules where viral RNA is degraded and the interferon response is enhanced. Image adapted from (Decroly et al. 2011).

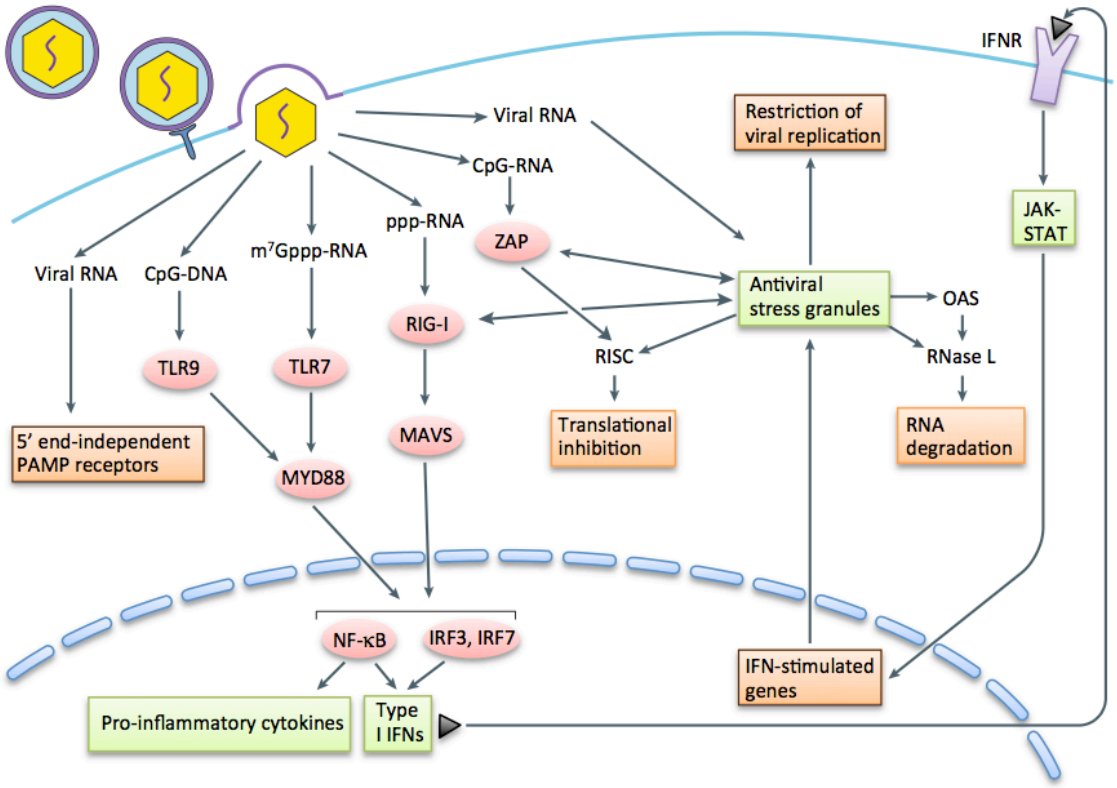
IFNR
Viral RNA
CpG-RNA
ppp-RNA
m7Gppp-RNA
Viral RNA
CpG-DNA
ZAP
RIG-I
TLR9
TLR7
MAVS
MYD88
5' end-independent PAMP receptors
RISC
Translational inhibition
Antiviral stress granules
Restriction of viral replication
OAS
RNase L
RNA degradation
JAK-STAT
NF-κB
IRF3, IRF7
Pro-inflammatory cytokines
Type I IFNs
IFN-stimulated genes

All IFNs signal through the Janus kinase-signal transducer and activator of transcription (JAK-STAT) signaling pathway (Rawlings, Rosler, and Harrison 2017). In brief detail, intracellular activation occurs when ligand, IFN, binding induces the multimerization of the IFN receptor. JAK phosphorylates the IFN receptor as well as the signaling molecule STAT. Phosphorylated STAT leads to an interaction between IFN regulatory factor (IRF) 9 and ISG factor 3 (ISGF3) (Schindler et al. 1992; Levy et al. 1989; Fu et al. 1990). ISGF3 then translocates to the nucleus, where it binds IFN-stimulated regulatory elements in the DNA upstream of interferon-stimulated genes (ISGs), resulting in the transcription of hundreds of ISGs (Rawlings, Rosler, and Harrison 2017) (**Fig. 2**).

Interferon-stimulated genes take on a number of diverse cellular roles. Collectively, they are highly effective in resisting and controlling pathogen infection. Many ISGs control infection by directly targeting pathways and functions required during pathogen life cycles. One method of viral restriction is the control of gene expression of viral nucleic acids in anti-viral stress granules (Jackson, Hellen, and Pestova 2010).

Stress Granules

Translation is one of the most energy-intensive cellular processes and must be tightly regulated. When subjected to acute stress conditions, such as viral infection, cells rapidly reprogram gene expression to deploy stress response measures to conserve energy and minimize damage. Stress granules (SGs) are large cytoplasmic foci that are nucleated by the aggregation of untranslated

messenger ribonucleoproteins (mRNPs), which accumulate as a result of stress-induced translational arrest (Kedersha et al. 2000) (**Fig. 2)**.

A diverse set of intermolecular interactions is essential for granule assembly. Protein modifications like methylation, phosphorylation, glycosylation, and poly-ADP ribosylation (PARylation) influence stress granule assembly presumably by altering specific protein-protein interactions (Leung et al. 2011; S. Kwon, Zhang, and Matthias 2007; Wippich et al. 2013; Ohn et al. 2008; Goulet et al. 2008; Nott et al. 2015; Tourrière et al. 2003; Yang et al. 2014; Jackson, Hellen, and Pestova 2010) Moreover, stress granules appear to form through the crosslinking of untranslated mRNAs that can provide a scaffold for multivalent mRNP interactions (Protter and Parker 2016).

Hundreds of proteins have been identified to associate with stress granules (Jain et al. 2016). For example, SG-recruited members of the 40s ribosome stall translation of host and viral proteins, the ribonucleases XRN1 and RNase L degrade available RNA (McCormick and Khaperskyy 2017), both of which lead to decreased translation of viral proteins. Many SG-recruited proteins are also ISGs; namely, retinoic acid-inducible gene I (RIG-I), zinc-finger antiviral protein (ZAP), and tripartite motif-containing protein 25 (TRIM25) (Bock, Todorova, and Chang 2015; Todorova, Bock, and Chang 2015; Sánchez-Aparicio et al. 2017). RIG-I and ZAP are both cytosolic PRRs of foreign nucleic acids. Functionally, their respective antiviral activities act independently of each other, but at the same time complement one another. Of particular importance to this dissertation, the anti-viral functions of both RIG-I and ZAP are enhanced by the enzymatic

activity of TRIM25 (Gack et al. 2007; J. Sanchez et al. 2016; Li et al. 2017; Zheng et al. 2017). The trafficking of RIG-I, ZAP, and TRIM25 into SGs provides an opportune moment for these proteins to synergize an anti-viral response.

ZAP

ZAP belongs to the poly ADP-ribose polymerase family of proteins (PARPs), which regulate fundamental cellular processes through the modification of target proteins with ADP-ribose. ZAP antiviral function was initially identified in a screen for novel antiviral proteins (Bick et al. 2003). Since then, ZAP has been implicated as a host restriction factor against a variety of RNA viruses (**Table 1**) including filoviruses, retroviruses, and alphaviruses (Wang et al. 2012; Mao et al. 2013; Zhu et al. 2011; Muller et al. 2007; Gao 2002). The domain architecture of ZAP consists of an N-terminal RNA binding domain containing 4 CCCH zinc fingers, a putatively unstructured serine and glycine-rich region, a WWE domain, and a C-terminal PARP domain. Humans naturally express two ZAP isoforms through alternative splicing, ZAP-long (ZAPL) and ZAP-short (ZAPS) (**Fig. 3)**. ZAPL is farnesylated at a CaaX-motif within the PARP domain, which serves a membrane localization signal, possibly allowing ZAPL to target viruses with an endocytic life cycle (Charron et al. 2013). In contrast, ZAPS does not contain a PARP domain, and therefore likely samples cytosolic substrates. Interestingly, ZAPS, rather than ZAPL, is transcriptionally activated by interferon during viral infection (Schoggins and Rice 2011; Atasheva, Frolova, and Frolov 2014; McCormick and Khaperskyy 2017).

Table 1. Viruses detected by ZAP and RIG-I

Viruses Detected by ZAP	
Alphaviruses	(Bick et al. 2003)
Filoviruses **Ebola Virus** **Marburg Virus**	(Muller et al. 2007)
Hepatitis B virus	(Mao et al. 2013)
Maloney MuLV	(Gao 2002)

Viruses Detected by RIG-I	
Paramyxoviridae **Sendai virus** **Newcastle disease virus** **Respiratory syncytial virus** **Measles** **Nipah** **Human parainfluenza 5 mRNA**	(Kato et al. 2005; Yoneyama et al. 2004; Loo et al. 2008; Plumet et al. 2007; Habjan et al. 2008; Luthra et al. 2011)
Rhabdoviridae **Vesicular stomatitis virus** **Rabies virus**	(Kato et al. 2005; Yoneyama et al. 2004; Hornung et al. 2006)
Orthomyxoviridae **Influenza A** **Influenza B**	(Kato et al. 2006; Loo et al. 2008)
Filoviridae **Ebola**	(Habjan et al. 2008)
Arenaviridae **Lassa** **Lymphocytic choriomeningitis virus**	(Habjan et al. 2008; Zhou et al. 2010)
Bunyaviridae **Rift Valley fever virus**	(Habjan et al. 2008)
Flaviviridae **Hepatitis C virus**	(Sumpter Jr. et al. 2005; Saito et al. 2007)
Coronaviridae **Murine hepatitis virus**	(Roth-Cross, Bender, and Weiss 2008)
Caliciviridae **Murine norovirus-1**	(McCartney et al. 2008)
DNA viruses **Epstein-Barr virus EBER** **myxoma virus**	(Samanta et al. 2006; Wang et al. 2008)
Flaviviridae **Japanese encephalitis virus** **Dengue virus** **West Nile virus**	(Kato et al. 2006; Loo et al. 2008; Fredericksen et al. 2008)
Reoviridae dsRNA S **Reovirus**	(Kato et al. 2008; Loo et al. 2008)

Fig. 3. Humans naturally express two ZAP isoforms through alternative splicing, ZAP-long (ZAPL) and ZAP-short (ZAPS).

ZAPL lacks critical residues of the HYE motif present in other PARPs required for ADP-ribosylation activity, whereas ZAPS lacks a PARP domain altogether. Therefore, both isoforms lack PARP activity and are unable to ADP-ribosylate target proteins. Interestingly, both ZAPL and ZAPS contain a nuclear localization and export signal, and likely shuttle between the nucleus and the cytoplasm in a XPO1-dependent manner.


CCCH Zinc Fingers
WWE
PARP
ZAPL
ZAPS

A recent study has determined that ZAP distinguishes between self and non-self RNA through recognition of an RNA CpG motif, which is vastly underrepresented in vertebrates (Takata et al. 2017). In double-stranded DNA the CpG dinucleotide is subject to G to T mutations, driven by CG-specific DNA methyltransferases (C. P. Walsh and Xu 2006; Ng and Bird 1999). Therefore, vertebrate evolution has resulted in the selection against CpG dinucleotides within their genomes due to the commonality of G to T mutations (Bird 1980).

The four CCCH zinc fingers situated within the N-terminus of ZAP mediate RNA binding. The zinc fingers cooperate to form two RNA-interacting clefts that are thought to provide specificity and selectivity of binding (Chen et al. 2012). RNA-bound ZAP serves as a recruiting element for RNA destabilizing factors, and likely other effector proteins involved in the cellular stress response (Atasheva, Frolova, and Frolov 2014; Guo et al. 2007; Seo et al. 2013).

Recent genome-wide siRNA screens have revealed that TRIM25 enhances the antiviral actions of ZAP but does not seem to be in a ubiquitin-dependent manner (Li et al. 2017; Zheng et al. 2017). Immunoprecipitation of both ZAPS and ZAPL found that the TRIM25 SPRY domain interacts with the ZAP N-terminal RNA-binding domain (Li et al. 2017). Interestingly, both of these domains are required for RNA binding, so it remains unclear whether or not RNA in fact bridges the putative ZAP-TRIM25 interaction. Two explanations of TRIM25 function could be: 1) the E3 ligase activity of TRIM25 enhances ZAP function by ubiquitylating other host factors, 2) TRIM25 is mediating optimal ZAP

binding to target RNA. The role of TRIM25 in the enhancement of ZAP anti-viral activity remains an outstanding question.

RIG-I

The RLR family of DExD/H box RNA helicases plays a pivotal role in detecting cytoplasmic viral RNA. The RLRs signal downstream transcription factor activation to drive type-I IFN production and antiviral gene expression that elicit an intracellular immune response to control viral infection. RLR expression is typically maintained at low levels in resting cells but is greatly increased with IFN exposure and after virus infection (Kang et al. 2004; Yoneyama et al. 2004). RIG-I is a prototypical member of this family that recognizes RNA from a broad range of viruses (**Table 1**). Many studies have led to the characterization of the RIG-I substrate (reviewed in Loo and Gale 2017) as 5'-triphosphorylated (5'ppp) blunt-ended dsRNA.

RIG-I consists of 3 distinct domains: (1) an N-terminal region consisting of tandem caspase activation and recruitment domains (2CARD), (2) a central DExD/H box RNA helicase domain with the capacity to hydrolyze ATP, and (3) a C-terminal domain (CTD) that is involved in auto-regulation of RIG-I (**Fig. 4A)**. Signal transduction of an anti-viral response occurs through 2CARD interaction with the downstream adaptor protein mitochondria anti-viral signaling protein (MAVS) (Peisley et al. 2014; Wu et al. 2014; Cai et al. 2014). RNA binding to RIG-I is mediated both by the CTD, which specifically binds the 5'ppp end and the helicase domain (Kowalinski et al. 2011; Luo et al. 2012; F. Jiang et al. 2011).

Figure 4. Mechanism of RIG-I activation and signaling.

A) RIG-I is composed of three major domains: 2CARD, helicase, and CTD.

B) RIG-I takes on an auto-inhibited state in the absence of a substrate. A proper substrate along with ATP binding allows for RIG-I translocation along the RNA as well as releases 2CARD.

C) K63-linked polyubiquitin chains stabilize the 2CARD tetramer, in which 2CARD tetramerization is required to nucleate the MAVS filament. The adaptor protein MAVS activates transcription factors leading to the production of NF-κB and interferon.

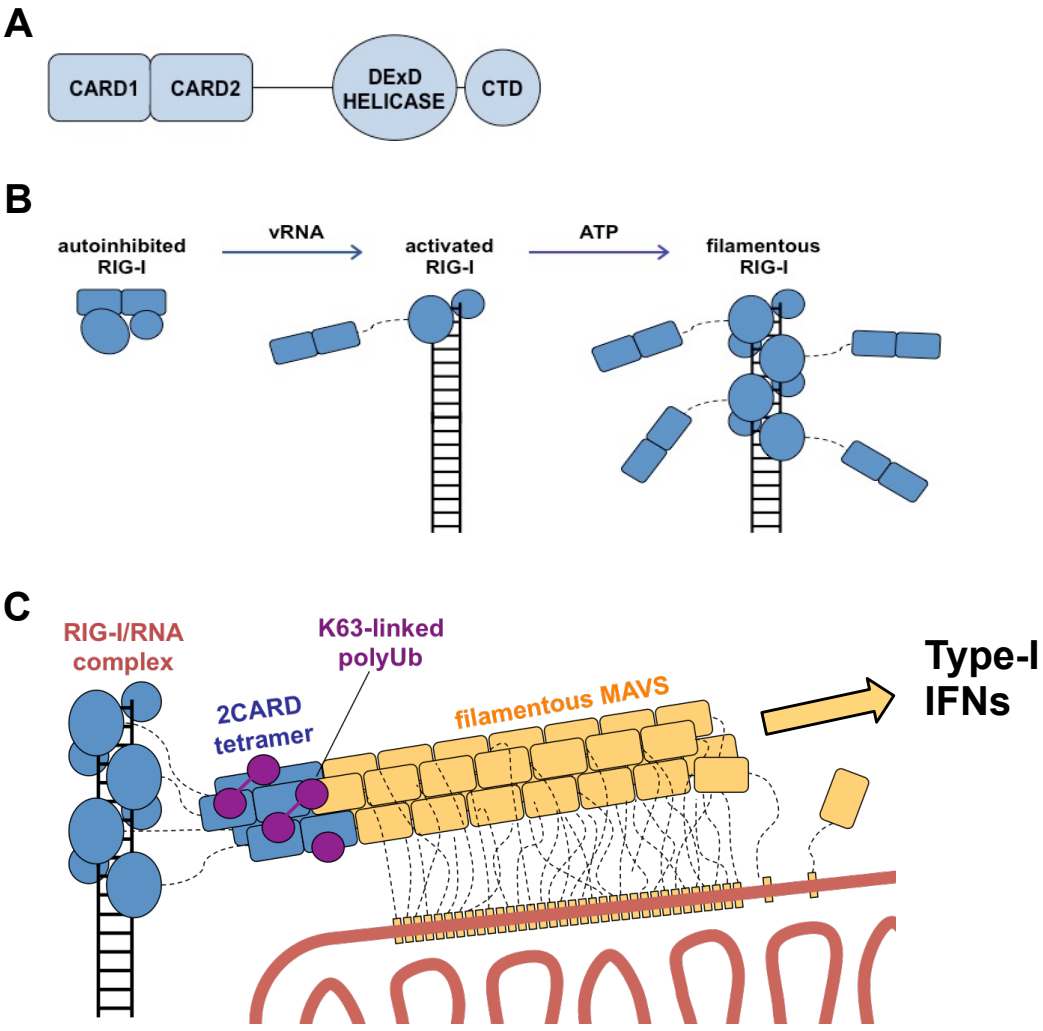
A
CARD1
CARD2
DExD
HELICASE
CTD
B
autoinhibited
RIG-I
vRNA
activated
RIG-I
ATP
filamentous
RIG-I
C
RIG-I/RNA
complex
K63-linked
polyUb
2CARD
tetramer
filamentous MAVS
Type-I
IFNs

In the absence of an RNA substrate, RIG-I adopts an autoinhibited conformation that is unable to signal type-I IFN production, stabilized by salt bridges and hydrophobic interactions between 2CARD and a helicase subdomain (Kowalinski et al. 2011) (**Fig. 4B)**. The autoinhibited RIG-I maintains a high degree of structural flexibility that facilitates its surveillance for viral RNAs. Various studies have demonstrated that the ligand-free helicase domain has significant flexibility between the helicase subdomains (Luo et al. 2012; F. Jiang et al. 2011). Similarly a structural study of full-length RIG-I found the CTD was disordered in the crystal structure, suggestive of flexibility (Kowalinski et al. 2011). RIG-I substrate binding occurs through the flexible CTD sampling the surrounding space for 5'ppp dsRNA, allowing for cooperative binding of ATP and RNA to the helicase domain. RIG-I translocates along the RNA in an ATP-dependent manner, exposing the 5'ppp, and allowing further RIG-I molecules to bind the same RNA (Peisley et al. 2013) (**Fig. 4B)**. Helicase binding to RNA releases 2CARD and results in a signaling-competent state. 2CARD release allows its interaction with the N-terminal CARD of the downstream signaling adaptor molecule, MAVS (Peisley et al. 2014). Upon interaction with RIG-I 2CARD, MAVS CARD forms a self-perpetuating filament, ultimately generating a type-I interferon (IFN) response (Wu et al. 2014; Cai et al. 2014; Peisley et al. 2014) (**Fig. 4C)**.

Recent studies have uncovered the interaction of the N-terminal CARD of MAVS with a tetrameric assembly of 2CARD from RNA-bound RIG-I initiates the MAVS prion-like filament formation (X. Jiang et al. 2012; Peisley et al. 2014; Wu

et al. 2014). The helical tetrameric “lock washer” architecture of RIG-I 2CARD serves as a template that recruits individual MAVS CARD along the extended helical trajectory predefined by the RIG-I 2CARD tetramer. As a result, the helical architecture of the RIG-I 2CARD is precisely preserved in the MAVS CARD filament (Peisley et al. 2014). MAVS formation of protease-resistant prion-like fibrils effectively converts endogenous monomeric MAVS on the mitochondria into a functional signaling platform for the induction of an anti-viral response (Hou et al. 2011) (**Fig. 4C)**. Importantly, MAVS filament formation is dependent upon an activated RNA-bound RIG-I that then allows for RIG-I 2CARD tetramerization. Otherwise, uncontrolled MAVS assembly will have harmful consequences to the cell, and so a variety of mechanisms have evolved to dictate where, when and how the RIG-I 2CARD seeds MAVS CARDs assembly (Chiang, Davis, and Gack 2014).

Ubiquitin (Ub) is a well-characterized regulator of the RIG-I 2CARD/MAVS CARD seeding mechanism (Gack et al. 2007, 2008; Q. X. Jiang and Chen 2012; Peisley et al. 2014; Zeng et al. 2010). Activated 2CARD has been shown to be modified with both anchored and unanchored K63-linked poly-ubiquitin chains (K63-polyUb) (Gack et al. 2007; Q. X. Jiang and Chen 2012; Zeng et al. 2010). Structural and biochemical studies have revealed that K63-polyUb wrap around four RIG-I 2CARD molecules to induce and stabilize the “lock washer” configuration (Q. X. Jiang and Chen 2012; Peisley et al. 2014) (**Fig. 4C)**. Furthermore, ubiquitylation at a key residue within RIG-I 2CARD, Lys172, located at the aqueous surface that faces the helicase domain, is proposed to promote

steric hindrance for the autoinhibited RIG-I state (Kowalinski et al. 2011). Both types of K63-polyUb are synthesized by the E3 ubiquitin ligase, TRIM25, which is an essential component of the RIG-I pathway (Gack et al. 2007; Zeng et al. 2010; J. Sanchez et al. 2016).

TRIM25

TRIM25 belongs to the tripartite motif (TRIM) protein family, which consists of over 70 distinct members (Meroni and Diez-Roux 2005). The family derives its name from three conserved N-terminal domains: a really interesting new gene (RING) domain, one or two B-Boxes (B1/B2) and a coiled-coil domain (CCD). A variable C-terminal domain follows the tripartite motif RING-B1/B2-CCD (RBCC) (**Fig. 5**). The RING domain recognizes the ubiquitin-loaded E2 conjugating enzyme and promotes ubiquitin conjugation to target proteins (Plechanovova et al. 2012; Dou et al. 2012). The B-boxes mediate self-association and could also contribute to the E3 ubiquitin ligase activity of TRIM proteins (Wagner et al. 2016). The CCD is necessary for TRIM oligomerization (Cainarca et al. 1999; Reymond et al. 2001) Finally, the variable C-terminal domain may mediate interactions with specific substrates.

A unifying theme for all TRIMs is that their ability to catalyze ubiquitin transfer is an important functional requirement. Ubiquitin conjugation requires an E1-activating enzyme and ATP as an energy source, an E2-conjugating enzyme, an E3-ligase (**Fig. 6**). The RING domain of TRIM proteins confers E3 ligase activity by facilitating interaction with E2 enzymes, while their unique C-terminal domain allows for substrate specificity.

Fig. 5. TRIM25 organization.

TRIM proteins are composed of a conserved set of N-terminal domains: a really interesting new gene (RING) domain, one or two B-Boxes (B1/B2) and a coiled-coil (CC) domain. A variable C-terminal domain follows the tripartite motif RING-B1/B2-CC (RBCC). TRIM25 contains a C-terminal SPRY domain.

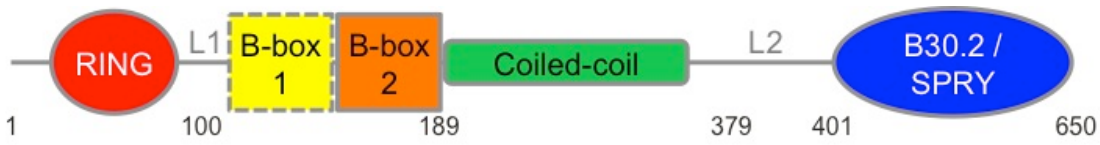
RING
L1
B-box 1
B-box 2
Coiled-coil
L2
B30.2 / SPRY
1
100
189
379
401
650

Fig. 6. The ubiquitination system

Ubiquitin is a 76-amino-acid protein involved in a wide variety of cellular processes. The free C-terminal glycine residue of Ub is most commonly conjugated to a lysine residue of specific substrate proteins (Trempe 2011). In turn, Ub itself contains seven lysines (K6, K11, K27, K29, K33, K48, and K63) on which polyUb chains can be formed when the C-terminal glycine of one Ub molecule is conjugated to a lysine of another Ub molecule. The conjugated Ub linkage type dictates the downstream cellular function of the substrate (Komander and Rape 2012). For example, proteins covalently modified with K48-linked polyUb are degraded by the Ub-proteasome system. In contrast, proteins modified with K63-linked polyUb chains are involved in activation of antiviral signaling. Moreover, Ub does not require covalent conjugated to a protein to exert a signaling effect on that protein (Yau and Rape 2016). Ub conjugation requires an E1-activating enzyme, an E2-conjugating enzyme, an E3-ligase, and ATP as an energy source. Humans encode for 1 E1 protein, ~40 E2 proteins, and hundreds of E3 proteins (Stewart et al. 2016). The ubiquitination process starts with the activation of the ubiquitin C-terminus by the E1 enzyme in an ATP dependent manner to create an E1~Ub conjugate. The activated Ub is then passed over to an E2 enzyme. Finally, an E3 ligase facilitates the transfer of Ub from the E2 onto the substrate.

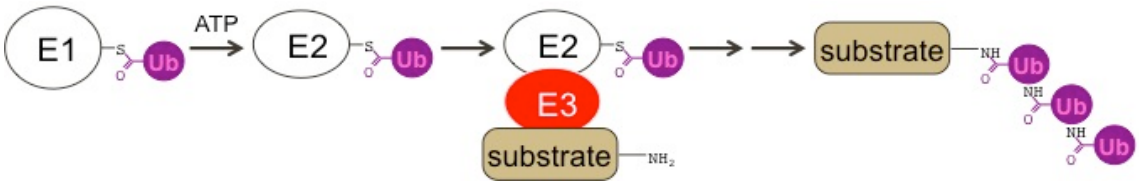
E1
Ub
ATP
E2
Ub
E2
Ub
E3
substrate
NH2
substrate
NH
Ub
NH
Ub
NH
Ub

TRIM proteins contribute to a broad range of cellular functions, including antiviral activity, oncogenesis, autophagy, apoptosis and transcriptional regulation (Hatakeyama 2011; Napolitano and Meroni 2012; Rajsbaum, García-Sastre, and Versteeg 2014). Moreover, most TRIMs undergo alternative splicing, promoting additional diversity in protein function (Rajsbaum, García-Sastre, and Versteeg 2014; Versteeg et al. 2013). Interestingly, several TRIM proteins have been implicated in more than one cellular process. This multi-functionality extends to TRIM25.

TRIM25, the main subject of this dissertation, is composed of the RBCC domain and a C-terminal SPRY domain. TRIM25 was first annotated as estrogen-responsive finger protein (EFP), due to its transcriptional upregulation by estrogen (Inoue et al. 1993). TRIM25 was found to target 14-3-3σ (a negative cell cycle regulator that causes G2 arrest) for proteolysis, resulting in increased cell growth and tumorigenesis (Urano et al. 2002; Horie et al. 2003). TRIM25 is now a key biomarker for the detection of breast cancer (Horie et al. 2003; L. A. Walsh et al. 2017)

Regulation of RIG-I signaling is one of the best-characterized roles of TRIM25 (Gack et al. 2007, 2008). RIG-I recognition of viral RNA exposes its 2CARD domain for binding to the SPRY domain of TRIM25 (D 'Cruz et al. 2013; Gack et al. 2007, 2008). TRIM25 then synthesizes and conjugates K63-polyUb to residues K99, K169, K172, K181, K190 and K193 of RIG-I 2CARD (Gack et al. 2007, 2009; D 'Cruz et al. 2013). As mentioned earlier, these polyUb chains stabilize the 2CARD “lock washer” configuration (Peisley et al. 2014).

TRIM25 is also involved in the translational inhibition of viral RNA through interaction with ZAP, a broad-spectrum inhibitory protein. TRIM25 interacts with ZAP through the SPRY domain, and TRIM25 mutants lacking the RING fail to stimulate ZAP's antiviral activity (Li et al. 2017; Zheng et al. 2017).

The importance of TRIM25 in anti-viral signaling is further underscored by the fact that the NS1 protein of influenza A viruses directly antagonize TRIM25 activity. NS1 specifically inhibits TRIM25-mediated RIG-I 2CARD ubiquitination and decreases the cellular interferon response to Influenza A infection (Gack et al. 2009).

Most recently, TRIM25 has been identified as a novel RNA binding protein. TRIM25 RNA binding has been linked to cellular processes such as: microRNA processing linked to tumor growth (N R Choudhury et al. 2014), serving as a target for Dengue subgenomic RNA (Manokaran et al. 2015), and having a role in stem-cell physiology through interactions with mRNA (S. C. Kwon et al. 2013).

The aforementioned TRIM25-regulated binding-partners provide insight into the variable substrates that are recognized by the C-terminal SPRY domain. Evolutionary analysis of TRIM proteins have found that the SPRY domain has had a marked selective advantage over the other C-terminal domains (Rhodes, De Bono, and Trowsdale 2005). Approximately 50% of human TRIM proteins contain a B30.2 (PRY/SPRY) domain at the C-terminus (Rajsbaum, García-Sastre, and Versteeg 2014; Nisole, Stoye, and Saib 2005). The SPRY domain is found in ~100 human proteins and is involved in protein-protein interactions and RNA binding (Nisole, Stoye, and Saib 2005). The typical

structure of the SPRY domain is a six to seven-stranded antiparallel β-sheets, arranged in a β-sandwich fold, similar to that of an immunoglobulin-like fold (James et al. 2007; D 'Cruz et al. 2013) The antibody-like flexible loops that connect β-strands termed variable loops, grant substrate-binding specificity.

The goal of this dissertation research was to elucidate the mechanisms by which TRIM25 modulates anti-viral innate immune responses. Chapter 2 describes how the CCD dictates the tertiary structure of TRIM25 as well as many other TRIMs (Sanchez et al. 2014). Chapter 3 describes the requirement of TRIM25 higher-order oligomerization for E3 ligase activity as well as cellular anti-viral activity (Sanchez et al. 2016). Chapter 4 describes that the RNA binding property of TRIM25 is integral to its anti-viral activity. Overall, the collective data demonstrate the structural factors engaged in TRIM25 E3 ligase activation. The data reflect the quality control requirements involved in TRIM25 signal propagation.

REFERENCES

"2014-2016 Ebola Outbreak in West Africa | Ebola Hemorrhagic Fever | CDC." 2017. Accessed November 16. https://www.cdc.gov/vhf/ebola/outbreaks/2014-west-africa/index.html.

Aderem, Alan, and Richard J Ulevitch. 2000. "Toll-like Receptors in the Induction of the Innate Immune Response." *Nature* 406 (August). Macmillan Magazines Ltd.: 782. http://dx.doi.org/10.1038/35021228.

Akira, Shizuo, Satoshi Uematsu, and Osamu Takeuchi. 2006. "Pathogen Recognition and Innate Immunity." *Cell* 124 (4). Elsevier: 783–801. doi:10.1016/j.cell.2006.02.015.

Atasheva, Svetlana, Elena I Frolova, and Ilya Frolov. 2014. “Interferon-Stimulated poly(ADP-Ribose) Polymerases Are Potent Inhibitors of Cellular Translation and Virus Replication.” *Journal of Virology* 88 (4). American Society for Microbiology (ASM): 2116–30. doi:10.1128/JVI.03443-13.

Barré-Sinoussi, F, J C Chermann, F Rey, M T Nugeyre, S Chamaret, J Gruest, C Dauguet, et al. 1983. “Isolation of a T-Lymphotropic Retrovirus from a Patient at Risk for Acquired Immune Deficiency Syndrome (AIDS).” *Science (New York, N.Y.)* 220 (4599): 868–71. http://www.ncbi.nlm.nih.gov/pubmed/6189183.

Berke, Ian C., Yue Li, and Yorgo Modis. 2013. “Structural Basis of Innate Immune Recognition of Viral RNA.” *Cell Microbiol* 15 (3). Department of Molecular Biophysics & Biochemistry, Yale University, New Haven, CT 06520, USA.: 386–94. doi:10.1111/cmi.12061.

Bick, Matthew J, John-William N Carroll, Guangxia Gao, Stephen P Goff, Charles M Rice, and Margaret R Macdonald. 2003. “Expression of the Zinc-Finger Antiviral Protein Inhibits Alphavirus Replication.” *JOURNAL OF VIROLOGY* 77 (21). American Society for Microbiology: 11555–62. doi:10.1128/JVI.77.21.11555–11562.2003.

Bird, A P. 1980. “DNA Methylation and the Frequency of CpG in Animal DNA.” *Nucleic Acids Research* 8 (7). Oxford University Press: 1499–1504. http://www.ncbi.nlm.nih.gov/pubmed/6253938.

Bock, Florian J, Tanya T Todorova, and Paul Chang. 2015. “Molecular Cell Review RNA Regulation by Poly(ADP-Ribose) Polymerases.” *Molecular Cell* 58: 959–69. doi:10.1016/j.molcel.2015.01.037.

Bouloy, M., C. Janzen, P. Vialat, H. Khun, J. Pavlovic, M. Huerre, and O. Haller. 2001. “Genetic Evidence for an Interferon-Antagonistic Function of Rift Valley Fever Virus Nonstructural Protein NSs.” *Journal of Virology* 75 (3): 1371–77. doi:10.1128/JVI.75.3.1371-1377.2001.

Bray, Mike. 2001. “The Role of the Type I Interferon Response in the Resistance of Mice to Filovirus Infection.” *Journal of General Virology* 82 (6): 1365–73. doi:10.1099/0022-1317-82-6-1365.

Breman, Joel G., David L. Heymann, Graham Lloyd, Joseph B. McCormick, Malonga Miatudila, Frederick A. Murphy, Jean-Jacques Muyembé-Tamfun, et al. 2016. “Discovery and Description of Ebola Zaire Virus in 1976 and Relevance to the West African Epidemic During 2013–2016.” *Journal of Infectious Diseases* 214 (suppl 3). Oxford University Press: S93–101. doi:10.1093/infdis/jiw207.

Broek, M F van den, U Müller, S Huang, M Aguet, and R M Zinkernagel. 1995. “Antiviral Defense in Mice Lacking Both Alpha/beta and Gamma Interferon Receptors.” *Journal of Virology* 69 (8). American Society for Microbiology (ASM): 4792–96. http://www.ncbi.nlm.nih.gov/pubmed/7609046.

Cai, Xin, Jueqi Chen, Hui Xu, Siqi Liu, Qiu-Xing X Jiang, Randal Halfmann, and Zhijian J Chen. 2014. “Prion-like Polymerization Underlies Signal Transduction in Antiviral Immune Defense and Inflammasome Activation.” *Cell* 156 (6). NIH Public Access: 1207–22. doi:10.1016/j.cell.2014.01.063.

Cainarca, S, S Messali, A Ballabio, and G Meroni. 1999. “Functional Characterization of the Opitz Syndrome Gene Product (Midin): Evidence for Homodimerization and Association with Microtubules throughout the Cell Cycle.” *Human Molecular Genetics* 8 (8): 1387–96. http://www.ncbi.nlm.nih.gov/pubmed/10400985.

CDC. 2017. “CDC FACT SHEET: Today’s HIV/AIDS Epidemic.” Accessed November 21. https://www.cdc.gov/nchhstp/newsroom/docs/factsheets/todaysepidemic-508.pdf.

Center for Disease Control and Prevention. 2017. “Statistics Overview | Statistics Center | HIV/AIDS | CDC.” doi:https://doi.org/10.1016/S0092-8674(00)80412-2.

Centers for Disease Control (CDC). 1981. “Kaposi’s Sarcoma and Pneumocystis Pneumonia among Homosexual Men--New York City and California.” *MMWR. Morbidity and Mortality Weekly Report* 30 (25): 305–8. http://www.ncbi.nlm.nih.gov/pubmed/6789108.

Charron, Guillaume, Melody M H Li, M. R. MacDonald, and Howard C Hang. 2013. “Prenylome Profiling Reveals S-Farnesylation Is Crucial for Membrane Targeting and Antiviral Activity of ZAP Long-Isoform.” *Proceedings of the National Academy of Sciences* 110 (27): 11085–90. doi:10.1073/pnas.1302564110.

Chen, Shoudeng, Yihui Xu, Kuo Zhang, Xinlu Wang, Jian Sun, Guangxia Gao, and Yingfang Liu. 2012. “Structure of N-Terminal Domain of ZAP Indicates How a Zinc-Finger Protein Recognizes Complex RNA.” *Nature Structural & Molecular Biology* 19 (4): 430–35. doi:10.1038/nsmb.2243.

Chiang, Jessica J., Meredith E. Davis, and Michaela U. Gack. 2014. “Regulation of RIG-I-like Receptor Signaling by Host and Viral Proteins.” *Cytokine and Growth Factor Reviews*. doi:10.1016/j.cytogfr.2014.06.005.

Choudhury, N R, J S Nowak, J Zuo, J Rappsilber, S H Spoel, and G Michlewski. 2014. “Trim25 Is an RNA-Specific Activator of Lin28a/TuT4-Mediated Uridylation.” *Cell Rep* 9 (4): 1265–72. doi:10.1016/j.celrep.2014.10.017.

Choudhury, Nila Roy, Gregory Heikel, Maryia Trubitsyna, Peter Kubik, Jakub Stanislaw Nowak, Shaun Webb, Sander Granneman, et al. 2017. “RNA-Binding Activity of TRIM25 Is Mediated by Its PRY/SPRY Domain and Is Required for Ubiquitination.” *BMC Biology* 15 (1). BioMed Central: 105. doi:10.1186/s12915-017-0444-9.

D ’cruz, Akshay A, Nadia J Kershaw, Jessica J Chiang, May K Wang, Nicos A Nicola, Jeffrey J Babon, Michaela U Gack, et al. 2013. “Crystal Structure of the TRIM25 B30.2 (PRYSPRY) Domain: A Key Component of Antiviral Signalling.” *Biochem J* 456 (2): 231–40. doi:10.1042/BJ20121425.

Decroly, Etienne, Fran?ois Ferron, Julien Lescar, and Bruno Canard. 2011. “Conventional and Unconventional Mechanisms for Capping Viral mRNA.” *Nature Reviews Microbiology* 10 (December). doi:10.1038/nrmicro2675.

Dou, H, L Buetow, G J Sibbet, K Cameron, and D T Huang. 2012. “BIRC7-E2 Ubiquitin Conjugate Structure Reveals the Mechanism of Ubiquitin Transfer by a RING Dimer.” *Nat Struct Mol Biol* 19 (9): 876–83. doi:10.1038/nsmb.2379.

Dupuis, Stéphanie, Emmanuelle Jouanguy, Sami Al-Hajjar, Claire Fieschi, Ibrahim Zaid Al-Mohsen, Suliman Al-Jumaah, Kun Yang, et al. 2003. “Impaired Response to Interferon-A/β and Lethal Viral Disease in Human STAT1 Deficiency.” *Nature Genetics* 33 (3): 388–91. doi:10.1038/ng1097.

Ferrao, Ryan, and Hao Wu. 2012. “Helical Assembly in the Death Domain (DD) Superfamily.” *Current Opinion in Structural Biology* 22 (2). NIH Public Access: 241–47. doi:10.1016/j.sbi.2012.02.006.

Feschotte, Cédric, and Clément Gilbert. 2012. “Endogenous Viruses: Insights into Viral Evolution and Impact on Host Biology.” *Nature Reviews Genetics* 13 (4). Nature Publishing Group: 283–96. doi:10.1038/nrg3199.

Finlay, B Brett, and Grant McFadden. 2006. “Anti-Immunology: Evasion of the Host Immune System by Bacterial and Viral Pathogens.” *Cell* 124 (4): 767–82. doi:10.1016/j.cell.2006.01.034.

Forterre, Patrick, and David Prangishvili. 2009. “The Origin of Viruses.” *Research in Microbiology* 160 (7): 466–72. doi:10.1016/j.resmic.2009.07.008.

Fredericksen, B. L., B. C. Keller, J. Fornek, M. G. Katze, and M. Gale. 2008. “Establishment and Maintenance of the Innate Antiviral Response to West Nile Virus Involves Both RIG-I and MDA5 Signaling through IPS-1.” *Journal of Virology* 82 (2): 609–16. doi:10.1128/JVI.01305-07.

Fu, X Y, D S Kessler, S A Veals, D E Levy, and J E Darnell. 1990. “ISGF3, the Transcriptional Activator Induced by Interferon Alpha, Consists of Multiple Interacting Polypeptide Chains.” *Proceedings of the National Academy of Sciences of the United States of America* 87 (21): 8555–59. http://www.ncbi.nlm.nih.gov/pubmed/2236065.

Gack, M U, R A Albrecht, T Urano, K S Inn, I C Huang, E Carnero, M Farzan, S Inoue, J U Jung, and A Garcia-Sastre. 2009. “Influenza A Virus NS1 Targets the Ubiquitin Ligase TRIM25 to Evade Recognition by the Host Viral RNA Sensor RIG-I.” *Cell Host Microbe* 5 (5): 439–49. doi:10.1016/j.chom.2009.04.006.

Gack, M U, A Kirchhofer, Y C Shin, K S Inn, C Liang, S Cui, S Myong, T Ha, K P Hopfner, and J U Jung. 2008. “Roles of RIG-I N-Terminal Tandem CARD and Splice Variant in TRIM25-Mediated Antiviral Signal Transduction.” *Proc Natl Acad Sci U S A* 105 (43): 16743–48. doi:10.1073/pnas.0804947105.

Gack, M U, Y C Shin, C H Joo, T Urano, C Liang, L Sun, O Takeuchi, et al. 2007. “TRIM25 RING-Finger E3 Ubiquitin Ligase Is Essential for RIG-I-Mediated Antiviral Activity.” *Nature* 446 (7138): 916–20. doi:10.1038/nature05732.

Gallo, R C, S Z Salahuddin, M Popovic, G M Shearer, M Kaplan, B F Haynes, T J Palker, R Redfield, J Oleske, and B Safai. 1984. “Frequent Detection and Isolation of Cytopathic Retroviruses (HTLV-III) from Patients with AIDS and at Risk for AIDS.” *Science (New York, N.Y.)* 224 (4648): 500–503. http://www.ncbi.nlm.nih.gov/pubmed/6200936.

Gao, G. 2002. “Inhibition of Retroviral RNA Production by ZAP, a CCCH-Type Zinc Finger Protein.” *Science* 297 (5587): 1703–6. doi:10.1126/science.1074276.

Gerlier, D, and D S Lyles. 2011. “Interplay between Innate Immunity and Negative-Strand RNA Viruses: Towards a Rational Model.” *Microbiol Mol Biol Rev* 75 (3). INSERM U758, CERVI, 21 avenue Tony Garnier, 69007 Lyon, France. denis.gerlier@inserm.fr: 468–90, second page of table of contents. doi:10.1128/MMBR.00007-11.

Goulet, I., S. Boisvenue, S. Mokas, R. Mazroui, and J. Cote. 2008. “TDRD3, a Novel Tudor Domain-Containing Protein, Localizes to Cytoplasmic Stress Granules.” *Human Molecular Genetics* 17 (19): 3055–74. doi:10.1093/hmg/ddn203.

Gourbeyre, Pascal, Mustapha Berri, Yannick Lippi, F. Meurens, Silvia Vincent-Naulleau, J. Laffitte, Claire Rogel-Gaillard, Philippe Pinton, and Isabelle P Oswald. 2015. “Pattern Recognition Receptors in the Gut: Analysis of Their Expression along the Intestinal Tract and the Crypt/villus Axis.” *Physiological Reports* 3 (2). INRA, UMR1331, Toxalim, Toxicologie Alimentaire, Toulouse, France Universite de Toulouse, INP, UMR1331, Toxalim, Toulouse, France. INRA, UR1282, ISP, Infectiologie et Sante Publique, Nouzilly, France Universite Francois Rabelais, UMR1282 Infectiologie et: e12225–e12225. doi:10.14814/phy2.12225.

Greene, Warner C. 2007. “A History of AIDS: Looking back to See Ahead.” *European Journal of Immunology* 37 (S1): S94–102. doi:10.1002/eji.200737441.

Grieder, Franziska B, and Stefanie N Vogel. 2017. “Role of Interferon and Interferon Regulatory Factors in Early Protection against Venezuelan Equine Encephalitis Virus Infection.” Accessed November 21. https://ac.els-cdn.com/S0042682299996629/1-s2.0-S0042682299996629-main.pdf?_tid=ba2b2272-cf3b-11e7-9793-00000aab0f02&acdnat=1511324289_75a6c5aa76b5349b517142ddb56206a4.

Guo, Xuemin, Jing Ma, Jing Sun, and Guangxia Gao. 2007. “The Zinc-Finger Antiviral Protein Recruits the RNA Processing Exosome to Degrade the Target mRNA.” *Proceedings of the National Academy of Sciences of the United States of America* 104 (1). National Academy of Sciences: 151–56. doi:10.1073/pnas.0607063104.

Habjan, Matthias, Ida Andersson, Jonas Klingström, Michael Schümann, Arnold Martin, Petra Zimmermann, Valentina Wagner, et al. 2008. “Processing of Genome 5’ Termini as a Strategy of Negative-Strand RNA Viruses to Avoid RIG-I-Dependent Interferon Induction.” *PloS One* 3 (4). Public Library of Science: e2032. doi:10.1371/journal.pone.0002032.

Hatakeyama, Shigetsugu. 2011. “TRIM Proteins and Cancer.” *Nature Reviews Cancer*. doi:10.1038/nrc3139.

Horie, Kuniko, Tomohiko Urano, Kazuhiro Ikeda, and Satoshi Inoue. 2003. “Estrogen-Responsive RING Finger Protein Controls Breast Cancer Growth.” *The Journal of Steroid Biochemistry and Molecular Biology*. doi:10.1016/S0960-0760(03)00209-7.

Hornung, V., J. Ellegast, S. Kim, K. Brzozka, A. Jung, H. Kato, H. Poeck, et al. 2006. “5’-Triphosphate RNA Is the Ligand for RIG-I.” *Science* 314 (5801): 994–97. doi:10.1126/science.1132505.

Hou, F, L Sun, H Zheng, B Skaug, Q X Jiang, and Z J Chen. 2011. “MAVS Forms Functional Prion-like Aggregates to Activate and Propagate Antiviral Innate Immune Response.” *Cell* 146 (3): 448–61. doi:10.1016/j.cell.2011.06.041.

Hwang, S Y, P J Hertzog, K A Holland, S H Sumarsono, M J Tymms, J A Hamilton, G Whitty, I Bertoncello, and I Kola. 1995. “A Null Mutation in the Gene Encoding a Type I Interferon Receptor Component Eliminates Antiproliferative and Antiviral Responses to Interferons Alpha and Beta and Alters Macrophage Responses.” *Proceedings of the National Academy of Sciences of the United States of America* 92 (24): 11284–88. http://www.ncbi.nlm.nih.gov/pubmed/7479980.

Inoue, S, a Orimo, T Hosoi, S Kondo, H Toyoshima, T Kondo, a Ikegami, Y Ouchi, H Orimo, and M Muramatsu. 1993. “Genomic Binding-Site Cloning Reveals an Estrogen-Responsive Gene That Encodes a RING Finger Protein.” *Proceedings of the National Academy of Sciences of the United States of America*. doi:10.1073/pnas.90.23.11117.

Iwasaki, Akiko, and Ruslan Medzhitov. 2010. “Regulation of Adaptive Immunity by the Innate Immune System.” *Science* 327 (5963): 291–95. doi:10.1126/science.1183021.

Jackson, Richard J, Christopher U T Hellen, and Tatyana V Pestova. 2010. “The Mechanism of Eukaryotic Translation Initiation and Principles of Its Regulation.” *Nature Reviews. Molecular Cell Biology* 11 (2): 113–27. doi:10.1038/nrm2838.

Jain, Saumya, Joshua R Wheeler, Robert W Walters, Anurag Agrawal, Anthony Barsic, Roy Parker Correspondence, and Roy Parker. 2016. “ATPase-Modulated Stress Granules Contain a Diverse Proteome and Substructure.” *Cell* 164. Elsevier Inc: 487–98. doi:10.1016/j.cell.2015.12.038.

James, Leo C, Anthony H Keeble, Zahra Khan, David A Rhodes, and John Trowsdale. 2007. “Structural Basis for PRYSPRY-Mediated Tripartite Motif (TRIM) Protein Function.” *Proceedings of the National Academy of Sciences of the United States of America* 104 (15): 6200–6205. doi:10.1073/pnas.0609174104.

Janeway, Charles A. 2013. “Pillars Article: Approaching the Asymptote? Evolution and Revolution in Immunology. Cold Spring Harb Symp Quant Biol. 1989. 54: 1–13.” *The Journal of Immunology* 191 (9). http://www.jimmunol.org.proxy.its.virginia.edu/content/191/9/4475.

Jeong, Eunshil, and Joo Young Lee. 2011. “Intrinsic and Extrinsic Regulation of Innate Immune Receptors.” *Yonsei Medical Journal* 52 (3). Yonsei University College of Medicine: 379–92. doi:10.3349/ymj.2011.52.3.379.

Jiang, Fuguo, Anand Ramanathan, Matthew T Miller, Guo-Qing Q Tang, Michael Gale, Smita S Patel, Joseph Marcotrigiano, et al. 2011. “Structural Basis of RNA Recognition and Activation by Innate Immune Receptor RIG-I.” *Nature* 479 (7373). Center for Advanced Biotechnology and Medicine, Department of Chemistry and Chemical Biology, Rutgers University, 679 Hoes Lane West, Piscataway, New Jersey 08854, USA.: NIH Public Access: 423–27. doi:10.1038/nature10537.

Jiang, Q X, and Z J Chen. 2012. “Structural Insights into the Activation of RIG-I, a Nanosensor for Viral RNAs.” *EMBO Rep* 13 (1): 7–8. doi:10.1038/embor.2011.239.

Jiang, X, L N Kinch, C A Brautigam, X Chen, F Du, N V Grishin, and Z J Chen. 2012. “Ubiquitin-Induced Oligomerization of the RNA Sensors RIG-I and MDA5 Activates Antiviral Innate Immune Response.” *Immunity* 36 (6): 959–73. doi:10.1016/j.immuni.2012.03.022.

Kang, Dong Chul, Rahul V. Gopalkrishnan, Lin Lin, Aaron Randolph, Kristoffer Valerie, Sidney Pestka, and Paul B. Fisher. 2004. “Expression Analysis and Genomic Characterization of Human Melanoma Differentiation Associated Gene-5, Mda-5: A Novel Type I Interferon-Responsive Apoptosis-Inducing Gene.” *Oncogene* 23 (9): 1789–1800. doi:10.1038/sj.onc.1207300.

Kato, Hiroki, Shintaro Sato, Mitsutoshi Yoneyama, Masahiro Yamamoto, Satoshi Uematsu, Kosuke Matsui, Tohru Tsujimura, et al. 2005. “Cell Type-Specific Involvement of RIG-I in Antiviral Response.” *Immunity* 23 (1): 19–28. doi:10.1016/j.immuni.2005.04.010.

Kato, Hiroki, Osamu Takeuchi, Eriko Mikamo-Satoh, Reiko Hirai, Tomoji Kawai, Kazufumi Matsushita, Akane Hiiragi, Terence S. Dermody, Takashi Fujita, and Shizuo Akira. 2008. “Length-Dependent Recognition of Double-Stranded Ribonucleic Acids by Retinoic Acid–inducible Gene-I and Melanoma Differentiation–associated Gene 5.” *The Journal of Experimental Medicine* 205 (7): 1601–10. doi:10.1084/jem.20080091.

Kato, Hiroki, Osamu Takeuchi, Shintaro Sato, Mitsutoshi Yoneyama, Masahiro Yamamoto, Kosuke Matsui, Satoshi Uematsu, et al. 2006. “Differential Roles of MDA5 and RIG-I Helicases in the Recognition of RNA Viruses.” *Nature* 441 (1): 101–5. doi:10.1038/nature04734.

Kedersha, Nancy, Michael R Cho, Wei Li, Patrick W Yacono, Samantha Chen, Natalie Gilks, David E Golan, and Paul Anderson. 2000. “Dynamic Shuttling of TIA-1 Accompanies the Recruitment of mRNA to Mammalian Stress Granules.” *The Journal of Cell Biology* 151 (6): 1257–68. http://www.jcb.org/cgi/content/full/151/6/1257.

Kilbourne, Edwin D. 2006. “Influenza Pandemics of the 20th Century.” *Emerging Infectious Diseases* 12 (1). Centers for Disease Control and Prevention: 9–14. doi:10.3201/eid1201.051254.

Killip, Marian J, Ervin Fodor, and Richard E Randall. 2015. “Influenza Virus Activation of the Interferon System.” *Virus Research* 209 (November). Biomedical Sciences Research Complex, University of St Andrews, North Haugh, St Andrews, Fife KY16 9ST, UK; Sir William Dunn School of Pathology, University of Oxford, South Parks Road, Oxford OX1 3RE, UK. Electronic address: mjk3@st-andrews.ac.uk. Sir Wi: 11–22. doi:10.1016/j.virusres.2015.02.003.

Komander, David, and Michael Rape. 2012. “The Ubiquitin Code.” *Annual Review of Biochemistry* 81 (1): 203–29. doi:10.1146/annurev-biochem-060310-170328.

Koonin, Eugene V, Tatiana G Senkevich, and Valerian V Dolja. 2006. “The Ancient Virus World and Evolution of Cells.” *Biology Direct* 1 (1): 29. doi:10.1186/1745-6150-1-29.

Kowalinski, Eva, Thomas Lunardi, Andrew A. McCarthy, Jade Louber, Joanna Brunel, Boyan Grigorov, Denis Gerlier, and Stephen Cusack. 2011. “Structural Basis for the Activation of Innate Immune Pattern-Recognition Receptor RIG-I by Viral RNA.” *Cell* 147 (2). Elsevier Inc.: 423–35. doi:10.1016/j.cell.2011.09.039.

Kwon, S Chul, Hyerim Yi, Katrin Eichelbaum, S Fohr, Bernd Fischer, Kwon Tae You, Alfredo Castello, Jeroen Krijgsveld, Matthias W Hentze, and V Narry Kim. 2013. “The RNA-Binding Protein Repertoire of Embryonic Stem Cells.” *Nat Struct Mol Biol* 20 (9): 1122–30. doi:10.1038/nsmb.2638.

Kwon, Sohee, Yu Zhang, and Patrick Matthias. 2007. “The Deacetylase HDAC6 Is a Novel Critical Component of Stress Granules Involved in the Stress Response.” *Genes and Development* 21 (24): 3381–94. doi:10.1101/gad.461107.

Leung, Anthony K L, Sejal Vyas, Jennifer E Rood, Arjun Bhutkar, Phillip A Sharp, and Paul Chang. 2011. “Poly(ADP-Ribose) Regulates Stress Responses and microRNA Activity in the Cytoplasm.” *Molecular Cell* 42 (4). NIH Public Access: 489–99. doi:10.1016/j.molcel.2011.04.015.

Levy, D E, D S Kessler, R Pine, and J E Darnell. 1989. “Cytoplasmic Activation of ISGF3, the Positive Regulator of Interferon-Alpha-Stimulated Transcription, Reconstituted in Vitro.” *Genes & Development* 3 (9): 1362–71. http://www.ncbi.nlm.nih.gov/pubmed/2606351.

Li, Melody M. H., Zerlina Lau, Pamela Cheung, Eduardo G. Aguilar, William M. Schneider, Leonia Bozzacco, Henrik Molina, et al. 2017. “TRIM25 Enhances the Antiviral Action of Zinc-Finger Antiviral Protein (ZAP).” Edited by Ana Fernandez-Sesma. *PLoS Pathogens* 13 (1). Public Library of Science: e1006145. doi:10.1371/journal.ppat.1006145.

Loo, Y.-M., J. Fornek, N. Crochet, G. Bajwa, O. Perwitasari, L. Martinez-Sobrido, S. Akira, et al. 2008. “Distinct RIG-I and MDA5 Signaling by RNA Viruses in Innate Immunity.” *Journal of Virology* 82 (1): 335–45. doi:10.1128/JVI.01080-07.

Loo, Y.-M, and · M Gale. 2017. “Viral Regulation and Evasion of the Host Response.” Accessed October 7. https://link-springer-com.proxy.its.virginia.edu/content/pdf/10.1007%2F978-3-540-71329-6_14.pdf.

“LPS/TLR4 Signal Transduction Pathway.” 2008. *Cytokine* 42 (2). Academic Press: 145–51. doi:10.1016/J.CYTO.2008.01.006.

Luo, Dahai, Andrew Kohlway, Adriana Vela, and Anna Marie Pyle. 2012. “Visualizing the Determinants of Viral RNA Recognition by Innate Immune Sensor RIG-I.” *Structure* 20 (11): 1983–88. doi:10.1016/j.str.2012.08.029.

Luthra, Priya, Dengyun Sun, Robert H Silverman, and Biao He. 2011. “Activation of IFN-β Expression by a Viral mRNA through RNase L and MDA5.” *Proceedings of the National Academy of Sciences of the United States of America* 108 (5): 2118–23. doi:10.1073/pnas.1012409108.

Manokaran, Gayathri, Esteban Finol, Chunling Wang, Jayantha Gunaratne, Justin Bahl, Eugenia Z Ong, Hwee Cheng Tan, et al. 2015. “Dengue Subgenomic RNA Binds TRIM25 to Inhibit Interferon Expression for Epidemiological Fitness.” *Science* 350 (6257): 217 LP-221. http://science.sciencemag.org/content/350/6257/217.abstract.

Mao, Richeng, Hui Nie, Dawei Cai, Jiming Zhang, Hongyan Liu, Ran Yan, Andrea Cuconati, Timothy M. Block, Ju-Tao Tao Guo, and Haitao Guo. 2013. “Inhibition of Hepatitis B Virus Replication by the Host Zinc Finger Antiviral Protein.” Edited by Aleem Siddiqui. *PLoS Pathogens* 9 (7). Public Library of Science: e1003494. doi:10.1371/journal.ppat.1003494.

McCartney, Stephen A., Larissa B. Thackray, Leonid Gitlin, Susan Gilfillan, Herbert W. Virgin IV, and Marco Colonna. 2008. “MDA-5 Recognition of a Murine Norovirus.” *PLoS Pathogens* 4 (7). doi:10.1371/journal.ppat.1000108.

McCormick, Craig, and Denys A Khaperskyy. 2017. “Translation Inhibition and Stress Granules in the Antiviral Immune Response.” *Nature Publishing Group*. doi:10.1038/nri.2017.63.

Medzhitov, Ruslan, and Charles A Janeway. 1997. “Innate Immunity: The Virtues of a Nonclonal System of Recognition.” *Cell* 91 (3). Cell Press: 295–98. doi:10.1016/S0092-8674(00)80412-2.

Mogensen, Trine H. 2009. “Pathogen Recognition and Inflammatory Signaling in Innate Immune Defenses.” *Clinical Microbiology Reviews* 22 (2). American Society for Microbiology (ASM): 240–73, Table of Contents. doi:10.1128/CMR.00046-08.

Muller, S., P. Moller, Matthew J. Bick, Stephanie Wurr, Stephan Becker, S. Gunther, B. M. Kummerer, et al. 2007. “Inhibition of Filovirus Replication by the Zinc Finger Antiviral Protein.” *Journal of Virology* 81 (5). American Society for Microbiology: 2391–2400. doi:10.1128/JVI.01601-06.

Napolitano, L M, and G Meroni. 2012. “TRIM Family: Pleiotropy and Diversification through Homomultimer and Heteromultimer Formation.” *IUBMB Life* 64 (1): 64–71. doi:10.1002/iub.580.

Ng, H H, and A Bird. 1999. “DNA Methylation and Chromatin Modification.” *Current Opinion in Genetics & Development* 9 (2): 158–63. http://www.ncbi.nlm.nih.gov/pubmed/10322130.

Nisole, S, J P Stoye, and A Saib. 2005. “TRIM Family Proteins: Retroviral Restriction and Antiviral Defence.” *Nat Rev Microbiol* 3 (10): 799–808. doi:10.1038/nrmicro1248.

Nott, Timothy J., Evangelia Petsalaki, Patrick Farber, Dylan Jervis, Eden Fussner, Anne Plochowietz, Timothy D. Craggs, et al. 2015. “Phase Transition of a Disordered Nuage Protein Generates Environmentally Responsive Membraneless Organelles.” *Molecular Cell* 57 (5): 936–47. doi:10.1016/j.molcel.2015.01.013.

Nürnberger, Thorsten, and Frédéric Brunner. 2002. “Innate Immunity in Plants and Animals: Emerging Parallels between the Recognition of General Elicitors and Pathogen-Associated Molecular Patterns.” *Current Opinion in Plant Biology* 5 (4): 318–24. http://www.ncbi.nlm.nih.gov/pubmed/12179965.

Ohn, Takbum, Nancy Kedersha, Tyler Hickman, Sarah Tisdale, and Paul Anderson. 2008. “A Functional RNAi Screen Links O-GlcNAc Modification of Ribosomal Proteins to Stress Granule and Processing Body Assembly.” *Nature Cell Biology* 10 (10): 1224–31. doi:10.1038/ncb1783.

Peisley, Alys, Bin Wu, Hui Xu, Zhijian J. Chen, and Sun Hur. 2014. “Structural Basis for Ubiquitin-Mediated Antiviral Signal Activation by RIG-I.” *Nature* 509 (7498). Nature Publishing Group: 110–14. doi:10.1038/nature13140.

Peisley, Alys, Bin Wu, Hui Yao, Thomas Walz, and Sun Hur. 2013. “RIG-I Forms Signaling-Competent Filaments in an ATP-Dependent, Ubiquitin-Independent Manner.” *Molecular Cell* 51 (5). Elsevier Inc.: 573–83. doi:10.1016/j.molcel.2013.07.024.

Plechanovova, A, E G Jaffray, M H Tatham, J H Naismith, and R T Hay. 2012. “Structure of a RING E3 Ligase and Ubiquitin-Loaded E2 Primed for Catalysis.” *Nature* 489 (7414): 115–20. doi:10.1038/nature11376.

Plumet, Sébastien, Florence Herschke, Jean Marie Bourhis, Hélène Valentin, Sonia Longhl, and Denis Gerlier. 2007. “Cytosolic 5′-Triphosphate Ended Viral Leader Transcript of Measles Virus as Activator of the RIG I-Mediated Interferon Response.” *PLoS ONE* 2 (3). doi:10.1371/journal.pone.0000279.

Popovic, M, M G Sarngadharan, E Read, and R C Gallo. 1984. “Detection, Isolation, and Continuous Production of Cytopathic Retroviruses (HTLV-III) from Patients with AIDS and Pre-AIDS.” *Science (New York, N.Y.)* 224 (4648): 497–500. http://www.ncbi.nlm.nih.gov/pubmed/6200935.

Protter, David S W, and Roy Parker. 2016. “Principles and Properties of Stress Granules.” doi:10.1016/j.tcb.2016.05.004.

Rajsbaum, Ricardo, Adolfo García-Sastre, and Gijs A Versteeg. 2014. “TRIMmunity: The Roles of the TRIM E3-Ubiquitin Ligase Family in Innate Antiviral Immunity.” *Journal of Molecular Biology* 426 (6): 1265–84. doi:10.1016/j.jmb.2013.12.005.

Rawlings, Jason S, Kristin M Rosler, and Douglas A Harrison. 2017. “The JAK/STAT Signaling Pathway.” *Journal of Cell Science* 117: 1281–83. Accessed November 21. doi:10.1242/jcs.00963.

Reymond, Alexandre, Germana Meroni, Anna Fantozzi, Giuseppe Merla, Stefano Cairo, Lucilla Luzi, Daniela Riganelli, et al. 2001. “The Tripartite Motif Family Identifies Cell Compartments.” *EMBO Journal* 20 (9): 2140–51. doi:10.1093/emboj/20.9.2140.

Rhodes, David A., Bernard De Bono, and John Trowsdale. 2005. “Relationship between SPRY and B30.2 Protein Domains. Evolution of a Component of Immune Defence.” *Immunology*. doi:10.1111/j.1365-2567.2005.02248.x.

Roth-Cross, Jessica K, Susan J Bender, and Susan R Weiss. 2008. “Murine Coronavirus Mouse Hepatitis Virus Is Recognized by MDA5 and Induces Type I Interferon in Brain Macrophages/microglia.” *Journal of Virology* 82 (20): 9829–38. doi:10.1128/JVI.01199-08.

Ryman, K D, W B Klimstra, K B Nguyen, C A Biron, and R E Johnston. 2000. “Alpha/beta Interferon Protects Adult Mice from Fatal Sindbis Virus Infection and Is an Important Determinant of Cell and Tissue Tropism.” *Journal of Virology* 74 (7). American Society for Microbiology (ASM): 3366–78. http://www.ncbi.nlm.nih.gov/pubmed/10708454.

Saito, Takeshi, Reiko Hirai, Yueh-Ming Loo, David Owen, Cynthia L Johnson, Sangita C Sinha, Shizuo Akira, Takashi Fujita, and Michael Gale. 2007. “Regulation of Innate Antiviral Defenses through a Shared Repressor Domain in RIG-I and LGP2.” *Proceedings of the National Academy of Sciences of the United States of America* 104 (2): 582–87. doi:10.1073/pnas.0606699104.

Samanta, Mrinal, Dai Iwakiri, Teru Kanda, Tadaatsu Imaizumi, and Kenzo Takada. 2006. “EB Virus-Encoded RNAs Are Recognized by RIG-I and Activate Signaling to Induce Type I IFN.” *EMBO Journal* 25 (18): 4207–14. doi:10.1038/sj.emboj.7601314.

Sánchez-Aparicio, M. T., J. Ayllón, A. Leo-Macias, T. Wolff, and A. García-Sastre. 2017. “Subcellular Localizations of RIG-I, TRIM25, and MAVS Complexes.” *Journal of Virology* 91 (2): e01155-16. doi:10.1128/JVI.01155-16.

Sanchez, Jacint G., Jessica J. Chiang, Konstantin M.J. Sparrer, Steven L. Alam, Michael Chi, Marcin D. Roganowicz, Banumathi Sankaran, Michaela U. Gack, and Owen Pornillos. 2016. “Mechanism of TRIM25 Catalytic Activation in the Antiviral RIG-I Pathway.” *Cell Reports* 16 (5): 1315–25. doi:10.1016/j.celrep.2016.06.070.

Sanchez, Jacint G, Katarzyna Okreglicka, Viswanathan Chandrasekaran, Jordan M Welker, Wesley I Sundquist, and Owen Pornillos. 2014. “The Tripartite Motif Coiled-Coil Is an Elongated Antiparallel Hairpin Dimer.” *Proceedings of the National Academy of Sciences* 111 (7): 2494–99. doi:10.1073/pnas.1318962111.

Schindler, C, X Y Fu, T Improta, R Aebersold, J E Darnell, and Jr. 1992. “Proteins of Transcription Factor ISGF-3: One Gene Encodes the 91-and 84-kDa ISGF-3 Proteins That Are Activated by Interferon Alpha.” *Proceedings of the National Academy of Sciences of the United States of America* 89 (16). National Academy of Sciences: 7836–39. http://www.ncbi.nlm.nih.gov/pubmed/1502203.

Schneider, William M, Meike Dittmann Chevillotte, and Charles M Rice. 2014. “Interferon-Stimulated Genes: A Complex Web of Host Defenses.” *Annual Review of Immunology* 32. NIH Public Access: 513–45. doi:10.1146/annurev-immunol-032713-120231.

Schoggins, John W, and Charles M Rice. 2011. “Interferon-Stimulated Genes and Their Antiviral Effector Functions.” *Current Opinion in Virology* 1 (6). NIH Public Access: 519–25. doi:10.1016/j.coviro.2011.10.008.

Seo, Gil Ju, Rodney P Kincaid, Teva Phanaksri, James M Burke, Justin M Pare, Jennifer E Cox, Tien-Ying Ying Hsiang, Robert M Krug, and Christopher S Sullivan. 2013. “Reciprocal Inhibition between Intracellular Antiviral Signaling and the RNAi Machinery in Mammalian Cells.” *Cell Host and Microbe* 14 (4). Elsevier: 435–45. doi:10.1016/j.chom.2013.09.002.

Stewart, Mikaela D, Tobias Ritterhoff, Rachel E Klevit, and Peter S Brzovic. 2016. “E2 Enzymes: More than Just Middle Men.” *Cell Research* 2635: 423–40. doi:10.1038/cr.2016.35.

Sumpter Jr., R, Y M Loo, E Foy, K Li, M Yoneyama, T Fujita, S M Lemon, and M Gale Jr. 2005. “Regulating Intracellular Antiviral Defense and Permissiveness to Hepatitis C Virus RNA Replication through a Cellular RNA Helicase, RIG-I.” *J Virol* 79 (5): 2689–99. doi:10.1128/JVI.79.5.2689.

Takata, Matthew A, Daniel Gonçalves-Carneiro, Trinity M. Zang, Steven J Soll, Ashley York, Daniel Blanco-Melo, and Paul D Bieniasz. 2017. “CG Dinucleotide Suppression Enables Antiviral Defence Targeting Non-Self RNA.” *Nature*, September. doi:10.1038/nature24039.

Taubenberger, Jeffery K., and David M. Morens. 2006. “1918 Influenza: The Mother of All Pandemics.” *Emerging Infectious Diseases* 12 (1): 15–22. doi:10.3201/eid1201.050979.

Taubenberger, Jeffery K, Ann H Reid, Raina M Lourens, Ruixue Wang, Guozhong Jin, and Thomas G Fanning. 2017. “Characterization of the 1918 Influenza Virus Polymerase Genes.” Accessed November 16. doi:10.1038/nature04230.

Todorova, Tanya, Florian J. Bock, and Paul Chang. 2015. “Poly(ADP-Ribose) Polymerase-13 and RNA Regulation in Immunity and Cancer.” *Trends in Molecular Medicine* 21 (6). NIH Public Access: 373–84. doi:10.1016/j.molmed.2015.03.002.

Tourrière, Hélène, Karim Chebli, Latifa Zekri, Brice Courselaud, Jean Marie Blanchard, Edouard Bertrand, and Jamal Tazi. 2003. “The RasGAP-Associated Endoribonuclease G3BP Assembles Stress Granules.” *The Journal of Cell Biology* 160 (6): 823–31. doi:10.1083/jcb.200212128.

Trempe, Jean François. 2011. “Reading the Ubiquitin Postal Code.” *Current Opinion in Structural Biology*. doi:10.1016/j.sbi.2011.09.009.

Urano, Tomohiko, Tomoyuki Saito, Tohru Tsukui, Masayo Fujita, Takayuki Hosoi, Masami Muramatsu, Yasuyoshi Ouchi, and Satoshi Inoue. 2002. “Efp Targets 14-3-3σ for Proteolysis and Promotes Breast Tumour Growth.” *Nature* 417 (6891): 871–75. doi:10.1038/nature00826.

Versteeg, Gijs A, Ricardo Rajsbaum, Maria Teresa Sánchez-Aparicio, Ana M Maestre, Julio Valdiviezo, Mude Shi, Kyung Soo Inn, Ana Fernandez-Sesma, Jae Jung, and Adolfo García-Sastre. 2013. “The E3-Ligase TRIM Family of Proteins Regulates Signaling Pathways Triggered by Innate Immune Pattern-Recognition Receptors.” *Immunity* 38 (2): 384–98. doi:10.1016/j.immuni.2012.11.013.

Wagner, Jonathan M., Marcin D. Roganowicz, Katarzyna Skorupka, Steven L. Alam, Devin Christensen, Ginna Doss, Yueping Wan, et al. 2016. “Mechanism of B-Box 2 Domain-Mediated Higher-Order Assembly of the Retroviral Restriction Factor TRIM5α.” *eLife* 5 (JUNE2016). doi:10.7554/eLife.16309.

Walsh, C. P., and G. L. Xu. 2006. “Cytosine Methylation and DNA Repair.” In *Current Topics in Microbiology and Immunology*, 301:283–315. Berlin/Heidelberg: Springer-Verlag. doi:10.1007/3-540-31390-7_11.

Walsh, Logan A, Mariano J Alvarez, Erich Y Sabio, Linda T Vahdat, Andrea Califano, Timothy A Chan, Marsha Reyngold, et al. 2017. “An Integrated Systems Biology Approach Identifies TRIM25 as a Key Determinant of Breast Cancer Metastasis.” *Cell Reports* 20. doi:10.1016/j.celrep.2017.07.052.

Wang, Fuan, Xiujuan Gao, John W. Barrett, Qing Shao, Eric Bartee, Mohamed R. Mohamed, Masmudur Rahman, et al. 2008. “RIG-I Mediates the Co-Induction of Tumor Necrosis Factor and Type I Interferon Elicited by Myxoma Virus in Primary Human Macrophages.” *PLoS Pathogens* 4 (7). doi:10.1371/journal.ppat.1000099.

Wang, Xinlu, Fan Tu, Yiping Zhu, and Guangxia Gao. 2012. “Zinc-Finger Antiviral Protein Inhibits XMRV Infection.” Edited by Karin E. Peterson. *PLoS ONE* 7 (6). Public Library of Science: e39159. doi:10.1371/journal.pone.0039159.

“WHO | Influenza (Seasonal).” 2017. *WHO*. World Health Organization. http://www.who.int/mediacentre/factsheets/fs211/en/.

“WHO | Statement on the 1st Meeting of the IHR Emergency Committee on the 2014 Ebola Outbreak in West Africa.” 2014. *WHO*. World Health Organization. http://www.who.int/mediacentre/news/statements/2014/ebola-20140808/en/.

Wippich, Frank, Bernd Bodenmiller, Maria Gustafsson Trajkovska, Stefanie Wanka, Ruedi Aebersold, and Lucas Pelkmans. 2013. “Dual Specificity Kinase DYRK3 Couples Stress Granule Condensation/Dissolution to mTORC1 Signaling.” *Cell* 152 (4): 791–805. doi:10.1016/j.cell.2013.01.033.

Wu, Bin, Alys Peisley, David Tetrault, Zongli Li, Edward H. Egelman, Katharine E. Magor, Thomas Walz, Pawel A. Penczek, and Sun Hur. 2014. “Molecular Imprinting as a Signal-Activation Mechanism of the Viral RNA Sensor RIG-I.” *Molecular Cell* 55 (4). Elsevier Inc.: 511–23. doi:10.1016/j.molcel.2014.06.010.

Yang, Xiaoxue, Yi Shen, Elena Garre, Xinxin Hao, Daniel Krumlinde, Marija Cvijović, Christina Arens, Thomas Nyström, Beidong Liu, and Per Sunnerhagen. 2014. “Stress Granule-Defective Mutants Deregulate Stress Responsive Transcripts.” Edited by Paul Anderson. *PLoS Genetics* 10 (11): e1004763. doi:10.1371/journal.pgen.1004763.

Yau, Richard, and Michael Rape. 2016. “The Increasing Complexity of the Ubiquitin Code.” *Nature Cell Biology*. doi:10.1038/ncb3358.

Yoneyama, Mitsutoshi, Mika Kikuchi, Takashi Natsukawa, Noriaki Shinobu, Tadaatsu Imaizumi, Makoto Miyagishi, Kazunari Taira, Shizuo Akira, and Takashi Fujita. 2004. “The RNA Helicase RIG-I Has an Essential Function in Double-Stranded RNA-Induced Innate Antiviral Responses.” *Nature Immunology* 5 (7): 730–37. doi:10.1038/ni1087.

Zeng, Wenwen, Lijun Sun, Xiaomo Jiang, Xiang Chen, Fajian Hou, Anirban Adhikari, Ming Xu, and Zhijian J Chen. 2010. “Reconstitution of the RIG-I Pathway Reveals a Signaling Role of Unanchored Polyubiquitin Chains in Innate Immunity.” *Cell* 141 (2): 315–30. doi:10.1016/j.cell.2010.03.029.

Zheng, Xiaojiao, Xinlu Wang, Fan Tu, Qin Wang, Zusen Fan, and Guangxia Gao. 2017. “TRIM25 Is Required for the Antiviral Activity of Zinc-Finger Antiviral Protein (ZAP).” *Journal of Virology*, JVI.00088-17. doi:10.1128/JVI.00088-17.

Zhou, Shenghua, Anna M Cerny, An Zacharia, Katherine A Fitzgerald, Evelyn A Kurt-Jones, and Robert W Finberg. 2010. “Induction and Inhibition of Type I Interferon Responses by Distinct Components of Lymphocytic Choriomeningitis Virus.” *JOURNAL OF VIROLOGY* 84 (18): 9452–62. doi:10.1128/JVI.00155-10.

Zhu, Yiping, Guifang Chen, Fengxiang Lv, Xinlu Wang, Xin Ji, Yihui Xu, Jing Sun, Li Wu, Y.-T. Yong-Tang Zheng, and Guangxia Gao. 2011. “Zinc-Finger Antiviral Protein Inhibits HIV-1 Infection by Selectively Targeting Multiply Spliced Viral mRNAs for Degradation.” *Proceedings of the National Academy of Sciences* 108 (38). National Academy of Sciences: 15834–39. doi:10.1073/pnas.1101676108.

CHAPTER 2

THE TRIPARTITE MOTIF COILED-COIL IS AN ELONGATED ANTIPARALLEL HAIRPIN DIMER

Jacint G. Sanchez, Katarzyna Okreglicka, Viswanathan Chandrasekaran, Jordan M. Welker, Wesley I. Sundquist, and Owen Pornillos

Reprinted from Proceedings of the National Academy of Sciences
Volume 111, number 7, pages 2494-2499

ABSTRACT

Tripartite motif (TRIM) proteins make up a large family of coiled-coil-containing RING E3 ligases that function in many cellular processes, particularly innate antiviral response pathways. Both dimerization and higher-order assembly are important elements of TRIM protein function, but the atomic details of TRIM tertiary and quaternary structure have not been fully understood. Here, we present crystallographic and biochemical analyses of the TRIM coiled-coil and show that TRIM proteins dimerize by forming interdigitating antiparallel helical hairpins that position the N-terminal catalytic RING domains at opposite ends of the dimer and the C-terminal substrate-binding domains at the center. The dimer core comprises an antiparallel coiled-coil with a distinctive, symmetric pattern of flanking heptad and central hendecad repeats that appear to be conserved across the entire TRIM family. Our studies reveal how the coiled-coil organizes TRIM25 to polyubiquitylate the RIG-I/viral RNA recognition complex and how dimers of the TRIM5α protein are arranged within hexagonal arrays that recognize the HIV-1 capsid lattice and restrict retroviral replication.

INTRODUCTION

Tripartite motif (TRIM) proteins make up the largest super-family of RING E3 ubiquitin ligases, with more than 100 members in the human proteome (1, 2). TRIM proteins function in a variety of cellular pathways, and many regulate innate immunity and/or mediate antiviral responses. Antiviral TRIMs include TRIM25, which regulates the IFN response to RNA viruses (3,4), and TRIM5α, which senses and inhibits early stages of retroviral replication (5, 6).

TRIM proteins share a common N-terminal domain organization, termed the tripartite or RBCC (RING, B-box, coiled-coil) motif, followed by variable C-terminal protein recognition domains (**Fig. 1 A-B**). “Linker” segments of unknown structure typically separate both the RING and B-box domains (L1) and the coiled-coil and terminal effector domains (L2). The coiled-coil region mediates oligomerization, and both homooligomeric and hetero-oligomeric TRIMs have been described (7–13). Furthermore, many TRIM proteins form higher-order assemblies in vitro and form punctate or fibrous structures in cells (14–16). For example, TRIM5α assembly allows the protein to function as a cytosolic pattern-recognition receptor that can intercept the incoming capsids of diverse retroviruses, including HIV-1 (6). This results in species-specific “restriction” of viral replication (5), capsid dissociation (5, 6), and induction of innate immune responses (17). Retroviral capsids are recognized through a remarkable mechanism of multivalent pattern recognition. TRIM5α forms a homo-dimer (10, 11, 18), which can further assemble into a 2D lattice of linked hexagons (18). The hexagonal TRIM5α net matches the symmetry and spacing

Fig. 1. Domain organization and dimerization of TRIM proteins.

(A) Schematic of the domain structure of TRIM25. The principal domains and linker regions are RING (red), L1 (gray), B-box 1 (yellow), B-box 2 (orange), coiled-coil (green), L2 (gray), and B30.2/SPRY (blue). The $TRIM25_{189–379}$ construct used in this study is shown beneath (black), with the secondary structure derived from the crystal structure (rectangles represent helices).

(B) Analogous schematic of the domain structure of TRIM5α. TRIM5α does not contain a B-box 1 domain and has a shorter L2. The $TRIM5α_{133–300}$ construct used in this study is shown beneath (black). The asterisk denotes a predicted helix (H3) that crosses from L2 into the B30.2 domain.

(C) $TRIM_{189–379}$ is a stable dimer in solution. Equilibrium sedimentation distributions of the indicated protein concentrations are shown for the rotor speed of 12,000 rpm. (Upper) Absorbance measurements (open symbols; 280 nm) and best-fit curves (solid lines). (Lower) Residual differences. Equilibrium distributions were also measured at rotor speeds of 17,000 and 23,000 rpm (not shown for clarity), and all of the data were globally fit to a single-species model in which the molecular weight (M_{obs}) was allowed to float (M_{obs} = 41,674 Da; M_{calc} = 21,835 Da; M_{obs}/M_{calc} = 1.91). Fits in which the molecular weight was fixed to that of a dimer are shown in **Fig. 2A**.

(D) $TRIM5α_{133–300}$ is also a stable dimer in solution (M_{obs} = 43,505 Da; M_{calc} = 23,038 Da; M_{obs}/M_{calc} = 1.89). See **Fig. 2D** for fits to a single-species model with a fixed dimer molecular weight.

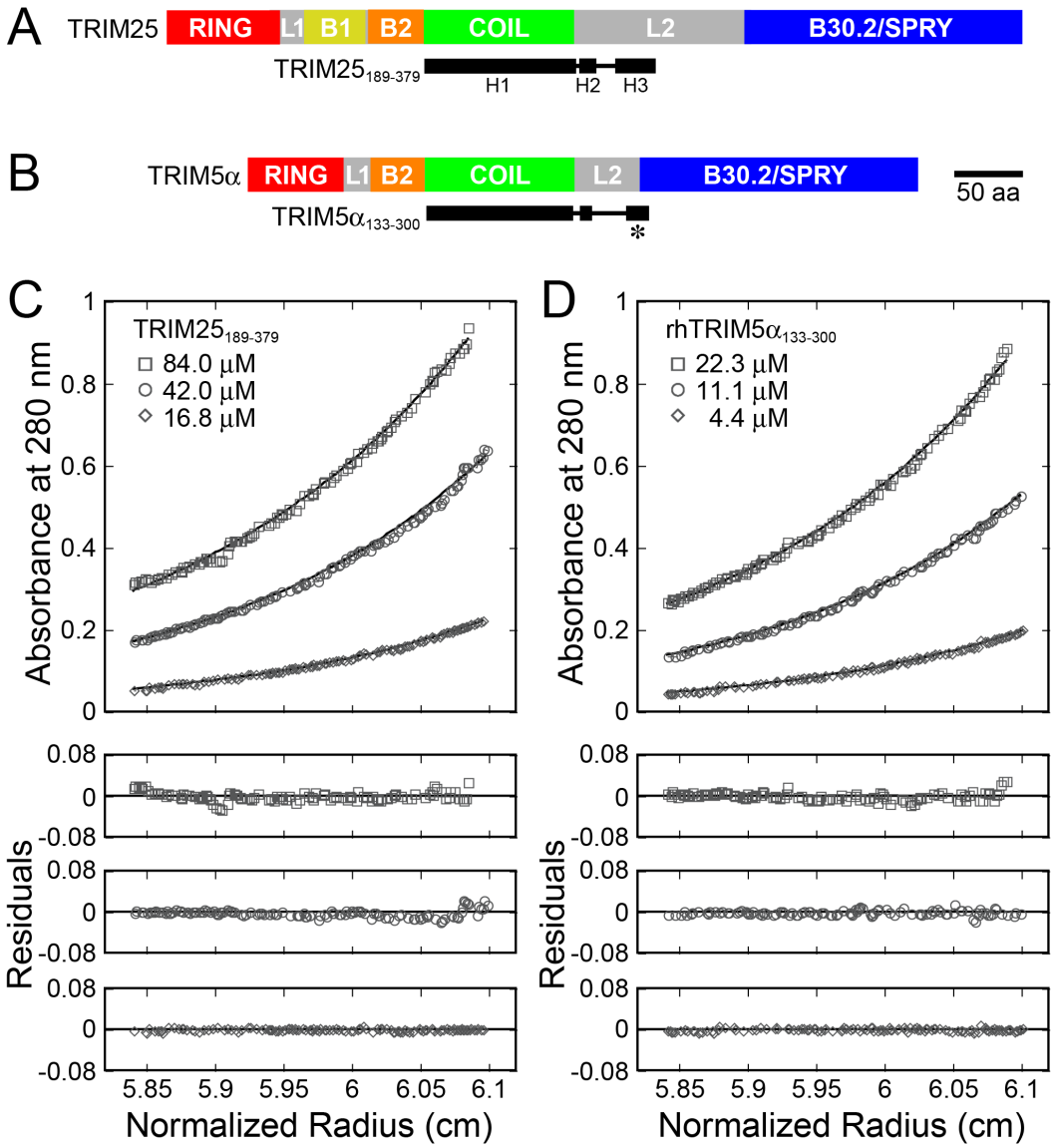
A
TRIM25
RING
L1
B1
B2
COIL
L2
B30.2/SPRY
TRIM25189-379
H1
H2
H3
B
TRIM5α
RING
L1
B2
COIL
L2
B30.2/SPRY
50 aa
TRIM5α133-300
C
TRIM25189-379
84.0 μM
42.0 μM
16.8 μM
Absorbance at 280 nm
Residuals
Normalized Radius (cm)
D
rhTRIM5α133-300
22.3 μM
11.1 μM
4.4 μM
Absorbance at 280 nm
Residuals
Normalized Radius (cm)

of the retroviral capsid surface lattice, thereby positioning multiple C-terminal B30.2/SPRY domains to interact with their repeating binding epitopes on the capsid.

Structures of isolated RING, B-box, and C-terminal domains of several TRIM proteins have been described, but the molecular details of TRIM oligomerization and high-order assembly have yet to be defined. Here, we report biochemical and crystallographic characterization of a coiled-coil-containing fragment of TRIM25. The crystallized construct forms a stable dimer in solution, and the structure reveals an elongated dimer composed of interdigitating hairpin-shaped subunits. We also present evidence that this dimer architecture is conserved across other TRIM family members, including TRIM5α. Finally, our studies allow us to assign the domain organization in the low-resolution EM reconstruction of the TRIM5α lattice (18) and thereby gain new insights into the mechanism of retroviral capsid pattern recognition.

RESULTS

TRIM25$_{189–379}$ Forms an Elongated, Antiparallel Dimer. We chose human TRIM25 for analysis because it lacks the propensity of TRIM5α to form high-order assemblies and is therefore more tractable biochemically. In initial experiments, we found that a series of coiled-coil-containing TRIM25 constructs, including the full tripartite motif and the full-length protein, behaved as single species during purification. All of these constructs eluted rapidly on gel filtration

chromatographs, indicating they had elongated shapes and/or were oligomers. The shortest well-behaved construct spanned residues 189–379, which includes the entire coiled-coil region as well as the N-terminal half of the L2 linker region that connects the coiled-coil to the B30.2/SPRY domain (**Fig. 1A**). Analytical ultracentrifugation experiments revealed that this construct is a stable dimer (**Fig. 1C; Fig. 2 A-C**), implying that the full-length protein is also probably dimeric.

To determine the molecular basis for TRIM25 dimerization, we crystallized native and selenomethionine-labeled $TRIM25_{189–379}$ and determined its structure to 2.6 Å resolution (**Fig. 3; Table 1**). The asymmetric unit comprises a single, elongated dimer ~17 nm in length (**Fig. 4**). Each subunit in the symmetrical dimer folds back into a hairpin configuration with long and short arms. The elements annotated as the coiled-coil and L2 linker are structurally distinct, with the coiled-coil residues forming the long arm of each subunit (helix H1, colored green in **Fig. 4A**) and the L2 residues forming the short arm that folds back and packs against H1 (helices H2, H3, and an irregular but well-ordered intervening segment, colored gray). The two subunits dimerize intimately in an antiparallel orientation, similar to two interdigitated bobby pins (**Fig. 4B**). Almost all hydrophobic side-chains are involved in packing interactions, which occur along the entire length of each hairpin and bury a total surface area of 5,102 $Å^2$. Polar and charged side-chains also form numerous hydrogen bonding and salt bridge interactions.

TRIM proteins have been predicted to contain two distinct coiled-coil segments separated by a helical, but noncoil, segment (19, 20). The TRIM25

Fig. 2. TRIM25$_{189–379}$ and TRIM5α$_{133–300}$ proteins form stable dimers.

(A–C) Equilibrium distributions of the indicated protein concentrations were measured at rotor speeds of 12,000, 17,000, and 23,000 rpm. (Upper panel) Absorbance measurements (open symbols) and best-fit curves (solid lines). (Lower panel) Residual differences. All data were globally fit to a single-species model in which the molecular weight was constrained to that of a dimer (M = 2 × 21,835 Da = 43,670 Da).

(D–F) Equilibrium distributions for TRIM5α$_{133–300}$ also fit a single-species dimer model (M = 2 × 20,238 Da = 40,476 Da).

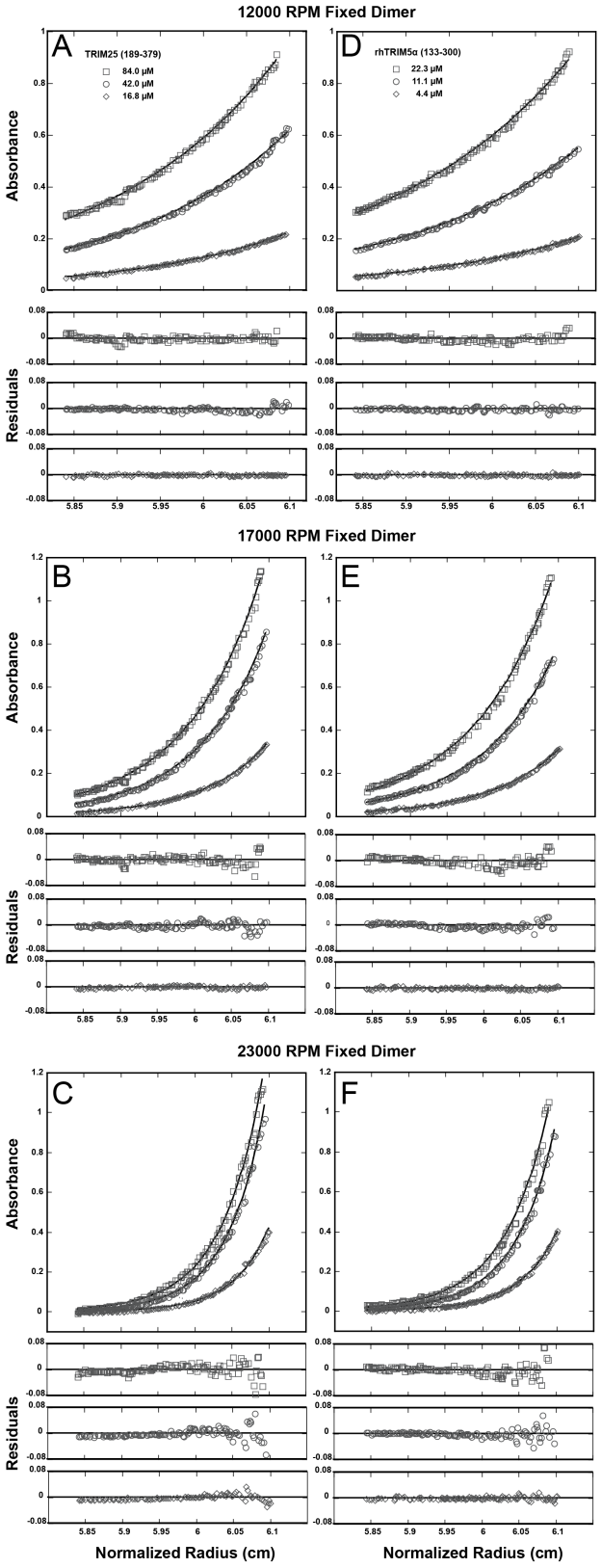
12000 RPM Fixed Dimer
A
TRIM25 (189-379)
84.0 μM
42.0 μM
16.8 μM
D
rhTRIM5α (133-300)
22.3 μM
11.1 μM
4.4 μM
17000 RPM Fixed Dimer
B
E
23000 RPM Fixed Dimer
C
F
Absorbance
Residuals
Normalized Radius (cm)
Normalized Radius (cm)

Fig. 3. Structure determination of TRIM25$_{189–379}$.

(A) Stereoview showing a section of the experimental 2mFo-DFc density modified map (blue mesh, 1.5σ) and anomalous Se difference map (magenta mesh, 8σ) overlaid with a Cα trace of the partially refined model for the selenomethionine data set. Residues shown are in the area surrounding Met209.

(B) Stereoview showing unbiased 2mFo-DFc density (magenta mesh, 1.5σ) after a round of rigid body and real space refinement (R = 0.45) of the molecular replacement solution (residues 195–200 for each subunit). Blue mesh shows 2mFo-DFc density (1σ) calculated with phases from the final, full model. Residues shown are in helix H3, which was not present in the initial molecular replacement model.

(C) Superposition of the TRIM25$_{189–379}$ heptad repeat regions with PDB accession no. 1CXZ chain B, which is a canonical left-handed antiparallel coiled-coil hairpin (14). The average root mean square deviation over 61 equivalent Cα atoms was 0.75 Å. The structure-based alignment with corresponding heptad assignments is indicated below.

(D) Superposition of the TRIM25$_{189–379}$ hendecad repeat regions with PDB accession no. 3VEM, which is an antiparallel dimer containing 4 hendecads (15). The average root mean square deviation over 90 equivalent Cα atoms was 1.42 Å. The structure-based alignment with corresponding hendecad assignments is indicated below.

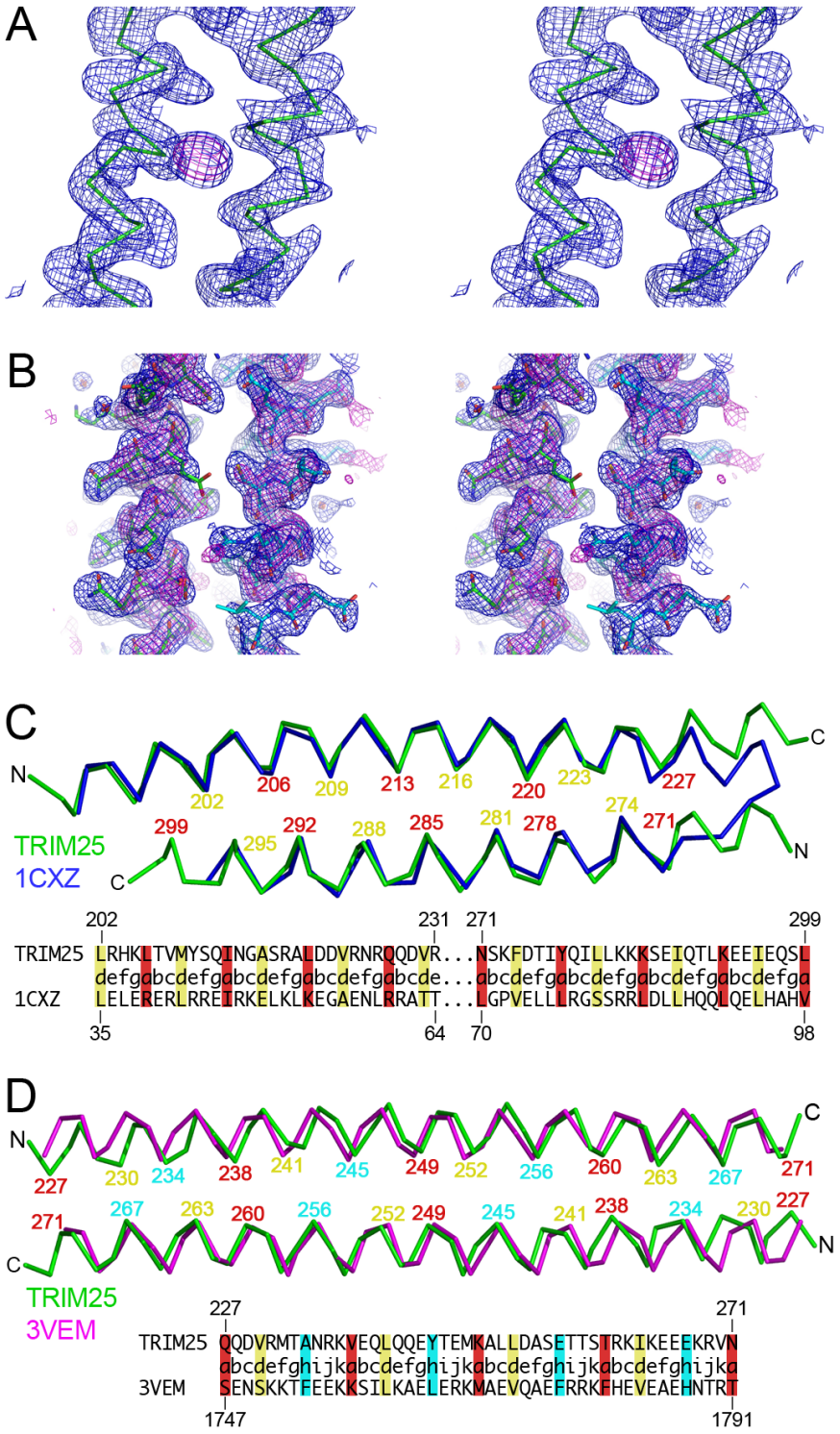
A
B
C
N
C
202
206
209
213
216
220
223
227
TRIM25
1CXZ
299
295
292
288
285
281
278
274
271
C
N
202
231
271
299
TRIM25 LRHKLTVMYSQINGASRALDDVRNRQQDVR...NSKFDTIYQILLKKKSEIQTLKEEIEQSL
defgabcdefgabcdefgabcdefgabcde...abcdefgabcdefgabcdefgabcdefga
1CXZ LELERERLRREIRKELKLKEGAENLRRATT...LGPVELLLRGSSRRLDLLHQQLQELHAHV
35
64
70
98
D
N
C
227
230
234
238
241
245
249
252
256
260
263
267
271
271
267
263
260
256
252
249
245
241
238
234
230
227
C
N
TRIM25
3VEM
227
271
TRIM25 QQDVRMTANRKVEQLQQEYTEMKALLDASETTSTRKIKEEEKRVN
abcdefghijkabcdefghijkabcdefghijkabcdefghijka
3VEM SENSKKTFEEKKSILKAELERKMAEVQAEFRRKFHEVEAEHNTRT
1747
1791

Table 1. Diffraction data and refinement statistics for $TRIM25_{189–379}$

	Se	Native
Diffraction		
Beamline	APS 22-ID	APS 22-ID
Wavelength (Å)	0.9791	1.000
Space group	$P2_12_12_1$	$P2_12_12_1$
Cell dimensions	a = 52.8 Å	a = 57.7 Å
	b = 69.6 Å	b = 83.2 Å
	c = 108.5 Å	c = 92.8 Å
	α = β = γ = 90°	α = β = γ = 90°
Resolution range (Å)	50–3.2 (3.31–3.2)	50–2.59 (2.69–2.59)
R_{sym}	0.12 (0.43)	0.14 (0.78)
Mean I/σ<I>	14.8 (2.3)	17.3 (2.2)
Completeness (%)	86.8 (46.7)	96.9 (81.4)
Average redundancy	11.0 (4.6)	13.1 (9.1)
Mosaicity range (°)	0.49–1.4	0.72–1.22
Wilson B-factor ($Å^2$)	65.5	43.6
Phasing		
Number of sites, expected/found	6/6	
Figure of merit	0.31	
Refinement		
Resolution range		42.2–2.59 (2.75–2.59)
No. of unique reflections		13,042 (892)
Reflections in free set		1,296 (94)
R_{work}		0.20 (0.30)
R_{free}		0.26 (0.38)
Number of nonhydrogen atoms		
Protein		2,778
Solvent		55
Average B-factor ($Å^2$)		
Protein		53.1
Solvent		47.7
Coordinate deviations		
Bond lengths (Å)		0.009
Bond angles (°)		1.17
Ramachandran plot		
Favored (%)		97
Outliers (%)		0
Molprobity clash score		4.07
Protein Data Bank ID		4LTB

Values in parenthesis are for the highest-resolution shell.

Fig. 4. Structure of the TRIM25$_{189–379}$ dimer.

(A) Orthogonal views of the dimer in ribbons representation, with the coiled-coil and L2 segments colored in green and gray, respectively (matching the color scheme of Fig. 1).

(B) Orthogonal views of the dimer with one subunit colored in rainbow gradient, with blue at the N-terminus and red at the C-terminus, and the other subunit in white.

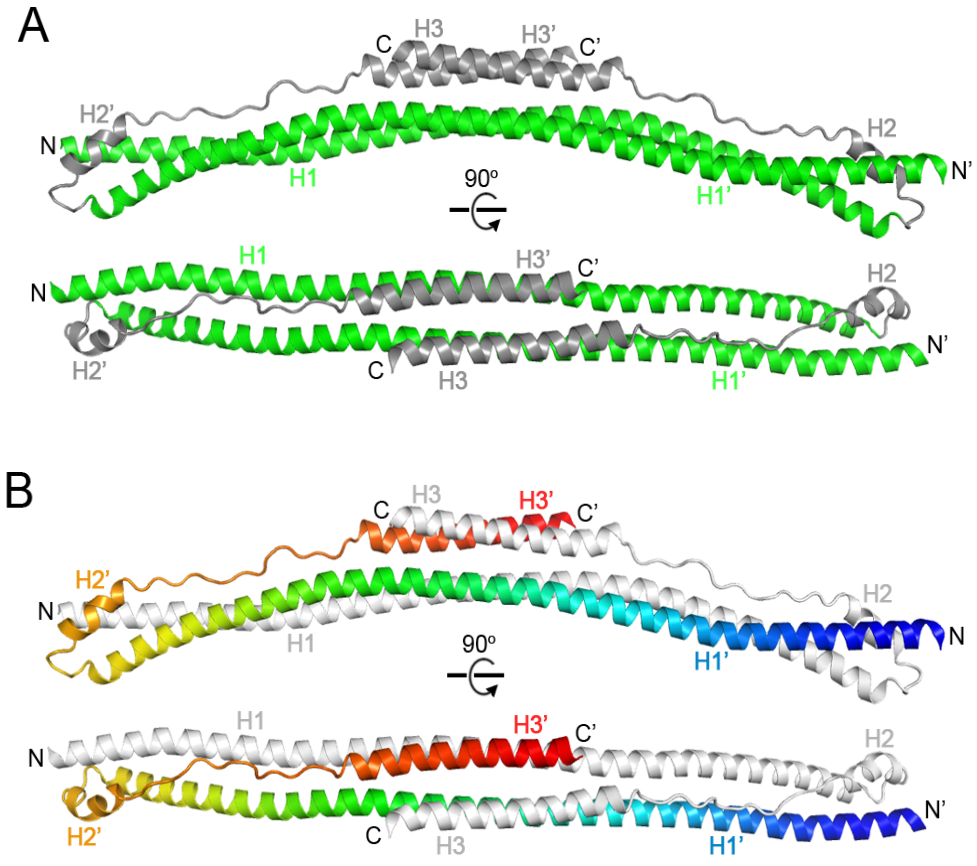
A
C
H3
H3'
C'
H2'
N
H2
N'
H1
90°
H1'
H1
H3'
C'
H2
N
N'
H2'
C
H3
H1'
B
C
H3
H3'
C'
H2'
N
H2
N
H1
90°
H1'
H1
H3'
C'
H2
N
H2'
C
H3
N'
H1'

structure reveals that these segments actually make up a single contiguous coil, helix H1, which forms the long arm of each subunit. The dimeric H1–H1′ interaction is mediated by classic “knobs-into-holes” packing of both heptad repeats (wherein amino acid residue positions in each repeat are denoted by the letters *abcdefg*) and hendecad repeats (*abcdefghijk*) (**Fig. 5, Fig. 3 C-D**). Residues in the h positions of the hendecads also form “knobs-to-knobs” interactions (21). The repeats are arranged in a symmetric 7-7-7-7-11-11-11-11-7-7-7-7 pattern, which produces a supercoil that is canonically left-handed at the ends but is underwound and slightly right-handed in the middle. This unusual configuration likely explains why sequence analysis programs failed to predict H1 as a single, contiguous coil. The hendecads mediate interactions at the center of the coiled-coil, and superhelical underwinding allows H1 and H1′ to sit side by side and form an amphipathic platform. Here, the terminal H3 helices from the short arm of each hairpin pack against one side of the platform to form a 4-helix bundle. Thus, the structure indicates that both ensuing C-terminal B30.2 domains will be centrally located on the same side of the dimer.

TRIM25 Dimerization Requires Hydrophobic Residues at the Center of the Coiled-Coil. The central region of the coiled-coil platform (boxed in **Fig. 5A,** expanded in **Fig. 5B**) has a particularly high density of intermolecular interactions because of tight packing of the H1 helices against one another and against the H3 helices (**Fig. 3**). Key H1–H1′ interactions in this region include the Leu252 side-chain, which packs against Tyr245′, Met248′, Lys249′, and the

Fig. 5. Dimeric packing of TRIM coiled-coil helices.

(A) Coiled-coil formed by the H1 and H1′ helices in the $TRIM25_{189–379}$ structure. Side-chains that mediate interhelix packing interactions are numbered and shown as spheres, with the *a, d*, and *h* positions colored in red, yellow, and cyan, respectively. Circled numbers indicate mutation sites analyzed in C. The dimer symmetry axis (black oval) runs perpendicular to the page.

(B) Expanded view of the central region boxed in A. Side-chains that mediate important packing interactions are shown as spheres, colored as in A and labeled, as are buried water molecules (orange).

(C) Thermofluor melting curves of wild-type (filled circles), L252A (open circles), M209A (filled diamonds), and V223A (filled squares). The high fluorescence signal for L252A at 25 °C indicates that the hydrophobic residues of this mutant are already exposed. Error bars represent the standard deviations from 4 replicates performed in parallel.

(D) Structure-to-sequence alignment. The graph shows a multiple sequence alignment of 54 different human TRIM coiled-coil/L2 sequences (see **Fig. 7**) displayed in logo format. The sequence alignment is overlaid with percentage buried surface area plots calculated using the entire $TRIM25_{189–379}$ structure (light gray bars) or the H1/H1′ helices only (dark gray bars). Heptad/hendecad residue assignments are color coded as in A. The TRIM25 sequence is shown at the top and the aligned TRIM5α sequence at the bottom, with the first and last residue numbers indicated.

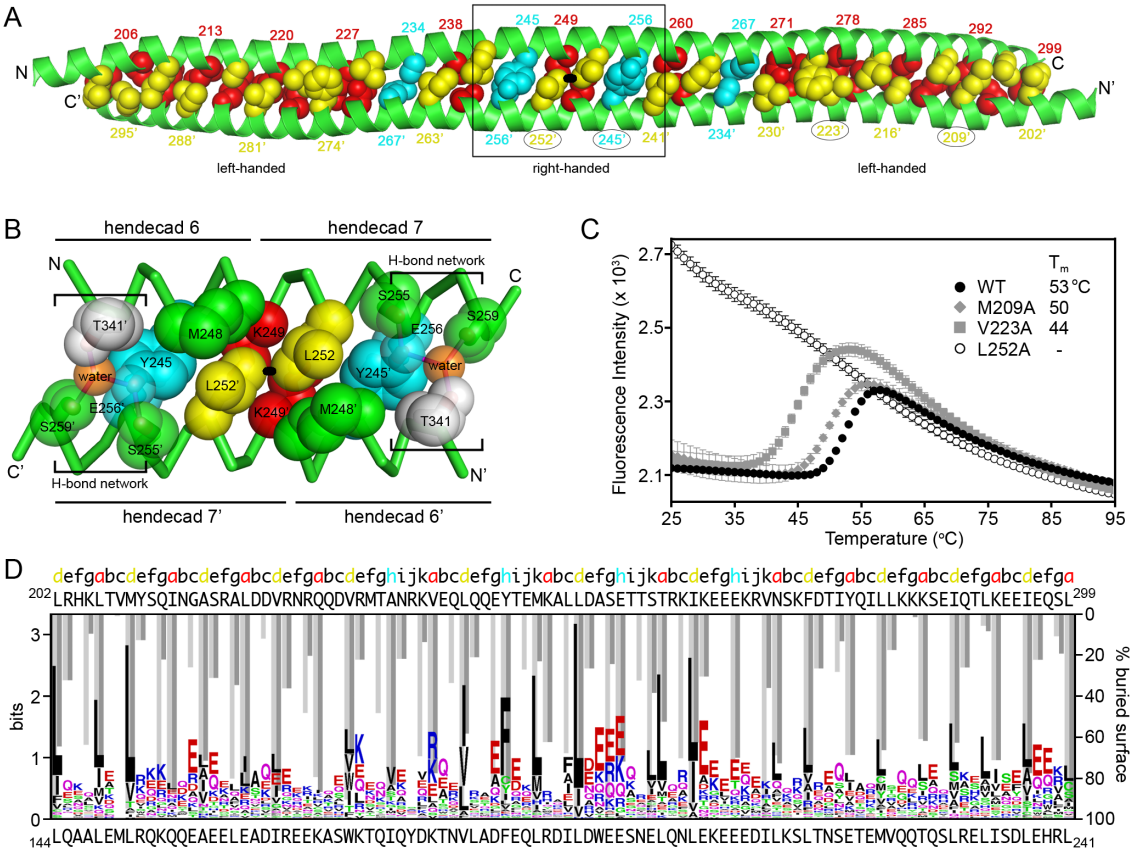
A
206
213
220
227
234
238
245
249
256
260
267
271
278
285
292
299
N
C
C'
N'
295'
288'
281'
274'
267'
263'
256'
252'
245'
241'
234'
230'
223'
216'
209'
202'
left-handed
right-handed
left-handed
B
hendecad 6
hendecad 7
N
C
H-bond network
T341'
M248
K249
L252
S255
E256
S259
Y245
water
L252'
Y245
water
E256'
K249'
M248'
T341
S259'
S255'
C'
N'
H-bond network
hendecad 7'
hendecad 6'
C
Fluorescence Intensity (x 10³)
2.7
2.5
2.3
2.1
25
35
45
55
65
75
85
95
Temperature (°C)
T_m
WT 53 °C
M209A 50
V223A 44
L252A -
D
defgabcdefgabcdefgabcdefgabcdefghijkabcdefghijkabcdefghijkabcdefghijkabcdefgabcdefgabcdefgabcdefga
202 LRHKLTVMYSQINGASRALDDVRNRQQDVRMTANRKVEQLQQEYTEMKALLDASETTSTRKIKEEEKRVNSKFDTIYQILLKKKSEIQTLKEEIEQSL 299
bits
3
2
1
0
% buried surface
0
20
40
60
80
100
144 LQAALEMLRQKQQEAEELEADIREEKASWKTQIQYDKTNVLADFEQLRDILDWEESNELQNLEKEEEDILKSLTNSETEMVQQTQSLRELISDLEHRL 241

symmetry equivalent Leu252′ in the apposing helix (**Fig. 5B**). This segment is further stabilized by salt bridges between the Lys249 and Asp253 side-chains and is flanked on either end by a buried hydrogen bond network (indicated by square brackets in **Fig. 5B**) involving the Tyr245 side-chain hydroxyl, a buried water molecule (orange sphere), Ser255 (H1′), Glu256 (H1′), Ser259 (H1′), Thr341 (H3′), and Gln356 (H3, not shown for clarity). This region therefore appears to be particularly important for dimer stability.

Coiled-coils represent a special case of protein folding in which formation of the hydrophobic core is coupled to oligomerization (dimerization in this case). We therefore used differential scanning fluorescence thermal melting assays to examine the coupled folding/dimerization transition. In this assay, the signal comes from a dye that fluoresces on binding hydrophobic side-chains that become exposed as the protein unfolds with in-creasing temperature (22). As shown in **Fig. 5C** (filled circles), wild-type $TRIM25_{189–397}$ displayed a typical coiled-coil differential scanning fluorescence profile with a single transition and an apparent melting temperature (T_m) of 53 °C. Consistent with the structure, the L252A mutant was difficult to purify and did not display a sigmoidal melting curve, indicating it was already unfolded (or misfolded), even at 25 °C (**Fig. 5C**, open circles). The Y245A mutant was also apparently misfolded and could not even be purified. In contrast, two control proteins with alanine substitutions for completely buried residues elsewhere in H1 (M209A and V223A) were properly folded, albeit with reduced stability (**Fig. 5C**, gray symbols). These results confirm that the

center of the coiled-coil helix is critical for proper folding of the TRIM25 dimer, perhaps making up the “trigger site” that directs coiled-coil formation (23–25).

This central region of TRIM25 is also where the terminal H3 helices pack to form the 4-helix bundle and contribute hydrophobic residues to the compact core. Unlike H1 mutants, however, alanine substitutions in buried hydrophobic H3 residues (T341A, L344A, and L348A) did not prevent $TRIM25_{189–379}$ coiled-coil formation (**Fig. 6A**). These results are consistent with the observation that TRIM5 protein dimerization requires only the coiled-coil domain and that both upstream (RING and B-boxes) and downstream (L2 equivalents and beyond) elements are dispensable (8, 19, 26, 27). Thus, even though the coiled-coil and L2 regions appear to form an integrated “domain” in our structure, the L2 segment is apparently not critical for dimerization and may be dynamic. Consistent with this idea, the average temperature factor for the short arm was 15% higher than the long arm in the native structure. In the selenomethionine crystal, one of the L2 arms had extremely poor density, likely because it had dissociated from the coiled-coil (**Fig. 6B**).

The H1 Coiled-Coil Heptad/Hendecad Pattern Is Conserved in the TRIM Family. The TRIM25 coiled-coil sequence diverges significantly from other human TRIM proteins (e.g., TRIM25 and TRIM5α share only ~10% sequence identity in this region). Nevertheless, our analysis of the human TRIM family using the secondary structure prediction program JPRED (28) indicated that the putative coiled-coil regions of most TRIM proteins are embedded within a contiguous helix of about 110 amino acids, consistent with the TRIM25

Fig. 6. Analysis of L2 packing against the coiled-coil.

(A) Differential scanning fluorimetry melting profiles of H3 mutants: T341A (blue), L344A (green), and L348A (red). The wild-type curve is in black.

(B) Electron density (magenta mesh, 1.2σ) for the selenomethionine-labeled crystal after multiple rounds of model building and refinement. Note the poor density for one of the H3 helices (Upper, labeled in cyan).

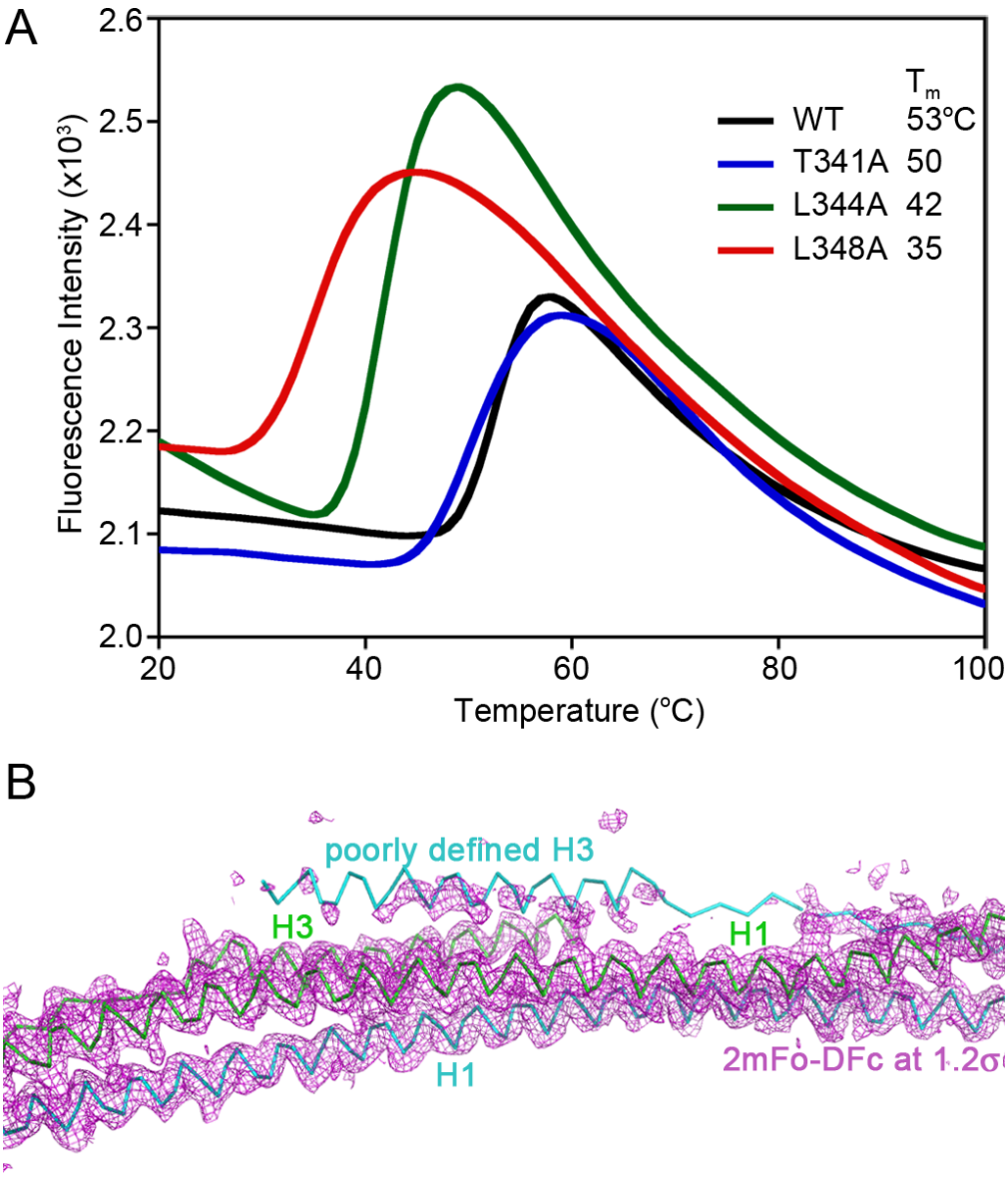
A
2.6
2.5
2.4
2.3
2.2
2.1
2.0
Fluorescence Intensity (x10³)
20
40
60
80
100
Temperature (°C)
T_m
WT 53°C
T341A 50
L344A 42
L348A 35
B
poorly defined H3
H3
H1
H1
2mFo-DFc at 1.2σ

structure. To align these regions, we performed a structure-to-sequence comparison by first generating a multiple sequence alignment (MSA) of the coiled-coil regions of 54 different human TRIM family members (**Fig. 7**). The alignment revealed a pattern of conserved hydrophobic amino acids, with leucine being the most highly represented residue. We next calculated and plotted the percentage buried surface area (BSA) for each residue in the H1/H1′ portion of the TRIM25 structure (i.e., not including the L2 arms) and aligned this plot with the MSA. As shown in **Fig. 5D**, there is excellent correspondence between the pattern of conserved hydrophobic positions in the MSA plot and the *a*, *d*, and *h* positions that mediate formation of the H1/H1′ dimer (dark gray bars; see also **Fig. 7**). These results indicate that the unusual pattern of heptad and hendecad repeats is conserved across the TRIM protein family and that the structures of other dimeric TRIM coiled-coils likely resemble the TRIM25 structure.

We also calculated a BSA plot for the entire structure (**Fig. 5D**, light gray bars). Comparison of the two BSA plots revealed that packing of the long and short arms of the TRIM25 subunits is mediated by H1 residues in the *c, g,* and *k* positions. Importantly, these residues are also conserved in the MSA, particularly at the center of the dimer (e.g., Glu244, Met248, Leu251). These results indicate that the hairpin configuration of the subunits and the central 4-helix bundle are also likely to be conserved.

TRIM5α and TRIM25 Have Similar Dimer Architectures. The 17-nm length of the $TRIM25_{189–379}$ dimer corresponds almost exactly to the length of each edge of the assembled TRIM5α hexagon (18), suggesting that the TRIM25

Fig. 7. **Multiple sequence alignment of the coiled-coil domains from 54 human TRIM family members, corresponding to the H1 and H2 helices in the TRIM25 structure.**

The corresponding TRIM25 sequence, secondary structure, H1 heptad/hendecad assignments, and residue numbers are shown at the top for reference. Residues shaded in black indicate side-chains in the TRIM25 structure that bury 60% or more of their available surface area within the H1–H1′ dimer interface (corresponding to dark gray bars in **Fig. 5D**). Residues shaded in gray are at least 60% buried within the entire $TRIM25_{189–379}$ structure (light gray bars in **Fig. 5D**) and also mediate packing of L2 against H1. The *a*, *d*, and *h* positions are shaded as in **Fig. 3** and **Fig. 5**. The last zinc-coordinating His/Cys pairs of the B-box 2 domains are shaded in green for reference. Colored dots indicate cysteine substitution sites in **Fig. 8**. TRIM family branch groupings (16) are indicated by square brackets on the left.

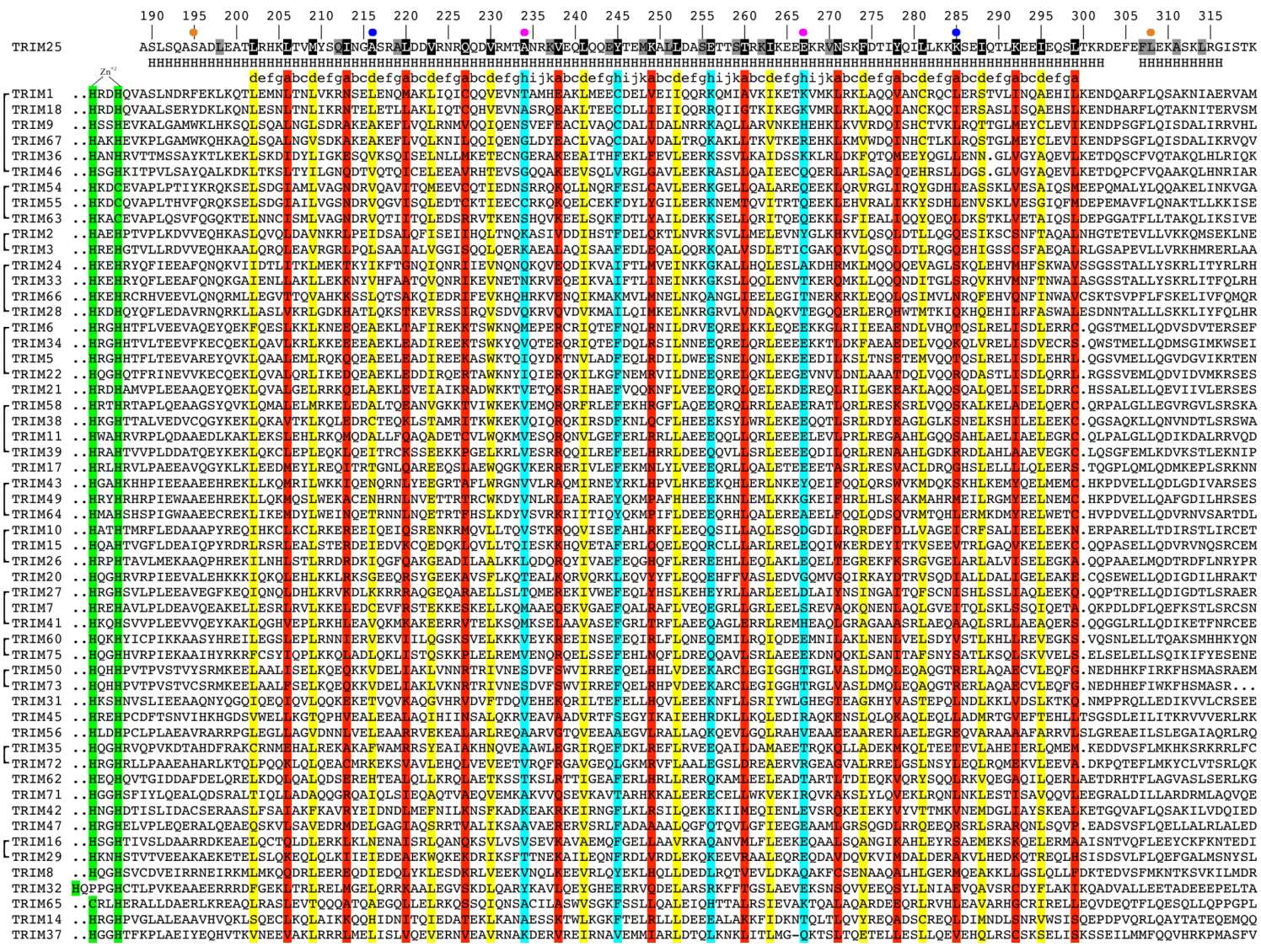
190 195 200 205 210 215 220 225 230 235 240 245 250 255 260 265 270 275 280 285 290 295 300 305 310 315
TRIM25 ASLSQASADLEATLRHKLTVMYSQINGASRALDDVRNRQQDVRMTANRKVEQLQQEYTEMKALLDASETTSTRKIKEEEKRVNSKFDTIVQILLKKKSEIQTLKEEIEQSLTKRDEFEFLEKASKLRGISTK
Zn+2
TRIM1 ..HRDHQVASLNDRFEKLKQTLEMNLTNLVKRNSELENQMAKLIQICQQVEVNTAMHEAKLMEECDELVEIIQQRKQMIAVKIKETKVMKLRKLAQQVANCRQCLERSTVLINQAEHILKENDQARFLQSAKNIAERVAM
TRIM18 ..HRDHQVAALSERYDKLKQNLESNLTNLIKRNTELETLLAKLIQTCQHVEVNASRQEAKLTEECDLLIEIIQQRKQIIGTKIKEGKVMRLRKLAQQIANCKQCIERSASLISQAEHSLKENDQARFLQTAKNITERVSM
TRIM9 ..HSSHEVKALGAMWKLHKSQLSQALNGLSDRAKEAKEFLVQLRNMVQQIQENSVEFEACLVAQCDALIDALNRRKAQLLARVNKEHEHKLKVVRDQISHCTVKLRQTTGLMEYCLEVIKENDPSGFLQISDALIRRVHL
TRIM67 ..HAKHEVKPLGAMWKQHKAQLSQALNGVSDKAKEAKEFLVQLKNILQQIQENGLDYEACLVAQCDALVDALTRQKAKLLTKVTKEREHKLKMVWDQINHCTLKLRQSTGLMEYCLEVIKENDPSGFLQISDALIKRVQV
TRIM36 ..HANHRVTTMSSAYKTLKEKLSKDIDYLIGKESQVKSQISELNLLMKETECNGERAKEEAITHFEKLFEVLEERKSSVLKAIDSSKKLRLDKFQTQMEEYQGLLENN.GLWGYAQEVLKETDQSCFVQTAKQLHLRIQK
TRIM46 ..HSGHKITPVLSAYQALKDKLTKSLTYILGNQDTVQTQICELEEAVRHTEVSGQQAKEEVSQLVRGLGAVLEEKRASLLQAIEECQQERLARLSAQIQEHRSLLDGS.GLWGYAQEVLKETDQPCFVQAAKQLHNRIAR
TRIM54 ..HKDCEVAPLPTIYKRQKSELSDGIAMLVAGNDRVQAVITQMEEVCQTIEDNSRRQKQLLNQRFESLCAVLEERKGELLQALAREQEEKLQRVRGLIRQYGDHLEASSKLVESAIQSMEEPQMALYLQQAKELINKVGA
TRIM55 ..HKDCQVAPLTHVFQRQKSELSDGIAILVGSNDRVQGVISQLEDTCKTIEECCRKQKQELCEKFDYLYGILEERKNEMTQVITRTQEEKLEHVRALIKKYSDHLENVSKLVESGIQFMDEPEMAVFLQNAKTLLKKISE
TRIM63 ..HKACEVAPLQSVFQGQKTELNNCISMLVAGNDRVQTIITQLEDSRRVTKENSHQVKEELSQKFDTLYAILDEKKSELLQRITQEQEKKLSFIEALIQQYQEQLDKSTKLVETAIQSLDEPGGATFLLTAKQLIKSIVE
TRIM2 ..HAEHPTVPLKDVVEQHKASLQVQLDAVNKRLPEIDSALQFISEIIHQLTNQKASIVDDIHSTFDELQKTLNVRKSVLLMELEVNYGLKHKVLQSQLDTLLQGQESIKSCSNFTAQALNHGTETEVLLVKKQMSEKLNE
TRIM3 ..HREHGTVLLRDVVEQHKAALQRQLEAVRGRLPQLSAAIALVGGISQQLQERKAEALAQISAAFEDLEQALQQRKQALVSDLETICGAKQKVLQSQLDTLRQGQEHIGSSCSFAEQALRLGSAPEVLLVRKHMRERLAA
TRIM24 ..HKEHRYQFIEEAFQNQKVIIDTLITKLMEKTKYIKFTGNQIQNRIIEVNQNQKQVEQDIKVAIFTLMVEINKKGKALLHQLESLAKDHRMKLMQQQQEVAGLSKQLEHVMHFSKWAVSSGSSTALLYSKRLITYRLRH
TRIM33 ..HKEHRYQFLEEAFQNQKGAIENLLAKLLEKKNYVHFAATQVQNRIKEVNETNKRVEQEIKVAIFTLINEINKKGKSLLQQLENVTKERQMKLLQQQNDITGLSRQVKHVMNFTNWALASGSSTALLYSKRLITFQLRH
TRIM66 ..HKEHRCRHVEEVLQNQRMLLEGVTTQVAHKKSSLQTSAKQIEDRIFEVKHQHRKVENQIKMAKMVLMNELNKQANGLIEELEGITNERKRKLEQQLQSIMVLNRQFEHVQNFINWAVCSKTSVPFLFSKELIVFQMQR
TRIM28 ..HKDHQYQFLEDAVRNQRKLLASLVKRLGDKHATLQKSTKEVRSSIRQVSDVQKRVQVDVKMAILQIMKELNKRGRVLVNDAQKVTEGQQERLERQHWTMTKIQKHQEHILRFASWALESDNNTALLLSKKLIYFQLHR
TRIM6 ..HRGHHTFLVEEVAQEYQEKFQESLKKLKNEEQEAEKLTAFIREKKTSWKNQMEPERCRIQTEFNQLRNILDRVEQRELKKLEQEEKKGLRIIEEAENDLVHQTQSLRELISDLERRC.QGSTMELLQDVSDVTERSEF
TRIM34 ..HRGHHTVLTEEVFKECQEKLQAVLKRLKKEEEEAEKLEADIREEKTSWKYQVQTERQRIQTEFDQLRSILNNEQRELQRLEEEEKKTLDKFAEAEDELVQQKQLVRELISDVECRS.QWSTMELLQDMSGIMKWSEI
TRIM5 ..HRGHHTFLTEEVAREYQVKLQAALEMLRQKQQEAEELEADIREEKASWKTQIQYDKTNVLADFEQLRDILDWEESNELQNLEKEEEDILKSLTNSETEMVQQTQSLRELISDLEHRL.QGSVMELLQGVDGVIKRTEN
TRIM22 ..HQGHQTFRINEVVKECQEKLQVALQRLIKEDQEAEKLEDDIRQERTAWKNYIQIERQKILKGFNEMRVILDNEEQRELQKLEEGEVNVLDNLAAATDQLVQQRQDASTLISDLQRRL.RGSSVEMLQDVIDVMKRSES
TRIM21 ..HRDHAMVPLEEAAQEYQEKLQVALGELRRKQELAEKLEVEIAIKRADWKKTVETQKSRIHAEFVQQKNFLVEEEQRQLQELEKDEREQLRILGEKEAKLAQQSQALQELISELDRRC.HSSALELLQEVIIVLERSES
TRIM58 ..HRTHRTAPLQEAAGSYQVKLQMALELMRKELEDALTQEANVGKKTVIWKEKVEMQRQRFRLEFEKHRGFLAQEEQRQLRRLEAEERATLQRLRESKSRLVQQSKALKELADELQERC.QRPALGLLEGVRGVLSRSKA
TRIM38 ..HKGHTTALVEDVCQGYKEKLQKAVTKLKQLEDRCTEQKLSTAMRITKWKEKVQIQRQKIRSDFKNLQCFLHEEEKSYLWRLEKEEQQTLSRLRDYEAGLGLKSNELKSHILELEEKC.QGSAQKLLQNVNDTLSRSWA
TRIM11 ..HWAHRVRPLQDAAEDLKAKLEKSLEHLRKQMQDALLFQAQADETCVLWQKMVESQRQNVLGEFERLRRLLAEEEQQLLQRLEEEELEVLPRLREGAAHLGQQSAHLAELLAELEGRC.QLPALGLLQDIKDALRRVQD
TRIM39 ..HRAHTVVPLDDATQEYKEKLQKCLEPLEQKLQEITRCKSSEEKKPGELKRLVESRRQQILREFEELHRRLDEEQQVLLSRLEEEEQDILQRLRENAAHLGDKRRDLAHLAAEVEGKC.LQSGFEMLKDVKSTLEKNIP
TRIM17 ..HRLHRVLPAEEAVQGYKLKLEEDMEYLREQITRTGNLQAREEQSLAEWQGKVKERRERIVLEFEKMNLYLVEEEQRLLQALETETEEETASRLRESVACLDRQGHSLELLLLQLEERS.TQGPLQMLQDMKEPLSRKNN
TRIM43 ..HGAHKHHPIEEAAEEHREKLLKQMRILWKKIQENQRNLYEEGRTAFLWRGNVVLRAQMIRNEYRKLHPVLHKEEKQHLERLNKEYQEIFQQLQRSWVKMDQKSKHLKEMYQELMEMC.HKPDVELLQDLGDIVARSES
TRIM49 ..HRYHRHRPIEWAAEEHREKLLQKMQSLWEKACENHRNLNVETTRTRCWKDYVNLRLEAIRAEYQKMPAFHHEEEKHNLEMLKKKGKEIPHRLHLSKAKMAHRMEILRGMYEELNEMC.HKPDVELLQAFGDILHRSES
TRIM64 ..HMAHSHSPIGWAAEECREKLIKEMDYLWEINQETRNNLNQETRTFHSLKDYVSVRKRIITIQYQKMPIFLDEEEQRHLQALEREAEELFQQLQDSQVRMTQHLERMKDMYRELWETC.HVPDVELLQDVRNVSARTDL
TRIM10 ..HATHTMRFLEDAAAPYREQIHKCLKCLRKEREEIQEIQSRENKRMQVLLTQVSTKRQQVISEFAHLRKFLEEQQSILAQLESQDGDILRQRDEFDLLVAGEICRFSALIEELEEKN.ERPARELLTDIRSTLIRCET
TRIM15 ..HQAHTVGFLDEAIQPYRDRLRSRLEALSTERDEIEDVKCQEDQKLQVLLTQIESKKHQVETAFERLQQELEQQRCLLLARLRELEQQIWKERDEYITKVSEEVTRLGAQVKELEEKC.QQPASELLQDVRVNQSRCEM
TRIM26 ..HRPHTAVLMEKAAQPHREKILNHLSTLRRDRDKIQGFQAKGEADILAALKKLQDQRQYIVAEFEQGHQFLREREEHLLEQLAKLEQELTEGREKFKSRGVGELARLALVISELEGKA.QQPAAELMQDTRDFLNRYPR
TRIM20 ..HQGHRVRPIEEVALEHKKKIQKQLEHLKKLRKSGEEQRSYGEEKAVSFLKQTEALKQRVQRKLEQVYFLEQQEHFFVASLEDVGQMVGQIRKAYDTRVSQDILALLDALIGELEAKE.CQSEWELLQDIGDILHRAKT
TRIM27 ..HRGHSVLPLEEAVEGFKEQIQNQLDHLKRVKDLKKRRRAQGEQARAELLSLTQMERKIVWEFEQLYHSLKEHEYRLLARLEELDLAIYNSINGAITQFSCNISHLSSLLAQLEEKQ.QQPTRELLQDIGDTLSRAER
TRIM7 ..HREHAVLPLDEAVQEAKELLESRLRVLKKELEDCEVFRSTEKKESKELLKQMAAEQEKVGAEFQALRAFLVEQEGRLLGRLEELSREVAQKQNENLAQLGVETTQLSKLSSQIQETA.QKPDLDFLQEFKSTLSRCSN
TRIM41 ..HKQHSVVPLEEVVQEYKAKLQGHVEPLRKHLEAVQKMKAKEERRVTELKSQMKSELAAVASEFGRLTRFLAEEQAGLERRLREMHEAQLGRAGAAASRLAEQAAQLSRLLAEAQERS.QQGGLRLLQDIKETFNRCEE
TRIM60 ..HQKHYICPIKKAASYHREILEGSLEPLRNNIERVEKVIILQGSKSVELKKKVEYKREEINSEFEQIRLFLQNEQEMILRQIQDEEMNILAKLNENLVELSDYVSTLKHLLREVEGKS.VQSNLELLTQAKSMHHKYQN
TRIM75 ..HQGHHVRPIEKAAIHYRKRFCSYIQPLKKQLADLQKLISTQSKKPLELREMVENQRQELSSEFEHLNQFLDREQQAVLSRLAEEEKDNQQKLSANITAFSNYSSATLKSQLSKVVELS.ELSELELLSQIKIFYESENE
TRIM50 ..HQHHPVTPVSTVYSRMKEELAALISELKQEQKKVDELLAKLVNNRTRIVNESDVFSWVIRREFQELHHLVDEEKARCLEGIGGHTRGLVASLDMQLEQAQGTRERLAQAECVLEQFG.NEDHHKFIRKFHSMASRAEM
TRIM73 ..HQHHPVTPVSTVCSRMKEELAALFSELKQEQKKVDELLAKLVKNRTRIVNESDVFSWVIRREFQELRHPVDEEKARCLEGIGGHTRGLVASLDMQLEQAQGTRERLAQAECVLEQFG.NEDHHEFIWKFHSMASR...
TRIM31 ..HKSHNVSLIEEAAQNYQGQIQEQIQVLQQKEKETVQVKAQGVHRVDVFTDQVEEKQRILTEFELLHQVLEEEKNFLLSRIYWLGHEGTEAGKHYVASTEPQLNDLKKLVDSLKTKQ.NMPPRQLLEDIKVVLCRSEE
TRIM45 ..HREHPCDFTSNVIHKHGDSVWELLKGTQPHVEALEEALAQIHIINSALQKRVEAVAADVRTFSEGYIKAIEEHRDKLLKQLEDIRAQKENSLQLQKAQLEQLLADMRTGVEFTEHLLTSGSDLEILITKRVVVERLRK
TRIM56 ..HLDHPCLPLAEAVRARRPGLEGLLAGVDNNLVELEAARRVEKEALARLREQAARVGTQVEEAAEGVLRALLAQKQEVLGQLRAHVEAAEEAARERLAELEGREQVARAAAAFARRVLSLGREAEILSLEGAIAQRLRQ
TRIM35 ..HQGHRVQPVKDTAHDFRAKCRNMEHALREKAKAFWAMRRSYEAIAKHNQVEAAWDRIQEFDKLREFLRVEEQAILDAMAEETRQKQLLADEKMKQLTEETEVLAHEIERLQMEM.KEDKVSFLMKHKSRKRRLFC
TRIM72 ..HRGHRLLPAAEAHARLKTQLPQQKLQLQEACMRKEKSVAVLEHQLVEVEETVRQFRGAVGEQLGKMRVVFLAALEGSLDREAERVRGEAGVALRREIGSLNSYLEQLRQMEKVLEEVA.DKPQTEFLMKYCLVTSRLQK
TRIM62 ..HEQHQVTGIDDAFDELQRELKDQLQALQDSEREHTEALQLLKRQLAETKSSTKSLRTTIGEAFERLHRLLRERQKAMLEELEADTARTLTDIEQKVQRYSQQLRKVQEGAQILQERLAETDRHTFLAGVASLSERLKG
TRIM71 ..HGGHSFIYLQEALQDSRALTIQLLADAQQGRQAIQLSIEQAQTVAEQVEMKAKVVQSEVKAVTARHKKALEERECELLWKVEKIRQVKLASKLYLQVEKLRQNLNKLESTISAVQQVLEEGRALDILLARDRMLAQVQE
TRIM42 ..HNGHDTISLIDACSERAASLFSAIAKFKAVRYEIDNDLMEFNILKNSFKADKEAKRKEIRNGFLKLRSILQEKEKIIMEQIENLEVSRQKEIEKYYVYTTMKVNEMDGLIAYSKEALKETGQVAFLQSAKILVDQIED
TRIM47 ..HRGHELVPLEQERALQEAEQSKVLSAVEDRMDELGAGIAQSRRTVALIKSAAVAERERVSRLFADAAAALQGFQTQVLGFIEEGEAAMLGRSQGDLRRQEEQRSRLSRARQNLSQVP.EADSVSFLQELLALRLALED
TRIM16 ..HSGHTIVSLDAARRDKEAELQCTQLDLERKKLNENAISRLQANQKSVLVSVSEVKAVAEMQFGELLAAVRKAQANVMLFLEEKEQAALSQANGIKAHLEYYSAEMEKSKQELERMAAISNTVQFLEEYCKFKNTEDI
TRIM29 ..HKNHSTVTVEEAKAEKETELSLQKEQLQLKIIEIEDEAEKWQKEKDRIKSFTTNEKAILEQNFRDLVRDLEKQKEEVRAALEQREQDAVDQVKVIMDALDERAKVLHEDKQTREQLHSISDSVLFLQEFGALMSNYSL
TRIM8 ..HQGHSVCDVEIRRNEIRKMLMKQQDRLEERERQDIEDQLYKLESDKRLVEEKVNQLKEEVRLQYEKLHQLLDEDLRQTVEVLDKAQAKFCSENAAQALHLGERMQEAKKLLGSLQLLFDKTEDVSFMKNTKSVKILMDR
TRIM32 HQPPGHCTLPVKEAAEERRRDFGEKLTRLRELMGELQRRKAALEGVSKDLQARYKAVLQEYGHEERRVQDELARSRKFFTGSLAEVEKSNSQVVEEQSYLLNIAEVQAVSRQDYFLAKIKQADVALLEETADEEEPELTA
TRIM65 ..CRLHERALLDAERLKREAQLRASLEVTQQQATQAEGQLLELRKQSSQIQNSACILASWVSGKFSSLLQALEIQHTTALRSIEVAKTQALAQARDEEQRLRVHLEAVARHGCRIRELLEQVDEQTFLQESQLLQPPGPL
TRIM14 ..HRGHPVGLALEAAVHVQKLSQECLKQLAIKKQQHIDNITQIEDATEKLKANAESSKTWLKGKFTELRLLLDEEEALAKKFIDKNTQLTLQVYREQADSCREQLDIMNDLSNRVWSISQEPDPVQRLQAYTATEQEMQQ
TRIM37 ..HGGHTFKPLAEIYEQHVTKVNEEVAKLRRRLMELISLVQEVERNVEAVRNAKDERVREIRNAVEMMIARLDTQLKNKLITLMG-QKTSLTQETELLESLLQEVEHQLRSCSKSELISKSSEILMMFQQVHRKPMASFV

structure can also inform our understanding of the TRIM5α hexagonal lattice. Intermolecular disulfide bond formation was used to probe and compare the structures of the TRIM25 and TRIM5α dimers in solution. The $TRIM25_{189–379}$ crystal structure was analyzed using a disulfide prediction program (29) to identify three pairs of residues that are in close proximity in the dimer and are predicted to form intermolecular disulfides when mutated into cysteines (**Fig. 8A**). Two of the designed disulfides, A216C/K285C and A234C/E267C, probe for packing and phase of the H1/H1′ helices (i.e., antiparallel coiled-coil formation), and the third, S195C/L308C, probes for packing of H1 in one subunit against H2 in the other subunit (i.e., the fold-back configuration). These disulfide bonds collectively sample the entire length of the dimer (**Fig. 8A**).

As shown in **Fig. 8B**, all three double-cysteine mutant $TRIM25_{189–379}$ proteins behaved as designed. Each formed intermolecular disulfide crosslinks very efficiently under nonreducing conditions and migrated exclusively as crosslinked dimers on a denaturing polyacrylamide gel (lanes 7, 9, and 11). In contrast, three negative controls that contained scrambled pairs of cysteines migrated almost exclusively as monomers under the same conditions (**Fig. 8B**, even-numbered lanes). Thus, disulfide crosslinking can be used as a sensitive probe of the dimeric conformation of TRIM25.

Analogous disulfide crosslinking experiments were performed on rhesus $TRIM5α_{133–300}$ to test whether the TRIM5α protein also adopts a similar dimeric structure. Equilibrium sedimentation distributions of the wild-type $TRIM5α_{133–300}$ fit well to a single-species dimer model, confirming that this region was sufficient

Fig. 8. Disulfide crosslinking of TRIM25 and TRIM5α dimers.

(A) H1 and H2 regions of the $TRIM25_{189–379}$ structure showing positions of residue pairs chosen for cysteine mutagenesis. Equivalent TRIM25 and TRIM5α residues are labeled in black and gray, respectively.

(B) Electrophoretic profiles of purified $TRIM25_{189–379}$ double-cysteine mutants that were dialyzed under nonreducing conditions, then denatured in SDS-PAGE buffer under reducing (Left) or nonreducing (Right) conditions. Molecular weight marker positions are labeled on the left. Positions of monomers and crosslinked dimers are labeled on the right. Note that the symmetric dimer is expected to produce two types of intermolecular disulfide-crosslinked species: one in which both cysteine pairs are oxidized (lower bands) and another in which one of the pairs is reduced (upper bands). Data are representative of 3 independent experiments.

(C) Profiles of rhesus $TRIM5α_{133–300}$ cysteine mutants that were dialyzed under mildly reducing conditions and then prepared for SDS-PAGE, as described for $TRIM25_{189–379}$. Data are representative of 3 independent experiments.

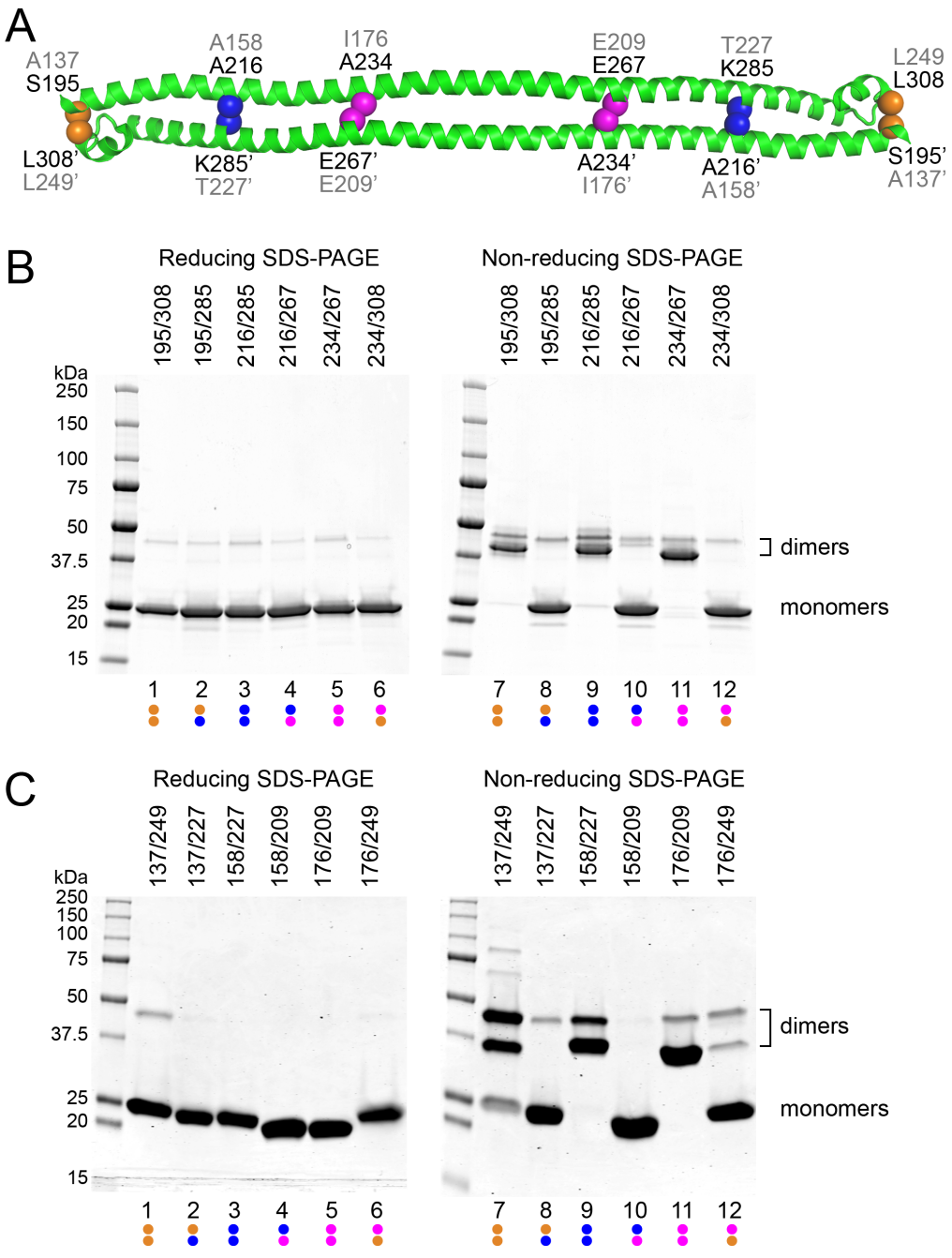
A
A137
S195
A158
A216
I176
A234
E209
E267
T227
K285
L249
L308
L308'
L249'
K285'
T227'
E267'
E209'
A234'
I176'
A216'
A158'
S195'
A137'
B
Reducing SDS-PAGE
Non-reducing SDS-PAGE
195/308
195/285
216/285
216/267
234/267
234/308
kDa
250
150
100
75
50
37.5
25
20
15
dimers
monomers
1
2
3
4
5
6
7
8
9
10
11
12
C
Reducing SDS-PAGE
Non-reducing SDS-PAGE
137/249
137/227
158/227
158/209
176/209
176/249
kDa
250
150
100
75
50
37.5
25
20
15
dimers
monomers
1
2
3
4
5
6
7
8
9
10
11
12

for dimerization (**Fig. 1D; Fig. 2 D-F**). Three pairs of TRIM5α$_{133–300}$ cysteine mutants were then created in positions that were equivalent to the three crosslinking pairs of TRIM25$_{189–379}$ (**Fig. 8A**). As shown in **Fig. 8C**, these TRIM5α$_{133–300}$ Cys pairs also formed intermolecular disulfides efficiently (lanes 7, 9, and 11), although the A137C/L249C disulfide crosslink formed somewhat less efficiently than did the A158C/T227C and I176C/E209C crosslinks, suggesting that H2 may not reside in precisely the same position in TRIM25 and TRIM5α. The crosslinks were judged to be stable because the proteins migrated almost exclusively as dimers, even after extended incubation under mildly reducing conditions (2 mM β-mercaptoethanol), consistent with the favorable disulfide geometries predicted by the homology model. We therefore conclude that TRIM5α and TRIM25 form dimers of similar structure.

DISCUSSION

Mechanistic Implications for TRIM25-Mediated Polyubiquitylation of RIG-I. TRIM25 is an established effector of the RIG-I signaling pathway, which mediates the intracellular innate immune response to RNA viruses. TRIM25 recognizes and catalyzes Lys63-linked polyubiquitylation of the RIG-I/viral RNA recognition complex, thereby activating downstream effectors in the pathway and establishing an antiviral state (3). RIG-I/viral RNA complexes are recognized by the C-terminal B30.2 domain of TRIM25 (3, 30), and ubiquitin transfer is facilitated by the N-terminal RING domain, in cooperation with a ubiquitin E2 ligase. Our structure indicates that in the full-length TRIM25 dimer, the two

catalytic RING domains will be separated by at least 17 nm at either end of the elongated dimer (**Fig. 9**). In this geometry, the two RING domains within one TRIM25 dimer probably could not cooperate during catalysis, at least not in the same manner as well-characterized cooperative homodimeric RING domains such as RNF4 (31) or BIRC7 (32). As illustrated in **Fig. 9**, the fold-back configuration of the TRIM25 subunits explains how the RING domains can approach the B30.2 domains to enable RIG-I ubiquitylation. It is likely, however, that there is a more precise positioning mechanism than we can currently describe, as TRIM25 has been shown to modify RIG-I at a specific lysine residue (3, 30). We speculate that dynamics of the L2 arm (including possibly the L2 region that is missing from our structure) and other factors (33, 34) may make important contributions in this regard. In addition, RNA-bound RIG-I has been shown to dimerize (35). It will therefore be interesting to learn whether both subunits of the TRIM25 dimer can engage both subunits of the RIG-I dimer simultaneously.

Implications for Dimerization of the Tripartite Motif. Our analysis indicates that TRIM25 is likely to be an obligate dimer. Furthermore, the distinctive 7-7-7-7-11-11-11-11-7-7-7-7 pattern of heptad and hendecad repeats in the TRIM25 coiled-coil appears to be conserved, and we speculate that it may be a “signature” of the TRIM family. Studies of dimeric coiled-coils have shown that short sequence elements or “trigger sites” of 7–14 amino acids are critically important for proper folding because they are the first segments to become

Fig. 9. Model for coiled-coil mediated coupling of the TRIM25 RING and B30.2 domains to facilitate RIG-I polyubiquitylation.

The tandem B-boxes are likely to form an integrated unit by analogy to the structure of homologous domains from MID1/TRIM18 (17). We assume that the B-box 2 domain is closely associated with the coiled-coil on the basis of their sequence connectivity. The connecting linker (L1) between the RING domain and the B-box domain is shown as dashes because its configuration is unknown. For the same reason, the C-terminal portion of L2 (about 60 residues) that connects the last ordered residue in our structure and the first ordered residue in the recently published structure of the B30.2 domain (blue) (18) is also shown as dashes. The B30.2 domain of TRIM25 binds to the first CARD of RIG-I, and the RING domain ubiquitylates Lys172 in the second CARD (19, 20). CARD, caspase activation and recruitment domain; CTD, C-terminal domain; B1, B-box 1; B2, B-box 2; E2, E2 ubiquitin ligase; Ub, ubiquitin; vRNA, viral RNA.

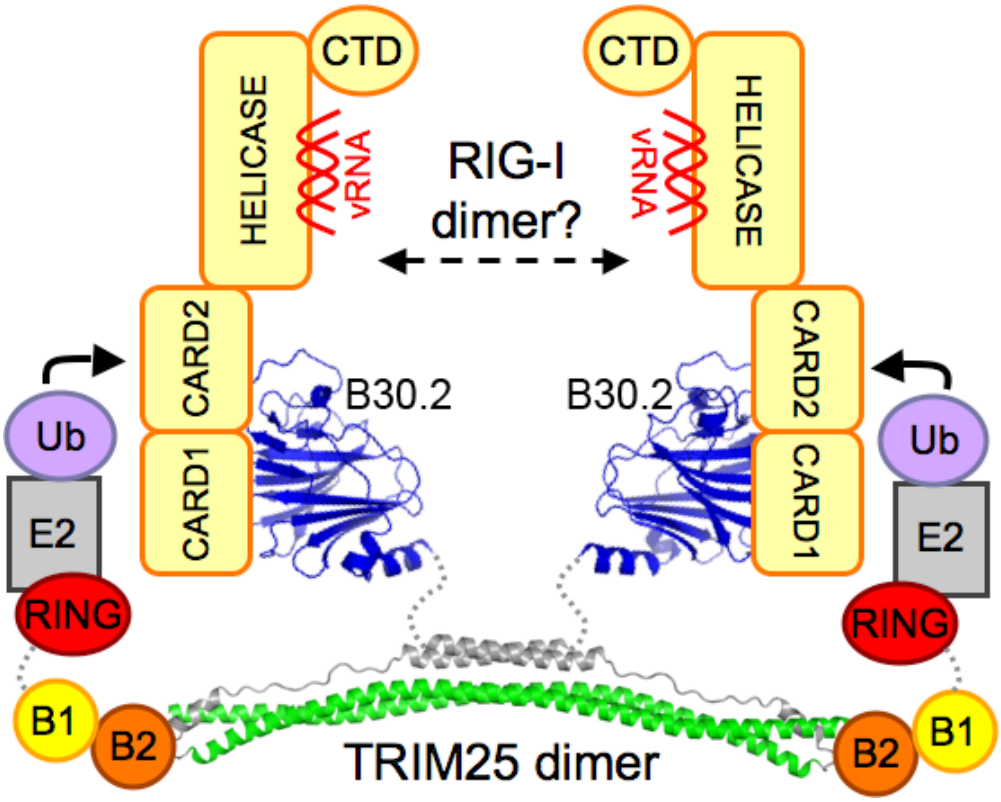
CTD
HELICASE
vRNA
RIG-I
dimer?
CTD
HELICASE
vRNA
CARD2
CARD1
B30.2
B30.2
CARD2
CARD1
Ub
E2
RING
Ub
E2
RING
B1
B2
TRIM25 dimer
B2
B1

helical, and therefore nucleate dimerization (23–25). Once the initial dimer contact is established, the peripheral residues then “zip up” to form the fully folded coiled-coil. This general model implies that associating helices, whether homodimeric or heterodimeric, must have compatible trigger sites. Our structural and mutational analyses indicate that the center of the H1 helix is likely to be the TRIM25 coiled-coil trigger site. This element includes Tyr245 and Leu252 (hendecads 6 and 7) and is flanked by polar residues that form a buried hydrogen bond network (**Fig. 5B**). It is likely that these buried polar interactions help to define pairing specificity and helix packing registry in TRIM proteins, as has been seen in SNARE coiled-coil complexes (36). Our sequence analysis indicates that almost every human TRIM protein has a unique central sequence, although there is conservation within the same branches of the TRIM family tree (**Fig. 7**). This likely explains why TRIM proteins apparently do not form heterodimers promiscuously and why reports of TRIM heterodimerization generally involve closely related TRIM proteins (7, 9, 12, 13).

Implications for Dimerization and High-Order Assembly of TRIM5α. Our structural and biochemical data establish that the coiled-coil and L2 regions of TRIM25 and TRIM5α form similar structures. We have therefore used the TRIM25 structure to interpret the protein density seen in the 2D cryoEM reconstruction of the assembled TRIM5α hexagonal lattice (18) (**Fig. 10**). This analysis indicates that each edge of the TRIM5α hexagon corresponds to a single coiled-coil dimer (each 17 nm in length). This interpretation, in turn, implies that the threefold symmetric densities observed at each vertex

Fig. 10. Models of quaternary TRIM5α interactions.

(A) Schematic model of the TRIM5α hexagonal lattice, showing the deduced positions of the different domains and overlaid with the cryoEM projection map (gray contours) (18). Domains are colored as in **Fig. 1B**.

(B) Schematic model of the full-length TRIM5α dimer. The C-terminal B30.2 domains (blue) are shown packed against one side of the coiled-coil domain via a putative extended H3 helix (colored in gray to blue gradient and outlined in black) that spans both L2 and B30.2 sequences and forms a 4-helix bundle with the coiled-coil, as seen in the TRIM25 structure.

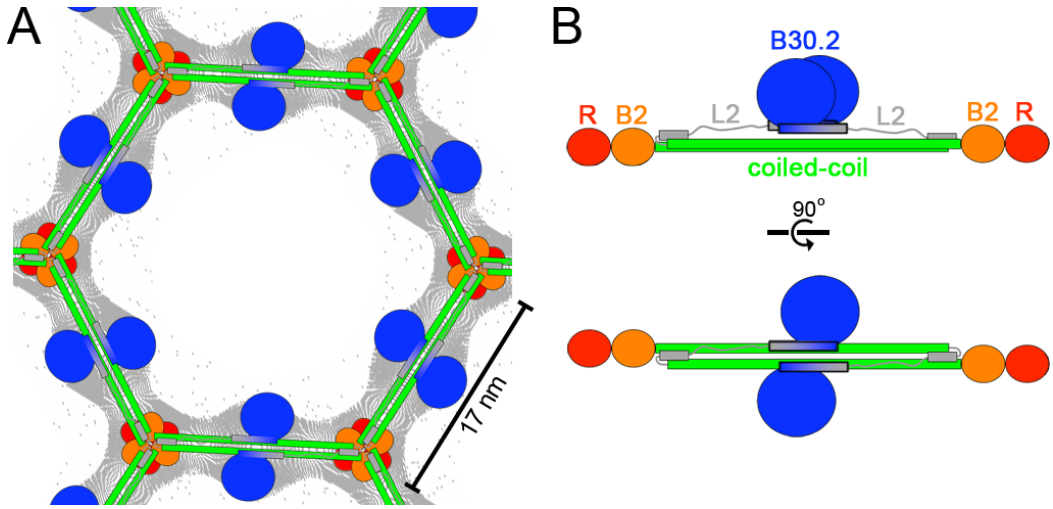
A
17 nm
B
B30.2
R
B2
L2
L2
B2
R
coiled-coil
90°

correspond to the N-terminal RING and B-box 2 domains and that the twofold symmetric densities at the midpoint of each hexagon edge correspond to the B30.2/SPRY domains (18) (**Fig. 10A**). These assignments are consistent with the known requirement for the B-box 2 domain in high-order TRIM5α assembly (18, 37, 38) and could also explain how assembly can activate the RING domains by bringing them into close proximity, consistent with the observation that capsid binding enhances E3 ligase activity (17). We envision two possible subunit configurations for the hexagonal lattice, which differ in domain connectivity at the local threefold vertex (**Fig. 11**). In one configuration, the intact dimers would interact at the vertex through the RING, B-box 2, and/or ends of the coiled-coil. In the alternative configuration, the associated coiled-coil dimers would "swap" arms in a fashion reminiscent of clathrin triskelion assembly (39). We cannot yet unambiguously discriminate between these different possible assembly modes but note that domain swapping would provide a mechanism for autoinhibition, and thereby prevent unregulated assembly, and would be consistent with recent studies indicating that the L2 linker plays an important role in high-order TRIM5α assembly (40, 41).

Our domain assignments, together with the density distribution in the EM map of the TRIM5α lattice, further suggest that the B30.2 domain may interact with the coiled-coil. The sequences of TRIM5α and TRIM25 diverge considerably beyond the short-arm H2 helix, but secondary structure algorithms predict an α-helix at the TRIM5α L2/B30.2 boundary (residues 283–300) that is equivalent in position to TRIM25 H3 (asterisks in **Fig. 1B** and **Fig. 12**). Interestingly,

Fig. 11. Two possible configurations of domain connectivity at the threefold symmetry axes of the TRIM5α hexagonal lattice.

The RING and B-box domains are not shown.

(A) Three dimers with loops (magenta) connecting the coiled-coil helices (green) and L2 (gray) in the “fold-back” configuration, as observed in the TRIM25 crystal structure.

(B) Three dimers in which the adjacent subunits have “swapped” their short arms. Note that this will also result in a domain swapping of downstream L2 and B30.2 elements.

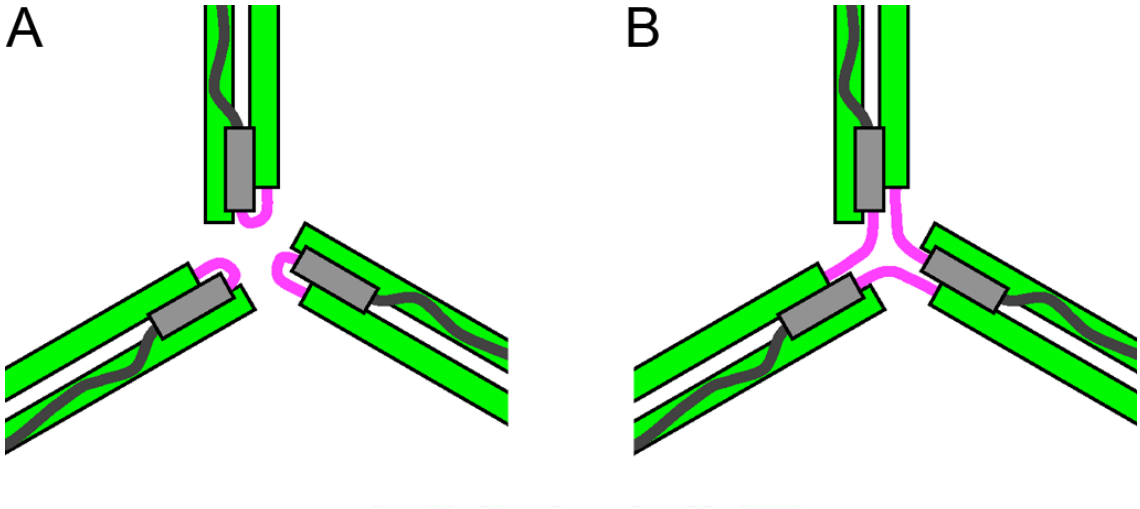
A
B

Fig. 12. Secondary structure predictions for rhesus TRIM5α$_{133–300}$ performed with the program JPRED (21) (H, helix; E, strand).

Residues that fold into an α-helix in X-ray structures of the isolated B30.2 domain are colored in blue and boxed. The “domain” boundaries are indicated at the bottom, following the color scheme of **Fig. 1B**. Black rectangles depict the deduced helix H1 and H2 positions and the predicted H3 helix.

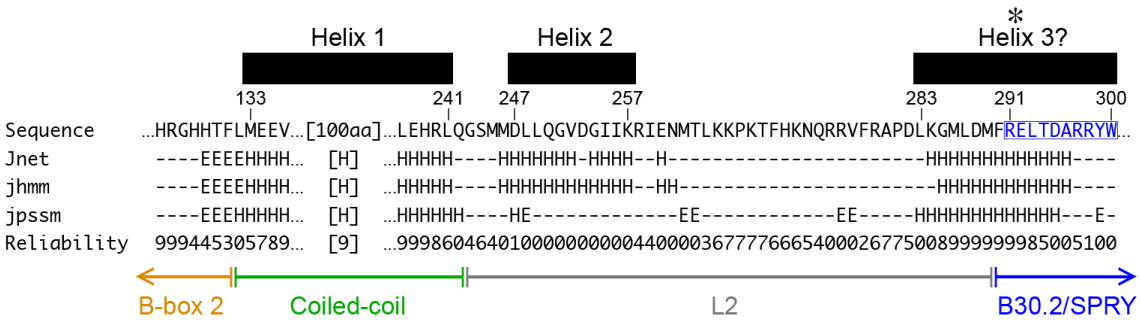
Helix 1
Helix 2
Helix 3?
133
241
247
257
283
291
300
Sequence …HRGHHTFLMEEV…[100aa]…LEHRLQGSMMDLLQGVDGIIKRIENMTLKKPKTFHKNQRRVFRAPDLKGMLDMFRELTDARRYW…
Jnet ----EEEEHHHH… [H] …HHHHH----HHHHHHH-HHHH--H----------HHHHHHHHHHHHH----
jhmm ----EEEEHHHH… [H] …HHHHH----HHHHHHHHHHHH--HH----------HHHHHHHHHHHHH----
jpssm ----EEEHHHHH… [H] …HHHHHH----HE----------EE----------EE-----HHHHHHHHHHHHH---E-
Reliability 999445305789… [9] …9998604640100000000004400003677776665400026775008999999985005100
B-box 2
Coiled-coil
L2
B30.2/SPRY

residues 291–300 of rhesus TRIM5α (**Fig. 12**) do indeed form a helix in two independent crystal structures of the isolated B30.2 domain (42, 43), although the immediately preceding residues (287–290) adopt a nonhelical loop configuration with high temperature factors in one of the structures (43). These observations lead us to speculate that the N-terminal helix of the TRIM5α B30.2 domain (or the longer, predicted helix) may pack against the center of the upstream coiled-coil to form a 4-helix bundle, as seen in the TRIM25 structure. In support of this idea, alanine substitutions of surface-exposed residues on the TRIM5α B30.2 helix (Arg297, Arg298, and Tyr299) impair both restriction activity and capsid binding. These residues are far removed from the capsid-binding surface (44) but could mediate interaction of the TRIM5α B30.2 domain against its coiled-coil. Such interactions would not only position the B30.2 domains on the same side of the dimer but also possibly define their spacing and orientation, as has been postulated to be a “minimum design feature” of retroviral capsid restriction factors (45). Consistent with this general idea, residues within the TRIM5α coiled-coil domain are under positive selection (46, 47), implying they can influence capsid recognition, and the coiled-coil itself may be a determinant of binding specificity (47).

In summary, we propose that the tripartite motif coiled-coil has a conserved structure and a conserved scaffolding function that organizes the biochemical activities of TRIM proteins, thereby facilitating selective substrate polyubiquitylation by TRIM25 and capsid pattern recognition by TRIM5α. Thus, the TRIM domains are organized spatially, consistent with the idea that they have

coevolved and behave as an integrated module, rather than as a collection of independent functional elements (14, 20, 48).

METHODS

Construct Design and Protein Expression. Human tripartite motif 25 (TRIM25) was subcloned from a plasmid kindly provided by Dong-Er Zhang (University of California, San Diego, La Jolla, CA) (Addgene plasmid 12449) (1). Rhesus TRIM5α (GI: 44890114) was subcloned from a pLPCX/TRIM5α-HA plasmid kindly provided by Joseph Sodroski (Harvard University, Cambridge, MA) (2). $TRIM25_{189–379}$ and $TRIM5α_{133–300}$ were ex-pressed from pET24a-derived vectors (3) with His_6-tagged SUMO leader sequences (Table S2). Asp85 in the SUMO coding region of the TRIM5α vectors was mutated to serine to destroy a Shine-Dalgarno-like sequence that caused a nearby Ile to be used as an alternative start site for translation. Residue pairs for cysteine mutagenesis were selected with the program Disulfide-by-Design (4). The cysteine mutants were generated by PCR-based mutagenesis (Table S2). Proteins were expressed in Escherichia coli BL21(DE3) (TRIM25) or Rosetta(DE3) pLysS (TRIM5α), using the autoinduction method as described (5), except that the cultures were grown at 37 °C until saturation and then at 18–19 °C for 16 h.

Purification of $TRIM25_{189–379}$. Cells expressing $TRIM25_{189–379}$ from 1 L of culture were resuspended in 30 mL lysis buffer [50 mM Tris at pH 9.0, 0.3 M NaCl, 20 mM β-mercaptoethanol (βME)] supplemented with 2 mM phenylmethylsulfonylfluoride. Cells were lysed using a microfluidizer

(Microfluidics model M110P) at 20,000 psi chamber pressure. Cell debris was removed by centrifugation (45,000 × g for 45 min at 4 °C). Filtered super-natant was incubated in a gravity flow chromatography column with 10 mL Ni-NTA resin (Qiagen) for 1 h on a rocker at 4 °C. The resin was washed with 150 mL lysis buffer, followed by 500 mL wash buffer (25 mM Tris at pH 8.0, 0.1 M NaCl, 10 mM βME, 20 mM imidazole). Bound protein was eluted in wash buffer containing 400 mM imidazole. Ulp1 protease was added to the pooled fractions (~1:100 mass ratio), and the sample was dialyzed overnight at 4 °C against cleavage buffer (25 mM Hepes at pH 7.0, 20 mM NaCl, 10 mM βME). The sample was applied to a 5-mL HiTrap SP FF column (GE Healthcare) and eluted with a linear salt gradient (0.02–1 M NaCl) in cleavage buffer. Pooled fractions were concentrated to ~3 mL and purified to homogeneity on a HiLoad 16/600 Superdex 75 gel filtration column (GE Healthcare) in crystallization buffer (10 mM Tris at pH 8.0, 0.1 M NaCl). Selenomethionine-labeled protein was purified in the same manner except that the final buffer contained 10 mM βME. The pure proteins were concentrated to ~18 mg/mL, flash-frozen in liquid nitrogen, and stored at −80 °C. The mass of freshly purified wild-type protein was determined by electrospray ionization mass spectrometry to be 21,832 Da (expected mass from sequence, 21,835 Da). Typical yields for the wild-type protein were ~5 mg/L culture. Flash-freezing or long-term incubation in solution induced a minor fraction of the protein to form an SDS-resistant 40-kDa (dimer) species (e.g., see Fig. 4B, lanes 1–12). Cysteine mutants were purified in the same manner as wild-type, except that 20 mM βME was added to all buffers. All

cysteine mutants displayed the same elution behavior as wild-type during size-exclusion chromatography.

Purification of TRIM5α$_{133–300}$. Cells expressing TRIM5α$_{133–300}$ from 1 L of culture were collected and resuspended in 100 mL lysis buffer (100 mM Hepes at pH 8, 1 M LiCl, 300 mM NaCl, 30 mM imidazole) supplemented with 0.5% Triton X-100, 5% glycerol, 1 tablet cOmplete EDTA-free protease inhibitors (Roche), and 10 µg/mL DNase I (Roche). Cells were lysed by freeze-thaw and sonication (Qsonica; 2 min at 80% amplitude on ice). The lysate was clarified by centrifugation (37,000 × g for 45 min at 4 °C), and the 0.45-µm-filtered supernatant was incubated with 4 mL cOmplete His-tag purification resin (Roche) for 1 h with rocking. The resin was washed with 200 mL lysis buffer and 200 mL protease cleavage buffer (50 mM Tris at pH 8, 500 mM NaCl, 5% glycerol), eluted in 50 mL elution buffer (50 mM Tris at pH 8, 500 mM NaCl, 5% glycerol, 1.125 M imidazole), and dialyzed for 12 h against two changes of 2 L each of protease cleavage buffer supplemented with 0.5 mM EDTA. The sample was diluted fivefold in 50 mM Tris at pH 8, 0.5 mM EDTA, 1 mM TCEP, and the His$_6$-SUMO tag was removed by incubating with 3 mg Ulp1 protease for 6 h at 23 °C. The sample was loaded onto two 5 mL HiTrap Q HP columns (GE Healthcare) connected in series and eluted with a 100-mL linear NaCl gradient (0.05–1 M). The protein eluted in two distinct peaks, which we speculate correspond to dimers and monomers, as previously observed for longer TRIM5 constructs (6). Both peaks were pooled, concentrated, loaded on a HiLoad 16/600 Superdex 75 gel filtration column (GE Healthcare), and eluted in

size-exclusion buffer (50 mM Tris at pH 8, 150 mM NaCl, 1 mM TCEP). Fractions from the major peak (corresponding to the protein dimer) were pooled and concentrated to 1 mg/mL. The average mass of the purified protein was determined by electrospray ionization mass spectrometry to be 20,236 Da (expected mass from sequence, 20,238 Da). Typical yields for the wild-type protein were ~15 mg/L culture. Cysteine mutants were purified in the same way as wild-type except that 1 mM TCEP was added to all buffers. All mutants displayed the same elution behavior as wild-type during size-exclusion chromatography.

Analytical Ultracentrifugation. Equilibrium sedimentation experiments were performed at 4 °C, using a Beckman Optima XL-I centrifuge, at rotor speeds of 12,000, 17,000, and 23,000 rpm. For each speed, three protein concentrations were tested (16.8, 42, and 84 μM for $TRIM25_{189–379}$ and 4.4, 11.1, and 22.3 μM for $TRIM5\alpha_{133–300}$), and each centrifugation run was performed for 24 h to reach equilibrium. TRIM25 samples were in 10 mM Hepes at pH 7.4, 40 mM NaCl, 0.5 mM TCEP. TRIM5α samples were in 50 mM Tris at pH 8, 150 mM NaCl, 1 mM TCEP. Nonlinear least-squares data fitting was performed using the Heteroanalysis software (7). Solvent density and protein partial-specific volumes were calculated with the program SEDNTERP (8). The same analyses were also performed with a TRIM25 construct that contained two additional tryptophan residues to access lower loading concentrations (6.5, 16.2, and 32.3 μM), and the results were the same.

Crystallization and Data Collection. Crystals of native TRIM25$_{189–379}$ were obtained at 17 °C in sitting drops that were set up as a 1:1:1 mix of protein solution, water, and precipitant (6–12% PEG 4,000 at pH 5.3–6.6, 10 mM sodium acetate). Selenomethionine-labeled crystals were obtained in the same manner except that the precipitant solution was 16% PEG 3,350, 80 mM Bis-Tris propane at pH 8.8, and 20 mM citric acid. Crystals were cryoprotected in mother liquor containing 25% PEG 400. The protein crystallized in at least 4 distinct space groups within the same drop, and the diffraction quality was highly variable, with most crystals diffracting poorly. After extensive screening, a native data set extending to 2.6 Å resolution ($I/\sigma \geq 2$ criterion) and anomalous Se data extending to 3.2 Å were collected at Advanced Photon Source beamline 22-ID. Diffraction data were processed using HKL2000 (9). Data statistics are reported in **Table 1**.

Structure Determination. TRIM25$_{189–379}$ structure determination, model building, and initial refinement were performed with the AutoSol, AutoMR, and AutoBuild Wizards of the PHENIX suite (version 1.8.2–1309) (10). The Se and native data both indexed as $P2_12_12_1$, but with different unit cell dimensions (**Table 1**). Each had one dimer in the asymmetric unit, which packed in different ways. The initial structure was determined by single-wavelength anomalous dispersion from the Se derivative. The coiled-coil region of this structure was partially built and refined mostly as a polyalanine model (**Fig. 3A**). Further refinement of this crystal form was not continued because one of the L2 arms had extremely poor density, likely because it had dissociated from the coiled-coil (**Fig. 6B**). The partially built structure was used as a molecular replacement

search model to phase the native data (**Fig. 3B**). Automated model building/rebuilding and refinement against the 2.6 Å native data resulted in a model that was about 80% complete. The rest of the model was built manually using the program Coot (11). To take advantage of the twofold improvement in data-to-parameter ratio afforded by noncrystallographic symmetry while taking into account the flexibility of the subunits, residues were binned into 16 noncrystallographic symmetry segments and equivalent sections were re-strained to match each other [approach adapted from ref. 12; see Protein Data Bank (PDB) file header for details on the binned segments]. Multiple rounds of refinement (phenix.re-fine; version 1.8.2-dev-1427) and manual model building resulted in good geometry and R/R_{free} of 0.20/0.26 (**Table 1**). The final model consists of amino acid residues 190–360 for both chains in the dimer. Density was lacking for residues 189 and 361–379, which were not included in the final model. Model validation with Molprobity (13) was performed throughout the structure refinement process. Coordinates and structure factors have been deposited in the PDB under ac-cession code 4LTB.

Sequence and Structure Analysis. Sequences aligned in **Fig. 5D and 7** started from the last zinc-coordinating pair of the B-box 2 domain (typically His-X-X-His) and spanned the subsequent 130 residues. Sixty-seven members of the human TRIM family (Table 1 in ref. 20), excluding TRIM25, were initially used to generate a multiple sequence alignment with the ClustalW2 program. Duplicates and sequences with gaps of 3 or more residues within H1 were removed, resulting in a final alignment of 54 sequences. To facilitate

structure-to-sequence comparisons, a consensus sequence plot was generated using the Weblogo program (49), total buried surface areas for each residue in the TRIM25 structure were calculated using the PISA Web server (50), and the Weblogo and buried surface area plots were aligned manually.

Differential Scanning Fluorimetry. Thermofluor melting assays (22) were performed with a Bio-Rad CFX96 thermal cycler. Proteins in crystallization buffer were mixed with a 1:400 dilution of “10,000×” SYBR Safe dye (Invitrogen). Final protein concentrations were 2 mg/mL, except for the L252A and L348A mutants, which were 1 mg/mL and 2.6 mg/mL, respectively. Samples were held at 20 °C for 5 min, and the temperature was then raised to 100 °C in 1 °C increments every 15 s, taking fluorescence readings at each increment. Each sample was set up in 4 replicates, and melting curves for each protein were determined at least twice, with independent protein preparations. T_m was determined from the maximum of the first derivative of the melting curve. The maximal variation in wild-type $TRIM25_{189–379}$ T_m was <1 °C in seven independent determinations.

Crosslinking Analysis. Double-cysteine mutant proteins were reduced by dilution to 30 μM in reducing buffer [50 mM Tris at pH 8.0, 150 mM NaCl, 20 mM β-mercaptoethanol (βME)] and then dialyzed overnight at 4 °C into the same buffer containing 0 mM (TRIM25) or 2 mM (TRIM5α) βME to allow formation of stable disulfide crosslinks. Aliquots were then mixed with the same volume of 2× SDS-PAGE sample buffer containing either 1 M βME (reducing) or no

additional βME (nonreducing), incubated for 5 min at 99 °C in a dry bath and immediately analyzed by SDS-PAGE with Coomassie blue staining.

ACKNOWLEDGMENTS

We thank Barbie Ganser-Pornillos, Chris Hill, and members of the O.P. and W.I.S. laboratories for critical reading of the manuscript; Ed Campbell for helpful discussions; Kate Skorupka and Peter Horanyi for technical support; Debra Eckert and Steve Alam for assistance with the equilibrium sedimentation analyses. We also thank an anonymous reviewer for helpful suggestions on the analysis of the helical repeats in the antiparallel coiled-coil. This project was supported by a Research and Development grant from the University of Virginia School of Medicine (to O.P.) and National Institutes of Health Grant P50 GM082545 (to W.I.S.). J.G.S. is supported by a predoctoral Cell and Molecular Biology Training Grant from the National Institutes of Health (T32 GM008136). K.O. participated in this study while on leave from Jagiellonian University, Krakow, Poland.

REFERENCES

1. Han K, Lou DI, Sawyer SL (2011) Identification of a genomic reservoir for new TRIM genes in primate genomes. PLoS Genet 7(12):e1002388.

2. McNab FW, Rajsbaum R, Stoye JP, O'Garra A (2011) Tripartite-motif proteins and in-nate immune regulation. Curr Opin Immunol 23(1):46–56.

3. Gack MU, et al. (2007) TRIM25 RING-finger E3 ubiquitin ligase is essential for RIG-I-mediated antiviral activity. Nature 446(7138):916–920.

4. Oshiumi H, Matsumoto M, Seya T (2012) Ubiquitin-mediated modulation of the cytoplasmic viral RNA sensor RIG-I. J Biochem 151(1):5–11.

5. Stremlau M, et al. (2004) The cytoplasmic body component TRIM5α restricts HIV-1 infection in Old World monkeys. Nature 427(6977):848–853.

6. Grütter MG, Luban J (2012) TRIM5 structure, HIV-1 capsid recognition, and innate immune signaling. Curr Opin Virol 2(2):142–150.

7. Centner T, et al. (2001) Identification of muscle specific ring finger proteins as potential regulators of the titin kinase domain. J Mol Biol 306(4):717–726.

8. Short KM, Cox TC (2006) Subclassification of the RBCC/TRIM superfamily reveals a novel motif necessary for microtubule binding. J Biol Chem 281(13):8970–8980.

9. Li X, et al. (2007) Unique features of TRIM5α among closely related human TRIM family members. Virology 360(2):419–433.

10. Kar AK, Diaz-Griffero F, Li Y, Li X, Sodroski J (2008) Biochemical and biophysical characterization of a chimeric TRIM21-TRIM5α protein. J Virol 82(23):11669–11681.

11. Langelier CR, et al. (2008) Biochemical characterization of a recombinant TRIM5α protein that restricts human immunodeficiency virus type 1 replication. J Virol 82(23): 11682–11694.

12. Herquel B, et al. (2011) Transcription cofactors TRIM24, TRIM28, and TRIM33 associate to form regulatory complexes that suppress murine hepatocellular carcinoma. Proc Natl Acad Sci USA 108(20):8212–8217.

13. Napolitano LM, Meroni G (2012) TRIM family: Pleiotropy and diversification through homomultimer and heteromultimer formation. IUBMB Life 64(1): 64–71.

14. Reymond A, et al. (2001) The tripartite motif family identifies cell compartments. EMBO J 20(9):2140–2151.

15. Javanbakht H, Diaz-Griffero F, Stremlau M, Si Z, Sodroski J (2005) The contribution of RING and B-box 2 domains to retroviral restriction mediated by monkey TRIM5α. J Biol Chem 280(29):26933–26940.

16. Campbell EM, et al. (2007) TRIM5 α cytoplasmic bodies are highly dynamic structures. Mol Biol Cell 18(6):2102–2111.

17. Pertel T, et al. (2011) TRIM5 is an innate immune sensor for the retrovirus capsid lattice. Nature 472(7343):361–365.

18. Ganser-Pornillos BK, et al. (2011) Hexagonal assembly of a restricting TRIM5α protein. Proc Natl Acad Sci USA 108(2):534–539.

19. Javanbakht H, et al. (2006) Characterization of TRIM5α trimerization and its contri-bution to human immunodeficiency virus capsid binding. Virology 353(1):234–246.

20. Sardiello M, Cairo S, Fontanella B, Ballabio A, Meroni G (2008) Genomic analysis of the TRIM family reveals two groups of genes with distinct evolutionary properties. BMC Evol Biol 8:225.

21. Brown JH, Cohen C, Parry DA (1996) Heptad breaks in alpha-helical coiled coils: Stutters and stammers. Proteins 26(2):134–145.

22. Matulis D, Kranz JK, Salemme FR, Todd MJ (2005) Thermodynamic stability of car-bonic anhydrase: Measurements of binding affinity and stoichiometry using Ther-moFluor. Biochemistry 44(13):5258–5266.

23. Kammerer RA, et al. (1998) An autonomous folding unit mediates the assembly of two-stranded coiled coils. Proc Natl Acad Sci USA 95(23):13419–13424.

24. Kammerer RA, et al. (2001) An intrahelical salt bridge within the trigger site stabilizes the GCN4 leucine zipper. J Biol Chem 276(17):13685–13688.

25. Steinmetz MO, et al. (2007) Molecular basis of coiled-coil formation. Proc Natl Acad Sci USA 104(17):7062–7067.

26. Mische CC, et al. (2005) Retroviral restriction factor TRIM5α is a trimer. J Virol 79(22): 14446–14450.

27. Perez-Caballero D, Hatziioannou T, Yang A, Cowan S, Bieniasz PD (2005) Human tripartite motif 5α domains responsible for retrovirus restriction activity and specificity. J Virol 79(14):8969–8978.

28. Cole C, Barber JD, Barton GJ (2008) The Jpred 3 secondary structure prediction server. Nucleic Acids Res 36(Web Server issue):W197-201.

29. Dombkowski AA (2003) Disulfide by Design: A computational method for the rational design of disulfide bonds in proteins. Bioinformatics 19(14): 1852–1853.

30. Gack MU, et al. (2008) Roles of RIG-I N-terminal tandem CARD and splice variant in TRIM25-mediated antiviral signal transduction. Proc Natl Acad Sci USA 105(43): 16743–16748.

31. Plechanovová A, Jaffray EG, Tatham MH, Naismith JH, Hay RT (2012) Structure of a RING E3 ligase and ubiquitin-loaded E2 primed for catalysis. Nature 489(7414):115–120.

32. Dou H, Buetow L, Sibbet GJ, Cameron K, Huang DT (2012) BIRC7-E2 ubiquitin conjugate structure reveals the mechanism of ubiquitin transfer by a RING dimer. Nat Struct Mol Biol 19(9):876–883.

33. Liu HM, et al. (2012) The mitochondrial targeting chaperone 14-3-3e regulates a RIG-I translocon that mediates membrane association and innate antiviral immunity. Cell Host Microbe 11(5):528–537.

34. Kwon SC, et al. (2013) The RNA-binding protein repertoire of embryonic stem cells. Nat Struct Mol Biol 20(9):1122–1130.

35. Feng M, et al. (2013) Structural and biochemical studies of RIG-I antiviral signaling. Protein Cell 4(2):142–154.

36. Fasshauer D, Sutton RB, Brunger AT, Jahn R (1998) Conserved structural features of the synaptic fusion complex: SNARE proteins reclassified as Q- and R-SNAREs. Proc Natl Acad Sci USA 95(26):15781–15786.

37. Diaz-Griffero F, et al. (2009) A B-box 2 surface patch important for TRIM5α self-association, capsid binding avidity, and retrovirus restriction. J Virol 83(20): 10737–10751.

38. Li X, Sodroski J (2008) The TRIM5α B-box 2 domain promotes cooperative binding to the retroviral capsid by mediating higher-order self-association. J Virol 82(23):11495–11502.

39. Fotin A, et al. (2004) Molecular model for a complete clathrin lattice from electron cryomicroscopy. Nature 432(7017):573–579.

40. Sastri J, et al. (2010) Identification of residues within the L2 region of rhesus TRIM5α that are required for retroviral restriction and cytoplasmic body localization. Virology 405(1):259–266.

41. Li X, Yeung DF, Fiegen AM, Sodroski J (2011) Determinants of the higher order association of the restriction factor TRIM5α and other tripartite motif (TRIM) proteins. J Biol Chem 286(32):27959–27970.

42. Biris N, et al. (2012) Structure of the rhesus monkey TRIM5α PRYSPRY domain, the HIV capsid recognition module. Proc Natl Acad Sci USA 109(33):13278–13283.

43. Yang H, et al. (2012) Structural insight into HIV-1 capsid recognition by rhesus TRIM5α. Proc Natl Acad Sci USA 109(45):18372–18377.

44. Sebastian S, et al. (2009) An invariant surface patch on the TRIM5α PRYSPRY domain is required for retroviral restriction but dispensable for capsid binding. J Virol 83(7): 3365–3373.

45. Yap MW, Mortuza GB, Taylor IA, Stoye JP (2007) The design of artificial retroviral restriction factors. Virology 365(2):302–314.

46. Sawyer SL, Wu LI, Emerman M, Malik HS (2005) Positive selection of primate TRIM5α identifies a critical species-specific retroviral restriction domain. Proc Natl Acad Sci USA 102(8):2832–2837.

47. Maillard PV, Ecco G, Ortiz M, Trono D (2010) The specificity of TRIM5 α-mediated restriction is influenced by its coiled-coil domain. J Virol 84(11):5790–5801.

48. Meroni G, Diez-Roux G (2005) TRIM/RBCC, a novel class of ‘single protein RING finger’ E3 ubiquitin ligases. Bioessays 27(11):1147–1157.

49. Crooks GE, Hon G, Chandonia JM, Brenner SE (2004) WebLogo: A sequence logo generator. Genome Res 14(6):1188–1190.

50. Krissinel E, Henrick K (2007) Inference of macromolecular assemblies from crystalline state. J Mol Biol 372(3):774–797.

CHAPTER 3

MECHANISM OF TRIM25 CATALYTIC ACTIVATION IN THE RIG-I PATHWAY

Jacint G. Sanchez, Jessica J. Chiang, Konstantin M.J. Sparrer, Steven L. Alam, Michael Chi, Marcin D. Roganowicz, Banumathi Sankaran, Michaela U. Gack, Owen Pornillos

Reprinted with permission from Cell Reports

Volume 16, Issue 5, pages 1315-1325

ABSTRACT

Antiviral response pathways induce interferon by higher-order assembly of signaling complexes called signalosomes. Assembly of the RIG-I signalosome is regulated by K63-linked polyubiquitin chains, which are synthesized by the E3 ubiquitin ligase, TRIM25. We have previously shown that the TRIM25 coiled-coil domain is a stable, antiparallel dimer that positions two catalytic RING domains on opposite ends of an elongated rod. We now show that the RING domain is a separate self-association motif that engages ubiquitin-conjugated E2 enzymes as a dimer. RING dimerization is required for catalysis, TRIM25-mediated RIG-I ubiquitination, interferon induction, and antiviral activity. We also provide evidence that RING dimerization and E3 ligase activity are promoted by binding of the TRIM25 SPRY domain to the RIG-I effector domain. These results indicate that TRIM25 actively participates in higher-order assembly of the RIG-I signalosome and helps to fine-tune the efficiency of the RIG-I-mediated antiviral response.

INTRODUCTION

Higher-order assembly of large protein complexes is a recognized signal amplification mechanism that operates in many cellular signaling pathways (Wu, 2013). In the innate immune system, filamentous assemblies of the mitochondrial protein, MAVS (also known as CARDIF, VISA, or IPS-1), comprise one such type of signalosome (reviewed by Cai and Chen, 2014). MAVS filaments amplify signals from RIG-I-like pattern recognition receptors bound to viral RNA and recruit downstream effectors that ultimately generate a type I interferon (IFN) response. IFN-a/b gene expression induced by the RIG-I/MAVS signaling axis suppresses the replication of a variety of clinically important viral pathogens, including influenza A virus (IAV), hepatitis C virus, and dengue virus (reviewed by Goubau et al., 2013 and Loo and Gale, 2011).

Recent studies have shown that RIG-I-induced MAVS filament formation requires a remarkably simple biochemical trigger: interaction of the amino-terminal CARD (caspase activation and recruitment domain) of MAVS with a tetrameric assembly of the amino-terminal tandem CARDs (2CARD) of RNA-bound RIG-I (Jiang et al., 2012; Peisley et al., 2014; Wu et al., 2014). The RIG-I 2CARD tetramer is a helix with a single CARD as repeat unit, and so the 2CARD architecture restricts it to a ‘‘lock washer’’ configuration with only two helical turns (Peisley et al., 2014). The 2CARD ‘‘lock washer’’ acts as a template or seed for the single CARD of MAVS, which assembles along the helical trajectory to form long filaments containing several hundreds of MAVS CARD molecules (Peisley et al., 2014; Wu et al., 2014; Xu et al., 2014). MAVS filaments

behave like prion fibers and thus are thought to commit the RIG-I pathway to an all-or-none or digital response to viral infection (Cai et al., 2014; Cai and Chen, 2014; Hou et al., 2011). Uncontrolled MAVS assembly will have harmful consequences to the cell, and so a number of mechanisms have evolved to regulate where, when, and how the RIG-I 2CARD seeds MAVS CARD assembly (reviewed by Chiang et al., 2014).

Ubiquitin (Ub) is a well-characterized regulator of the RIG-I 2CARD/MAVS CARD seeding mechanism (Gack et al., 2007, 2008; Jiang et al., 2012; Peisley et al., 2013, 2014; Zeng et al., 2010). Activated 2CARD is modified with K63-linked polyubiquitin chains (K63-polyUb) (Gack et al., 2007), and unanchored K63-polyUb chains were also shown to associate with RIG-I in biochemical reconstitution studies (Jiang et al., 2012; Zeng et al., 2010). Structural and biochemical studies have revealed that these K63-polyUb chains can wrap around four RIG-I 2CARD molecules to induce and stabilize the ‘‘lock washer’’ configuration (Jiang et al., 2012; Peisley et al., 2014). Both types of K63-polyUb chains are synthesized by the E3 ubiquitin ligase, TRIM25, which is an essential component of the RIG-I pathway (Gack et al., 2007; Zeng et al., 2010).

TRIM25 belongs to the tripartite motif (TRIM) protein family, which is characterized by a conserved domain organization at the N terminus (known as the TRIM or RBCC motif) composed of a catalytic RING domain, one or two B-box domains, and a coiled-coil dimerization domain (Meroni and Diez-Roux, 2005; **Fig. 1A**). In addition, TRIM25 has a C-terminal SPRY domain that binds to

Fig. 1. Primary Structure and E3 Ligase Activity of TRIM25.

(A) Schematic of TRIM25 domain organization. Approximate amino acid boundaries of the different domains are indicated. B1, B-box 1; B2, B-box 2.

(B) Schematic of the elongated, antiparallel TRIM25 dimer, which places the catalytic RING domains around 170 Å apart. In this context, the RING domains are effectively monomeric.

(C) The isolated TRIM25 RING domain is active with Ubc5 isoforms and Ubc13/Uev1A. Purified RING (5 μM), E1 (50 nM), indicated E2s (1 μM), Ub (20 μM), and Mg-ATP (3 mM) were incubated at 37°C for 30 min. Ubiquitination products were observed by immunoblotting (IB) with anti-Ub antibody. **Fig. 2** shows the full screen of 26 different E2-conjugating enzymes, as well as a control experiment to confirm that chains made with Ubc13/Uev1A were not simply due to the known E3-independent activity of this heterodimeric E2.

(D) IB analysis, using K63-linkage specific anti-Ub, of the same samples in (C).

(E) The same reactions in (C) were performed but with K63-only Ub (wherein all Ub lysines except K63 are mutated to arginine). Only K63-linked polyUb chains are made in these reactions. IB was performed with anti-Ub. (F) Full-length TRIM25 is active with Ubc5 and Ubc13/Uev1A. Reactions contained partially purified FLAG-tagged TRIM25 (200 nM) and either Ubc13/Uev1A (280 nM; lanes 1–6), Ubc13 alone (1 μM; lanes 7–8), or Ubc5b alone (1 μM; lanes 9–10). IB was performed with anti-Ub (left) or anti-FLAG (right). TRIM25 made only unanchored K63-linked polyUb with Ubc13/Uev1A but anchored (autoubiquitinated) Ub with Ubc13 alone or Ubc5b alone. However, faint di-Ub and tri-Ub bands can be discerned in the Ubc5 reactions at longer exposures of the anti-Ub blot.

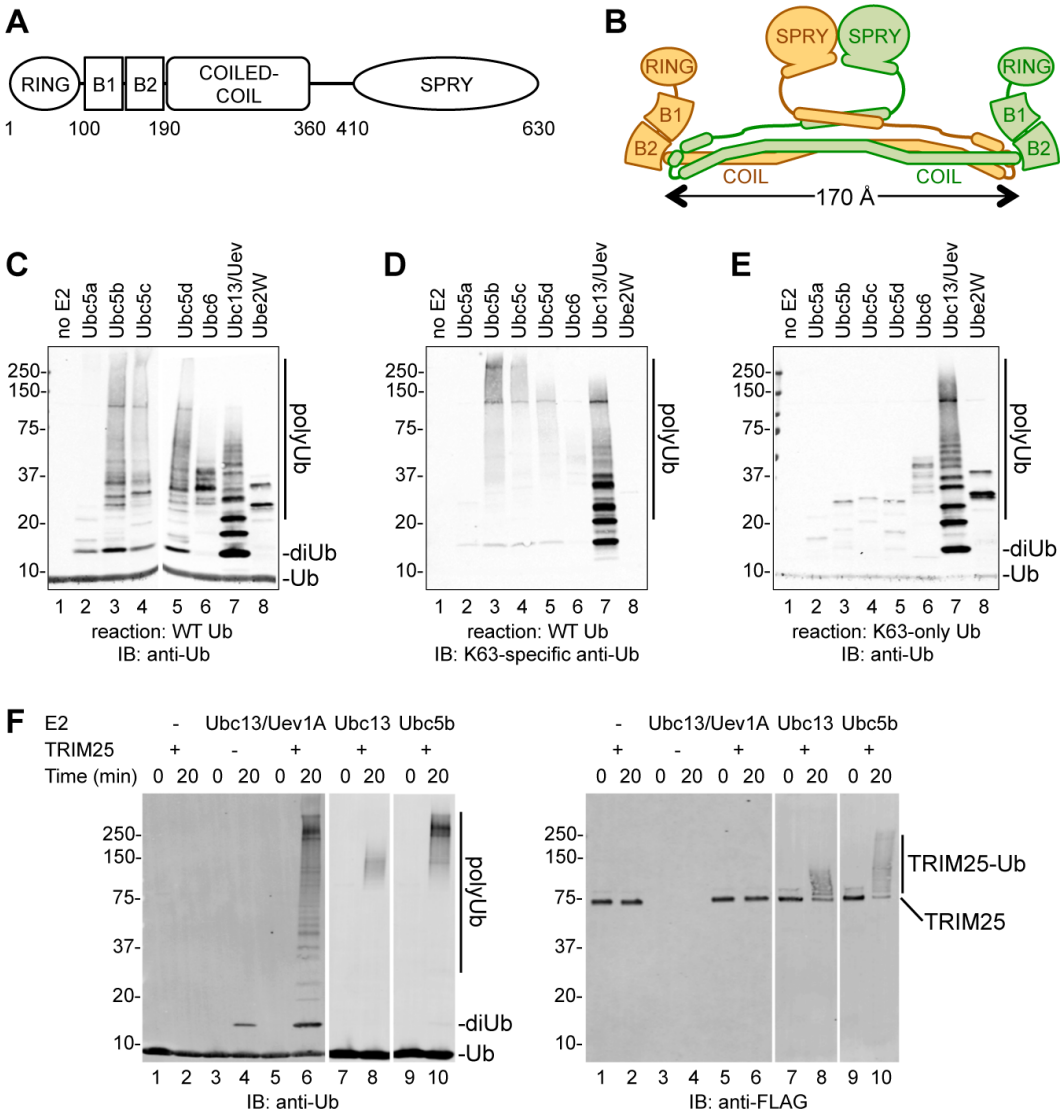
A
RING
B1
B2
COILED-COIL
SPRY
1
100
190
360
410
630
B
SPRY
SPRY
RING
B1
B2
RING
B1
B2
COIL
COIL
170 Å
C
no E2
Ubc5a
Ubc5b
Ubc5c
Ubc5d
Ubc6
Ubc13/Uev
Ube2W
250-
150-
75-
37-
20-
10-
polyUb
-diUb
-Ub
1 2 3 4 5 6 7 8
reaction: WT Ub
IB: anti-Ub
D
no E2
Ubc5a
Ubc5b
Ubc5c
Ubc5d
Ubc6
Ubc13/Uev
Ube2W
250-
150-
75-
37-
20-
10-
polyUb
1 2 3 4 5 6 7 8
reaction: WT Ub
IB: K63-specific anti-Ub
E
no E2
Ubc5a
Ubc5b
Ubc5c
Ubc5d
Ubc6
Ubc13/Uev
Ube2W
250-
150-
75-
37-
20-
10-
polyUb
-diUb
-Ub
1 2 3 4 5 6 7 8
reaction: K63-only Ub
IB: anti-Ub
F
E2
-
Ubc13/Uev1A
Ubc13
Ubc5b
TRIM25
+
-
+
+
+
Time (min)
0 20 0 20 0 20 0 20 0 20
250-
150-
75-
37-
20-
10-
polyUb
-diUb
-Ub
1 2 3 4 5 6 7 8 9 10
IB: anti-Ub
-
Ubc13/Uev1A
Ubc13
Ubc5b
+
-
+
+
+
0 20 0 20 0 20 0 20 0 20
250-
150-
75-
37-
20-
10-
TRIM25-Ub
TRIM25
1 2 3 4 5 6 7 8 9 10
IB: anti-FLAG

the RIG-I 2CARD (D'Cruz et al., 2013; Gack et al., 2007, 2008). TRIM proteins, like the well-characterized cullin ligases, are modular E3 enzymes. Similar to the cullin scaffold, the TRIM coiled-coil domain defines the spatial disposition of the catalytic and substrate-binding/recruitment domains. The coiled-coil domain of TRIM25 makes an elongated, antiparallel dimer of hairpin-shaped subunits, which positions two RING domains on opposite ends of a 170Å-long rod (Sanchez et al., 2014; **Fig. 1B**). In the TRIM25 dimer, two C-terminal SPRY domains emanate from a four-helix bundle in the middle of the coiled coil. The SPRY domains are located on the same side of the dimer, which presumably allows them to simultaneously engage two substrate molecules (Goldstone et al., 2014; Li et al., 2014; Sanchez et al., 2014; Weinert et al., 2015). Cooperation between the catalytic and substrate-binding domains is likely facilitated by flexible linkers connecting these domains to the coiled-coil scaffold.

TRIM25 is recruited by RIG-I when RNA recognition by the helicase and C-terminal domains of RIG-I releases the 2CARD from autoinhibition (Jiang and Chen, 2011; Kowalinski et al., 2011; Luo et al., 2011), and the exposed 2CARD binds to the C-terminal SPRY domain of the E3 enzyme (D'Cruz et al., 2013; Gack et al., 2007, 2008). It is not known whether 2CARD binding is simply a mechanism to localize an already active ligase (and therefore K63-polyUb) to sites of seed or signalosome assembly or whether such localization is coupled to TRIM25 catalytic activation. Here, we use structural, biochemical, and cell biological approaches to analyze the mechanism of catalytic activation of TRIM25. We found that the RING domain constitutes a self-association motif that

dimerizes to engage Ub-conjugated E2 enzymes and synthesize K63-pol-yUb. Because the two RING domains in the stable, coiled-coil-mediated TRIM25 dimer cannot self-associate and are effectively monomeric, our results imply that K63-polyUb synthesis is enabled only upon further, higher-order oligomerization of TRIM25. This is likely to be a quality control mechanism in the RIG-I pathway that couples TRIM25 catalytic activation to Ub-dependent 2CARD seed formation and MAVS assembly.

RESULTS

Structure of the TRIM25 RING Domain in Complex with E2-Ub. The antiparallel architecture of the TRIM25 coiled-coil dimerization domain implies that the associated RING domains are separated by about 170 Å and so are effectively monomeric in this context (**Fig. 1B**). Indeed, the TRIM25 RING was proposed to act as a monomer, similar to the CBL-B RING domain (Li et al., 2014). Nevertheless, many more RING domains engage E2 enzymes as dimers, as exemplified by the non-TRIM E3 ligases, RNF4 and BIRC7. Structures of these proteins, each bound to a covalent E2-Ub conjugate, have been demonstrated to represent the catalytically primed form of these enzymes (Dou et al., 2012; Plechanovova et al., 2012). We therefore reasoned that, if the TRIM25 RING domain catalyzes K63-polyUb synthesis as a dimer, then its crystal structure with the relevant E2-Ub should reveal an equivalent quaternary fold—including high-resolution details—as the RNF4 and BIRC7 complexes.

To facilitate structure determination, we first identified E2-conjugating enzymes suitable for such analysis from a ubiquitination activity screen of 26 E2 proteins (**Fig. 2**). Two Ubc5 isoforms (Ubc5b and Ubc5c; also known as Ube2D2 and Ube2D3, respectively) and Ubc13 (also known as Ube2N) have been previously shown to function in the RIG-I pathway (Liu et al., 2013; Zeng et al., 2009, 2010). Accordingly, we found that the isolated RING domain of TRIM25 (residues 1–83) efficiently synthesized polyUb with these E2 enzymes (**Fig. 1C**); however, K63-polyUb chains were most efficiently made in vitro with Ubc13 and its partner, Uev1A (also known as Ube2V1; **Fig. 1D and 1E**). Likewise, full-length TRIM25 is active with these E2 enzymes (**Fig. 1F**). Interestingly, full-length TRIM25 predominantly made anchored Ub chains (autoubiquitination) with Ubc5b or Ubc13 alone and, conversely, only unanchored chains with Ubc13/Uev1A.

We were successful in co-crystallizing the TRIM25 RING domain with Ub-conjugated Ubc13 (**Fig. 3; Table 1**). To prevent loss of the Ub moiety during crystallization, we used the previously described strategy of stably conjugating Ub to the E2 via an isopeptide linkage (Plechanovova et al., 2012) to make Ubc13^{C87K}-Ub. The structure of the TRIM25 RING/Ubc13^{C87K}-Ub complex was determined to 2.4-Å resolution (R/R_{free} = 0.19/0.23).

Although the isolated TRIM25 RING domain is predominantly a monomer in solution (**Fig. 4A**), it crystallized as a dimer in complex with Ubc13-Ub. This indicated that high protein concentrations during crystallization and binding of Ubc13-Ub promoted dimerization of the RING domain. The TRIM25

Fig. 2. E2 screen and control reactions.

(A) Full E2 screen with the isolated TRIM25 RING domain. E2 enzymes were purchased from UBPBio and the screen was performed according to manufacturer's instructions. Reaction products were visualized by immunoblotting (IB) with anti-Ub.

(B) Control reactions showing significantly elevated activity of the heterodimeric E2, Ubc13/Uev1A, in the presence of the TRIM25 RING domain.

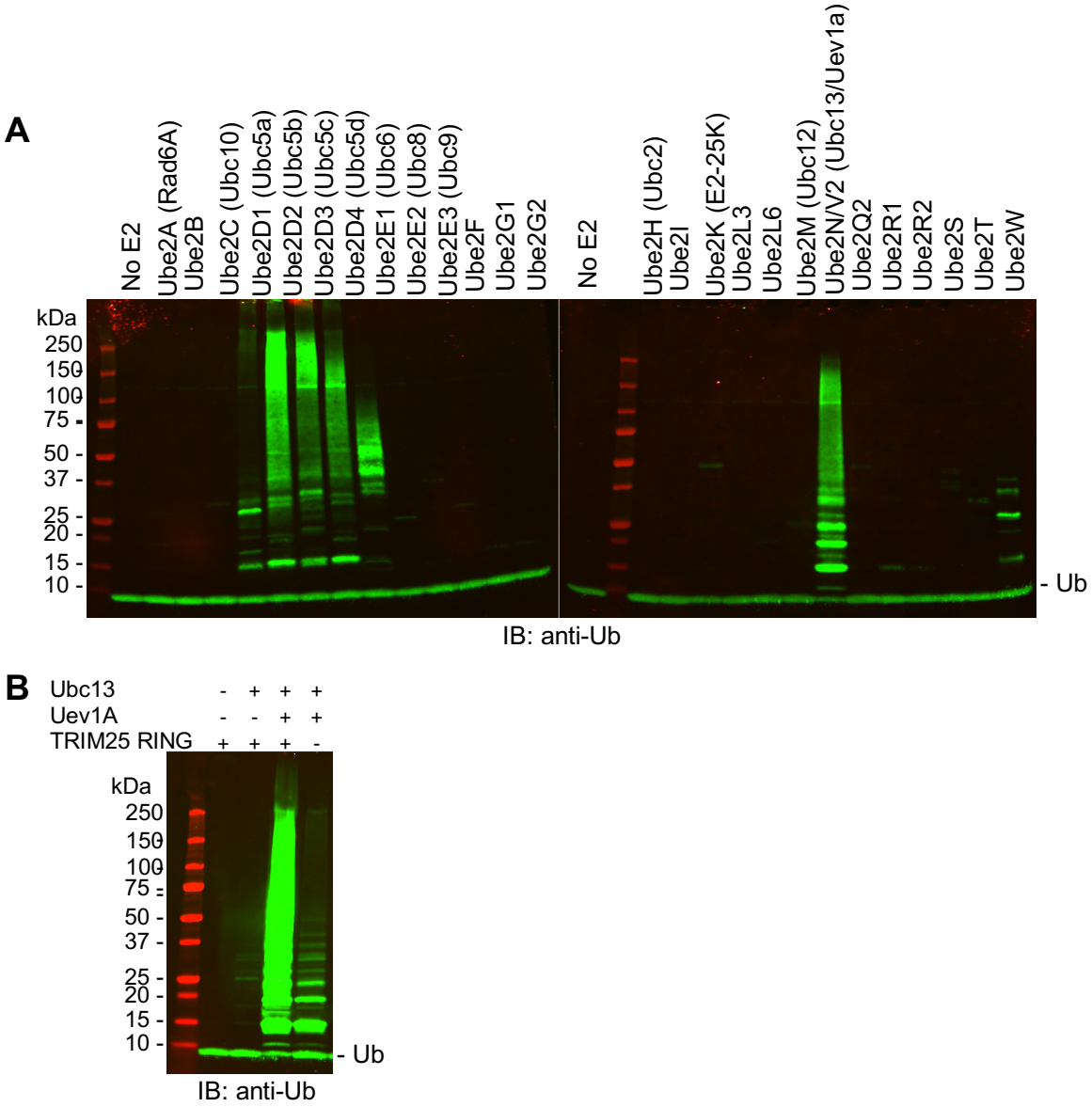
A
No E2
Ube2A (Rad6A)
Ube2B
Ube2C (Ubc10)
Ube2D1 (Ubc5a)
Ube2D2 (Ubc5b)
Ube2D3 (Ubc5c)
Ube2D4 (Ubc5d)
Ube2E1 (Ubc6)
Ube2E2 (Ubc8)
Ube2E3 (Ubc9)
Ube2F
Ube2G1
Ube2G2
No E2
Ube2H (Ubc2)
Ube2I
Ube2K (E2-25K)
Ube2L3
Ube2L6
Ube2M (Ubc12)
Ube2N/V2 (Ubc13/Uev1a)
Ube2Q2
Ube2R1
Ube2R2
Ube2S
Ube2T
Ube2W
kDa
250
150
100
75
50
37
25
20
15
10
- Ub
IB: anti-Ub
B
Ubc13 - + + +
Uev1A - - + +
TRIM25 RING + + + -
kDa
250
150
100
75
50
37
25
20
15
10
- Ub
IB: anti-Ub

Fig. 3. Structure of the TRIM25 RING Domain in Complex with Ub-Conjugated Ubc13.

(A) The TRIM25 RING dimer is at the center of the complex, colored in gray and rose. Ubc13 molecules are colored in yellow and magenta. Ub molecules are colored in cyan and green. Zinc atoms are colored in gray. Structure statistics are in **Table 1**.

(B) Superposition of the TRIM25/Ubc13-Ub complex with the RNF4/Ubc5a-Ub complex (Plechanovová et al., 2012) and BIRC7/Ubc5a-Ub complex (Dou et al., 2012). Proximal and distal RING positions are defined relative to the bound Ub (cyan). Boxed regions are expanded in (C) (blue) and (D) (red).

(C) Details of the proximal RING interactions showing that the TRIM25 RING dimer (left) positions the Ub tail against the E2 in the same way as RNF4 (middle; Plechanovová et al., 2012) and BIRC7 (right; Dou et al., 2012). Landmark residues are shown as sticks and labeled. Asterisks indicate the covalent E2-Ub linkages (isopeptide in the TRIM25 and RNF4 complexes; oxyester in the BIRC7 complex). Hydrogen bonds are colored in green.

(D) Details of the distal RING interactions that help hold Ub in the “closed” position primed for catalysis. Also shown is a hydrogen bond between the zinc-coordinating His30 side chain in the proximal TRIM25 RING and Ub Glu24 carbonyl (top panel). Both RNF4 (middle; Plechanovová et al., 2012) and BIRC7 (bottom; Dou et al., 2012) make equivalent interactions.

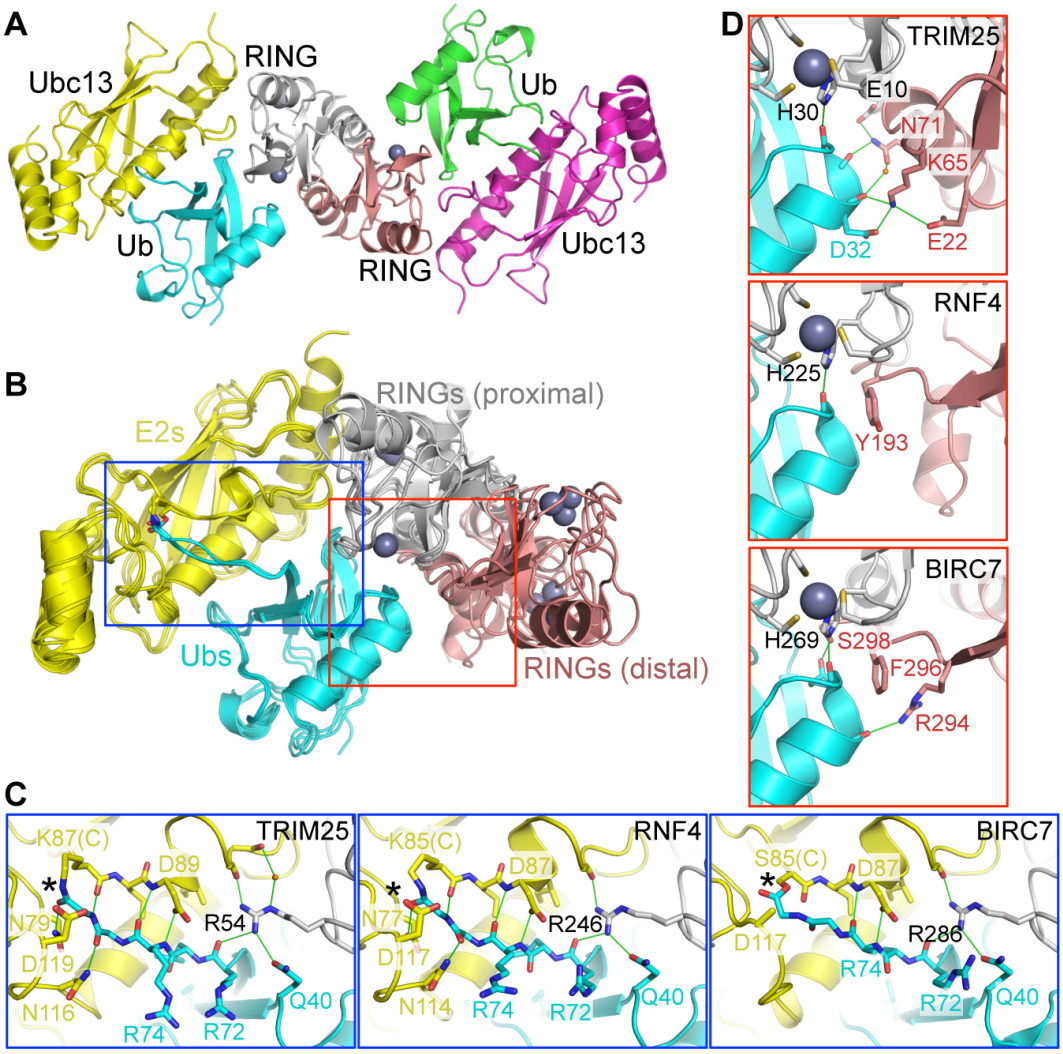
A
Ubc13
RING
Ub
Ub
RING
Ubc13
B
E2s
RINGs (proximal)
Ubs
RINGs (distal)
C
TRIM25
K87(C)
D89
N79
R54
D119
N116
Q40
R74
R72
RNF4
K85(C)
D87
N77
R246
D117
N114
R74
R72
Q40
BIRC7
S85(C)
D87
D117
R286
R74
R72
Q40
D
TRIM25
E10
H30
N71
K65
D32
E22
RNF4
H225
Y193
BIRC7
H269
S298
F296
R294

Table 1. Structure statistics.

Diffraction	
Beamline	ALS 5.0.1
Wavelength (Å)	0.9774
Processing	
Processing program	HKL2000
Space group	$P2_12_12_1$
Cell dimensions	*a* = 53.05 Å
	b = 75.78 Å
	c = 169.10 Å
	α = β = γ = 90°
Resolution range (Å)	50-2.40 (2.49-2.40)
R_{sym} / R_{meas} / R_{pim}	0.18 (0.74) / 0.19 (0.82) / 0.07 (0.33)
Mean I/σ<I>	9.6 (1.0)
Completeness (%)	98.2 (86.4)
Average redundancy	8.1 (4.8)
Mosaicity range (°)	0.24-0.31
Wilson B-factor (Å^2)	26.8
Refinement	
Refinement program	PHENIX
Resolution range	28.97-2.40 (2.84-2.40)
No. of unique reflections	24,622 (7,973)
Reflections in free set	1,786 (623)
R_{work}	0.19 (0.29)
R_{free}	0.23 (0.39)
No. of nonhydrogen atoms	
protein and zinc	4,838
solvent	188
Average B-factor (Å^2)	
protein and zinc	41.98
solvent	41.90
Coordinate deviations	
bond lengths (Å)	0.006
bond angles (°)	1.10
Validation and deposition	
Ramachandran plot	
Favored (%)	99
Outliers (%)	0
MolProbity clashscore	2.89
PDB ID	5EYA

Values in parenthesis are for the highest resolution shell.

Fig. 4. Solution oligomerization behavior of TRIM25.

(A) The isolated RING domain is predominantly monomeric. Equilibrium sedimentation distributions at the indicated protein concentrations are shown for the rotor speed of 28,000 rpm. The upper panel shows absorbance measurements at 280 nm (symbols) and best-fit curves (solid lines). Lower panels show residual differences. Data were also collected at a rotor speed of 25,000 rpm, and all six distributions were globally fit to a single-species model in which the molecular weight (MW_{obs}) was allowed to float. The value obtained (11 kDa) was about 15% higher than expected (MW_{calc} = 9.6 kDa). Fitting to a monomer-dimer equilibrium model wherein the molecular weight was fixed to 9.6 kDa also gave good residuals and a dissociation constant of about 1 mM. Thus, the RING domain is only very weakly dimeric in solution, if at all.

(B) Full-length TRIM25 is a dimer in solution. Sedimentation data at indicated protein concentrations are shown for the rotor speed of 9,000 rpm. Data were also collected at a rotor speed of 6,500 rpm, and all six distributions were globally fit to a single-species model wherein the molecular weight was allowed to float. MW_{obs} = 176 kDa. MW_{calc} = 75.7 kDa. MW_{obs}/MW_{calc} = 2.3.

(C) SEC-MALS analysis of full-length TRIM25 at a loading concentration of 20 μM. Protein concentrations were monitored using a refractive index detector (RI, blue trace). Mass measurements (M, red trace) indicate that the sample is almost pure dimer. A minor fraction eluting at 24.3 min (barely detectable by RI) has molecular weight consistent with a tetramer. Gray dashes indicate the theoretical masses.

(D) Coomassie-stained SDS-PAGE gel showing purified TRIM25.

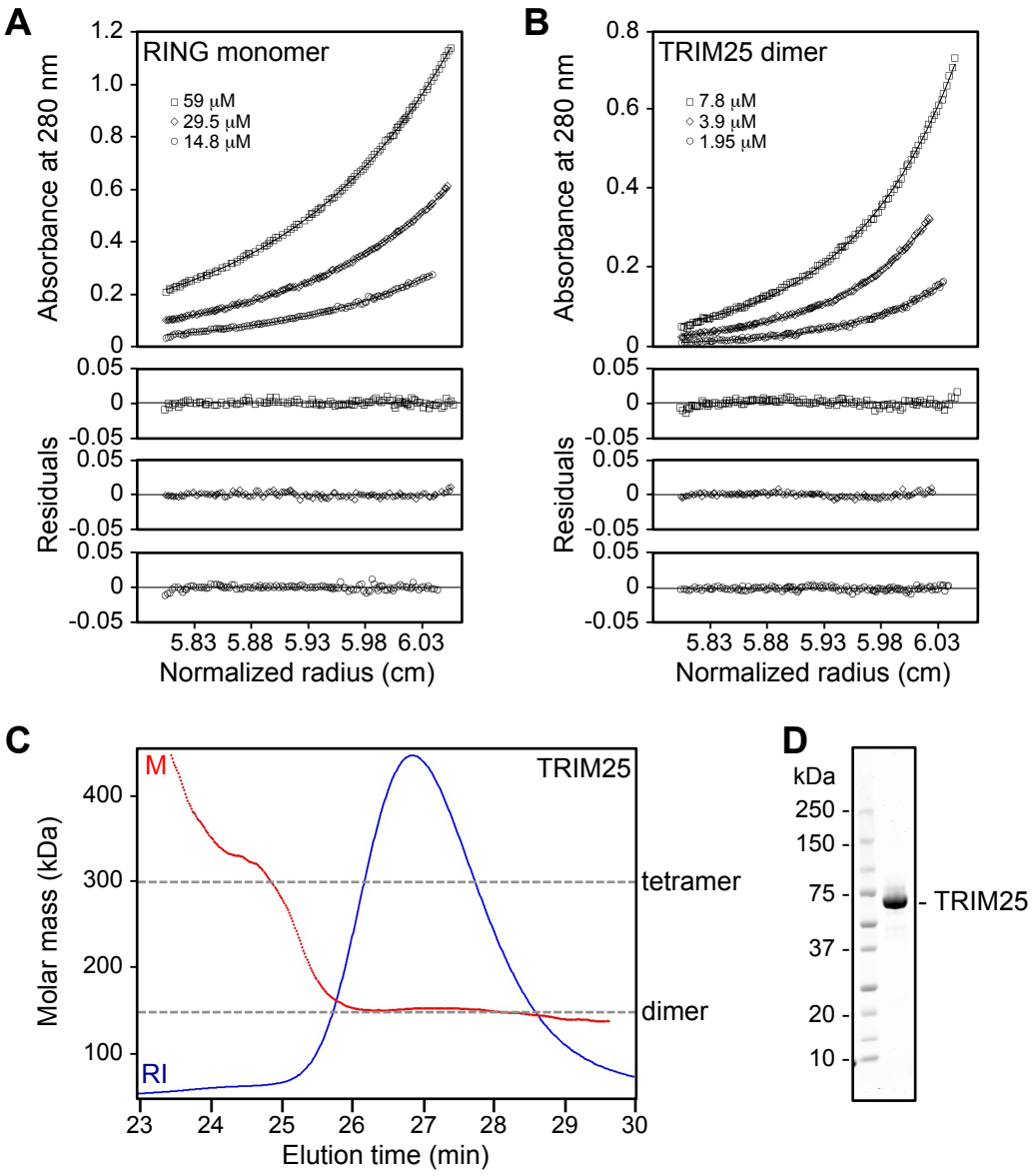
A
RING monomer
59 μM
29.5 μM
14.8 μM
Absorbance at 280 nm
Residuals
Normalized radius (cm)
B
TRIM25 dimer
7.8 μM
3.9 μM
1.95 μM
Absorbance at 280 nm
Residuals
Normalized radius (cm)
C
M
TRIM25
RI
tetramer
dimer
Molar mass (kDa)
Elution time (min)
D
kDa
250
150
75
37
20
10
TRIM25

RING/Ubc13-Ub complex is strikingly similar to the RING/E2-Ub complexes of RNF4 and BIRC7 (Dou et al., 2012; Plechanovova et al., 2012; **Fig. 3A and 3B**). Each RING domain interacts with Ubc13-Ub through an extensive three-way interface. TRIM25 Arg54 coordinates an extensive hydrogen bond network that packs the Ub C-terminal tail against a shallow groove leading to the E2 active site (**Fig. 3C**), and the zinc-bound His30 side chain makes a hydrogen bond with the Ub Glu32 carbonyl (**Fig. 3D**). These interactions help hold Ub in the so-called ‘‘closed’’ conformation primed for catalysis (Dou et al., 2012; Plechanovova et al., 2012; Pruneda et al., 2012). Complex formation also induces allosteric remodeling of the E2 active site, with the Ubc13 Asn79 side chain amide making a hydrogen bond with the isopeptide (normally thioester) carbonyl and the Asp119 side chain positioned to activate the incoming lysine nucleophile (**Fig. 3C**). Furthermore, the Ub moiety also makes hydrogen bonds with the second RING, involving RING side chains Glu22, Lys65, and Asn71; Ub backbone carbonyls; and the Ub Asp32 side chain (**Fig. 3D**). These high-resolution structural details are very similar, and in many aspects identical, to the previously described RING/E2-Ub complexes of RNF4 (Plechanovova et al., 2012) and BIRC7 (Dou et al., 2012; **Fig. 3B–3D**). The striking equivalence of the three structures strongly indicates that TRIM25 engages E2-Ub conjugates as a dimer.

TRIM25 RING Dimerization Is Required for Polyubiquitin Synthesis In Vitro. The TRIM25 RING domain dimer is mediated by two regions of contact (**Fig. 5A**). Thr25, Asn31, and Asn66 from the zinc-binding lobes coordinate

Fig. 5. Structure-Based Mutagenesis of the TRIM25 RING Dimer Interface.

(A) The TRIM25 RING dimer is stabilized by a buried network of hydrogen bonds (green lines) between the two zinc lobes and by a four-helix bundle made by residues that flank the zinc lobes in primary sequence. Residues in close contact within the dimer interface are shown as sticks and labeled.

(B) Coomassie-stained SDS-PAGE gel of purified WT and mutant recombinant RING proteins. See also **Fig. 6**.

(C) Ubiquitination activities of the RING mutants (5 μM) with Ubc13/Uev1A (250 nM; top panels) or Ubc5b (1 μM; bottom panels). Samples were analyzed by IB with anti-Ub.

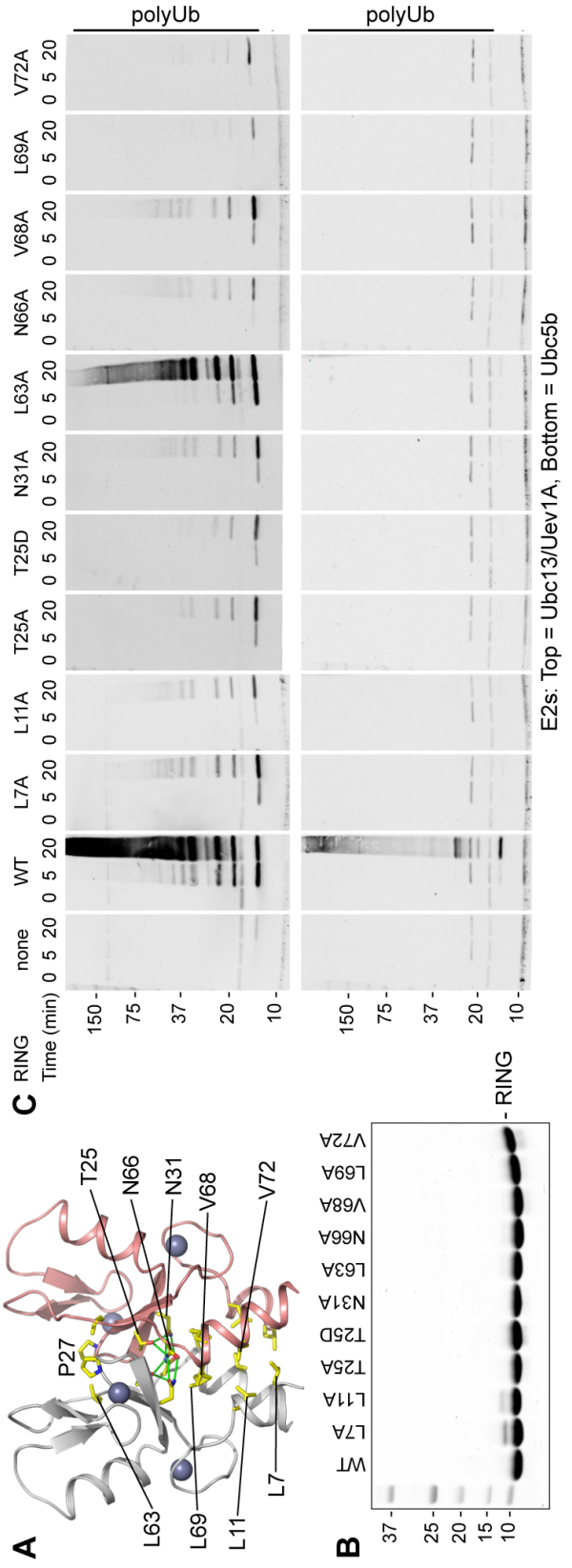
A
P27
T25
N66
N31
V68
V72
L63
L69
L11
L7
B
RING
WT
L7A
L11A
T25A
T25D
N31A
L63A
N66A
V68A
L69A
V72A
37
25
20
15
10
C
RING
Time (min)
none
WT
L7A
L11A
T25A
T25D
N31A
L63A
N66A
V68A
L69A
V72A
0 5 20
polyUb
150
75
37
20
10
E2s: Top = Ubc13/Uev1A, Bottom = Ubc5b

a buried hydrogen bond network, which is contiguous with the hydrophilic interactions at the RING/E2-Ub interface. A small four-helix bundle formed by residues that flank the zinc lobes in primary sequence also stabilizes the dimer via buried aliphatic side chains (Leu7, Leu11, Val68, Leu69, and Val72). The TRIM25 RING dimer is therefore reminiscent of the BRCA1/BARD1 heterodimer, in that helical elements outside the main zinc cores also mediate dimer formation (Brzovic et al., 2001). To validate the structure, we systematically substituted alanine for residues buried in both regions of the TRIM25 dimer interface and then purified the mutants (**Fig. 5B**) and tested their catalytic activity (**Fig. 5C**). Results showed that the RING mutants were invariably deficient in catalysis, with L69A and V72A showing the greatest deficiency (**Fig. 5C**). Importantly, the size-exclusion profiles of all the RING mutants were similar to that of the wild-type protein, indicating that the mutants were also monomeric on purification and that none of the mutations affected the tertiary fold of the domain (**Fig. 6A**). Similarly, the L69A and V72A mutations did not affect folding or the basal oligomerization of full-length TRIM25 (**Fig. 6B**).

RING dimerization facilitates Ub conjugation because the two RING domains cooperate in holding the Ub moiety in a configuration primed for catalysis (Dou et al., 2012; Plechanovova et al., 2012). The first RING interacts with both E2 and Ub using a conserved set of interactions (**Fig. 3C and 3D**), whereas the second RING contacts the same Ub using a different set of non-conserved residues (**Fig. 3D**). In RNF4 and BIRC7, the second set of interactions primarily consists of pi-stacking between a Ub backbone peptide and

Fig. 6. Size exclusion chromatography behavior of RING domain mutants.

(A) Superdex 75 size exclusion chromatography profiles of the RING domain mutants shown in Fig. 3 and 4, from the final purification steps. Mutant profiles are similar to WT, indicating that the mutations did not disrupt folding of the RING domain.

(B) SEC-MALS profiles of full-length TRIM25 with the L69A and V72A mutations. Dashed gray line indicates the expected dimer molecular weight.

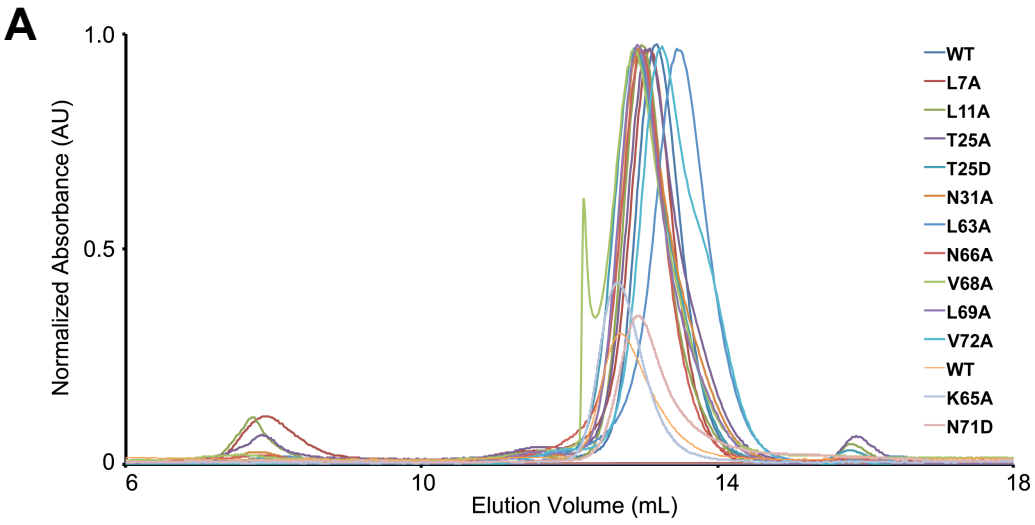
A
1.0
0.5
0
Normalized Absorbance (AU)
6
10
14
18
Elution Volume (mL)
WT
L7A
L11A
T25A
T25D
N31A
L63A
N66A
V68A
L69A
V72A
WT
K65A
N71D

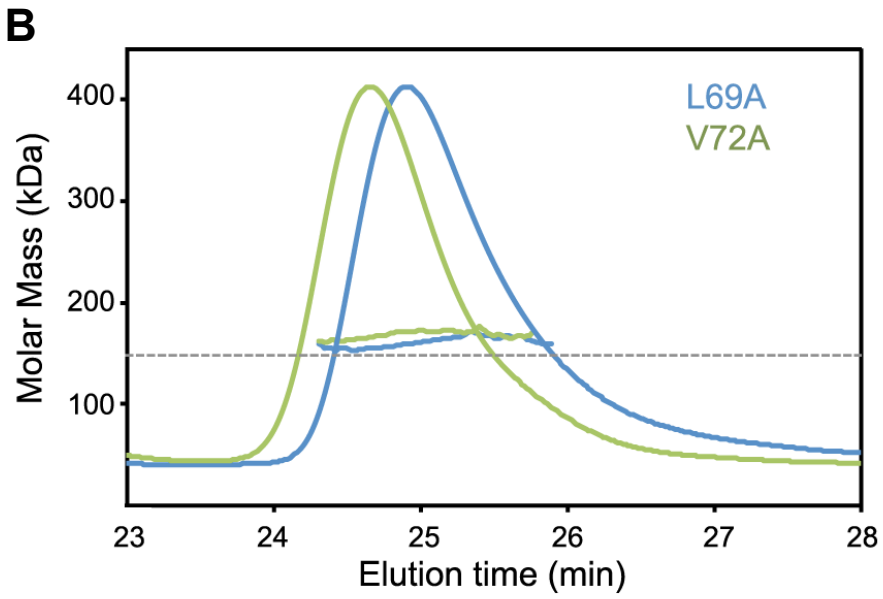
B
400
300
200
100
Molar Mass (kDa)
L69A
V72A
23
24
25
26
27
28
Elution time (min)

a tyrosine or phenylalanine side chain (**Fig. 3D**, middle and bottom panels; Dou et al., 2012; Plechanovova et al., 2012). In contrast, the TRIM25 interface consists of a hydrogen bond network mediated in part by Lys65 and Asn71 (**Fig. 3D**, top panel, and **4A**). To confirm that this set of interactions is important for catalysis, we also generated the K65A, N71A, and N71D mutants (**Fig. 7B**) and assayed them for ubiquitination activity (**Fig. 7C**). Although the N71A mutant was still catalytically active, both the K65A and N71D mutants were severely deficient. Thus, like RNF4 and BIRC7, the second set of RING/Ub interactions is also required for TRIM25 catalytic activity.

In summary, the results of our structure-based mutagenesis experiments support the conclusion that the TRIM25 RING domain is catalytically active as a dimer. This has now been further confirmed by an independent structure of the TRIM25 RING domain in complex with Ubc5a-Ub, which was reported while this paper was under review (Koliopoulos et al., 2016). The TRIM5a RING domain in complex with unconjugated Ubc13 is also a dimer (Yudina et al., 2015), as are uncomplexed structures of TRIM37 (PDB 3LRQ) and TRIM32 (Koliopoulos et al., 2016), and so this may be a general property of the TRIM family of E3 ligases.

TRIM25 RING Dimerization Is Required for RIG-I Signaling. Our structural and biochemical analyses identified the RING domain as a second self-association motif in TRIM25, in addition to the coiled-coil dimerization motif. We therefore sought to examine the requirement for both types of interactions in promoting RIG-I-mediated signaling. To test the signal-transducing activities of wild-type (WT) and mutant TRIM25 proteins without potentially confounding

Fig. 7. The Non-conserved Second Set of RING/Ub Interactions Is Required for Catalysis.

(A) Location of Asn71 and K65 (sticks) in context of the complex.

(B) Coomassie-stained SDS-PAGE gel of purified WT and mutant recombinant RING proteins. See also **Fig. 6**.

(C and D) Ubiquitination assays with indicated RING mutants (5 μM) and Ubc13/Uev1A (250 nM). WT panels show corresponding control experiments, performed in parallel. Samples were analyzed by IB with anti-Ub.

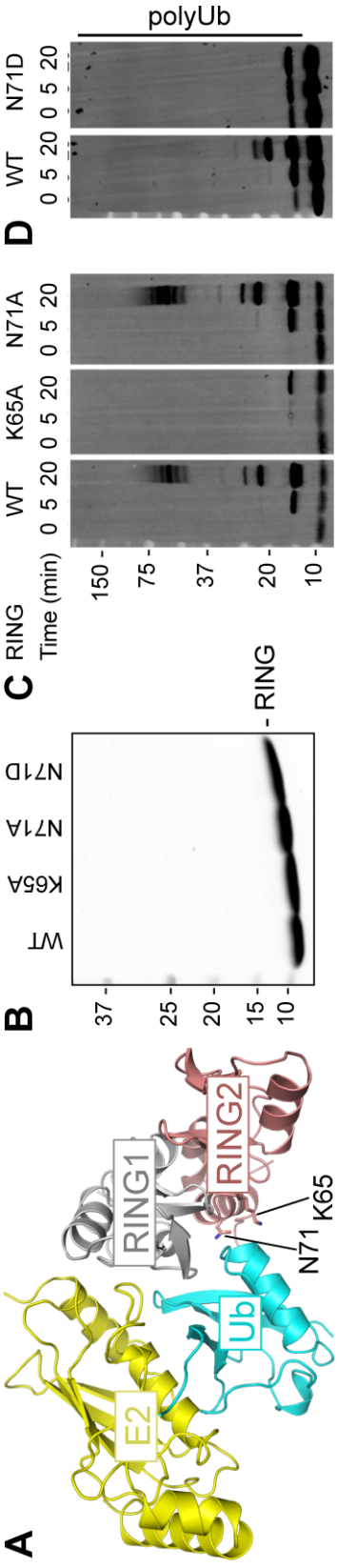
A
E2
Ub
RING1
RING2
N71
K65
B
WT
K65A
N71A
N71D
- RING
37
25
20
15
10
C
RING
Time (min)
WT
K65A
N71A
0 5 20 0 5 20 0 5 20
150
75
37
20
10
D
polyUb
WT
N71D
0 5 20 0 5 20

effects by the presence of endogenous TRIM25 protein, we utilized CRISPR technology to generate *TRIM25*-knockout (KO) HEK293T cells (**Fig. 8A**). Immunoblot (IB) analysis confirmed the absence of endogenous TRIM25 protein in these cells (**Fig. 8B**). To further validate the *TRIM25*-KO cells, we tested them for their ability to support RIG-I 2CARD-mediated IFN-b promoter activation by a luciferase assay (**Fig. 8B**). As previously shown (Gack et al., 2007), glutathione-S-transferase (GST)-fused RIG-I 2CARD (GST-2CARD) potently induced IFN-β promoter activation in normal (WT) HEK293T cells due to its constitutive signal-inducing activity. In contrast, IFN-β promoter activation induced by GST-2CARD was very low in *TRIM25*-KO cells (**Fig. 8C**). Consistent with these results, an IAV infection assay showed low viral NS1 protein expression in WT cells, indicative of well-controlled virus replication (**Fig. 8D**). In contrast, the expression of IAV NS1 protein was high in the *TRIM25*-KO cells, indicating that these cells are impaired in suppressing virus replication.

To determine the signal-promoting activity of TRIM25 mutants, we performed the IFN-β luciferase assay in *TRIM25*-KO cells that have been transfected with GST-2CARD together with two different amounts (1 or 5 ng) of plasmid encoding WT or structure-based mutants of TRIM25. As previously shown (Gack et al., 2007), WT TRIM25 strongly enhanced GST-2CARD-mediated signaling in a dose-dependent manner (**Fig. 9A**). In striking contrast, TRIM25 mutants harboring the L69A and V72A mutations, which disrupted the RING dimer interface, did not potentiate 2CARD-mediated signaling; that is, IFN-β promoter activation induced by GST-2CARD

Fig. 8. Generation and validation of *TRIM25*-KO HEK293T cells.

(A) Targeting strategy for CRISPR knockout. *TRIM25*-KO cells were generated using Cas9-mediated induction of a dsDNA break and insertion of a cassette encoding for a Blasticidin resistance gene (BSD) controlled by the HSV-1 thymidine kinase (TK) promoter into the TRIM25 open reading frame (ORF) through homologous recombination. Insertion of the HSV-1 TK-BSD cassette replaced the start codon and one additional G (ATGG) in the first exon of the TRIM25 ORF. Upon selection of resistant cell clones using Blasticidin, a single colony was isolated and propagated.

(B) Absence of TRIM25 protein in *TRIM25*-KO HEK293T cells. Normal (WT) and *TRIM25*-KO HEK293T cells were treated with 1,000 U/mL IFN-α2 for 24 h, or left untreated. WCLs were subjected to SDS-PAGE, followed by IB with anti-TRIM25, anti-RIG- I, and anti-actin antibodies.

(C) RIG-I 2CARD dependent signaling is strongly reduced in *TRIM25*-KO cells as compared to normal (WT) cells. WT or *TRIM25*-KO HEK293T cells were transfected with IFN-β-luciferase, β-galactosidase expressing pGK-β-gal, and GST or GST-2CARD. 12 h later, IFN-β promoter activity was measured by luciferase assay and luciferase values were normalized to β- galactosidase values. The results are expressed as mean ± s.d. (n = 3).

(D) Enhanced IAV replication in *TRIM25*-KO HEK293T cells. Normal (WT) and *TRIM25*-KO HEK293T cells were infected with IAV (PR8, H1N1) at an MOI of 0.001. 48 h later, cells were lysed and WCLs analyzed by IB for viral NS1 as well as endogenous TRIM25 and actin using anti-NS1, anti-TRIM25, and anti-actin antibodies.

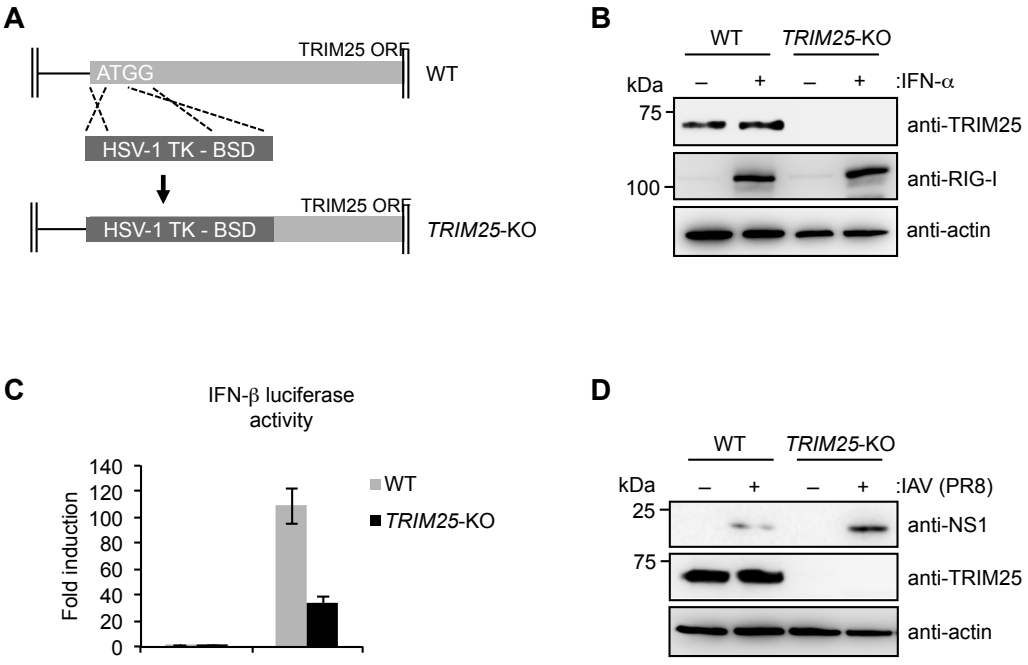
A
TRIM25 ORF
ATGG
WT
HSV-1 TK - BSD
TRIM25 ORF
HSV-1 TK - BSD
TRIM25-KO
B
WT
TRIM25-KO
kDa
–
+
–
+
:IFN-α
75
anti-TRIM25
100
anti-RIG-I
anti-actin
C
IFN-β luciferase activity
Fold induction
140
120
100
80
60
40
20
0
WT
TRIM25-KO
D
WT
TRIM25-KO
kDa
–
+
–
+
:IAV (PR8)
25
anti-NS1
75
anti-TRIM25
anti-actin

Fig. 9. IFN Induction, Ubiquitination, and Antiviral Activities of TRIM25.

(A) IFN-β induction by WT and TRIM25 mutants. *TRIM25*-KO HEK293T cells (**Fig. 8**) were transfected with plasmids encoding IFN-β-luciferase, β-galactosidase, GST, or GST-2CARD and empty vector (Vec) or the indicated FLAG-tagged TRIM25 (T25) constructs (see Experimental Procedures for details). Twelve hours later, IFN-β promoter activity was measured by a luciferase assay and values were normalized to β-galactosidase. Whole-cell lysates (WCLs) were analyzed by IB with the indicated antibodies. Results are expressed as mean ± s.d. (n = 2).

(B) Ubiquitination of RIG-I 2CARD. *TRIM25*-KO HEK293T cells were transfected with plasmid for GST or GST-2CARD, together with Vec or the indicated FLAG-TRIM25 constructs. Forty-eight hours later, cells were lysed and WCLs subjected to GST pull-down (GST-PD), followed by IB with anti-Ub and anti-GST antibodies. IB of WCLs was performed with anti-FLAG antibody to determine the expression levels of the TRIM25 WT and mutant proteins.

(C and D) Replication of influenza A virus (IAV) (H1N1 PR8 strain) in *TRIM25*-KO HEK293T cells reconstituted with TRIM25 WT or mutants. Cells were transfected with Vec or plasmids encoding FLAG-tagged TRIM25 WT or the indicated mutants. At 24 h post-transfection, cells were infected with IAV (MOI 0.01) for 96 hr. Expression levels of IAV NS1, actin, and TRIM25 constructs were analyzed by IB with anti-NS1, anti-actin, and anti-FLAG (TRIM25) antibodies (C). IAV titers in the supernatant of reconstituted *TRIM25*-KO cells were determined by TCID50 assay (D). The results shown are from two independent experiments.

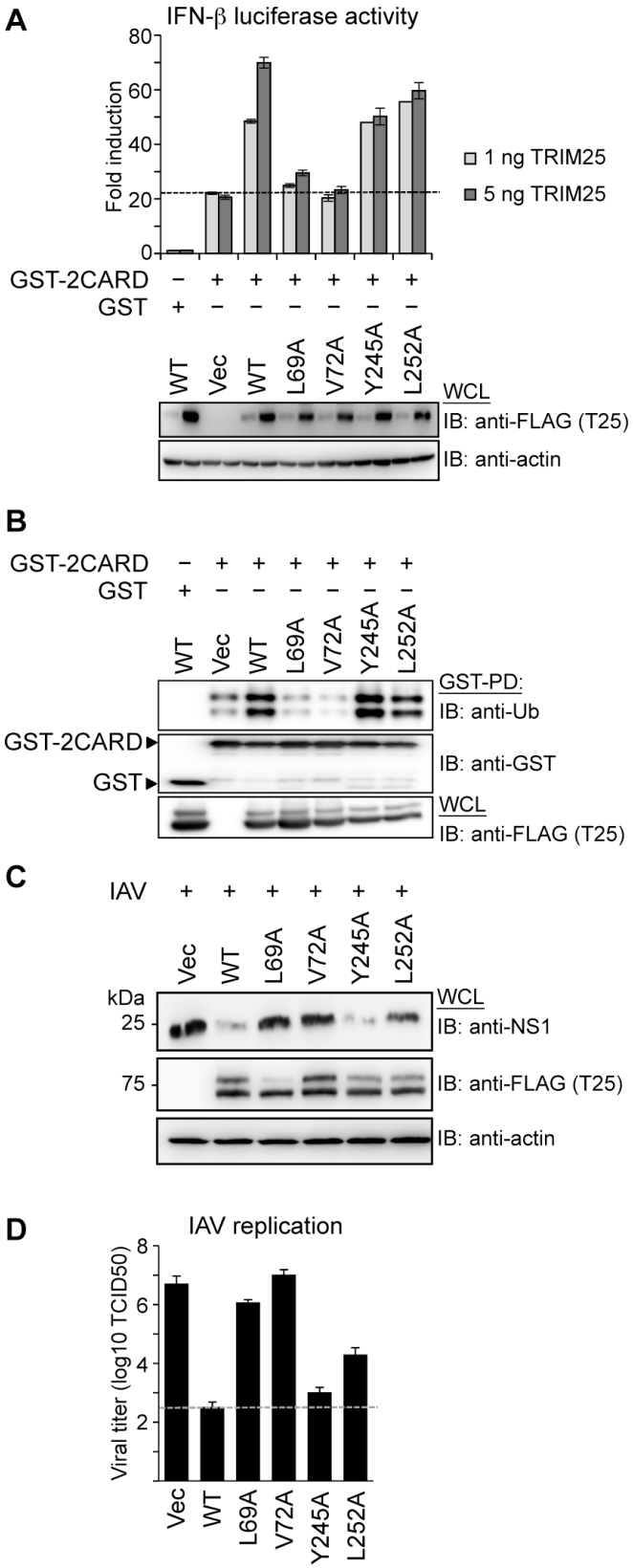
A
IFN-β luciferase activity
Fold induction
80
60
40
20
0
1 ng TRIM25
5 ng TRIM25
GST-2CARD – + + + + + +
GST + – – – – – –
WT Vec WT L69A V72A Y245A L252A
WCL
IB: anti-FLAG (T25)
IB: anti-actin
B
GST-2CARD – + + + + + +
GST + – – – – – –
WT Vec WT L69A V72A Y245A L252A
GST-PD:
IB: anti-Ub
GST-2CARD
IB: anti-GST
GST
WCL
IB: anti-FLAG (T25)
C
IAV + + + + + +
Vec WT L69A V72A Y245A L252A
kDa
25
75
WCL
IB: anti-NS1
IB: anti-FLAG (T25)
IB: anti-actin
D
IAV replication
Viral titer (log10 TCID50)
8
6
4
2
Vec WT L69A V72A Y245A L252A

co-expressed with TRIM25 L69A or V72A was similar to that of GST-2CARD expressed alone. The lack of IFN- β -inducing activity of the TRIM25 L69A and V72A mutants correlated very well with loss of ubiquitination of the RIG-I 2CARD (**Fig. 9B**), confirming that the abolished signal-promoting activity of TRIM25 L69A and V72A is due to defective E3 ligase activity.

We also tested TRIM25 proteins harboring Y245A and L252A mutations, which severely disrupted dimerization of the isolated coiled-coil domain (Sanchez et al., 2014). These TRIM25 mutants showed only slightly reduced activities in promoting GST-2CARD-mediated IFN-b promoter activation as compared to WT TRIM25 at higher expression, whereas they had similar activities to WT TRIM25 at low expression (**Fig. 9A**). The TRIM25 coiled-coil mutants also supported GST-2CARD ubiquitination, although this was somewhat reduced compared to WT TRIM25, in particular for the L252A mutant (**Fig. 9B**).

To determine the antiviral activity of TRIM25 mutants with disrupted RING dimer (L69A or V72A) or coiled-coil dimer (Y245A or L252A) interfaces, we reconstituted *TRIM25*-KO cells with the individual mutants and subsequently infected them with IAV. Cells transfected with empty vector or WT TRIM25 served as controls (**Fig. 9C and 9D**). Cells reconstituted with WT TRIM25 potently inhibited viral titers (by more than four log) and viral NS1 protein expression as compared to cells reconstituted with empty vector (Vec). In contrast, cells reconstituted with the TRIM25 L69A or V72A mutant had similar viral titers and NS1 protein levels as vector-complemented cells, indicating a profound defect in antiviral activity of these TRIM25 mutants. Furthermore,

cells reconstituted with the Y245A and L252A mutants showed only a slightly reduced antiviral activity as com-pared to WT TRIM25 (**Fig. 9C and 9D**), which is consistent with the IFN-b luciferase and 2CARD ubiquitination data (**Fig. 9A and 9B**).

The modest defect caused by the Y245A and L252A coiled-coil dimerization mutations was somewhat surprising, because these mutations resulted in severe misfolding of the isolated coiled-coil domain of TRIM25, as determined by a thermal melting assay (Sanchez et al., 2014). We therefore tested the effect of these mutations on the thermal melting profile of full-length TRIM25. In contrast to the isolated coiled-coil mutant proteins, the full-length mutants were more easily purifiable and remained dimeric, although, as expected, they were less stable than WT (**Fig. 10**). Thus, the folding defect caused by Y245A and L252A was much less pronounced in context of full-length TRIM25, explaining the modest effect of these mutations in the cell-based assays. We surmise that the presence of eukaryotic chaperones during expression of the full-length mutants likely compensates for the folding and dimerization defect caused by the coiled-coil mutations.

Analysis of TRIM25 Self-Association in Solution. The above results indicated that the stable, coiled-coil-mediated TRIM25 dimer (Sanchez et al., 2014) is insufficient for catalysis and that engagement of the E2-conjugating enzyme and polyUb synthesis occurs with further, higher-order assembly of the ligase. Indeed, TRIM5α, another antiviral TRIM family member, becomes catalytically active precisely by this mechanism. Higher-order assembly of

Fig. 10. Stability and Folding of Coiled-Coil Mutants.

(A) Coomassie-stained SDS-PAGE gel showing purified proteins.

(B) Differential scanning fluorimetry thermal melting profiles were measured using proteins at 1 mg/mL as described (Sanchez et al., 2014). Upper panel shows raw fluorescence curves; error bars represent ± s.d. from quadruplicate measurements. Lower panel shows negative first derivatives of the raw curves indicate Y245A had 2 transitions. These results indicate that, in context of full-length TRIM25, the coiled-coil mutations did not disrupt dimerization but did reduce stability.

(C) SEC-MALS profiles of full-length TRIM25 with the Y245A and L252A mutations show that the coiled-coil mediated dimers are intact. Dashed gray line indicates the expected dimer molecular weight.

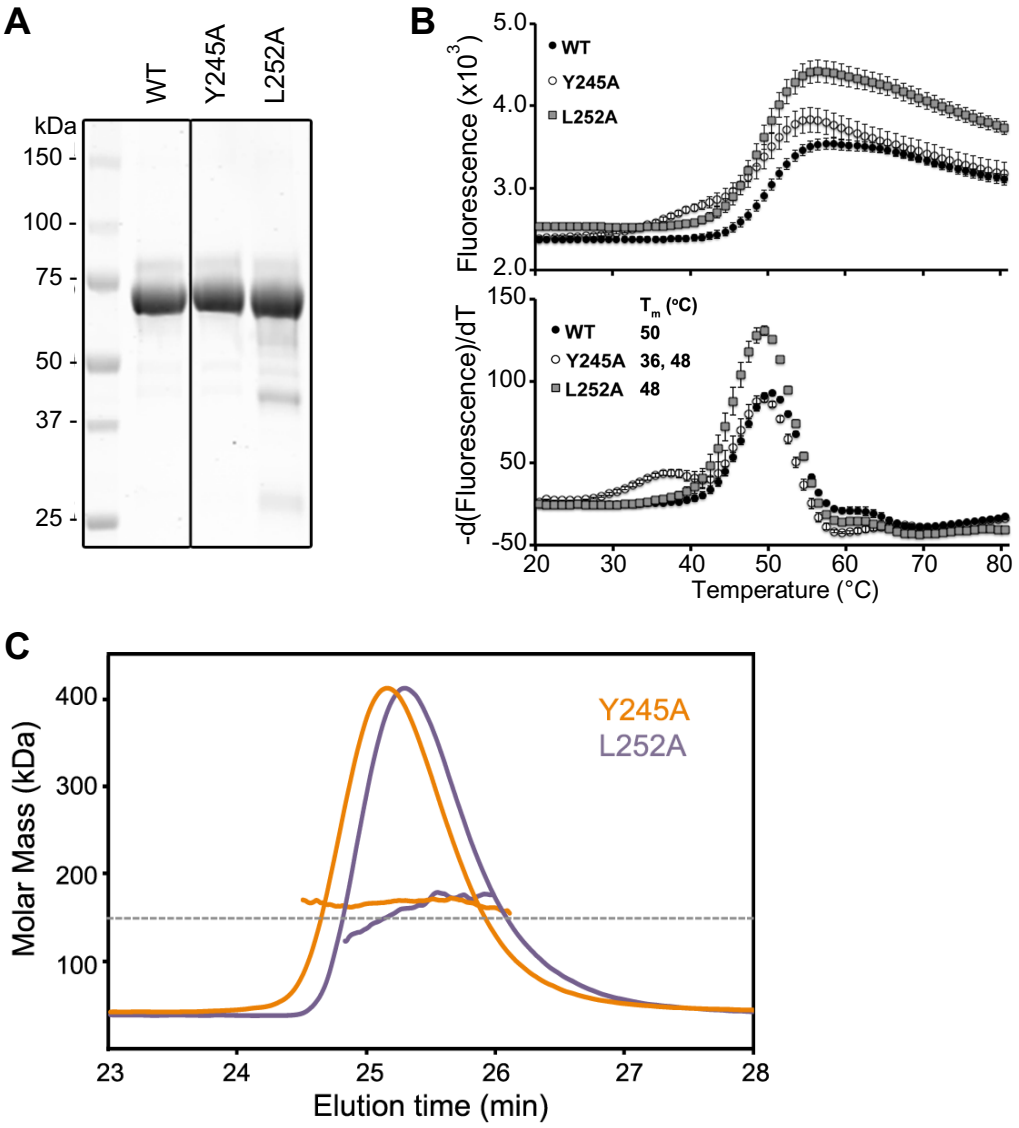
A
WT
Y245A
L252A
kDa
150
100
75
50
37
25
B
Fluorescence (x10^3)
5.0
4.0
3.0
2.0
WT
Y245A
L252A
-d(Fluorescence)/dT
150
100
50
-50
T_m (°C)
WT 50
Y245A 36, 48
L252A 48
20
30
40
50
60
70
80
Temperature (°C)
C
Molar Mass (kDa)
400
300
200
100
Y245A
L252A
23
24
25
26
27
28
Elution time (min)

TRIM5a is mediated by its single B-box domain, which facilitates spontaneous assembly of coiled-coil-mediated TRIM5α dimers into an extended lattice (Diaz-Griffero et al., 2009; Ganser-Pornillos et al., 2011; Li and Sodroski, 2008; Li et al., 2016; Wagner et al., 2016). Note that, in contrast to TRIM5α, TRIM25 has a tandem of B-boxes (**Fig. 1A**). To determine whether TRIM25 also assembles spontaneously in a B-box-dependent manner, we analyzed the solution behavior of full-length TRIM25 (**Fig. 4B** and **4C**). Notably, we found that full-length TRIM25 had significant E3 ligase activity at nanomolar concentrations (**Fig. 1F**). This was in contrast to the isolated RING domain, which catalyzed polyUb formation only at micromolar concentrations (**Fig. 1C**) and suggested that, in context of the full-length protein, RING-RING interactions occurred more readily. We have previously shown that the isolated coiled-coil domain of TRIM25 is a stable dimer in solution, and indeed, freshly purified full-length TRIM25 also behaved as a stable dimer at low-protein concentrations (**Fig. 4B**). Interestingly, at higher concentrations, we reproducibly detected the presence of a minor species with molecular weight consistent with a tetramer (**Fig. 4C**). However, extensive analysis by electron microscopy did not reveal convincing evidence of spontaneous higher-order or lattice-type assembly behavior for TRIM25. These results indicated that unlike the B-box 2 domain of TRIM5a, the equivalent domain in TRIM25 does not spontaneously self-associate. We conclude that efficient TRIM25 RING domain activation is likely to be facilitated by other factors.

RIG-I 2CARD Enhances TRIM25's Catalytic Activity In Vitro. What might be the factors that promote assembly of catalytically active TRIM25? Our data indicate that a minimum of two coiled-coil-mediated TRIM25 dimers (or four monomers) is required to generate a catalytically active E3 ligase. This matches the stoichiometry of the 2CARD tetramer that seeds MAVS filament assembly. Therefore, an appealing hypothesis is that TRIM25 and RIG-I mutually promote each other's oligomerization and activation. Indeed, it has been demonstrated that K63-linked poly-Ub chains synthesized by TRIM25 can promote 2CARD tetramerization in vitro (Peisley et al., 2014). We therefore performed the complementary experiment to ask whether 2CARD promotes higher-order oligomerization and catalytic activation of TRIM25.

We first titrated TRIM25 concentrations in our ubiquitination reactions and found that, with 100 nM of full-length TRIM25, poly-Ub chain formation was minimal with either Ubc13/Uev1A (**Fig. 11A**, lane 3) or Ubc5c (**Fig. 11A**, lane 7). The same reactions were then performed in the presence of 1 mM of freshly purified His-tagged 2CARD, and we found that polyUb synthesis was very significantly enhanced (**Fig. 11A**, compare lane 4 to lane 3 and lane 8 to lane 7). Thus, RIG-I 2CARD can promote TRIM25 RING/RING self-association in vitro and, by implication, higher-order oligomerization of coiled-coil-mediated TRIM25 dimers.

To determine whether polyUb-mediated 2CARD tetramerization was required for this effect, we measured catalysis using a Ub discharge assay in which polyUb chains were not being made (Middleton et al., 2014). In this assay,

Fig. 11. RIG-I 2CARD Enhances TRIM25's Catalytic Activity In Vitro.

(A) Ubiquitination activity of 100 nM FLAG-TRIM25 in the presence or absence of His-tagged RIG-I 2CARD. Reaction mixtures were analyzed by IB with anti-Ub (top), anti-FLAG (middle), and anti-His (bottom). As with the autoubiquitination reactions, substrate-attached Ub was observed only with Ubc5b and not with Ubc13/Uev1A. This experiment was performed with five independent protein preparations, with similar results.

(B) Oxyester hydrolysis assays showing the disappearance of Ubc5b$^{S22R/C85S}$-Ub conjugates and the appearance of free Ubc5b in the presence of full-length TRIM25 (1 μM), GST-tagged WT or T55D RIG-I 2CARD (8 μM), and/or K63-linked tetraUb (5 μM) over 180 min. (Top) Samples were resolved by using non-reducing SDS-PAGE and Coomassie blue staining. Experiments were performed in duplicate, and one set is shown. (Bottom) Densitometry quantification of gels follows the appearance of free Ubc5b over time. Error bars show the range values obtained in two independent experiments, performed with independent protein preparations of both TRIM25 and 2CARD.

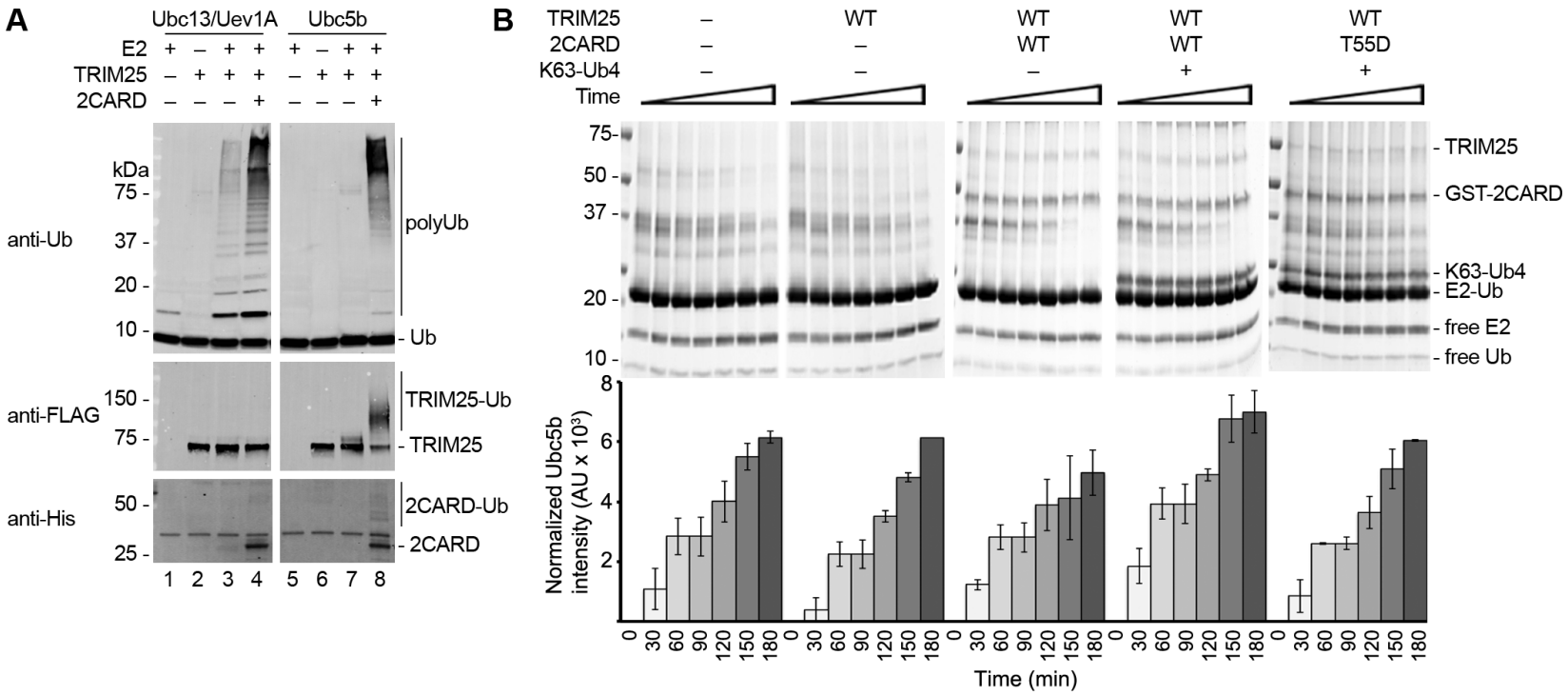
A
Ubc13/Uev1A
Ubc5b
E2
TRIM25
2CARD
kDa
anti-Ub
anti-FLAG
anti-His
polyUb
Ub
TRIM25-Ub
TRIM25
2CARD-Ub
2CARD
1 2 3 4 5 6 7 8
B
TRIM25
2CARD
K63-Ub4
Time
WT
T55D
TRIM25
GST-2CARD
K63-Ub4
E2-Ub
free E2
free Ub
Normalized Ubc5b intensity (AU x 10³)
Time (min)

E2-Ub conjugates were first synthesized by incubation of E1 and E2 enzymes with Ub and ATP. Discharge of the Ub moiety was then monitored by the disappearance of the E2-Ub conjugate and appearance of free E2, under conditions that prevent re-charging of the E2. To slow down the reaction, we used oxyester-linked Ubc5b$^{S22R/C85S}$-Ub conjugates and did not add excess Ub acceptor amine (Middleton et al., 2014; Wright et al., 2016). In this assay format, we found that TRIM25 did not significantly increase the basal rate of free E2 accumulation, probably because dissociation of the RING/RING dimer or RING/E2-Ub complex was fast relative to oxyester cleavage. We then found that the presence of 2CARD also did not result in increased discharge (**Fig. 11B**), even though we used a GST-2CARD fusion protein that was already dimeric due to the GST tag. On the other hand, when the added GST-2CARD was pre-incubated with K63-linked tetraUb, TRIM25-mediated discharge was increased. The effect was modest but was nevertheless evident, especially when comparing the initial time points (30–90 s), and was reproducibly observed in two independent experiments performed with independent protein preparations (**Fig. 11B**). Because incubation with K63-linked polyUb chains induces 2CARD tetramerization in vitro (Peisley et al., 2014), these results indicated that the presence of the 2CARD tetramer also stabilized the TRIM25 RING dimer and/or RING/E2-Ub complexes, i.e., that 2CARD oligomerization and TRIM25 oligomerization can occur cooperatively.

Finally, we found that mutation of T55 in the first CARD, which is a critical residue for TRIM25 SPRY domain binding (Gack et al., 2008), did not increase

TRIM25-mediated Ub discharge, even when the mutant GST-2CARD was pre-incubated with K63-linked polyUb (**Fig. 11B**). This result confirmed expectation that RIG-I 2CARD-mediated TRIM25 activation is dependent on binding of 2CARD to the SPRY domain of TRIM25.

DISCUSSION

The essential role of TRIM25 in the RIG-I pathway is underscored by findings that viruses, such as IAV and dengue virus, have evolved mechanisms to suppress RIG-I signaling by specifically targeting and disrupting TRIM25 function (Gack et al., 2009; Manokaran et al., 2015; Rajsbaum et al., 2012). In this study, we confirm the essential requirement for TRIM25's E3 ubiquitin ligase activity in RIG-I signaling (Gack et al., 2007) by showing that mutations that disrupt TRIM25 RING domain activation also reduce to background levels the ubiquitination of RIG-I 2CARD, 2CARD-dependent IFN induction, and antiviral activity against IAV. Furthermore, our results show that the TRIM25 RING domain must dimerize in order to productively engage Ub-conjugated E2 enzymes and become catalytically active, which is a common (but not universal) property of the RING family of E3 ubiquitin ligases (Lima and Schulman, 2012). Like other TRIM proteins, the basal oligomeric state of TRIM25 is a stable, coiled-coil-mediated dimer (Goldstone et al., 2014; Li et al., 2014; Sanchez et al., 2014; Weinert et al., 2015). The TRIM25 coiled-coil dimer has an antiparallel architecture, which places the two associated RING domains on opposite ends of an elongated rod (Sanchez et al., 2014). Therefore, TRIM25 RING dimers

very likely form by means of higher-order oligomerization (or assembly) of the coiled-coil-mediated dimers.

We envision at least two possible types of assembled, catalytically active TRIM25: a tetramer form wherein one coiled-coil-mediated dimer would interact with a second to allow head-to-head interactions of their RING domains or a filamentous or net form wherein the RING domains on opposite ends of the coiled coil would interact with RING domains from separate dimers (**Fig. 12**). TRIM5α, another well-characterized TRIM protein, makes higher-order complexes by the second mechanism; in this case, individual N-terminal RING domains are brought into close proximity by spontaneous trimerization of the downstream B-box 2 domains and assembly of TRIM5α dimers into an extended hexagonal network (Ganser-Pornillos et al., 2011; Li et al., 2016; Wagner et al., 2016; Yudina et al., 2015). Our analysis did not reveal a similar type of spontaneous high-order assembly behavior for TRIM25, indicating that its RING domains are brought into proximity by a different mechanism.

Initial recognition of viral RNA by RIG-I occurs at a tri- or di- phosphorylated blunt end of the viral RNA (Cui et al., 2008; Goubau et al., 2014; Hornung et al., 2006; Jiang and Chen, 2011; Kowalinski et al., 2011; Luo et al., 2011; Pichlmair et al., 2006). Multiple RIG-I molecules can decorate the same RNA (if it is of sufficient length) in an ATP-dependent manner (Peisley et al., 2013). This property of RIG-I is thought to promote clustering of activated 2CARDs, because a minimum of four 2CARD molecules is required to seed

Fig. 12. Models of TRIM25 RING Dimerization.

Shown are two possible modes of higher-order assembly of coiled-coil-mediated TRIM25 protein dimers that will promote RING/RING dimerization. The domains are color-coded as follows: red, RING (R); orange, B-boxes (B); green, coiled coil; blue, SPRY (S).

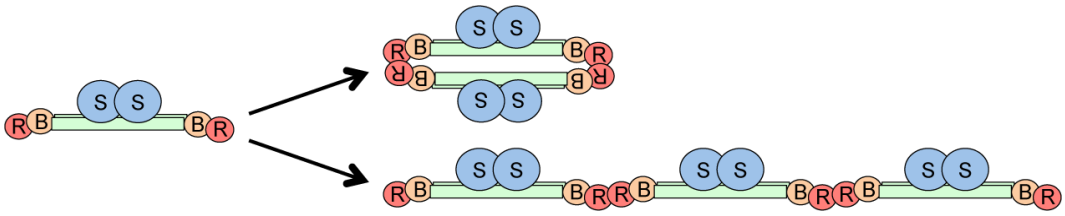
S
S
R
B
B
R

MAVS CARD filament assembly and initiate signaling (Peisley et al., 2014; Wu et al., 2014). We found that, at least in vitro, the isolated 2CARD can promote TRIM25 catalytic activation, in a manner that appears dependent on binding of 2CARD to the TRIM25 SPRY domain. These results indicate that RIG-I assembly on the viral RNA has the additional purpose of recruiting and clustering multiple TRIM25 dimers to activate K63-polyUb synthesis. Such a coupled recruitment and activation mechanism avoids any potential off-pathway effects of polyUb chains because these are synthesized only when needed and at the correct location.

Furthermore, we propose that mutually productive engagement of RIG-I and TRIM25 goes beyond simple proximity-induced self-association and activation. Because 2CARD-mediated enhancement of TRIM25 activity in vitro is also dependent on polyUb, it is very likely that formation of the tetrameric 2CARD seed is cooperative with TRIM25 RING dimerization and catalytic activation. Indeed, it is probable that there is an avidity component to the interaction, because a head-to-head TRIM25 tetramer should cluster four SPRY domains and allow simultaneous, stoichiometric SPRY/2CARD binding. A cooperative assembly mechanism is consistent with the finding that TRIM25, RNA-bound RIG-I, and the chaperone protein 14-3-3ε make a stable ternary complex that translocates from the cytosol to mitochondria in order to activate MAVS (Liu et al., 2012).

In summary, our results help to explain why TRIM25 is an essential player in the RIG-I-signaling pathway. In addition to its role as an enzymatic effector of

RIG-I, TRIM25 confers additional biochemical functionalities that promote 2CARD tetramerization and signal propagation. TRIM25 therefore helps to fine-tune the efficiency of RIG-I-mediated signaling to high degree, which is an important property that allows the pathway to respond effectively even if viral challenge is low.

METHODS

Ubiquitination Assay. E1 and E2 enzymes and Ub were either purified in house or purchased from Boston Biochem, UBPBio, or Enzo Life Sciences. Ubiquitination reactions were incubated at 37 C in 50 mM Tris (pH 7.5), 150 mM NaCl, 0.5 mM tris(2-carboxyethyl)phosphine (TCEP), or 1 mM β-mercaptoethanol (βME) and typically contained E1 (50 or 100 nM), E2 (280 μM Ubc13/Uev1A, 1 μM Ubc13, or 1 μM Ubc5b), E3 (200 nM TRIM25 or 5 μM RING), Ub (40 μM), ATP (3 mM), and $MgCl_2$ (5 mM). Reactions were stopped by addition of SDS-PAGE sample buffer and boiling for 10 min. Typically, time points were taken at 0, 5, and/or 20 min. Immunoblots were performed with anti-Ub (1:2,000; P4D1; Santa Cruz Biotechnology), K63-linkage-specific anti-Ub (1:1,000; Enzo Life Sciences), anti-pentaHis (1:1,000; QIAGEN), and anti-FLAG M2 (1:5,000; Sigma). Signals were detected with a fluorescent secondary antibody (Rockland) and a LI-COR Odyssey scanner.

Ubiquitin Discharge Assay. This assay was performed essentially as described (Wright et al., 2016). $Ubc5b^{S22R/C85S}$-Ub oxyester-linked conjugate was prepared by mixing the following: 200 μM Ubc5b, 300 μM Ub, 1 μM E1, 50 mM

Tris (pH 7.5), 150 mM NaCl, 5 mM ATP, 5 mM $MgCl_2$, 0.5 mM TCEP, and 0.1% Triton X-100. After overnight incubation at 37 C, the E1 enzyme and free ATP were removed by gel filtration in 20 mM Tris (pH 7.5) and 150 mM NaCl. Fractions containing E2-Ub, free E2, and free Ub were collected and concentrated to 4 mg/ml (5x concentration). Discharge reactions containing 1x Ubc5b$^{S22R/C85S}$-Ub, 1 μM TRIM25, and 8 μM GST-2CARD (WT or T55D), with or without 5 μM K63-linked tetraUb (Boston Biochem) in 50 mM Tris (pH 7.5) and 50 mM NaCl were incubated at 37°C. Time points were taken every 30 min over 3 h and quenched by addition of non-reducing SDS-PAGE and subsequent placement on ice. Reactions products were visualized by SDS-PAGE and Coomassie staining. Free Ubc5b$^{S22R/C85S}$ was quantified by using a LI-COR Odyssey scanner. The experiment was performed twice, each with freshly purified batches of TRIM25 and 2CARD.

Structure Determination of the TRIM25 RING/Ubc13-Ub Complex. The purified RING and Ubc13^{C87K}-Ub conjugate samples were diluted to 20 μM using their respective size exclusion buffers, mixed at equal volumes, and then concentrated to 10 mg/ml. Crystallization was performed in sitting drops with commercial screens at a 2:1 protein-to-precipitant ratio. Crystals formed in Hampton PEG/Ion HT Screen condition no. D9 (0.2 M Li citrate and 20% polyethylene glycol (PEG) 3,350) after 2 days and were used for data collection without optimization. Ethylene glycol (10% [v/v] in mother liquor) was used as cryoprotectant. Diffraction data collected at beamline 5.0.1 at the Advanced Light Source were indexed and scaled using HKL2000 (Otwinowski and Minor, 1997).

The phase problem was solved by molecular replacement with crystal structures of human Ubc13 (PDB 1J7D) and Ub (PDB 1UBQ). The Ubc13 active site loop and Ub tail were removed from the search models to obtain unbiased densities for these regions. After positioning of the Ubc13 and Ub moieties, rigid body refinement also revealed strong densities for the zinc atoms in the RING domains as well as coordinating side chains and associated loops. These served as guides for calculation of 2-fold noncrystallographic symmetry (NCS) averaged maps, which were used to build the RING domains. Iterative refinement and manual model building were performed with PHENIX (version 1.9-1692; Adams et al., 2010) and Coot (Emsley et al., 2010). Secondary structure, torsion angle NCS, covalent bond and angle restraints for the Ubc13 K87-Ub G76 isopeptide, and zinc coordination (bond and angle) restraints were applied during refinement. Structure validation tools (as implemented in PHENIX and Coot) were used throughout the refinement process. Structure statistics are summarized in **Table 1**.

IFN-β Luciferase Assay. *TRIM25*-KO HEK293T cells were seeded into 24-well plates. The next day, the cells were transfected with 100 ng of IFN-β luciferase reporter plasmid and 150 ng of b-galactosidase-expressing pGK-β-gal. To stimulate IFN-β promoter activity, cells were also transfected with 1 ng of plasmid encoding GST-2CARD together with 1 or 5 ng of empty pCMV vector or pCMV-FLAG-TRIM25 WT or mutant constructs. Twelve hours later, whole-cell lysates (WCLs) were prepared and subjected to a luciferase assay

(Promega). Luciferase values were normalized to β-galactosidase activity to measure the transfection efficiency.

GST Pull-Down Assay and Immunoblot Analysis. Pelleted cells were lysed in NP-40 buffer (50 mM HEPES [pH 7.4], 150 mM NaCl, 1% [v/v] NP-40, and protease inhibitor cocktail [Roche]), followed by centrifugation at 13,000 rpm for 25 min. Lysates were mixed with a 50% slurry of glutathione-conjugated Sepharose beads (GE Healthcare), and the binding reaction was incubated for 3 h at 4°C. Precipitates were washed extensively with lysis buffer. Proteins bound to the beads were separated by SDS-PAGE and transferred to a polyvinylidene difluoride (PVDF) membrane (Bio-Rad). Immunoblots were performed with anti-Ub (1:5,000; P4D1; Santa Cruz), anti-FLAG (1:2,000; Sigma), anti-GST (1:2,000; Sigma), anti-RIG-I (1:1,000; Adipogen), anti-TRIM25 (1:2,000; BD Biosciences), anti-actin (1:5,000–1:15,000; Sigma), or anti-NS1 (polyclonal rabbit; 1:3,000; kindly provided by Adolfo Garcia-Sastre, Mount Sinai). The proteins were visualized by a chemiluminescence reagent (Pierce) and detected with a GE Healthcare Amersham Imager.

Influenza Replication Assays. *TRIM25*-KO HEK293T cells, seeded into 12-well plates, were transfected with 2 mg of pCMV empty vector or pCMV-FLAG-TRIM25 WT or mutant constructs. At 24 hr post-transfection, cells were infected with IAV (MOI 0.01) for 96 hr. To determine viral titers, supernatants were subjected to an endpoint titration (TCID50) assay on MDCK cells in DMEM supplemented with Pen-Strep, 0.2% BSA (Sigma), 25 mM HEPES, and 2 mg/mL TPCK-trypsin (Worthington Biochemical), as described

previously (Balish et al., 2013). Furthermore, cells were harvested and WCLs prepared and subjected to SDS-PAGE and IB analysis using anti-NS1, anti-FLAG, and anti-actin antibodies.

Purification of the TRIM25 RING Domain. DNA encoding the TRIM25 RING domain (residues 1-83) was subcloned into the NdeI and BamHI sites of pET28a (Novagen) in-frame with a His-tag leader and a thrombin cleavage site. Mutants were made from this construct by the Quikchange method (Agilent). Proteins were expressed in *E. coli* BL21(DE3) cells using the auto-induction method (Studier, 2005). Cells from 1 L of culture were resuspended in 30 mL lysis buffer (50 mM Tris, pH 9.0, 0.3 M NaCl, 1 mM TCEP) supplemented with 2 mM phenylmethylsulfonylfluoride (PMSF). Cells were lysed using a microfluidizer (Microfluidics model M110P) at 20,000 psi chamber pressure. Cell debris was removed by centrifugation (45,000 g for 45 min at 4 °C). Filtered supernatant was incubated in a gravity flow chromatography column with ~4 mL Ni-NTA resin (Qiagen) for 1 h on a rocker at 4 °C. The resin was washed with 200 mL lysis buffer, followed by 500 mL of wash buffer (25 mM Tris, pH 8.0, 300 mM NaCl, 1 mM TCEP, 15 mM imidazole). Bound protein was eluted in wash buffer containing 400 mM imidazole. Thrombin (Sigma) was added to the pooled fractions (50 units), and the sample was dialyzed overnight at room temperature against cleavage buffer (20 mM Tris, pH 8.0, 20 mM NaCl, 1 mM TCEP, 2 mM $CaCl_2$). Pooled fractions were concentrated to ~4 mL and purified to homogeneity on a HiLoad 16/600 Superdex 75 gel filtration column (GE Healthcare) in crystallization buffer (20 mM HEPES, pH 7.4, 100 mM NaCl,

1 μM $ZnCl_2$, 1 mM TCEP). Dimerization mutants were purified in the same manner. Typical yields were ~2.5 mg/L culture. The pure proteins were concentrated to ~25 mg/mL (WT) or ~2 mg/mL (mutants), flash -frozen in liquid nitrogen, and stored at -80°C. The mass of freshly purified WT protein was determined by electrospray ionization mass spectrometry to be 9,496 Da, which exactly matched the expected value.

Purification of full-length TRIM25. Full-length TRIM25 was subcloned into pFastBac1 (Invitrogen) with an N-terminal Strep/FLAG tag and a human rhinovirus 3C protease cleavage site using the InFusion system (Clontech). Mutants were made from this construct by the Quikchange method (Agilent). Proteins were expressed in SF9 insect cells using a modification of the Invitrogen Bac-to-Bac baculovirus expression system (Hanson et al., 2007). Cells from 1.6 L of culture were resuspended in lysis buffer (50 mM Tris, pH 8.0, 20 mM NaCl, 200 mM $(NH_4)_2SO_4$, 10% (v/v) glycerol, 1.5% (v/v) Triton X-100, 1 mM TCEP) supplemented with 2 mM PMSF, 2 tablets of protease inhibitor cocktail tablets (Roche), and 25 units/mL Benzonase nuclease (Sigma). Cells were lysed using a dounce homogenizer, and debris was removed by centrifugation (45,000 *g* for 45 min at 4°C). To remove contaminating nucleic acids, a 9% solution of polyethyleneimine (PEI) was added dropwise to the clarified cell lysate to a final concentration of 0.1%, followed by stirring for 40 min in ice. The resulting precipitate was removed by centrifugation (20,000 *g* for 30 min at 4°C). The supernatant was incubated in a gravity flow chromatography column with 4 mL of StrepTactin resin (GE Healthcare) for 3 h on a rocker at 4 °C. The resin was

washed four times with 40 mL of wash buffer (50 mM Tris, pH 8.0, 300 mM NaCl, 10% (v/v) glycerol, 1 mM TCEP). Bound protein was eluted in wash buffer containing 5 mM desthiobiotin (Sigma). Pooled fractions were concentrated to ~4 mL and purified to homogeneity on a HiLoad 16/600 Superdex 200 gel filtration column (GE Healthcare) in size-exclusion buffer (20 mM CHES, pH 9.0, 300 mM NaCl, 1 mM TCEP). The purified protein was concentrated to ~4.5 mg/mL, flash-frozen with liquid nitrogen, and stored at -80°C. Typical yields were ~1.25 mg/L of culture.

Purification of His-tagged RIG-I 2CARD. The expression plasmid for His-tagged human RIG-I 2CARD was a kind gift of Sun Hur (Harvard Univ.). Protein was expressed and lysates prepared as described above for the TRIM25 RING domain. PEI precipitation was performed as described above for full-length TRIM25. The target protein was extracted from the supernatant by using 40% ammonium sulfate and centrifugation (9000 g for 20 min at 4°C). The pellet containing RIG-I 2CARD was resuspended in 50 mL wash buffer (50 mM HEPES, pH 8, 300 mM NaCl, 10% (v/v) glycerol, 20 mM imidazole, and 1 mM TCEP) and incubated in a gravity flow chromatography column with 4 mL Ni-NTA resin (Qiagen) for 1 h on a rocker at 4 °C. The resin was washed with 400 mL of wash buffer, followed by elution with wash buffer containing 500 mM imidazole at pH 8. The protein solution was concentrated to ~5 mL and purified to homogeneity on a HiLoad 16/600 Superdex 75 gel filtration column (GE Healthcare) and eluted in size-exclusion buffer (20 mM HEPES at pH 8, 300 mM NaCl, 1 mM TCEP). Purified protein was concentrated to ~160 μM.

Purification of GST-tagged RIG-I 2CARD. The 2CARD reading frame was subcloned into pGEX2T, in frame with an N-terminal GST tag and thrombin site (GE Healthcare). The T55D mutation was introduced into this vector using Quikchange (Agilent). Proteins were expressed in *E. coli* BL21(DE3) cells, induced at OD_{600} = 0.6 with 400 μM isopropyl β-D-1-thiogalactopyranoside (IPTG) and incubated at 16 °C for 16h. Cells from 3 L of culture were resuspended in 50 mL lysis buffer (50 mM Tris 8, 150 mM NaCl, 2 mM PMSF, 10% (v/v) glycerol, and 1 mM TCEP). Lysis and PEI precipitation were performed as described for the His-tagged 2CARD. Filtered supernatant was incubated in a gravity flow chromatography column with 2.5 mL glutathione agarose resin (Goldbio) for 4 h on a rocker at 4 °C. Bound protein was eluted with 2.5 mM glutathione after extensive washing of the resin with lysis buffer. Pooled fractions were concentrated to ~3 mL and purified to homogeneity on a HiLoad 16/600 Superdex 75 gel filtration column (GE Healthcare) in purification buffer (20 mM Tris, pH 7.5, 150 mM NaCl). Pooled protein fractions were concentrated to 40 μM.

Purification of Ubc13C87K. The human Ubc13 C87K mutant, with an N-terminal His-tag, was made by Quikchange mutagenesis from a plasmid template kindly provided by Chris Hill (Univ. of Utah). Protein was expressed in *E. coli* BL21(DE3) cells using the auto-induction method (Studier, 2005). Cells were lysed in the same manner as TRIM25 RING, and the protein was purified using a 5-mL Ni-NTA column (Qiagen) . Bound fractions were eluted in 20 mM Tris, pH 8.0, 150 mM NaCl, 1 mM TCEP, 400 mM imidazole. 3C protease was

added to the pooled fractions (~1:160 mass ratio), and the sample was dialyzed overnight at 4 °C against cleavage buffer (20 mM Tris at pH 8, 150 mM NaCl, 1 mM TCEP). The protein solution was concentrated to ~5 mL and purified to homogeneity with a HiLoad 16/600 Superdex 75 gel filtration column (GE Healthcare) in 20 mM HEPES, pH 7.4, 150 mM NaCl, 1 mM TCEP. The pure protein was concentrated to ~33 mg/mL, flash-frozen in liquid nitrogen, and stored at -80 °C.

Preparation of Ubc13^{C87K}-Ub conjugate. The stable Ubc13^{C87K}-Ub conjugate was prepared using a previously published protocol for Ubc5a (Plechanovová et al., 2012). Briefly, Ubc13 C87K (200 μM), His-tagged Ub (240 μM, UBPBio), and E1 (0.75 μM, Enzo Life Sciences) were mixed and then dialyzed overnight in reaction buffer (50 mM Tris, pH 10.0, 150 mM NaCl, 3 mM ATP, 5 mM $MgCl_2$, 0.5 mM TCEP). The reaction mix was then incubated at 35°C for 24 h, followed by overnight dialysis (50 mM Tris, pH 9.0, 150 mM NaCl, 1 mM TCEP) at 4 °C. Following purification using Ni-NTA resin (Qiagen), the His-tag was removed from the Ub moiety by overnight incubation with 50 units of thrombin (Sigma), and the E2-Ub conjugate was purified to homogeneity on a HiLoad 16/600 Superdex 75 gel filtration column (GE Healthcare) in size-exclusion buffer (20 mM HEPES, pH 7.4, 150 mM NaCl, 1 mM TCEP). The purified conjugate was concentrated to 0.6 mg/mL.

Purification of Ubc5b. Untagged human Ubc5b and Ubc5b$^{S22R/C85S}$ were expressed in *E. coli* BL21(DE3) cells in the same manner as GST-2CARD. Cells from 1 L of culture were resuspended in 50 mL lysis buffer (50mM Tris 8,

100 mM NaCl, 2 mM PMSF, 10 mM βME). After lysis and PEI precipitation, the protein was precipitated with ammonium sulfate at 65% saturation and centrifugation. The precipitate was resuspended in desalting buffer (20 mM MOPS, pH 6.5, 100 mM NaCl, 10% (v/v) glycerol, 10 mM βME). The resuspended protein solution was applied on a HiPrep 26/10 Desalting column (GE Healthcare) with desalting buffer as the running buffer. Collected fractions were diluted two-fold into buffer A (20 mM MOPS 6.5 and 10 mM βME), applied onto a HiTrap SP FF column (GE Healthcare), and eluted with a linear salt gradient (buffer A + 1 M NaCl). Pooled fractions were concentrated to ~3 mL and purified to homogeneity on a HiLoad 16/600 Superdex 75 gel filtration column in purification buffer (20 mM Tris, pH 7.5, 150 mM NaCl, 0.5 mM TCEP). Pooled protein fractions were concentrated to 1.3 mM.

Analytical ultracentrifugation. Sedimentation equilibrium data were collected using a Beckman Optima XL-A centrifuge at 4 °C. The isolated RING domain was analyzed at rotor speeds of 25,000 and 28,000 rpm, at loading concentrations of 59, 29.5, and 14.8 μM, in 25 mM HEPES, pH 7.4, 150 mM NaCl, 1 mM TCEP. Full-length FLAG-tagged TRIM25 was analyzed at speeds of 6,500 and 9,000 rpm and loading concentrations of 7.8, 3.9, and 1.95 μM, in 25 mM Tris, pH 9, 200 mM NaCl, 1 mM TCEP. Each centrifugation run was performed for 24 h to reach equilibrium. Nonlinear least-squares data fitting was performed using the Heteroanalysis software (Cole, 2004). Solvent density and protein partial-specific volumes were calculated with the program SEDNTERP (Laue et al., 1992).

SEC-MALS. Mass measurements were performed on a Dionex UltiMate3000 HPLC system (ThermoFisher) connected to a miniDAWN TREOS static light scattering detector (Wyatt Technology) and Optilab T-rEX differential refractometer (Wyatt Technology). Sample volumes of 40 µL at about 20 µM concentration were applied to a Superdex 200 HR 10/300 GL column (GE Healthcare) and developed in 50 mM Tris, pH 9, 200 mM NaCl, 0.5 mM TCEP at a flow rate of 0.4 mL/min. Data were recorded and processed using ASTRA software (Wyatt Technology).

Plasmids and viruses. The pEBG plasmids encoding GST or GST-2CARD have been previously described (Gack et al., Nature 2007). Plasmids encoding IFN-β luciferase and β-galactosidase (pGK-β-gal) have been previously described (Lin et al., 2000; Tanaka et al., 1995). pCMV-entry plasmid was purchased from Origene. The plasmids pcDNA3.3-hCas9, expressing human codon optimized Cas9, and pMH3 were gifts from George Church (Addgene plasmid #41815) and Klaus Foerstemann (Addgene plasmid #52528), respectively. pLKO.1 plasmid was purchased from ThermoFisher. pCMV-FLAG-TRIM25 was a gift from Dong-Er Zhang (Addgene plasmid #12449); mutations were introduced into this plasmid using the Quikchange method (Agilent).

Influenza A/PR/8/34 (H1N1) virus was kindly provided by Adolfo García-Sastre (Icahn School of Medicine at Mount Sinai). IFN-α2 was purchased from PBL Biomedical Laboratories.

Cell culture and transfection. HEK293T and MDCK (Madin-Darby canine kidney) cells were cultured in Dulbecco's Modified Eagle's Medium (DMEM) supplemented with 10% (v/v) fetal bovine serum (FBS; HyClone), 2 mM L-glutamine, and 1% (w/v) penicillin-streptomycin (Pen-Strep; Gibco). *TRIM25*-KO HEK293T cells were generated as described in Supplemental Experimental Methods, and cultured in DMEM (Gibco) supplemented with Pen-Strep (Gibco), 10% (v/v) FBS (HyClone) and 10 µg/mL Blasticidin (Gibco) for selection. Transfections were carried out using Lipofectamine 2000 or Lipofectamine and PLUS reagent (Invitrogen) in Opti-MEM (Gibco), or calcium phosphate (Clontech) according to the manufacturer's instructions.

Generation of *TRIM25*-KO HEK293T cells. *TRIM25*-KO HEK293T cells were generated according to a previous protocol (Bottcher et al., 2014) but with the following adaptations for human cells. HEK293T cells, seeded into 24-well plates, were transfected with 500 ng of a plasmid expressing hCas9, 250 ng of a dsDNA PCR product expressing a guide RNA (gRNA) directed against the start codon of the human *TRIM25* gene (targeting sequence: CCCGACCCCTGGGAGCGCCA) and controlled by the human U6 promoter, and 250 ng of a dsDNA PCR product as a homologous recombination template. The homologous recombination construct was composed of homologous sequences to the *TRIM25* first exon flanking a cassette consisting of Herpes Simplex Virus type 1 (HSV-1) thymidine kinase (TK) promoter followed by a blasticidin resistance gene (BSD). The construct was designed to delete the first 4 nucleotides including the *TRIM25* start codon (details shown in Figure S4)

in the recombined genome upon insertion of the TK-BSD cassette. Transfected cells were cultured for 10 days, followed by selection with 10 µg/mL Blasticidin. Resistant colonies were grown in 6-well plates until confluency. Single cell clones were isolated using serial dilutions in 96-well plates, propagated and analyzed for the absence of TRIM25 protein by IB analysis. Furthermore, genomic PCR (HiFi master mix; Thermo Fisher) confirmed the presence of the cassette.

The gRNA expression construct was generated by KOD (Millipore) PCR using pLKO.1 (Thermo Fisher) as a template for the human U6 promoter, and primers for the invariable part of the gRNA (GTTTAAGAGC TATGCTGGAA ACAGCATAGC AAGTTTAAAT AAGGCTAGTC CGTTATCAAC TTGAAAAAGT GGCACCGAGT CGGTGC), the specifically *TRIM25* targeting part (TGGAAAGGAC GAAACACCCC CGACCCCTGG GAGCGCCAGT TTAAGAGCTA TGCTG) and forward and reverse primers (GGAAGAGGGC CTATTTCCCA TGATTCCTTCAT, GCACCGACTCGGTGCCACT). The homologous recombination template was also generated by the same method using the pMH3-GFP vector harboring an insert coding for TK-BSD as the template. Long primers (Forward: GCTAGGTTTC GTTTCCTCGG CGGCCTCGGA GCGCGGGTGC AGCAGTTGTG TCCCGACCCC TGGGAGCGCC AATGAGTCTT CGGACCTCGC GGGGGCCG; Reverse: GTGACCGGCT CCTTGAAGGG CTCCAGGCAG ATGGAGCACG ACAGCTCCTC GGCCAGGGGG CACAGCTCTG CATATGTTA GAAACAAATT TATTTTTAAAG) adding 70 nt homologous sequences to the *TRIM25* locus on

each side of the cassette were used for the PCR. Both constructs were purified using a column (Omega BioTek) before transfection.

ACKNOWLEDGEMENTS

We thank Barbie Ganser-Pornillos for discussions and critical reading of the manuscript, Jonathan Wagner and Yueping Wan for technical support, and Adolfo Garcia-Sastre for providing influenza PR8 virus. The Berkeley Center for Structural Biology is supported in part by the NIH, National Institute of General Medical Sciences, and the Howard Hughes Medical Institute. The Advanced Light Source is supported by the Director, Office of Science, Office of Basic Energy Sciences, of the US Department of Energy under contract no. DE-AC02-05CH11231. This study was supported by NIH grants R01-AI087846 (to M.U.G.) and R01-GM112508 (to O.P.). Seed funding was also provided by the Annette Lightner Foundation (to O.P.). J.G.S. was supported by a predoctoral Cell and Molecular Biology Training grant from NIH (T32-GM008136) and the Robert R. Wagner Fellowship Fund. K.M.J.S. was supported by a fellowship from the German Research Foundation (SP 1600/1-1). M.D.R. participated in this study while on leave from Lodz Technical University, Poland.

REFERENCES

Adams, P.D., Afonine, P.V., Bunko´czi, G., Chen, V.B., Davis, I.W., Echols, N., Headd, J.J., Hung, L.W., Kapral, G.J., Grosse-Kunstleve, R.W., et al. (2010). PHENIX: a comprehensive Python-based system for macromolecular structure solution. Acta Crystallogr. D Biol. Crystallogr. *66*, 213–221.

Balish, A.L., Katz, J.M., and Klimov, A.I. (2013). Influenza: propagation, quantification, and storage. Curr. Protoc. Microbiol. *29*, 15G.1.1–15G.1.24.

Brzovic, P.S., Rajagopal, P., Hoyt, D.W., King, M.C., and Klevit, R.E. (2001). Structure of a BRCA1-BARD1 heterodimeric RING-RING complex. Nat. Struct. Biol. *8*, 833–837.

Cai, X., and Chen, Z.J. (2014). Prion-like polymerization as a signaling mechanism. Trends Immunol. *35*, 622–630.

Cai, X., Chen, J., Xu, H., Liu, S., Jiang, Q.X., Halfmann, R., and Chen, Z.J. (2014). Prion-like polymerization underlies signal transduction in antiviral immune defense and inflammasome activation. Cell *156*, 1207–1222.

Chiang, J.J., Davis, M.E., and Gack, M.U. (2014). Regulation of RIG-I-like receptor signaling by host and viral proteins. Cytokine Growth Factor Rev. *25*, 491–505.

Cui, S., Eisena¨cher, K., Kirchhofer, A., Brzo´zka, K., Lammens, A., Lammens, K., Fujita, T., Conzelmann, K.K., Krug, A., and Hopfner, K.P. (2008). The C-terminal regulatory domain is the RNA 5^0-triphosphate sensor of RIG-I. Mol. Cell *29*, 169–179

D'Cruz, A.A., Kershaw, N.J., Chiang, J.J., Wang, M.K., Nicola, N.A., Babon, J.J., Gack, M.U., and Nicholson, S.E. (2013). Crystal structure of the TRIM25 B30.2 (PRYSPRY) domain: a key component of antiviral signalling. Biochem. J. *456*, 231–240.

Diaz-Griffero, F., Qin, X.R., Hayashi, F., Kigawa, T., Finzi, A., Sarnak, Z., Lienlaf, M., Yokoyama, S., and Sodroski, J. (2009). A B-box 2 surface patch important for TRIM5a self-association, capsid binding avidity, and retrovirus restric-tion. J. Virol. *83*, 10737–10751.

Dou, H., Buetow, L., Sibbet, G.J., Cameron, K., and Huang, D.T. (2012). BIRC7-E2 ubiquitin conjugate structure reveals the mechanism of ubiquitin transfer by a RING dimer. Nat. Struct. Mol. Biol. *19*, 876–883.

Emsley, P., Lohkamp, B., Scott, W.G., and Cowtan, K. (2010). Features and development of Coot. Acta Crystallogr. D Biol. Crystallogr. *66*, 486–501.

Gack, M.U., Shin, Y.C., Joo, C.H., Urano, T., Liang, C., Sun, L., Takeuchi, O., Akira, S., Chen, Z., Inoue, S., and Jung, J.U. (2007). TRIM25 RING-finger E3 ubiquitin ligase is essential for RIG-I-mediated antiviral activity. Nature *446*, 916–920.

Gack, M.U., Kirchhofer, A., Shin, Y.C., Inn, K.S., Liang, C., Cui, S., Myong, S., Ha, T., Hopfner, K.P., and Jung, J.U. (2008). Roles of RIG-I N-terminal tandem CARD and splice variant in TRIM25-mediated antiviral signal transduction. Proc. Natl. Acad. Sci. USA *105*, 16743–16748.

Gack, M.U., Albrecht, R.A., Urano, T., Inn, K.S., Huang, I.C., Carnero, E., Farzan, M., Inoue, S., Jung, J.U., and Garcı´a-Sastre, A. (2009). Influenza A virus NS1 targets the ubiquitin ligase TRIM25 to evade recognition by the host viral RNA sensor RIG-I. Cell Host Microbe *5*, 439–449.

Ganser-Pornillos, B.K., Chandrasekaran, V., Pornillos, O., Sodroski, J.G., Sundquist, W.I., and Yeager, M. (2011). Hexagonal assembly of a restricting TRIM5a protein. Proc. Natl. Acad. Sci. USA *108*, 534–539.

Goldstone, D.C., Walker, P.A., Calder, L.J., Coombs, P.J., Kirkpatrick, J., Ball, N.J., Hilditch, L., Yap, M.W., Rosenthal, P.B., Stoye, J.P., and Taylor, I.A. (2014). Structural studies of postentry restriction factors reveal antiparallel dimers that enable avid binding to the HIV-1 capsid lattice. Proc. Natl. Acad. Sci. USA *111*, 9609–9614.

Goubau, D., Deddouche, S., and Reis e Sousa, C. (2013). Cytosolic sensing of viruses. Immunity *38*, 855–869.

Goubau, D., Schlee, M., Deddouche, S., Pruijssers, A.J., Zillinger, T., Goldeck, M., Schuberth, C., Van der Veen, A.G., Fujimura, T., Rehwinkel, J., et al. (2014). Antiviral immunity via RIG-I-mediated recognition of RNA bearing 5′-diphosphates. Nature *514*, 372–375.

Hornung, V., Ellegast, J., Kim, S., Brzo´zka, K., Jung, A., Kato, H., Poeck, H., Akira, S., Conzelmann, K.K., Schlee, M., et al. (2006). 5′-Triphosphate RNA is the ligand for RIG-I. Science *314*, 994–997.

Hou, F., Sun, L., Zheng, H., Skaug, B., Jiang, Q.X., and Chen, Z.J. (2011). MAVS forms functional prion-like aggregates to activate and propagate anti-viral innate immune response. Cell *146*, 448–461.

Jiang, Q.X., and Chen, Z.J. (2011). Structural insights into the activation of RIG-I, a nanosensor for viral RNAs. EMBO Rep. *13*, 7–8.

Jiang, X., Kinch, L.N., Brautigam, C.A., Chen, X., Du, F., Grishin, N.V., and Chen, Z.J. (2012). Ubiquitin-induced oligomerization of the RNA sensors RIG-I and MDA5 activates antiviral innate immune response. Immunity *36*, 959–973.

Koliopoulos, M.G., Esposito, D., Christodoulou, E., Taylor, I.A., and Rittinger, K. (2016). Functional role of TRIM E3 ligase oligomerization and regulation of catalytic activity. EMBO J. *35*, 1204–1218.

Kowalinski, E., Lunardi, T., McCarthy, A.A., Louber, J., Brunel, J., Grigorov, B., Gerlier, D., and Cusack, S. (2011). Structural basis for the activation of innate immune pattern-recognition receptor RIG-I by viral RNA. Cell *147*, 423–435.

Li, X., and Sodroski, J. (2008). The TRIM5a B-box 2 domain promotes cooperative binding to the retroviral capsid by mediating higher-order self-association. J. Virol. *82*, 11495–11502.

Li, Y., Wu, H., Wu, W., Zhuo, W., Liu, W., Zhang, Y., Cheng, M., Chen, Y.G., Gao, N., Yu, H., et al. (2014). Structural insights into the TRIM family of ubiquitin E3 ligases. Cell Res. *24*, 762–765.

Li, Y.-L., Chandrasekaran, V., Carter, S.D., Woodward, C.L., Christensen, D.E., Dryden, K.A., Pornillos, O., Yeager, M., Ganser-Pornillos, B.K., Jensen, G.J., and Sundquist, W.I. (2016). Primate TRIM5 proteins form hexagonal nets on HIV-1 capsids. eLife *5*, e16269.

Lima, C.D., and Schulman, B.A. (2012). Structural biology: a protein engagement RING. Nature *489*, 43–44.

Liu, H.M., Loo, Y.M., Horner, S.M., Zornetzer, G.A., Katze, M.G., and Gale, M., Jr. (2012). The mitochondrial targeting chaperone 14-3-3ε regulates a RIG-I translocon that mediates membrane association and innate antiviral immunity. Cell Host Microbe *11*, 528–537.

Liu, S., Chen, J., Cai, X., Wu, J., Chen, X., Wu, Y.T., Sun, L., and Chen, Z.J. (2013). MAVS recruits multiple ubiquitin E3 ligases to activate antiviral signaling cascades. eLife *2*, e00785.

Loo, Y.M., and Gale, M., Jr. (2011). Immune signaling by RIG-I-like receptors. Immunity *34*, 680–692.

Luo, D., Ding, S.C., Vela, A., Kohlway, A., Lindenbach, B.D., and Pyle, A.M. (2011). Structural insights into RNA recognition by RIG-I. Cell *147*, 409–422.

Manokaran, G., Finol, E., Wang, C., Gunaratne, J., Bahl, J., Ong, E.Z., Tan, H.C., Sessions, O.M., Ward, A.M., Gubler, D.J., et al. (2015). Dengue subgenomic RNA binds TRIM25 to inhibit interferon expression for epidemiological fitness. Science *350*, 217–221.

Meroni, G., and Diez-Roux, G. (2005). TRIM/RBCC, a novel class of 'single pro-tein RING finger' E3 ubiquitin ligases. BioEssays *27*, 1147–1157.

Middleton, A.J., Budhidarmo, R., and Day, C.L. (2014). Use of E2 ubiquitin conjugates for the characterization of ubiquitin transfer by RING E3 ligases such as the inhibitor of apoptosis proteins. Methods Enzymol. *545*, 243–263

Otwinowski, Z., and Minor, W. (1997). Processing of X-ray diffraction data collected in oscillation mode. Methods Enzymol. *276*, 307–326.

Peisley, A., Wu, B., Yao, H., Walz, T., and Hur, S. (2013). RIG-I forms signaling-competent filaments in an ATP-dependent, ubiquitin-independent manner. Mol. Cell *51*, 573–583.

Peisley, A., Wu, B., Xu, H., Chen, Z.J., and Hur, S. (2014). Structural basis for ubiquitin-mediated antiviral signal activation by RIG-I. Nature *509*, 110–114.

Pichlmair, A., Schulz, O., Tan, C.P., Na¨slund, T.I., Liljestro¨m, P., Weber, F., and Reis e Sousa, C. (2006). RIG-I-mediated antiviral responses to single-stranded RNA bearing 5^0-phosphates. Science *314*, 997–1001.

Plechanovova´, A., Jaffray, E.G., Tatham, M.H., Naismith, J.H., and Hay, R.T. (2012). Structure of a RING E3 ligase and ubiquitin-loaded E2 primed for catalysis. Nature *489*, 115–120.

Pruneda, J.N., Littlefield, P.J., Soss, S.E., Nordquist, K.A., Chazin, W.J., Brzovic, P.S., and Klevit, R.E. (2012). Structure of an E3:E2 Ub complex reveals an allosteric mechanism shared among RING/U-box ligases. Mol. Cell *47*, 933–942.

Rajsbaum, R., Albrecht, R.A., Wang, M.K., Maharaj, N.P., Versteeg, G.A., Nistal-Villa´n, E., Garcı´a-Sastre, A., and Gack, M.U. (2012). Species-specific inhibition of RIG-I ubiquitination and IFN induction by the influenza A virus NS1 protein. PLoS Pathog. *8*, e1003059.

Sanchez, J.G., Okreglicka, K., Chandrasekaran, V., Welker, J.M., Sundquist, W.I., and Pornillos, O. (2014). The tripartite motif coiled-coil is an elongated antiparallel hairpin dimer. Proc. Natl. Acad. Sci. USA *111*, 2494–2499.

Wagner, J.M., Roganowicz, M.D., Skorupka, K., Alam, S.L., Christensen, D.E., Doss, G.L., Wan, Y., Frank, G.A., Ganser-Pornillos, B.K., Sundquist, W.I., and Pornillos, O. (2016). Mechanism of B-box 2 domain-mediated higher-order assembly of the retroviral restriction factor TRIM5a. eLife *5*, e16309.

Weinert, C., Morger, D., Djekic, A., Grutter, M.G., and Mittl, P.R. (2015). Crystal structure of TRIM20 C-terminal coiled-coil/B30.2 fragment: implications for the recognition of higher order oligomers. Sci. Rep. *5*, 10819.

Wright, J.D., Mace, P.D., and Day, C.L. (2016). Secondary ubiquitin-RING docking enhances Arkadia and Ark2C E3 ligase activity. Nat Struct Mol Biol *23*, 45–52.

Wu, H. (2013). Higher-order assemblies in a new paradigm of signal transduction. Cell *153*, 287–292.

Wu, B., Peisley, A., Tetrault, D., Li, Z., Egelman, E.H., Magor, K.E., Walz, T., Penczek, P.A., and Hur, S. (2014). Molecular imprinting as a signal-activation mechanism of the viral RNA sensor RIG-I. Mol. Cell *55*, 511–523.

Xu, H., He, X., Zheng, H., Huang, L.J., Hou, F., Yu, Z., de la Cruz, M.J., Borkow-ski, B., Zhang, X., Chen, Z.J., and Jiang, Q.X. (2014). Structural basis for the prion-like MAVS filaments in antiviral innate immunity. eLife *3*, e01489.

Yudina, Z., Roa, A., Johnson, R., Biris, N., de Souza Aranha Vieira, D.A., Tsiperson, V., Reszka, N., Taylor, A.B., Hart, P.J., Demeler, B., et al. (2015). RING dimerization links higher-order assembly of TRIM5a to synthesis of K63-linked polyubiquitin. Cell Rep. *12*, 788–797.

Zeng, W., Xu, M., Liu, S., Sun, L., and Chen, Z.J. (2009). Key role of Ubc5 and lysine-63 polyubiquitination in viral activation of IRF3. Mol. Cell *36*, 315–325.

Zeng, W., Sun, L., Jiang, X., Chen, X., Hou, F., Adhikari, A., Xu, M., and Chen, Z.J. (2010). Reconstitution of the RIG-I pathway reveals a signaling role of unanchored polyubiquitin chains in innate immunity. Cell *141*, 315–330.

CHAPTER 4

TRIM25 BINDS RNA TO MODULATE CELLULAR ANTI-VIRAL ACTIVITY

Note: The data described in Figure 6 was generated by Konstantin Sparrer in the lab of Michaela Gack

ABSTRACT

TRIM25 is a member of the tripartite motif family of E3 ubiquitin ligases and regulates in diverse RNA-dependent pathways. Several studies have shown that TRIM25 is a bona fide RNA binding protein (RBP). However, the impact of RNA on TRIM25 activity has not yet been defined. In this study, we use purified TRIM25 proteins in combination with *in vitro* ubiquitination, gel shift, and cell-based antiviral assays to determine how RNA binding affects TRIM25 anti-viral activity. We show that RNA enhances TRIM25 E3 ligase activity *in vitro*, that multiple TRIM25 structural elements are required for RNA binding, and that disruption of RNA binding also disrupts TRIM25's antiviral activity. These results reveal new insights into how RNA binding may couple TRIM25 E3 ligase activity with the modulation of other RBPs, such as known TRIM25-interacting proteins RIG-I and ZAP.

INTRODUCTION

TRIM25 is a member of the tripartite motif family of E3 ubiquitin ligases that functions in multiple RNA-dependent pathways. It has been well established that TRIM25 plays a crucial role in the RIG-I anti-viral pathway, where TRIM25 is reported to bind viral RNA-activated RIG-I, leading to K63-linked polyubiquitination of the sensor to promote transcriptional upregulation of type I interferons (IFNs) (Gack, 2007, 2008). TRIM25 was also shown to be important for micro RNA processing, which also requires TRIM25's E3 ligase activity (Choudhury, 2014;Heikel, 2016). Most recently, TRIM25 was found to be an essential co-factor for messenger RNA (mRNA) degradation mediated by the ZAP protein (Zheng, 2017;Li, 2017), which recognizes viral mRNAs with high CG-dinucleotide content (Takata, 2017). TRIM25 is therefore an attractive model system for understanding the molecular mechanisms of how a single ubiquitin E3 enzyme is directed to specific cellular pathways to produce distinct biological outcomes.

The biophysical mechanism of TRIM25's E3 ubiquitin ligase activity has now been elucidated. Like a typical TRIM protein, TRIM25 contains an N-terminal tripartite or RBCC motif, consisting of RING, B-box 1, B-box 2, and coiled-coil domains. Additionally, TRIM25 has a C-terminal SPRY domain that is required for recruitment to the RIG-I, ZAP, and RNA processing pathways (Gack, 2007;Gack, 2008;Zheng, 2017;Li, 2017;Choudhury, 2014). The RBCC and SPRY domains are connected by a linker region (linker 2 or L2), part of which is integrated with the coiled-coil and likely facilitates functional coupling of these

structural elements (Sanchez, 2014). The basal oligomeric state of TRIM25 is a stable dimer mediated by the coiled-coil/L2 regions. This dimerization domain makes an elongated, anti-parallel scaffold, with the RINGs and B-boxes on opposite ends and separated by around 170 Å, and the SPRY domains positioned near the middle (Sanchez, 2014). The RING domain harbors the E3 ubiquitin ligase activity of TRIM25, and it is catalytically competent *in vitro* as an independent protein. Recent studies have shown that the RING domain engages E2 conjugating enzymes and catalyzes polyubiquitination as a dimer (Koliopoulos, 2016;Sanchez, 2016). In context of the full-length TRIM25 dimer, the two RING domains cannot interact with each other, and RING dimerization therefore requires higher-order oligomerization or self-association of at least two coiled-coil mediated TRIM25 dimers. How TRIM25 self-association and RING activation occurs in a pathway-specific manner in cells is currently unknown.

The simplest model would be that polyvalent protein-protein interactions between TRIM25 and cellular RNA-binding receptors, such as RIG-I or ZAP, simultaneously promotes recruitment, RING activation, and polyubiquitination activity of TRIM25. However, this simple model has been challenged by the finding that TRIM25 independently binds RNA (Kwon, 2013). Here, we use biochemical, biophysical, and cell biological approaches to characterize this interaction and its functional significance for TRIM25's anti-viral activity. We found that TRIM25 has a composite RNA binding site with energetically significant contributions from multiple domains. We also show that TRIM25's RNA-binding activity is required for its interaction with the RNA receptor, RIG-I,

in vitro, and also for its subcellular localization and overall anti-viral activity in cells. Taken together with other studies, our results support a model wherein pathway-specific TRIM25 recruitment and activation results from a complex interplay of both protein-protein and protein-RNA interactions.

RESULTS

RNA binding enhances TRIM25 E3 ligase activity *in vitro.* Previous pull-down studies have suggested that TRIM25 is associated with RNA in cells (Kwon, 2013). We confirmed this RNA-binding activity in the course of purifying the protein for biochemical studies. Specifically, we found that recombinant Strep/FLAG-tagged TRIM25 overexpressed in insect cells co-eluted from affinity columns with large quantities of nucleic acid (**Fig. 1**). The protein samples were not very pure (**Fig. 1B**, left) and had a UV absorbance profile with a peak at 260 nm, with an A_{260}/A_{280} ratio of ~1.9 (**Fig. 1C**, left). Use of polyethyleneimine (PEI) precipitation prior to affinity purification significantly reduced both the protein (**Fig. 1B**, right) and nucleic acid contaminations, giving an A_{260}/A_{280} ratio of ~0.7 (**Fig. 1C**, right). Agarose gel electrophoresis confirmed the presence of significant amounts of nucleic acid in the non-PEI-treated but not the PEI-treated samples (**Fig. 1D**).

Interestingly, *in vitro* ubiquitination assays revealed that the presence of nucleic acid significantly enhanced the enzymatic activity of TRIM25 (**Fig 2A**, compare lane 2 to lane 3 and lane 5 to lane 6). This effect was independent of

Fig. 1. Recombinant TRIM25 co-purifies with nucleic acid.

(A) Affinity purification scheme for Strep/FLAG-tagged TRIM25 expressed in insect cells.

(B) Coomassie-stained SDS-PAGE gels of TRIM25 fractions after initial affinity chromatography step.

(C) UV absorbance spectra of pooled protein fractions. Vertical dashed lines indicate the peak wavelength.

(D) Visualization by agarose gel electrophoresis and SYBR-green staining of the co-purifying nucleic acid (–PEI) and its removal by polyethyleneimine treatment (+PEI).

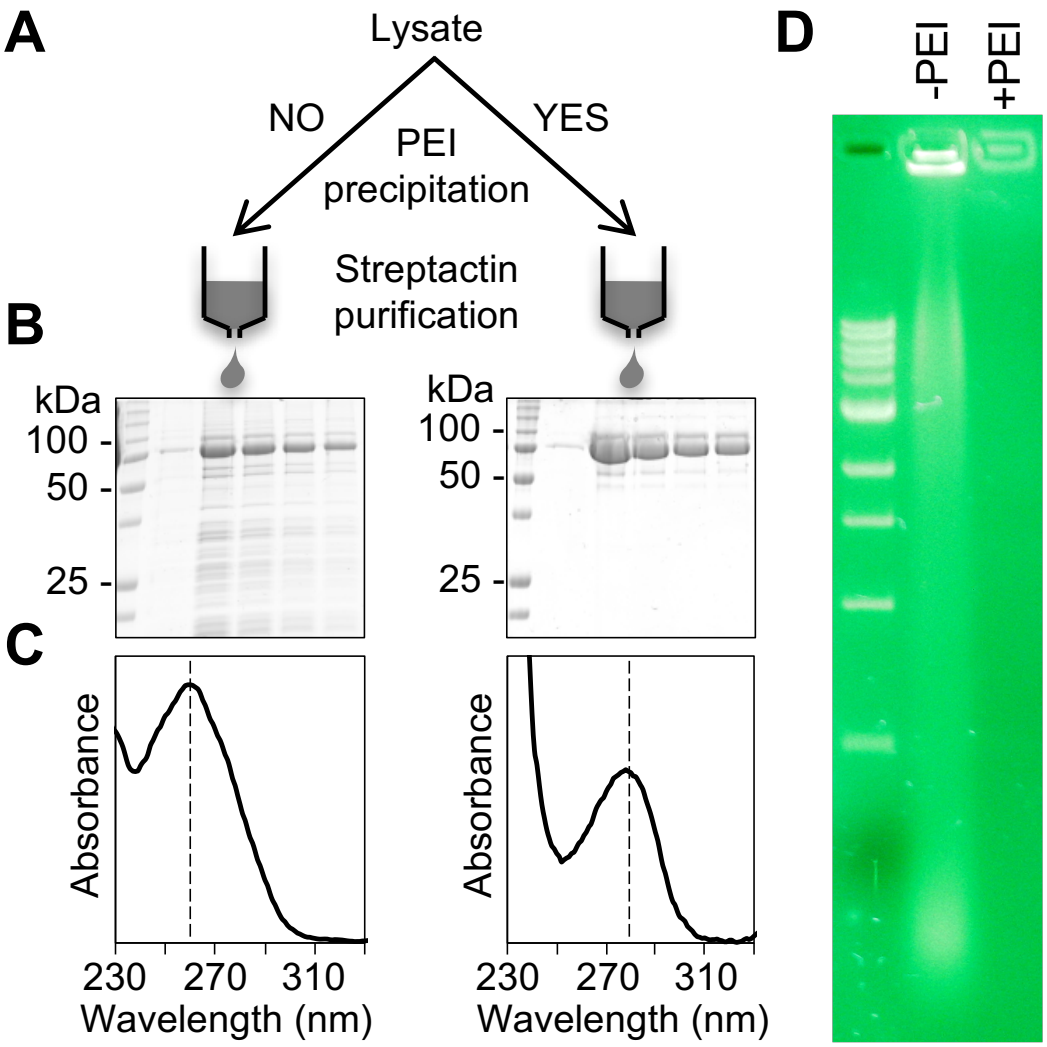
A
Lysate
NO
YES
PEI
precipitation
Streptactin
purification
B
kDa
100 -
50 -
25 -
kDa
100 -
50 -
25 -
C
Absorbance
230 270 310
Wavelength (nm)
Absorbance
230 270 310
Wavelength (nm)
D
-PEI
+PEI

Fig. 2. RNA enhances TRIM25's catalytic activity *in vitro*.

(A) Ubiquitination activities of ~200 nM TRIM25 purified with (lanes 1, 3, and 6) or without (lanes 2, 4, and 7) PEI precipitation. TRIM25 synthesizes anchored (self-attached) polyubiquitin (polyUb) chains with 1 μM Ubc5b and unanchored chains with 0.280 μM Ubc13/Mms2 (Sanchez, 2016). Reactions contained 100 nM E1, 40 μM Ub, and 5 mM Mg-ATP.

(B) TRIM25 purified in the absence of PEI treatment was pre-incubated with RNase A (lanes 5 and 9), DNase I (lanes 4 and 8), or buffer control (lanes 3 and 7) prior to setting up ubiquitination assays.

(C) TRIM25 purified with PEI treatment was pre-incubated with 500 ng of dsRNA (lanes 4 and 8), 500 ng of dsDNA (lanes 5 and 9), or buffer control (lanes 3 and 7) prior to ubiquitination assays.

(D) TRIM25 purified with PEI treatment was pre-incubated with the indicated concentrations of 14, 28, or 56 bp dsRNA prior to ubiquitination.

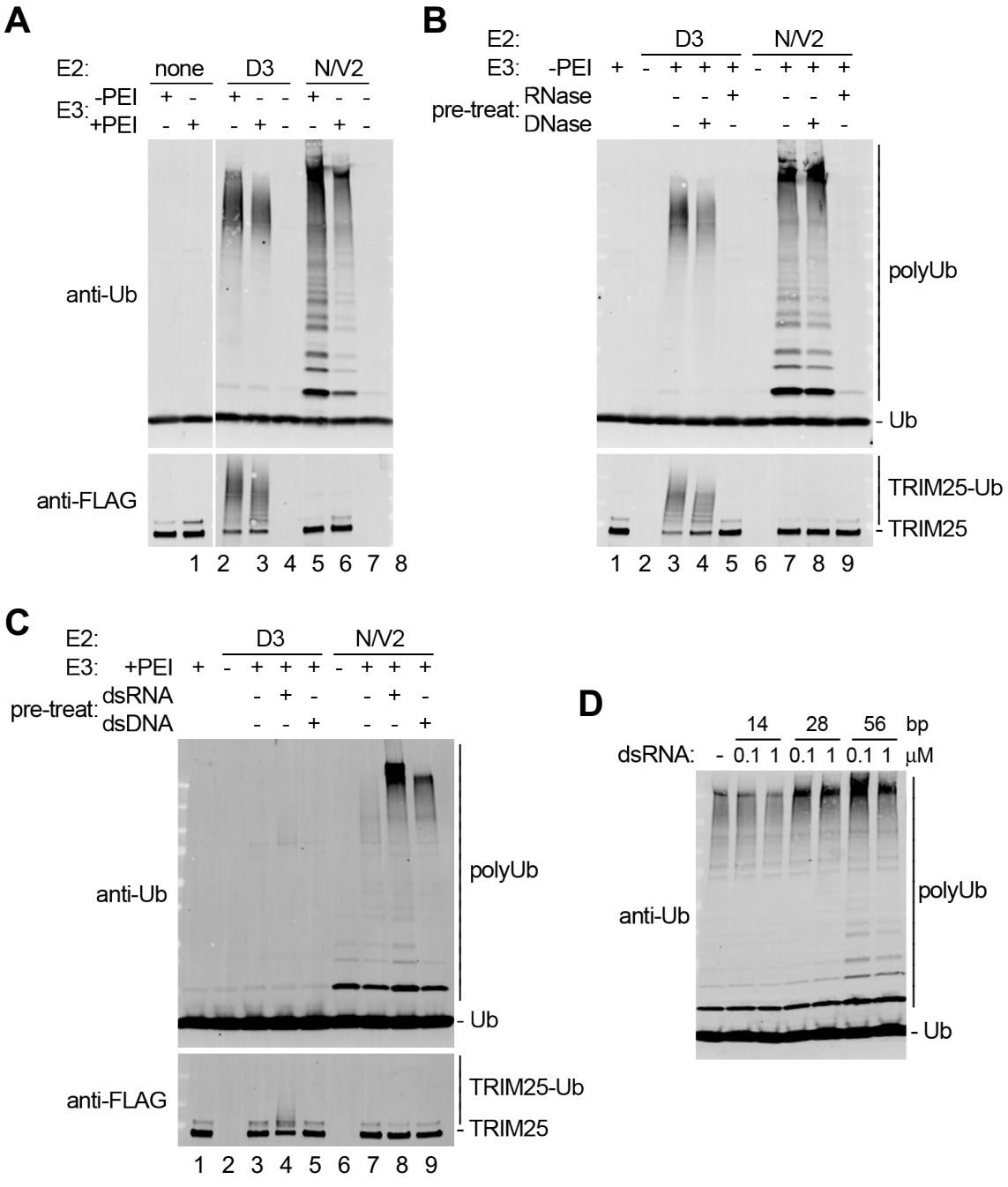
A
E2:
none
D3
N/V2
E3:
-PEI
+PEI
anti-Ub
anti-FLAG
1 2 3 4 5 6 7 8
B
E2:
D3
N/V2
E3:
-PEI
pre-treat:
RNase
DNase
polyUb
Ub
TRIM25-Ub
TRIM25
1 2 3 4 5 6 7 8 9
C
E2:
D3
N/V2
E3:
+PEI
pre-treat:
dsRNA
dsDNA
anti-Ub
anti-FLAG
polyUb
Ub
TRIM25-Ub
TRIM25
1 2 3 4 5 6 7 8 9
D
14
28
56
bp
dsRNA:
0.1 1 0.1 1 0.1 1 μM
anti-Ub
polyUb
Ub

the E2 conjugating enzyme, and was observed with both Ubc5b (which promotes *in vitro* auto-ubiquitination of TRIM25; **Fig. 2A**, lanes 2-4) and Ubc13/Mms2 (which promotes synthesis of free polyubiquitin chains; **Fig. 2A**, lanes 5-7). Incubation of the non-PEI-treated sample with RNase abrogated ubiquitination *in vitro*, again in an E2-independent manner (**Fig. 2B**, lanes 5 and 9), whereas incubation with DNase had little or no effect (**Fig. 2B**, lanes 4 and 8). This result confirmed that the co-purifying nucleic acids were indeed RNA. Conversely, incubation of PEI-treated samples with dsRNA significantly enhanced *in vitro* ubiquitination (**Fig. 2C**, lanes 4 and 8). Incubation with dsDNA also enhanced activity, but to a lesser extent (**Fig. 2C**, lanes 5 and 9); this result likely reflects the commonly observed non-specific interaction of RNA-binding proteins with DNA *in vitro*. Since the enzymatic activity of TRIM25 requires higher-order oligomerization of the coiled-coil-mediated dimers to allow for RING domain dimerization (Koliopoulos, 2016; Sanchez, 2016), a simple model for RNA-induced ubiquitination *in vitro* is through clustering of TRIM25 molecules. Typical dsRNA-binding proteins have a footprint of around 12-16 bp, and indeed, 14-bp dsRNA did not enhance the ubiquitination activity of PEI-treated TRIM25, whereas 28-bp and 56-bp dsRNA did (**Fig. 2D**). Thus, dsRNA promotes *in vitro* self-association of TRIM25 and RING domain activation, provided that the RNA is of sufficient length to bind more than one coiled-coil-mediated TRIM25 dimer.

RNA binding requires a lysine-rich motif in the L2 linker. Unlike full-length TRIM25, we found that a construct spanning the RBCC domain (amino acid residues 1-379) did not co-purify with nucleic acid, as evidenced by a low

A_{260}/A_{280} ratio after affinity purification without PEI treatment (**Fig. 3A**). Correspondingly, the *in vitro* ubiquitination activity of this RBCC construct was insensitive to added dsRNA (**Fig. 3B**, compare lanes 3 and 4; WT control, compare lanes 1 and 2). (Note that the ubiquitination experiment was performed with Ubc13/Mms2 to preclude having to account for differences in the number of potential lysine acceptors). Extension of the RBCC domain identified a lysine-rich sequence in the L2 linker that connects the coiled-coil and SPRY domains ($_{381}$KKVSKEEKKSKK$_{392}$, hereafter termed '7K motif'), the presence of which resulted in elevated A_{260}/A_{280} ratios in the affinity-purified fractions (**Fig. 3A**, constructs 1-401, 1-409, and 1-435). Interestingly, the TRIM25 7K motif resembles a segment in ribosomal protein S30 ($_{18}$KVAKQEKKKKK$_{28}$), in which the lysine sidechains mediate ionic contacts with the phosphodiester backbone of 18*s* ribosomal RNA (Anger, 2013). We therefore surmised that the TRIM25 7K motif might directly contact the bound RNA, and indeed alanine substitution of all 7 lysines in context of full-length TRIM25 (TRIM25 7KA) resulted in a low A_{260}/A_{280} ratio even in the absence of PEI precipitation (**Fig. 3A**). Consistent with this result, the ubiquitination activity of the purified 7KA mutant protein did not respond to dsRNA to the same extent as wildtype (WT) TRIM25 (**Fig. 3C**, compare lanes 3 and 4; WT control, compare lanes 1 and 2). However, dsRNA-dependent ubiquitination was still observed for the 7KA protein, indicating that this mutant still retained some ability to bind RNA (see also below).

To confirm that TRIM25 binds RNA directly, we performed SEC-MALS (size exclusion chromatography coupled with multi-angle light scattering)

Fig. 3. Identification of the 7K motif that mediates TRIM25 binding to RNA.

(A) Schematic of TRIM25's domain organization and summary of constructs used to map the RNA binding site. Observed A_{260}/A_{280} UV absorbance ratios with and without PEI treatment are indicated. The lysine-rich sequence spanning residues 381-392 is highlighted. Abbreviated domain names: B1 = B-box 1; B2 = B-box 2; CCD = coiled-coil dimerization domain.

(B-C) Ubiquitination activities of the indicated constructs (lanes 3 and 4) in the presence or absence of 1 mM 28-bp dsRNA, along with corresponding WT control assayed in parallel (lanes 1 and 2).

(D-E) SEC-MALS analysis of the indicated TRIM25 constructs prior to (blue) and after incubation with 56-bp dsRNA (red). Curves show the refractive index of the eluting species normalized to the peak intensity. Open circles indicate calculated molecular weights in kDa.

(F) SEC-MALS profile of the RNA alone, shown for reference.

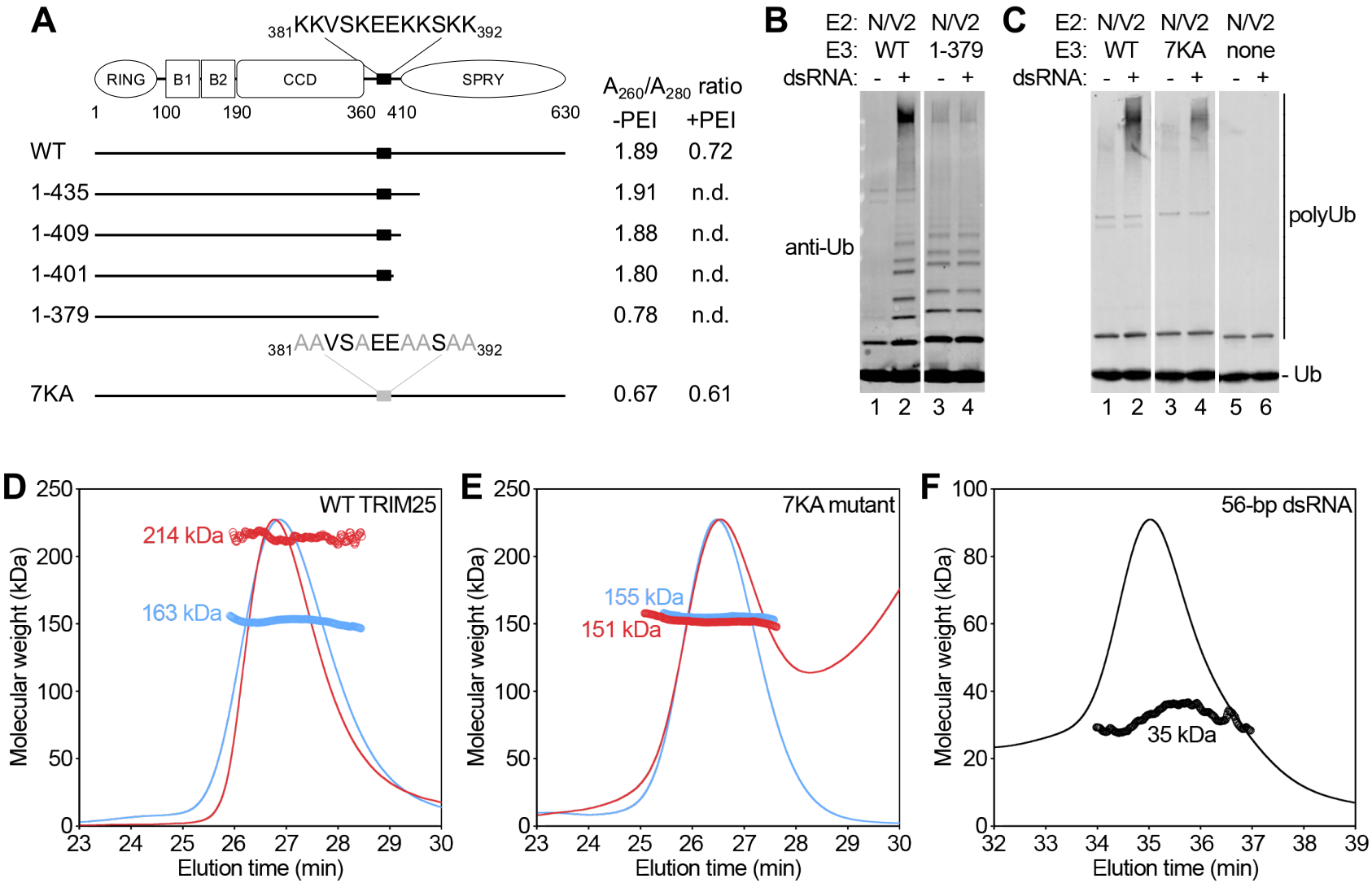
A
381KKVSKEEKKSKK392
RING
B1
B2
CCD
SPRY
1
100
190
360
410
630
A260/A280 ratio
-PEI
+PEI
WT
1.89
0.72
1-435
1.91
n.d.
1-409
1.88
n.d.
1-401
1.80
n.d.
1-379
0.78
n.d.
381AAVSAEEAASAA392
7KA
0.67
0.61
B
E2: N/V2 N/V2
E3: WT 1-379
dsRNA: - + - +
anti-Ub
1 2 3 4
C
E2: N/V2 N/V2 N/V2
E3: WT 7KA none
dsRNA: - + - + - +
polyUb
- Ub
1 2 3 4 5 6
D
WT TRIM25
214 kDa
163 kDa
Molecular weight (kDa)
Elution time (min)
E
7KA mutant
155 kDa
151 kDa
Molecular weight (kDa)
Elution time (min)
F
56-bp dsRNA
35 kDa
Molecular weight (kDa)
Elution time (min)

experiments, which allow direct measurements of particle mass, complex formation, and sample homogeneity. In control experiments, purified WT TRIM25 eluted in the absence of added RNA as a single major peak with a measured mass consistent with a dimer (**Fig. 3D**, blue curves; calculated mass from sequence = 2 x 75 kDa = 150 kDa). In the presence of an equimolar ratio of 56-bp dsRNA, the major peak did not significantly change in elution position (indicating that the particle shape did not change considerably from the elongated dimer of the protein alone), but now had a mass increase of ~70 kDa (**Fig. 3D**, red curves), which is equivalent to two 56-bp dsRNA molecules (**Fig. 3F**). Thus, TRIM25 bound to dsRNA at a 1:1 molar ratio in this experiment. In contrast, the 7KA mutant had the same population-averaged mass in the absence (**Fig. 3E**, blue) and presence (**Fig. 3E**, red) of dsRNA, confirming that this protein was significantly deficient in RNA binding *in vitro*. Importantly, our results also indicated that the 7KA mutations had no effect on the structure of the TRIM25 dimer, or on the fundamental biophysical mechanism of RING E3 ligase activation. These experiments provide proof, using biochemically pure reagents, that TRIM25 indeed binds RNA.

RNA binding requires the SPRY domain. The above experiments revealed that the 7KA mutation did not completely abolish the ability of TRIM25 to interact with RNA and that the SPRY domain also contributed to RNA binding. To explore this further, we used an electrophoretic mobility shift assay (EMSA) to quantify TRIM25's RNA binding activity *in vitro*. In this experiment, 250 nM of fluorescently-tagged 28-bp dsRNA was incubated with different concentrations of

purified TRIM25 proteins (0-10 μM), and then the free and TRIM25-bound RNA fractions were separated on a native polyacrylamide gel and quantified by densitometry. In control experiments with full-length WT TRIM25, the gel scans gave the appearance of an all-or-none or highly cooperative binding mechanism (**Fig. 4A**, WT). However, this conclusion was not fully supported by the data because the TRIM25/RNA complexes did not enter the gel and the homogeneity of the bound fractions cannot be rigorously established. We therefore estimated the amounts of bound RNA through densitometric quantification of the unbound RNA bands, and performed curve fitting to a simple binding isotherm (see Materials and Methods for details). This revealed that TRIM25 bound to 28-bp dsRNA with a dissociation constant (K_d) of 0.26 μM (**Fig. 4B**, blue and **Table 1**). Consistent with our purification data, the RBCC domain alone (residues 1-379) did not bind the RNA (**Fig. 4A**, RBCC). The 7KA mutant retained some RNA-binding activity, but with about 20-fold loss in affinity (K_d = 4.9 μM) (**Fig. 4A**, 7KA mutant; **Fig. 4B**, red; and **Table 1**). Interestingly, the lysine-rich peptide alone (**Fig. 4A**, 7K peptide) also did not bind RNA. This result demonstrated that the TRIM25 7K motif does not constitute an independent RNA-binding element. Our interpretation of these data is that the presence of the SPRY domain is required for the 7K motif to adopt the appropriate structural configuration for binding RNA.

TRIM25 binds RNA through multiple structural elements. Given the apparent requirement for both L2 and SPRY regions, we performed EMSA experiments on a series of TRIM25 constructs and full-length mutants to more

Fig. 4. Mapping of TRIM25 RNA binding elements.

(A) Electrophoretic mobility shift assays with 0.5 μM of 28 bp fluorescent dsRNA oligo incubated with 0, 0.05, 0.08, 0.12, 0.17, 0.26, 0.39, 0.59, 0.88, 1.32, 2.0, 3.0, 4.4, 7.0, and 10 μM of TRIM25 WT, ΔSPRY, 7KA mutant, or 7K peptide, which is an 18-mer peptide containing the lysine-rich sequence. Migration positions are indicated for unbound oligo and bound complexes, which did not enter the gel.

(B) Unbound fractions were quantified by densitometry and used to estimate the bound fractions, which were plotted as a function of total TRIM25 concentration. Curves indicate best fits to a standard binding isotherm.

(C-D) Assays with the indicated TRIM25 constructs and mutants.

(E) Diagram of the TRIM25 dimer, with locations of elements that contribute significantly to RNA binding indicated in blue.

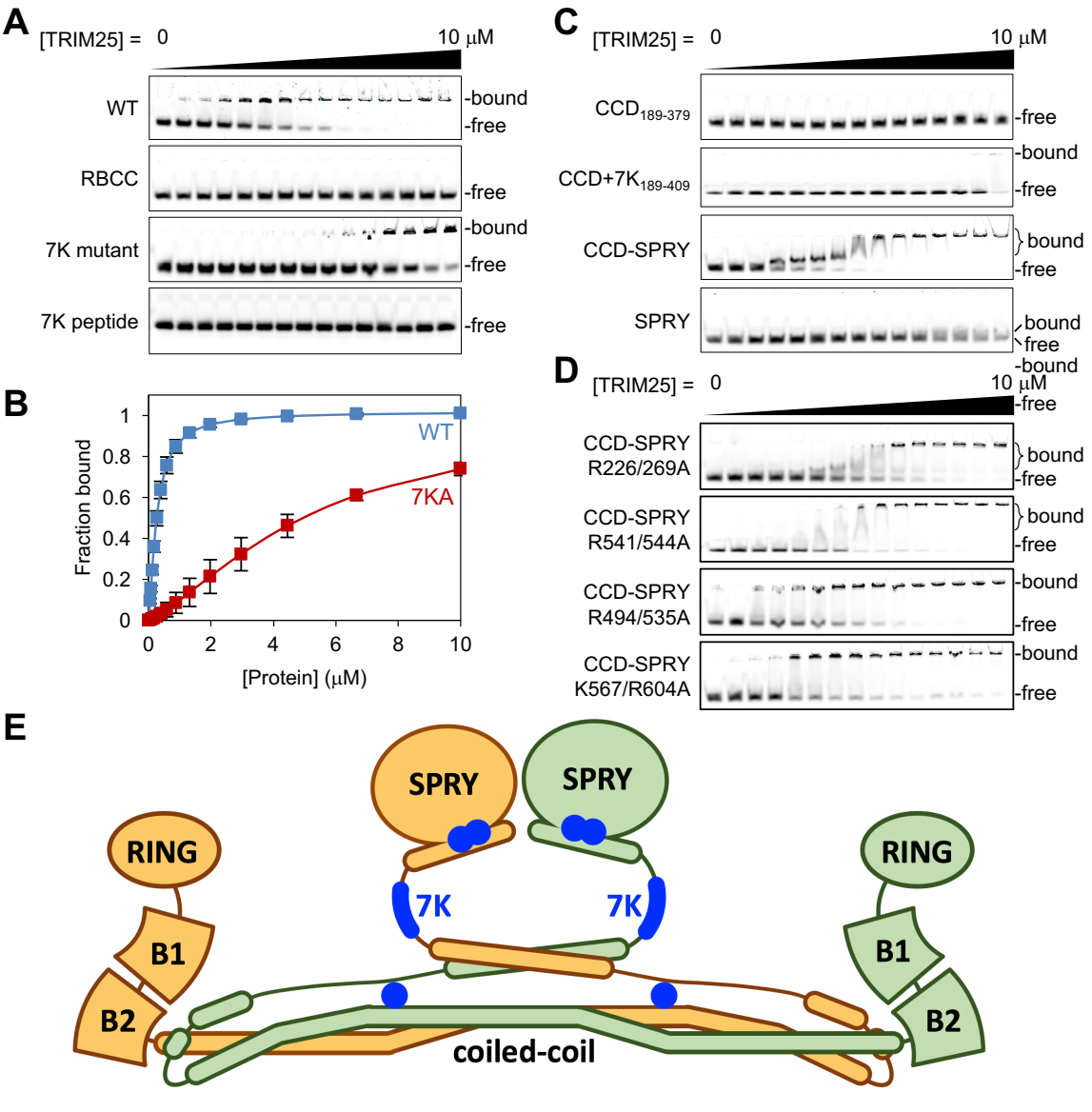
A
[TRIM25] = 0
10 μM
WT
RBCC
7K mutant
7K peptide
-bound
-free
B
Fraction bound
[Protein] (μM)
WT
7KA
C
[TRIM25] = 0
10 μM
CCD189-379
CCD+7K189-409
CCD-SPRY
SPRY
-free
-bound
bound
D
[TRIM25] = 0
10 μM
CCD-SPRY R226/269A
CCD-SPRY R541/544A
CCD-SPRY R494/535A
CCD-SPRY K567/R604A
E
SPRY
SPRY
RING
RING
7K
7K
B1
B2
B1
B2
coiled-coil

Table 1. RNA binding affinities of TRIM25 constructs.

Protein construct	Residues	K_d (μM)	Relative affinity[a]	Hill coefficient
WT	1-630	0.26 ± 0.03[b]	1.00	1.44 ± 0.10
7KA mutant	1-630	4.89 ± 0.03	0.05	1.73 ± 0.24
ΔSPRY	1-379	no binding		
7K peptide	379-394	no binding		
CCD	189-379	no binding		
CCD+7K	189-409	no binding		
CCD-SPRY	189-630	0.11 ± 0.02	2.36	2.24 ± 0.04
SPRY	410-630	3.47 ± 1.17	0.07	1.73 ± 0.92
CCD-SPRY R226/269A	189-630	0.45 ± 0.18	0.58	1.31 ± 0.10
CCD-SPRY R541/544A	189-630	0.27 ± 0.02	0.96	2.50 ± 0.55
CCD-SPRY R494/535A	189-630	0.22 ± 0.03	1.18	1.28 ± 0.07
CCD-SPRY R567/604A	189-630	0.47 ± 0.17	0.55	1.54 ± 0.20

[a] Compared to WT.

[b] Average values and standard deviations were calculated from at least three independent trials.

fully delineate the elements that contribute to TRIM25's RNA binding activity *in vitro* (**Fig. 4C-D**; results are summarized in **Table 1**). These experiments revealed that: (1) the RING and B-box 2 domains were not required for RNA binding, and indeed may even act inhibitory because deletion of both domains enhanced RNA-binding affinity by 2-fold; (2) the coiled-coil/L2 dimerization domain did not independently bind to RNA in the absence of the 7K motif, but alanine substitutions for exposed arginine residues (Arg226 and Arg229) in this domain in context of full-length protein resulted in 2-fold loss of affinity; (3) the isolated SPRY domain had independent, but weak RNA binding activity (K_d = 3.5 μM); and (4) alanine substitution of SPRY residues Lys567 and Arg604 in context of full-length TRIM25 also resulted in 2-fold loss of RNA binding. Thus, our aggregate data indicated that both the 7K motif in the L2 linker and the SPRY domain provide direct contacts to the bound RNA and are required for full-affinity binding. These elements circumscribe a region in the middle of the TRIM25 dimer, which in other TRIM proteins have been found to mediate interactions between their SPRY and coiled-coil domains (Weinert, 2015;Roganowicz, 2017) (**Fig. 4E**). We therefore speculate that binding to RNA is likely to have significant impact on the structural juxtaposition of the SPRY domain and RBCC dimer scaffold, and hence on mechanistic coupling of SPRY and RBCC functions.

TRIM25 preferentially binds RNA over DNA. We have not found evidence for sequence-specific binding by TRIM25 as yet, but did observe a clear preference for RNA over DNA in EMSA experiments. Pre-formed complexes of TRIM25 and fluorescently-labeled dsRNA were incubated with

unlabeled dsRNA, ssRNA, dsDNA, and ssDNA (all of the same lengths and sequence), and displacement of the labeled probe was quantified by polyacrylamide gel electrophoresis and densitometry (**Fig. 5**). Results showed that unlabeled ssRNA displaced about half the amount of labeled probe displaced by dsRNA, when compared on a molar basis. Since dsRNA has twice the number of strands as ssRNA, this result indicated that ssRNA was as competent as dsRNA in binding TRIM25 on a per-strand basis. In contrast, dsDNA displaced about 10-fold less probe compared to dsRNA, and ssDNA displaced also about half less than dsDNA. Thus, TRIM25 can bind both dsRNA and ssRNA *in vitro* and preferentially binds both forms of RNA over DNA.

RNA binding is required for TRIM25's overall anti-viral activity. Our collaborators, the Michaela Gack group at the University of Chicago, next tested whether TRIM25's RNA-binding ability is required for its anti-viral function. To this end, they reconstituted *TRIM25*-knockout (KO) HEK293T cells (Sanchez, 2016) by transfection with either empty vector, FLAG-tagged WT TRIM25, or the 7KA mutant. Results showed that WT TRIM25, but not the 7KA mutant, effectively suppressed replication of dengue virus, as monitored by expression levels of the viral prM protein in the infected cells (**Fig. 6A**). Specifically, dengue prM was expressed in only 15% of TRIM25 knock-out HEK293T cells that were reconstituted with WT TRIM25, but in more than 30% of cells reconstituted with the 7KA mutant or vector only control. The Gack lab also tested replication of influenza A virus (IAV) in reconstituted *TRIM25*-KO cells by measuring the abundance of the IAV non-structural protein 1 (NS1) in the whole cell lysates

Fig. 5. Competition binding experiments.

(A) The indicated concentrations of unlabeled competitor 28 bp oligos were incubated with 0.5 μM of TRIM25 in complex with fluorescent 28 bp RNA and electrophoretic migration of the fluorescent probe was analyzed.

(B) The amounts of fluorescent probe displaced by 5 μM competitor were quantified and plotted.

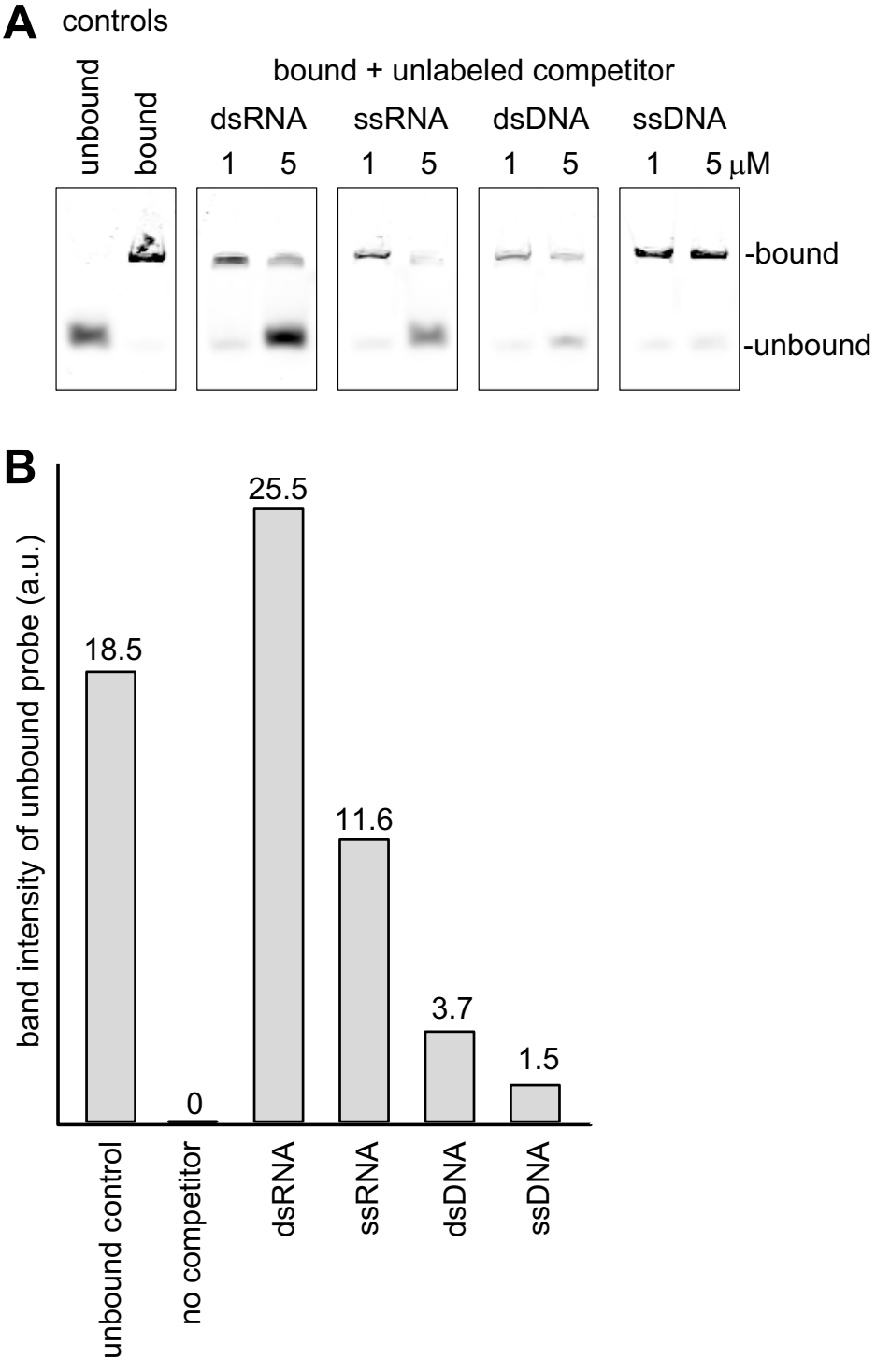
A
controls
unbound
bound
bound + unlabeled competitor
dsRNA
ssRNA
dsDNA
ssDNA
1 5 1 5 1 5 1 5 μM
-bound
-unbound
B
band intensity of unbound probe (a.u.)
18.5
0
25.5
11.6
3.7
1.5
unbound control
no competitor
dsRNA
ssRNA
dsDNA
ssDNA

Fig. 6. RNA binding is important for TRIM25's ability to inhibit virus replication.

(A) *TRIM25*-KO HEK293T cells were transiently transfected with either empty vector, or FLAG-tagged TRIM25 WT or the 7KA mutant, infected with dengue virus, and then stained for the viral prM protein. Percentage of prM-positive cells were determined by flow cytometry.

(B) Cells were infected with influenza A virus (H1N1 PR8, MOI 0.5), and then immunoblotted with anti-NS1 to determine expression levels of the viral NS1 protein. For both viral assays, whole cell lysates (WCLs) were further immunoblotted with anti-FLAG antibody to confirm expression of TRIM25 WT and 7KA proteins. Actin was used as loading control.

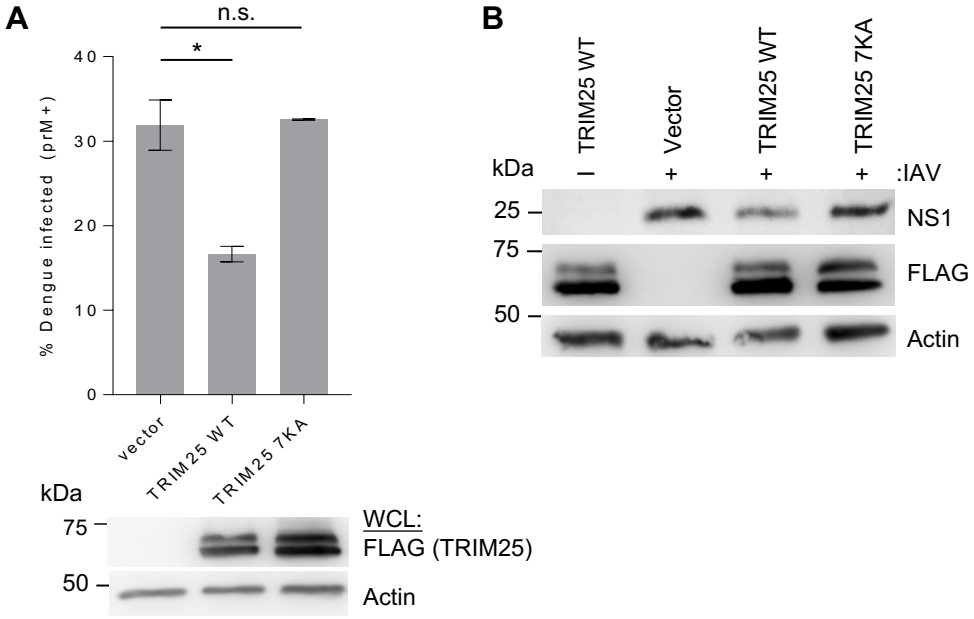
A
n.s.
*
40
30
20
10
0
% Dengue infected (prM+)
vector
TRIM25 WT
TRIM25 7KA
kDa
75
50
WCL:
FLAG (TRIM25)
Actin
B
- TRIM25 WT
+ Vector
+ TRIM25 WT
+ TRIM25 7KA
kDa
:IAV
25
75
50
NS1
FLAG
Actin

(WCLs) of infected cells through immunoblotting (**Fig. 6B**). This showed reduced NS1 protein levels in *TRIM25*-KO cells complemented with WT TRIM25 as compared to vector-transfected control cells. In contrast, cells reconstituted with the 7KA mutant had comparable NS1 protein expression levels as vector-transfected control. Consistent with these results, IAV titers in the supernatants of WT TRIM25-expressing cells were reduced, while cells reconstituted with the 7KA mutant had similar titers as cells reconstituted with empty vector (**Fig. 6C**). We conclude that the RNA-binding ability of TRIM25 is, indeed, important for its overall anti-viral activity.

DISCUSSION

TRIM25 functions in multiple RNA-dependent ubiquitination mechanisms, and was previously identified in an unbiased screen as an RNA-binding protein. Our studies provide biochemical proof, using purified components, that TRIM25 indeed directly binds to RNA with high affinity. Interestingly, our results show that multiple structural elements mediate TRIM25's RNA binding activity. In vitro binding experiments combined with mutagenesis showed that the SPRY and L2 linker regions are essential for high affinity binding, and that additional contacts may also be provided by the coiled-coil domain. In other TRIM proteins, the L2 linker has been shown to facilitate structural and mechanistic coupling of the SPRY and RBCC regions, and we therefore propose that RNA binding to likely modulates this functional coupling in TRIM25. Interestingly, the requirement for TRIM25 in both the anti-viral and RNA processing pathways have been shown to

be SPRY domain-dependent (Gack, 2007;Zheng, 2017;Li, 2017;Choudhury, 2014). Since the SPRY domain is also absolutely required for RNA binding, our results therefore indicate that the reported SPRY-dependent interactions may in fact be RNA-bridged interactions. We also found that, at least *in vitro*, RNA can promote higher-order oligomerization of TRIM25 and activation of its RING domain. Since TRIM25 appears to bind RNA promiscuously in the cell (Kwon, 2013; Choudhury, 2017), this raises the question of how TRIM25's ubiquitination activity is suppressed in the cell, because uncontrolled polyubiquitin synthesis is presumably harmful and needs to be avoided.

RNA binding by TRIM25 could facilitate pathway-specific ubiquitination by promoting dual recognition of RNA signals. In the simplest model, TRIM25 could function as a co-receptor that binds the same RNA molecule as the primary receptor, for example by co-binding to 5'-triphosphorylated viral RNA in the RIG-I pathway. We are currently performing experiments to determine whether or not TRIM25 and RIG-I are able to form a supercomplex on *in vitro* synthesized 5'ppp dsRNA of increasing lengths. Our data so far demonstrate that TRIM25 preferentially binds to free RNA rather than RIG-I bound RNA (data not shown). These results suggest that TRIM25 is not a co-receptor for the same RNA as RIG-I, and that modification of RIG-I may occur in *trans* from TRIM25 bound to a separate RNA molecule.

Recent studies showed that activation of RIG-I by viral RNA induces its co-localization with TRIM25 into punctate stress granules (Sanchez-Aparicio, 2017). Anti-viral stress granules form as a collection of viral and host RNAs

along with many interferon-stimulated genes and RNA binding proteins. We therefore speculate that RNA-binding may be part of an anti-viral stress granule localization signal for RIG-I and TRIM25. Once co-localized, TRIM25 and RIG-I may then act as co-receptors for the same RNA molecule. The induced proximity of RNA-bound and conformationally active RIG-I and TRIM25 may allow for the coordinated exposure of the RIG-I and TRIM25-mediated polyubiquitination of the RIG-I 2CARD, leading to an IFN response.

Furthermore, whether the co-receptor model holds true for other TRIM25-mediated pathways remains to be established. In this regard, TRIM25 was also recently implicated in the ZAP pathway, which induces degradation of CG-rich viral mRNAs (Zheng, 2017;Li, 2017;Takata, 2017). Notably, TRIM25's cellular RNA binding activity was initially reported in a study to identify mRNA binding proteins in the absence of viral infection (Kwon, 2013). It is therefore possible that TRIM25 is promiscuously but benignly associated with cellular mRNA, and that additional ZAP binding somehow triggers ubiquitin-dependent signaling to degrade the CG-rich subpopulation. However, it is not yet clear whether or how TRIM25's ubiquitination activity regulates ZAP, with some studies showing an absolute requirement for the RING domain and others not (Zheng, 2017;Li, 2017). Interestingly, ZAP is also reported to localize to RNA granules where it recruits deadenylase and exonuclease complexes, as well as mRNA decapping enzymes (Lee, 2013;Turner, 2014). In human cells, a variant of ZAP is reported to functionally associate with RIG-I (Hayakawa, 2011),

suggesting the possibility that TRIM25's overall anti-viral activity may in fact reflect an intersection of the RIG-I and ZAP pathways.

In summary, our studies define how TRIM25 binds to RNA and how this binding activity can promote both enzymatic activation of TRIM25 and interactions with RNA receptors *in vitro*. We also found that RNA binding is important for TRIM25 localization into cytoplasmic stress granules in cells. RNA binding by TRIM25 therefore imparts dual functionality to this protein, both of which are likely important for regulation of anti-viral and RNA processing mechanisms.

METHODS

Protein preparation. Full-length human TRIM25 was expressed using a baculovirus system and purified as described previously (Sanchez, 2016). In brief, clarified cell lysates were treated with PEI to remove nucleic acid contamination, and the Strep/FLAG-tagged protein was purified on a StrepTactin resin (GE Healthcare) and then on a Superdex 200 gel filtration column (GE Heathcare). The following protein constructs were expressed and purified in a similar manner: RBCC constructs spanning residues 1-379, 1-401, and 1-435, and the full-length 7KA mutant. Nucleic acid-contaminated protein used for experiments in **Fig. 2** were also purified similarly, except that the PEI precipitation step was omitted.

CCD constructs were expressed in *E. coli* as SUMO-fusion proteins and purified as described previously (Sanchez, 2014).

CCD-SPRY and SPRY were also expressed in as SUMO-fusion proteins. Cell pellets were resuspended in lysis buffer (20 mM Tris pH 8, 150 mM NaCl, 1 mM TCEP, 20 mM imidazole pH 8, 20 U/mL Benzonase (Sigma-Aldrich), and 1 tablet EDTA-free protease inhibitor) and lysed by a microfluidizer. Proteins were purified by a combination Ni-NTA affinity, Source 15Q ion exchange, and size exclusion chromatography into the final buffer (20 mM Sodium Phosphate pH 8, 100 mM NaCl, 1 mM TCEP).

RIG-I was expressed from a pET50b plasmid and purified as described in (Peisley, 2013). In brief, cell pellets were resuspended in lysis buffer (50 mM Sodium Phosphate pH 8.0, 300 mM NaCl, 10% glycerol, 0.2% NP-40, 20 mM imidazole pH 8.0, 1000 U/50 mL Benzonase (Sigma-Aldrich), and 1 tablet EDTA-free protease inhibitor) and lysed by a microfluidizer. The protein was purified by a combination of Ni-NTA affinity, heparin affinity and size exclusion chromatography (SEC) in SEC buffer (20 mM Hepes, pH 7.5, 150 mM NaCl and 2 mM DTT). The NusA tag was removed by overnight cleavage with HRV 3C protease at 4℃ prior to heparin affinity chromatography.

Ubiquitination assays. TRIM25 constructs were incubated at 37 C with E1 (100 nM), E2 (1 mM Ubc5b or 0.28 mM Ubc13/Mms2), and ubiquitin (40 μM) in buffer (50 mM Tris, pH 7.5, 150 mM NaCl, 0.5 mM TCEP, 5 mM ATP, 10 mM $MgCl_2$). Reactions were stopped by addition of SDS-PAGE sample buffer and

boiling for 10 min. Immunoblots were performed with anti-Ub (1:2,000; P4D1, Santa Cruz Biotechnoogy), and anti-FLAG M2 (1:5,000; Sigma). Experiments in **Fig. 2** used RNase A (Qiagen), DNase I (Sigma), dsRNA ladder (NEB), and 100-bp dsDNA ladder (NEB).

SEC-MALS. These experiments were performed as described previously (Sanchez, 2016).

EMSA. The fluorescent dsRNA used in EMSA and competition experiments (Integrated DNA Technologies) contained a 28 bp duplex with a 5' IRDye 800CW fluorophore. For EMSAs used to evaluate RNA binding, individual TRIM25 constructs were incubated with 250 nM fluorescent RNA ligand for 30 min on ice in binding buffer (25 mM HEPES pH 7.5, 150 mM NaCl, 1 mM TCEP, 5% glycerol, 0.3 mg/ml BSA) at concentrations ranging from 0 nM to 10 μM. After incubation, 5 μL of each sample was run on a 6% 0.5x TBE for 30 min at 50 V. The RNA was imaged on a Licor Odyssey Classic infrared scanner. The fraction unbound RNA bands were quantified with the Licor Image StudioLite software for each protein concentration and plotted as fraction RNA bound vs protein concentration. The data was fit to a simple binding isotherm model, using the equation:

$$\text{fraction bound} = \frac{[\text{TRIM25}]^{n}}{\text{Kd}^{n} + [\text{TRIM25}]^{n}}$$

, where Kd = dissociation constant and n = Hill coefficient.

RNA competition assay. To evaluate TRIM25 binding specificity to RNA or DNA, the 5' IRDye 800 28mer dsRNA (250 nM) was saturated with TRIM25 (4 μM), as guided from our EMSA experiments. Non-fluorescent competitors at 1 μM or 5 μM, with the same nucleotide sequence (Integrated DNA Technologies), were then added to the reaction mix and allowed to incubate on ice for an additional 30 minutes. Samples were resolved on a 6% 0.5x TBE gel for 30 min at 50V. The fraction of displaced fluorescent RNA was imaged on a Licor Odyssey Classic infrared scanner. The displaced RNA was quantified with the Licor Image StudioLite software and plotted as band intensity of unbound probe vs competitor.

Viral infection assays. *TRIM25*-KO HEK 293T cells, seeded into 12-well plates (~5 x 10^5 cells/well), were transfected with 2 μg of pCMV empty vector or the indicated FLAG-tagged TRIM25 constructs using linear polyethylenimine (PEI) (1 mg/mL solution in 20 mM Tris pH 6.8; Polysciences), according to the manufacturer's instructions. At 24 h post-transfection, cells were infected with the indicated viruses. For DenV replication experiments, cells were infected with an MOI of 4 of DENV (strain 16681, serotype 2) in serum-free medium (OPTI-MEM, Life Technologies). After 2 h, medium was replaced with supplemented DMEM. At 24 h post-infection, cells were harvested and stained for DenV prM protein via flow cytometry as previously described (Chan, 2016). Briefly, cells were washed once in phosphate-buffered saline (PBS) and then fixed in 1% (*w*/*v*) paraformaldehyde (PFA, in PBS) for 30 min, followed by permeabilization in 0.1% saponin (in 2% FBS in PBS) for 30 min. Cells were incubated for 1 h with

anti-prM (2H2, Merck Millipore) conjugated to DyLight 633 using a commercial kit (Thermo Scientific). Cells were washed twice with PBS, re-suspended in 1% PFA (*w*/*v*) (in PBS), and then analyzed on a BD LSRII. Analysis was performed using FlowJo software. For experiments with IAV, *TRIM25*-KO HEK 293T cells were infected with IAV (PR/8/1934(H1N1)) at the indicated MOI. At the indicated times post-infection, cells were lysed in NP-40 buffer (150 mM NaCl, 1% NP-40, 50 mM HEPES, pH 7.4, supplemented with protease inhibitors). Cell debris was pelleted by centrifugation at 13,000 rpm for 20 minutes at 4 ºC. WCLs were mixed with 6x Laemmli loading buffer and heated at 95ºC for 5 min. Protein expression of IAV NS1 was determined by immunoblotting using anti-NS1.

ACKNOWLEDGEMENTS

We thank Barbie Ganser-Pornillos for discussions, Marcin Roganowicz for technical support, Konstantin Sparrer and the lab of Michaela Gack for cell-based *in vitro* virus assays shown in Figures 6 and 9, and Sun Hur for providing 62bp ds RNA. This study was supported by NIH grants R01-AI087846 (to M.U.G.) and R01-GM112508 (to O.P.). Seed funding was also provided by the Annette Lightner Foundation (to O.P.). J.G.S. was supported by a predoctoral Cell and Molecular Biology Training grant from NIH (T32-GM008136) and the Robert R. Wagner Fellowship Fund.

REFERENCES

Anger, A.M., Armache, J.P., Berninghausen, O., Habeck, M., Subklewe, M., Wilson, D.N., and Beckmann, R. (2013). Structures of the human and Drosophila 80S ribosome. Nature *497*, 80-85.

Chan, Y.K., and Gack, M.U. (2016a). A phosphomimetic-based mechanism of dengue virus to antagonize innate immunity. Nat Immunol *17*, 523-530.
Chan, Y.K., and Gack, M.U. (2016b). Viral evasion of intracellular DNA and RNA sensing. Nat Rev Microbiol *14*, 360-373.

Choudhury, N.R., Nowak, J.S., Zuo, J., Rappsilber, J., Spoel, S.H., and Michlewski, G. (2014). Trim25 is an RNA-specific activator of Lin28a/TuT4-mediated uridylation. Cell Rep *9*, 1265-1272.

Choudhury, Nila Roy, Gregory Heikel, Maryia Trubitsyna, Peter Kubik, Jakub Stanislaw Nowak, Shaun Webb, Sander Granneman, et al. 2017. "RNA-Binding Activity of TRIM25 Is Mediated by Its PRY/SPRY Domain and Is Required for Ubiquitination." *BMC Biology* 15 (1). BioMed Central: 105. doi:10.1186/s12915-017-0444-9.

Gack, M.U., Kirchhofer, A., Shin, Y.C., Inn, K.S., Liang, C., Cui, S., Myong, S., Ha, T., Hopfner, K.P., and Jung, J.U. (2008). Roles of RIG-I N-terminal tandem CARD and splice variant in TRIM25-mediated antiviral signal transduction. Proc Natl Acad Sci U S A *105*, 16743-16748.

Gack, M.U., Shin, Y.C., Joo, C.H., Urano, T., Liang, C., Sun, L., Takeuchi, O., Akira, S., Chen, Z., Inoue, S.*, et al.* (2007). TRIM25 RING-finger E3 ubiquitin ligase is essential for RIG-I-mediated antiviral activity. Nature *446*, 916-920.

Hayakawa, S., Shiratori, S., Yamato, H., Kameyama, T., Kitatsuji, C., Kashigi, F., Goto, S., Kameoka, S., Fujikura, D., Yamada, T.*, et al.* (2011). ZAPS is a potent stimulator of signaling mediated by the RNA helicase RIG-I during antiviral responses. Nat Immunol *12*, 37-44.

Heikel, G., Choudhury, N.R., and Michlewski, G. (2016). The role of Trim25 in development, disease and RNA metabolism. Biochem Soc Trans *44*, 1045-1050.
Koliopoulos, M.G., Esposito, D., Christodoulou, E., Taylor, I.A., and Rittinger, K. (2016). Functional role of TRIM E3 ligase oligomerization and regulation of catalytic activity. EMBO J *35*, 1204-1218.

Kwon, S.C., Yi, H., Eichelbaum, K., Fohr, S., Fischer, B., You, K.T., Castello, A., Krijgsveld, J., Hentze, M.W., and Kim, V.N. (2013). The RNA-binding protein repertoire of embryonic stem cells. Nat Struct Mol Biol *20*, 1122-1130.

Lee, H., Komano, J., Saitoh, Y., Yamaoka, S., Kozaki, T., Misawa, T., Takahama, M., Satoh, T., Takeuchi, O., Yamamoto, N.*, et al.* (2013). Zinc-finger antiviral protein mediates retinoic acid inducible gene I-like receptor-independent antiviral response to murine leukemia virus. Proc Natl Acad Sci U S A *110*, 12379-12384.

Li, M.M., Lau, Z., Cheung, P., Aguilar, E.G., Schneider, W.M., Bozzacco, L., Molina, H., Buehler, E., Takaoka, A., Rice, C.M.*, et al.* (2017). TRIM25 enhances the antiviral action of zinc-finger antiviral protein (ZAP). PLoS Pathog *13*, e1006145.

Peisley, A., Wu, B., Xu, H., Chen, Z.J., and Hur, S. (2014). Structural basis for ubiquitin-mediated antiviral signal activation by RIG-I. Nature *509*, 110-114.

Peisley, A., Wu, B., Yao, H., Walz, T., and Hur, S. (2013). RIG-I forms signaling-competent filaments in an ATP-dependent, ubiquitin-independent manner. Mol Cell *51*, 573-583.

Roganowicz, M.D., Komurlu, S., Mukherjee, S., Plewka, J., Alam, S.L., Skorupka, K.A., Wan, Y., Dawidowski, D., Cafiso, D.S., Ganser-Pornillos, B.K.*, et al.* (2017). TRIM5alpha SPRY/coiled-coil interactions optimize avid retroviral capsid recognition. PLoS Pathog *13*, e1006686.

Saito, T., Owen, D.M., Jiang, F., Marcotrigiano, J., and Gale, M., Jr. (2008). Innate immunity induced by composition-dependent RIG-I recognition of hepatitis C virus RNA. Nature *454*, 523-527.

Sanchez, J.G., Chiang, J.J., Sparrer, K.M., Alam, S.L., Chi, M., Roganowicz, M.D., Sankaran, B., Gack, M.U., and Pornillos, O. (2016). Mechanism of TRIM25 catalytic activation in the antiviral RIG-I pathway. Cell Rep *16*, 1315-1325.

Sanchez, J.G., Okreglicka, K., Chandrasekaran, V., Welker, J.M., Sundquist, W.I., and Pornillos, O. (2014). The tripartite motif coiled-coil is an elongated antiparallel hairpin dimer. Proc Natl Acad Sci U S A *111*, 2494-2499.

Sanchez-Aparicio, M.T., Ayllon, J., Leo-Macias, A., Wolff, T., and Garcia-Sastre, A. (2017). Subcellular localizations of RIG-I, TRIM25, and MAVS complexes. J Virol *91*.
Schlee, M. (2013). Master sensors of pathogenic RNA - RIG-I like receptors. Immunobiology *218*, 1322-1335.

Sparrer, K.M.J., Gableske, S., Zurenski, M.A., Parker, Z.M., Full, F., Baumgart, G.J., Kato, J., Pacheco-Rodriguez, G., Liang, C., Pornillos, O.*, et al.* (2017). TRIM23 mediates virus-induced autophagy via activation of TBK1. Nat Microbiol.

Takata, M.A., Goncalves-Carneiro, D., Zang, T.M., Soll, S.J., York, A., Blanco-Melo, D., and Bieniasz, P.D. (2017). CG dinucleotide suppression enables antiviral defence targeting non-self RNA. Nature.

Turner, M., Galloway, A., and Vigorito, E. (2014). Noncoding RNA and its associated proteins as regulatory elements of the immune system. Nat Immunol *15*, 484-491.

Weinert, C., Morger, D., Djekic, A., Grutter, M.G., and Mittl, P.R. (2015). Crystal structure of TRIM20 C-terminal coiled-coil/B30.2 fragment: implications for the recognition of higher order oligomers. Sci Rep *5*, 10819.

Zeng, W., Sun, L., Jiang, X., Chen, X., Hou, F., Adhikari, A., Xu, M., and Chen, Z.J. (2010). Reconstitution of the RIG-I pathway reveals a signaling role of unanchored polyubiquitin chains in innate immunity. Cell *141*, 315-330.

Zheng, X., Wang, X., Tu, F., Wang, Q., Fan, Z., and Gao, G. (2017). TRIM25 is required for the antiviral activity of zinc finger antiviral protein. J Virol *91*.

CHAPTER 5

SUMMARY AND FUTURE PERSPECTIVES

SUMMARY

The importance of TRIM25 in cellular anti-viral defense is highlighted by findings that viruses, such as influenza and dengue, have evolved mechanisms to suppress innate immunity by specifically targeting and disrupting TRIM25 function (Gack et al. 2009; Manokaran et al. 2015). This dissertation describes a series of detailed structure-function studies to answer important questions on oligomerization and assembly of TRIM25 and the TRIM family of proteins; how assembly of TRIM25 regulates its E3 ligase activity; and how the polyubiquitination and RNA binding activities of TRIM25 facilitate its anti-viral function.

In Chapter 2, we describe the TRIM25 coiled-coil structure, which is the first example from the entire TRIM protein family. This study elucidated the fundamental oligomeric state of the TRIM family of proteins, and established the structural framework of TRIM protein function. The structure revealed that the TRIM25 coiled-coil forms an elongated antiparallel dimer. Our biophysical analysis demonstrated that the coiled-coil is dimeric even at nM concentrations, establishing that the basal oligomeric state of TRIM25 is a dimer. These data further revealed that in the full-length TRIM25 dimer, the two N-terminal catalytic RING domains are separated by the length of the coiled-coil, sterically hindering any potential RING/RING interactions within the dimer. Additionally, the fold-back configuration of the subunits places the substrate-binding SPRY domains at a central location of the TRIM25 dimer.

We also found within the coiled-coil structure a distinctive pattern of heptad and hendecad repeats of hydrophobic residues. The stability of the dimer requires two central hydrophobic residues (Tyr245 and Leu252). These residues perhaps comprise a “trigger site” that nucleates coiled-coil formation. A “structure-to-sequence” analysis revealed that the pattern of heptad and hendecad repeats is conserved within many other TRIM proteins, despite their highly divergent coiled-coil sequences. We then demonstrated the conservation of the antiparallel coiled-coil within a distantly related TRIM, TRIM5α. These data suggested that other TRIM proteins share the same tertiary and quaternary structure as TRIM25, which has since been confirmed by other groups (Y. Li et al. 2014; Goldstone et al. 2017; Weinert et al. 2015).

In Chapter 3, we describe a second TRIM25 dimerization site, found within a RING/RING interface, and the importance of TRIM25 higher-order oligomerization for E3 ligase activity. Previously published studies demonstrated that TRIM25 modified RNA-activated RIG-I with K63-linked polyubiquitin chains (Gack et al. 2007). However, the mechanism by which TRIM25 carries out RIG-I modification was not yet determined. This study filled in important gaps in our understanding of how the RIG-I pathway is regulated to avoid the harmful consequences of runaway signaling.

We demonstrated that Ubc13/Uev1a is the only E2 conjugating enzyme able to synthesize K63-linked polyubiquitin chains *in vitro* when combined with TRIM25 RING. Our structural and biochemical analysis of the TRIM25 RING in complex with ubiquitin-conjugated Ubc13 revealed that TRIM25 requires RING

dimerization for catalytic activity. We concluded that TRIM25 tetramerizes through the combination of the two distinct oligomerization sites within the RING and coiled-coil domains. Disruption of TRIM25 tetramerization, using the RING dimer-disrupting mutants L69A and V72A, leads to a significant decrease in TRIM25-mediated anti-viral activity against influenza virus. Interestingly, mutations that disrupt coiled-coil dimerization *in vitro* (Y245A and L252A) have relatively little effect on TRIM25 anti-viral activity, suggesting that the coiled-coil is significantly more stable inside the cell.

The TRIM25 substrate, RIG-I 2CARD, is well characterized to form a “lock washer” tetramer for MAVS activation (Peisley et al. 2014). We found that the ubiquitin-stabilized 2CARD tetramer enhances TRIM25’s E3 ligase activity *in vitro,* likely through aiding TRIM25 tetramerization. These results suggested to us a mutually productive activation of TRIM25 and RIG-I tetramerization through complementary oligomerization. We believe that this mechanism helps to define the fidelity of RIG-I signaling.

In Chapter 4, we describe how RNA enhances TRIM25 E3 ligase activity as well as TRIM25-dependent anti-viral activity. Together with published studies (Kwon et al. 2013; N R Choudhury et al. 2014; Nila Roy Choudhury et al. 2017), this work now establishes TRIM25 as an RNA binding protein. However, the TRIM25 RNA binding domain was not yet well characterized. We first demonstrated that RNA binding enhances TRIM25 E3 ligase activity *in vitro*, and then mapped the RNA-binding site to a lysine rich region within the Linker 2 (L2) region. Further analysis revealed that TRIM25 RNA binding is an orchestrated

event, requiring multiple TRIM25 structural elements, including the coiled-coil, L2, and SPRY. Viral infection assays demonstrated that RNA binding is required for TRIM25's overall anti-viral activity. Interestingly, the requirements for TRIM25 anti-viral and RNA processing pathways have been shown to be SPRY dependent. Since we demonstrated the SPRY domain is required for RNA binding, there is a possibility that reported SPRY-dependent interactions may in fact be RNA-bridged interactions.

In summary, our collective data demonstrate that the coiled-coil and RING domains of TRIM25 constitute two separate oligomerization sites. The basal oligomeric state of TRIM25 is a catalytically inactive dimer, mediated by the coiled-coil domain. Further oligomerization of TRIM25 through the RING domains, promoted by interactions with an E2 protein and ubiquitin and by interactions with substrate, forms a catalytically active tetramer. The formation of this tetramer may also be promoted by assembly onto an RNA strand mediated through coiled-coil, L2, and SPRY residues. Disruption of TRIM25 tetramerization or RNA binding activity abrogates cellular antiviral activity. These studies therefore provide important mechanistic insights on how TRIM25 helps to defend the cell from viral infections.

FUTURE PERSPECTIVES

TRIM25 anti-viral activity was initially identified through its modification of RIG-I with K63-linked polyubiquitin chains (Gack et al. 2007). In this signaling mechanism, RIG-I recognition of viral RNA exposes its N-terminal 2CARD,

followed by TRIM25 modification of the 2CARD. The polyubiquitin chains stabilize the “lock washer” configuration of 2CARD, which then serves as a nucleation site for the formation of a prion-like MAVS filament (Peisley et al. 2014; Wu et al. 2014). Current models of the TRIM25 and RIG-I interaction invokes either direct interactions between the RIG-I 2CARD and the TRIM25 SPRY domain, or indirect, RNA-mediated interactions between RIG-I and TRIM25. We have now performed extensive biochemical tests of these models, and have found that the TRIM25 SPRY domain does not significantly bind the RIG-I 2CARD, and that in competition experiments, TRIM25 preferentially binds free RNA over RNA-bound RIG-I (data not shown). These results do not support either model. Instead, it appears that TRIM25 and RIG-I may bind to separate RNA molecules and RIG-I modification occurs in *trans*. For this to occur, activated RIG-I and TRIM25 must be in close proximity to one another. Proximity-induced interaction appears to occur when viral RNA-bound RIG-I and TRIM25 co-localize in anti-viral stress granules, which are cytosolic sites with an enriched concentration of viral RNA and RNA binding proteins (Sánchez-Aparicio et al. 2017). Future studies should be directed at determining how RNA modulates TRIM25 and RIG-I interactions within these cytoplasmic granules.

TRIM25 is also required for the anti-viral activity of ZAP (M. M. H. Li et al. 2017; Zheng et al. 2017), which provides a different mechanism of viral restriction than RIG-I. ZAP promotes the degradation of viral mRNAs, resulting in translational inhibition of viral proteins (Gao 2002; MacDonald et al. 2007; Takata et al. 2017). Our preliminary data demonstrate that RNA also mediates

the interactions between ZAP and TRIM25. Interestingly, ZAP has an inhibitory effect on TRIM25 ubiquitination activity *in vitro*. This suggests that RIG-I and ZAP differentially modulate the E3 ligase activity of TRIM25. Future studies are required to reveal the importance of reducing TRIM25 E3 ligase activity for ZAP-mediated viral restriction.

REFERENCES

Choudhury, N R, J S Nowak, J Zuo, J Rappsilber, S H Spoel, and G Michlewski. 2014. “Trim25 Is an RNA-Specific Activator of Lin28a/TuT4-Mediated Uridylation.” *Cell Rep* 9 (4): 1265–72. doi:10.1016/j.celrep.2014.10.017.

Choudhury, Nila Roy, Gregory Heikel, Maryia Trubitsyna, Peter Kubik, Jakub Stanislaw Nowak, Shaun Webb, Sander Granneman, et al. 2017. “RNA-Binding Activity of TRIM25 Is Mediated by Its PRY/SPRY Domain and Is Required for Ubiquitination.” *BMC Biology* 15 (1). BioMed Central: 105. doi:10.1186/s12915-017-0444-9.

Gack, M U, R A Albrecht, T Urano, K S Inn, I C Huang, E Carnero, M Farzan, S Inoue, J U Jung, and A Garcia-Sastre. 2009. “Influenza A Virus NS1 Targets the Ubiquitin Ligase TRIM25 to Evade Recognition by the Host Viral RNA Sensor RIG-I.” *Cell Host Microbe* 5 (5): 439–49. doi:10.1016/j.chom.2009.04.006.

Gack, M U, Y C Shin, C H Joo, T Urano, C Liang, L Sun, O Takeuchi, et al. 2007. “TRIM25 RING-Finger E3 Ubiquitin Ligase Is Essential for RIG-I-Mediated Antiviral Activity.” *Nature* 446 (7138): 916–20. doi:10.1038/nature05732.

Gao, G. 2002. “Inhibition of Retroviral RNA Production by ZAP, a CCCH-Type Zinc Finger Protein.” *Science* 297 (5587): 1703–6. doi:10.1126/science.1074276.

Goldstone, David C, Philip A Walker, Lesley J Calder, Peter J Coombs, Joshua Kirkpatrick, Neil J Ball, Laura Hilditch, et al. 2017. “Structural Studies of Postentry Restriction Factors Reveal Antiparallel Dimers That Enable Avid Binding to the HIV-1 Capsid Lattice Divisions of a Molecular Structure.” Accessed September 12. doi:10.1073/pnas.1402448111.

Kwon, S Chul, Hyerim Yi, Katrin Eichelbaum, S Fohr, Bernd Fischer, Kwon Tae You, Alfredo Castello, Jeroen Krijgsveld, Matthias W Hentze, and V Narry Kim. 2013. “The RNA-Binding Protein Repertoire of Embryonic Stem Cells.” *Nat Struct Mol Biol* 20 (9): 1122–30. doi:10.1038/nsmb.2638.

Li, Melody M. H., Zerlina Lau, Pamela Cheung, Eduardo G. Aguilar, William M. Schneider, Leonia Bozzacco, Henrik Molina, et al. 2017. “TRIM25 Enhances the Antiviral Action of Zinc-Finger Antiviral Protein (ZAP).” Edited by Ana Fernandez-Sesma. *PLoS Pathogens* 13 (1). Public Library of Science: e1006145. doi:10.1371/journal.ppat.1006145.

Li, Yang, Han Wu, Wei Wu, Wei Zhuo, Weixiao Liu, Yixiao Zhang, Minzhang Cheng, et al. 2014. “Structural Insights into the TRIM Family of Ubiquitin E3 Ligases.” *Cell Research*. doi:10.1038/cr.2014.46.

MacDonald, Margaret R, Erica S Machlin, Owen R Albin, and David E Levy. 2007. “The Zinc Finger Antiviral Protein Acts Synergistically with an Interferon-Induced Factor for Maximal Activity against Alphaviruses.” *Journal of Virology* 81 (24). American Society for Microbiology: 13509–18. doi:10.1128/JVI.00402-07.

Manokaran, Gayathri, Esteban Finol, Chunling Wang, Jayantha Gunaratne, Justin Bahl, Eugenia Z Ong, Hwee Cheng Tan, et al. 2015. “Dengue Subgenomic RNA Binds TRIM25 to Inhibit Interferon Expression for Epidemiological Fitness.” *Science* 350 (6257): 217 LP-221. http://science.sciencemag.org/content/350/6257/217.abstract.

Peisley, Alys, Bin Wu, Hui Xu, Zhijian J. Chen, and Sun Hur. 2014. “Structural Basis for Ubiquitin-Mediated Antiviral Signal Activation by RIG-I.” *Nature* 509 (7498). Nature Publishing Group: 110–14. doi:10.1038/nature13140.

Sánchez-Aparicio, M. T., J. Ayllón, A. Leo-Macias, T. Wolff, and A. García-Sastre. 2017. “Subcellular Localizations of RIG-I, TRIM25, and MAVS Complexes.” *Journal of Virology* 91 (2): e01155-16. doi:10.1128/JVI.01155-16.

Takata, Matthew A, Daniel Gonçalves-Carneiro, Trinity M. Zang, Steven J Soll, Ashley York, Daniel Blanco-Melo, and Paul D Bieniasz. 2017. “CG Dinucleotide Suppression Enables Antiviral Defence Targeting Non-Self RNA.” *Nature*, September. doi:10.1038/nature24039.

Weinert, Christopher, Damien Morger, Aleksandra Djekic, Markus G. Grütter, and Peer R. E. Mittl. 2015. “Crystal Structure of TRIM20 C-Terminal Coiled-coil/B30.2 Fragment: Implications for the Recognition of Higher Order Oligomers.” *Scientific Reports* 5 (1): 10819. doi:10.1038/srep10819.

Wu, Bin, Alys Peisley, David Tetrault, Zongli Li, Edward H. Egelman, Katharine E. Magor, Thomas Walz, Pawel A. Penczek, and Sun Hur. 2014. “Molecular Imprinting as a Signal-Activation Mechanism of the Viral RNA Sensor RIG-I.” *Molecular Cell* 55 (4). Elsevier Inc.: 511–23. doi:10.1016/j.molcel.2014.06.010.

Zheng, Xiaojiao, Xinlu Wang, Fan Tu, Qin Wang, Zusen Fan, and Guangxia Gao. 2017. “TRIM25 Is Required for the Antiviral Activity of Zinc-Finger Antiviral Protein (ZAP).” *Journal of Virology*, JVI.00088-17. doi:10.1128/JVI.00088-17.

APPENDIX 1

ZAP STUDIES AND ZAP INFLUENCE ON TRIM25

Note: The data described in this text was generated by Katarzyna Zawada and Jacint Sanchez in the lab of Owen Pornillos and Barbie Ganser-Pornillos

INTRODUCTION

This appendix summarizes unpublished data encompassing efforts to structurally and biochemically characterize full-length ZAP, individual ZAP domains and their influence on TRIM25 E3 ligase activity. This study has been a cooperative project between Katarzyna Zawada and myself.

Appendix 1.1, Expression and purification of ZAP constructs

We purified ZAPL (aa 1-902) and ZAPS (aa 1-723), as well as the WWE (aa 498-723) and WWE-PARP (aa 498-902) domains to mimic the differences between the two isoforms (**Fig 1**)

1. Grow freshly transformed cells by autoinduction.
2. Lysis conditions: 50mM phosphate pH8, 100mM NaCl, 5% glycerol, 1mM TCEP, 0.2M (NH4)2SO4, 1 tablet complete EDTA free (protease inhibitor), 0.5ml PMSF, 0.75ml 100% TritonX, ddH20 till around 40ml (dilute till 50ml in the microfluidizer).
3. Lyse cells in microfluidizer – pass them through 2x.
4. Centrifugation 45 000xg, 30min, 4°C.
5. Transfer supernatant to clean beaker with stirrer (everything on ice) and do PEI precipitation:
   - Add 560ul 9% PEI pH8 dropwise to 50ml protein solution.
   - Stir on ice for 20min.
6. Centrifugation 20 000xg, 20min, 4°C.
7. Prepare Ni gravity column:
   - Wash Ni resin with ddH2O and with Lysis Buffer
8. Add supernatant from PEI precipitation to prepared Ni beads
   - Rock for about 20min at 4°C.
9. Let the protein solution flow through the beads 2x.
10. Wash beads:
    - 2x20ml & 1x10ml Lysis Wash Buffer
    - 1x5ml High Salt Buffer
    - 1x15ml Low pH Wash Buffer
11. Elution:
    - Elution in 4 steps: 3ml, 4ml, 3ml and 3ml of Elution Buffer.
    - IMPORTANT – Add some extra phosphate to freshly eluted fractions (to 40mM).
12. Dialysis of eluted fractions overnight against: 20mM phosphate pH8, 75mM NaCl, 10mM imidazole, 1mM TCEP
    - Add 25ul ULP1 to dialyzed protein solution – cutting TAG
13. Second Nickel:
    - Prepare 3ml Ni resin (wash with ddH20 and Dialysis Buffer)
    - Run protein with cut tag through the beads 5 times
    - Perform wash with 30mM imidazole (protein still binds to beads a little even without the tag)
14. Dilute fractions with ZAP 3x with Buffer A and run SourceQ column
    - ZAP does not bind to the column and comes out already pure!
15. Concentrate protein and run on S75 Column in: 20mM Tris pH8, 100mM NaCl, 1mM TCEP

- Instead of running S75 you can also dialyze ZAP into 20mM Tris pH8, 100mM NaCl, 1mM TCEP and concentrate after that for further analysis/crystallization.

BUFFERS for 1st Nickel:

Lysis Wash Buffer

- 20mM phosphate pH8, 100mM NaCl, 20mM imidazole, 1mM TCEP

High Salt Wash Buffer

- 20mM phosphate pH8, 500mM NaCl, 1mM TCEP

Low pH Wash Buffer

- 20mM phosphate pH7.5, 100mM NaCl, 20mM imidazole, 1mM TCEP

Elution Buffer

- 20mM phosphate pH8, 100mM NaCl, 400mM imidazole, 1mM TCEP

Source15Q column buffers

Buffer A

- 20mM phosphate pH8, 1mM TCEP

Buffer B

- 20mM phosphate pH8, 1M NaCl 1mM TCEP

Figure 1

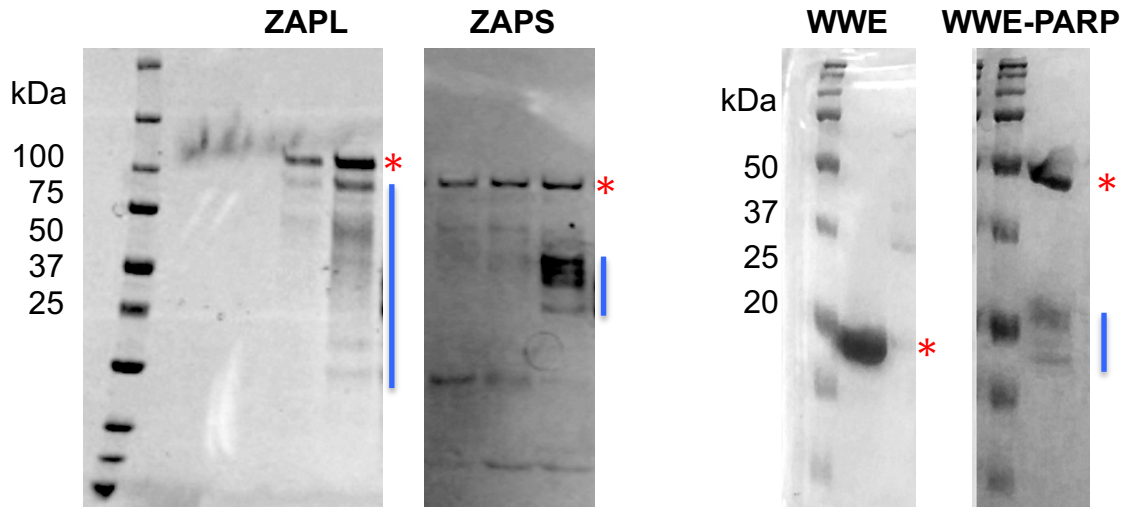
ZAPL
ZAPS
WWE
WWE-PARP
kDa
100
75
50
37
25
kDa
50
37
25
20
* Target protein
Proteolytic products

Appendix 1.2, ZAPL and ZAPS reduce TRIM25 E3 ligase activity

In this experiment we wanted to test whether ZAP has any influence on TRIM25's E3 ligase activity. The first experiment is a ubiquitylation assay (**Fig 2A**). In the second experiment, TRIM25 is co-transfected with ZAP or an empty vector (**Fig 2B**).

Ubiquitylation Assay

1. Components: 100 nM E1, 1 uM UbcH5b, 100 nM FLAG-TRIM25, 40 uM Ub, 5mM ATP, ~100 nM Smt3-ZAPL.
2. Mix components and allow the reaction to run for 20 minutes at room temperature,
3. Run reaction on SDS-PAGE, and visualize with western blot.

TRIM25 and ZAP co-expression

1. Transfection of 1 well in a 6-well plate of 293T cells requires 200 ng of FLAG-TRIM25 in pcDNA3 and 400 ng of HA-ZAP in pcDNA4.
2. Cells were harvested 48 hours after transfection.
3. Cells were lysed and proteins were visualized with western blot

Figure 2

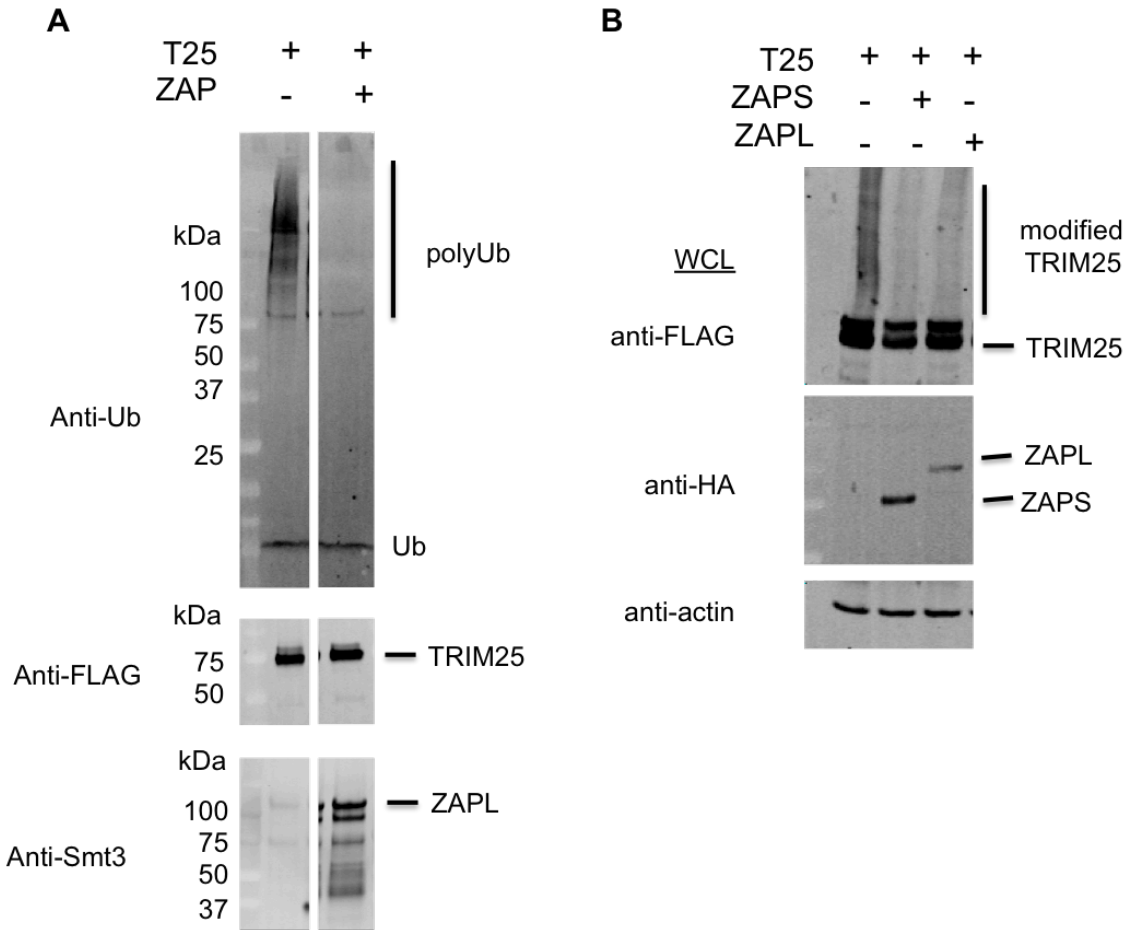
A
T25 + +
ZAP - +
kDa
100
75
50
37
25
Anti-Ub
polyUb
Ub
kDa
Anti-FLAG
75
50
TRIM25
kDa
100
75
50
37
Anti-Smt3
ZAPL
B
T25 + + +
ZAPS - + -
ZAPL - - +
WCL
anti-FLAG
modified TRIM25
TRIM25
anti-HA
ZAPL
ZAPS
anti-actin

Appendix 1.3, ATP stabilizes WWE structure

The WWE domain in ZAP is responsible for recognizing poly-ADP ribose; ATP is similar in structure to ADP-ribose. We sought to determine whether or not ATP would bind to the WWE domain of ZAP by observing the melting temperature (**Fig 3**).

1. The Z5-WWE (aa 498-723) construct was concentrated to 2 mg/mL, protein buffer alone or 10 uM ATP in protein buffer was added to the protein.
2. A final concentration of 100x SYPRO Orange was added to the mix, for a final volume of 25 uL.
3. The DSF experiment was performed using an RT-PCR, the data was analyzed in Excel.

Figure 3

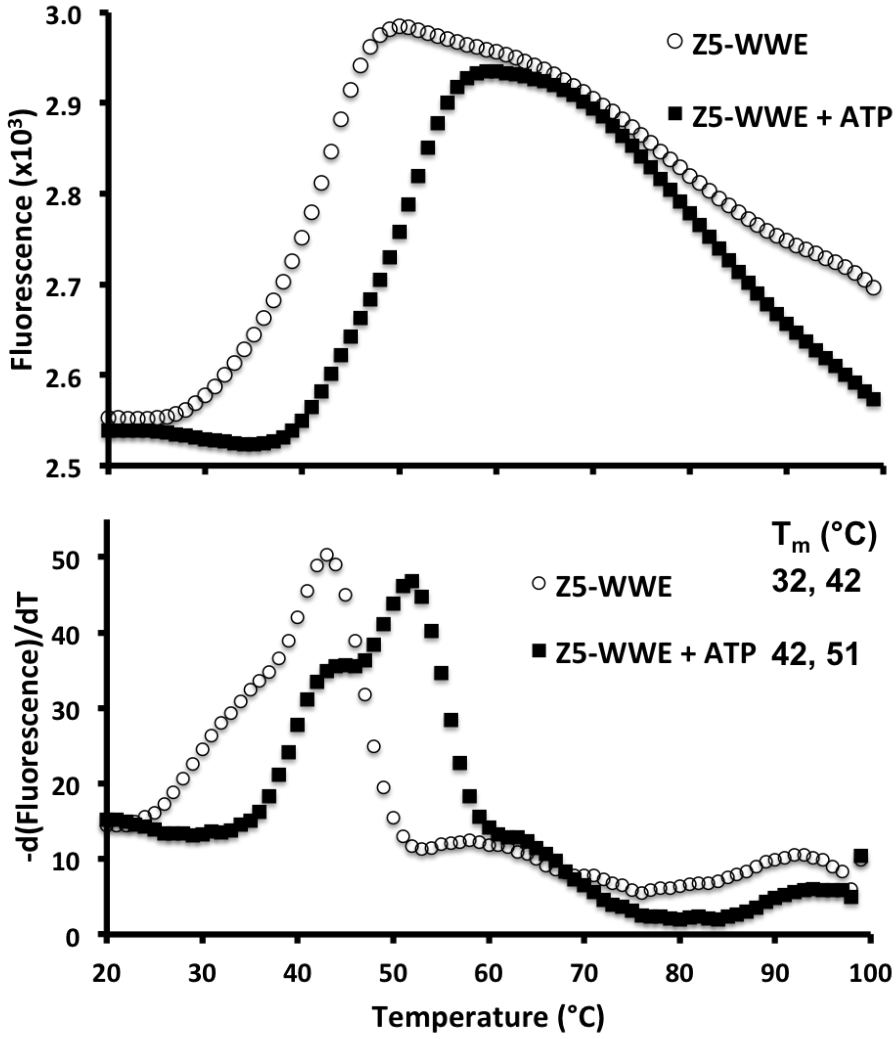
Fluorescence (x10³)
3.0
2.9
2.8
2.7
2.6
2.5
Z5-WWE
Z5-WWE + ATP
-d(Fluorescence)/dT
50
40
30
20
10
0
T_m (°C)
32, 42
Z5-WWE
Z5-WWE + ATP 42, 51
20
30
40
50
60
70
80
90
100
Temperature (°C)

Appendix 1.4, Crystallization of the WWE domain

At the moment, the only ZAP structure is of the N-terminal RNA binding domain. We sought to run crystallization trials with our purified proteins. The WWE (aa 498-723) construct was the only one that crystallized. Molecular replacement was not possible with currently available PDB structures. Selenomethionine labeled WWE failed to crystallize.

1. Proteins were purified as described in appendix 1.1 and concentrated to 8 mg/mL.
2. Crystals formed 3 days after setting up the drops.
3. Crystals were found in a 1:1 setup of protein to mother liquor.
4. Mother liquor contained: 0.2M Proline, 0.1M Hepes pH 7.5, 10% PEG 3350

Figure 4